MAGNETIC RESONANCE OF MICELLAR SYSTEMS

Ph.D.

1974

Katharine K. Fox

UMI Number: U419235

All rights reserved

INFORMATION TO ALL USERS
The quality of this reproduction is dependent upon the quality of the copy submitted.

In the unlikely event that the author did not send a complete manuscript
and there are missing pages, these will be noted. Also, if material had to be removed,
a note will indicate the deletion.

UMI®
Dissertation Publishing

UMI U419235
Published by ProQuest LLC 2015. Copyright in the Dissertation held by the Author.
Microform Edition © ProQuest LLC.
All rights reserved. This work is protected against
unauthorized copying under Title 17, United States Code.

ProQuest®

ProQuest LLC
789 East Eisenhower Parkway
P.O. Box 1346
Ann Arbor, MI 48106-1346

UNIVERSITY LIBRARY LEICESTER

THESIS
460237
15 8 74

Acknowledgements

I would like to thank Prof M C R Symons and Mr J Clifford for supervising this work, and Drs P J Anderson, W M Fox, I D Robb and G J T Tiddy for general discussions and encouragement. Specific thanks are due to Dr M A Turpin and Mrs J C Savage for adapting C S Johnson's computer program for my use, to Dr A L Smith and Mr J Boyd for help in investigating the dimerization phenomenon, to Dr P Richmond and Mr A Clark for discussions concerning things mathematical, to Drs H A Barnes and B Yates for discussions about rheology, to Mr D G Hall for discussions about thermodynamics, and Mr M L Bellis for help with instrumentation. The support of Unilever Research Laboratory, Port Sunlight and their provision of facilities and equipment for this research are also gratefully acknowledged.

CONTENTS

		PAGE
CHAPTER 1.	INTRODUCTION	
1.1.	Introduction	1
1.2.	Electron Paramagnetic Resonance	1
	1.2.1. The Basic Phenomenon	1
	1.2.2. Hyperfine Structure	3
	1.2.3. Rotational Mobility of Nitroxides	5
	1.2.4. Exchange Phenomena	6
1.3.	The Micellization of Surfactants	8
1.4.	Previous Applications of EPR to Colloid Chemistry	9
	1.4.1. Nitroxide Probes in Micellar Solutions	9
	1.4.2. Paramagnetic Counter-Ions in Micellar Solutions	12
	1.4.3. Electron Paramagnetic Resonance Studies of Colloidal Emulsions and Soap Films	13
1.5.	The Frequency of Exchange between Micelles and the Surrounding Solutions	14
1.6.	An EPR Investigation of the Monomer-Micelle Exchange Frequency	16
CHAPTER 2.	PREPARATION AND CHARACTERIZATION OF SOME NITROXIDE SURFACTANTS	19
2.1.	Preparation of 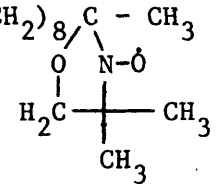	19
2.2.	Attempted Preparation of Paramagnetic Anionic Surfactants	20
2.3.	Preparation of Cationic Surfactants	22
	2.3.1. Preparation of $C_{12}TABN\dot{O}$	22
	2.3.2. Preparation of C_1, C_{10} and $C_{14}TABN\dot{O}$	24
2.4.	Characterization of the Cationic Surfactant Nitroxides	25
	2.4.1. Determination of the cmc from Surface Tension Measurements	25
	2.4.2. Determination of the cmc by a Conductivity Method	26
	2.4.3. Determination of the Number of Spins per Surfactant Molecule	27
CHAPTER 3.	EARLY EXPERIMENTAL WORK WITH $C_{12}TABN\dot{O}$	29
3.1.	Experimental Results	29
	3.1.1. Room Temperature Spectra	29
	3.1.2. Dilution of the Paramagnetic Surfactant with a Diamagnetic Analogue	31
	3.1.3. Temperature Dependence of $C_{12}TABN\dot{O}$ Spectra	32

CONTENTS (cont'd)

		PAGE
3.2.	Discussion	33
	3.2.1. Establishment of the Species Responsible for the Observed Spectra	33
	3.2.2. Determination of Exchange Frequencies and Activation Energies	34
CHAPTER 4.	FURTHER EXPERIMENTS WITH THE CATIONIC NITROXIDE SURFACTANTS	41
4.1.	Determination of the Energy of Activation of the Micellization Process for $C_{14}TABN\dot{O}$	41
4.2.	Experiments with $C_{10}TABN\dot{O}$	45
4.3.	Addition of Inorganic Salts to the Cationic Nitroxide Surfactant Systems	48
4.4.	Heisenberg Spin Exchange in the Cationic Nitroxide Systems	53
4.5.	Expected Arrhenius Plots and Linewidth vs. $^{T}/_{\eta}$ Graphs for a System Undergoing Two Rate Processes	55
CHAPTER 5.	THEORETICAL BASIS OF THE EXCHANGE EQUATIONS	59
5.1.	Equations for Monomer-Monomer Interactions	59
	5.1.1. Heisenberg Spin Exchange	59
	5.1.2. The Micellar Line	61
5.2.	Exchange between Monomeric and Micellar Sites	63
	5.2.1. Exchange Equations for the Central Line	64
	5.2.2. Exchange Equations for the Central Line - Method of Zimmerman & Brittin	67
	5.2.3. Exchange Equations for the Outer Lines	72
5.3.	The Effect of the Relative Numbers of Monomers and Micelles on the Observed Monomer Linewidth	73
CHAPTER 6.	DETERMINATION OF THE WIDTH OF THE PROTON HYPERFINE LINES	78
6.1.	NMR Measurements of Hyperfine Coupling Constants	78
	6.1.1. The Theory of the Determination of Small Hyperfine Coupling Constants by NMR	78
	6.1.2. The Pseudo-contact Interaction	80
	6.1.3. Determination of the Isotropic Proton Hyperfine Coupling Constants of the Paramagnetic Surfactants	81
6.2.	Computer Simulation of Nitroxide Spectra	85
	6.2.1. Description of the Program used to Computer-Simulate EPR Spectra	85
	6.2.2. Computer-Simulated Nitroxide Surfactant Spectra	85

CONTENTS (cont'd)

		PAGE
CHAPTER 7.	PRE-MICELLAR ASSOCIATION	95
7.1.	Introduction	95
7.2.	Measurements with $C_{12}TABN\dot{O}$	96
7.3.	Measurements with C_1 $TABN\dot{O}$	101
7.4.	Variable Temperature Measurements with $C_{10}TABN\dot{O}$	103
7.5.	An Attempted Detection of Pre-Micellar Association Using the Freezing Point Depression Method	105
7.6.	The Influence of Added Salt on the Pre-Micellar Association of $C_{10}TABN\dot{O}$	106
7.7.	Conclusions	107
CHAPTER 8.	CONCLUDING EXPERIMENTS WITH THE CATIONIC NITROXIDE SURFACTANTS	109
8.1.	Introduction	109
8.2.	De-oxygenation of the Surfactant Solutions	110
8.3.	Experiments with $C_{14}TABN\dot{O}$	111
8.4.	Experiments with $C_{12}TABN\dot{O}$	112
8.5.	Experiments with C_{10} $TABN\dot{O}$	117
8.6.	Conclusion	119
APPENDIX I.	SOIL REMOVAL STUDIES INVOLVING A PARAMAGNETIC SOIL	121
A-I.1.	Introduction	121
A-I.2.	The Paramagnetic Probe as a Component of Other Soils	122
A-I.3.	Dilute Paramagnetic Probe as the Only Soil Present	122
A-I.4.	Removal of Soils from Fabrics	123
	A-I.4.1. Removal of Soil Films	123
	A-I.4.2. Removal of Individual Soil Molecules	124
A-I.5.	Redeposition of (I) onto Nylon from SDS Solution	126
A-I.6.	Conclusions	126

CONTENTS (cont'd)

		PAGE
APPENDIX II.	A SIMULATED WASHING MACHINE EPR SAMPLE CELL	127
A-II.1.	Introduction	127
A-II.2.	Cell Description	127
A-II.3.	Discussion	128
A-II.4.	Conclusions	129
REFERENCES		130

CHAPTER 1

INTRODUCTION

1.1. Introduction

The bulk of the work described in this thesis concerns a novel application of the electron paramagnetic resonance (henceforth EPR) technique to the study of micellar systems. The background of this work lies in the diverse fields of magnetic resonance and colloid chemistry, and in previous uses of the former to investigate the latter. This chapter describes these various backgrounds, and introduces the problem arising from them which the remainder of the thesis describes in detail.

1.2. Electron Paramagnetic Resonance

1.2.1. The Basic Phenomenon

Isolated electrons possess a magnetic moment, the magnitude of which is $\frac{1}{2}g\beta$, where g is the Landé factor and β the Bohr magneton, and the sign of which may be either positive or negative in the presence of a magnetic field[1]. Most molecules contain an even number of electrons, which are paired in orbitals containing one electron of spin $+\frac{1}{2}$ and one electron of spin $-\frac{1}{2}$. The net electron magnetic moment of these molecules is zero. Some molecules, however, contain one or more unpaired electrons, each of which may have a magnetic moment of either $+\frac{1}{2}g\beta$ or $-\frac{1}{2}g\beta$. The net electron magnetic moment of these molecules may be either positive or negative in sign, and will have a magnitude which is an integral multiple of $\frac{1}{2}g\beta$.

An ensemble of molecules, each of which contains an integral number N of unpaired electrons, will contain molecules with N + 1 different net magnetic moments. In the presence of an external magnetic field, the

energies of these molecules will be given by[1]

$$\mathcal{H} = g\beta H_o S_z \tag{1.1}$$

where H_o is the strength of the external magnetic field, $-g\beta S_z$ is the net electron magnetic moment of the molecule concerned, and S_z, the component of the electron spin which is parallel to the magnetic field, may be any integral multiple of $\pm\frac{1}{2}$, up to and including $\pm N/2$. If a process exists which allows the transfer of energy and spin angular momentum from one molecule to another, then given enough time thermal equilibrium will be established between the molecules in the ensemble. When thermal equilibrium has been established, the number of spins in each of the N + 1 spin states will be governed by Boltzmann's law[1],

$$N_\alpha = N_o e^{-E_\alpha/kT} \tag{1.2}$$

where N_α is the number of spins in the αth spin state, N_o is the total number of spins in the ensemble, E_α is the energy of the αth spin state given by equation 1.1,k is Boltzmann's constant, and T is the temperature in K. This requires that at finite temperatures there will be a progressive excess of spins in the lower energy states.

For simplicity let us consider an ensemble of molecules, each of which contains one unpaired electron. If this ensemble is placed in a magnetic field, those molecules with an electron spin quantum number S_z of $+\frac{1}{2}$ will increase their energy as the magnetic field increases, while those molecules with $S_z = -\frac{1}{2}$ will simultaneously decrease their energy. This is shown schematically in Fig 1.1. At a given field strength H_o', the energy difference between the two states will be $g\beta H_o'$, as indicated in the figure. If thermal equilibrium is allowed to be established between the two spin states, then the number of spins N_α in the higher energy state will be related to the number of spins

FIG. I.I. ENERGY LEVELS OF AN ELECTRON IN A MAGNETIC FIELD

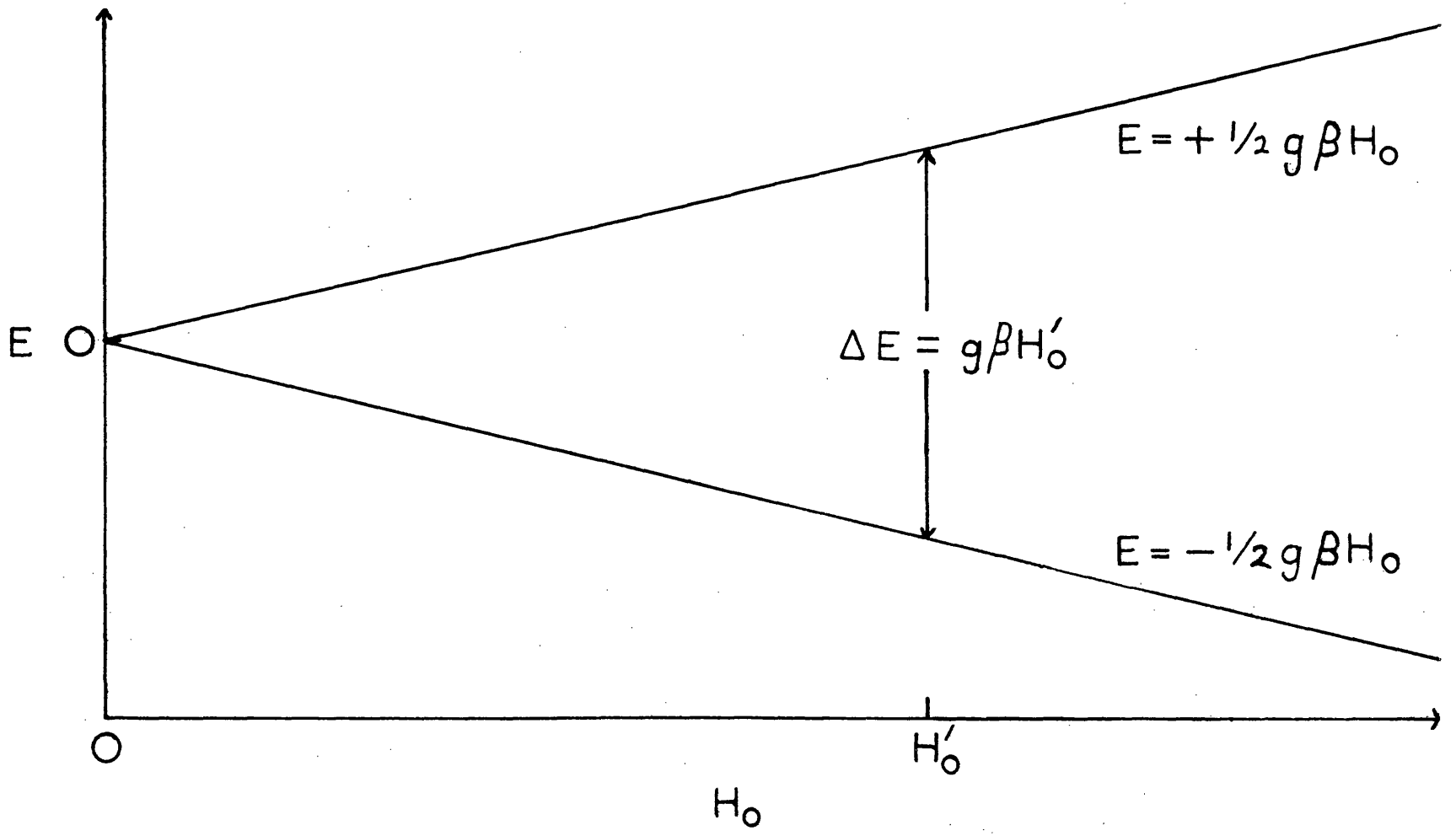

N_β in the lower energy state by

$$\frac{N_\alpha}{N_\beta} = \exp^{-g\beta H'_o / kT} \qquad (1.3)$$

(from equation 1.2). By supplying energy to the system at frequency ν so that

$$h\nu = g\beta H'_o$$

where h is Planck's constant, one can induce spins to transfer from one spin state to the other. Since the system at equilibrium has an excess of electrons in the lower energy state, there will be more induced transitions from the lower state to the upper than vice versa, with a resultant loss of energy from the incident radiation. It is this loss of energy from an applied microwave field which is amplified and recorded as the signal in a conventional EPR spectrometer.

The transfer of spins from one spin state to the other induced by the applied microwave field would soon equalize the number of spins in the two spin states, and thus halt the loss of energy from the applied microwave field, were it not for the presence of those relaxation processes which allowed the initial establishment of thermal equilibrium. These provide for the non-radiative transfer of energy from the spin system to the lattice, and thus allow the return of spins from the upper to the lower energy state. The characteristic time for relaxation through these processes is called T_1. In the experiments described in this thesis the applied microwave power was kept low enough so that the relaxation processes characterised by T_1 were able to maintain the thermal equilibrium number of spins in both the α and β spin states.

1.2.2. Hyperfine Structure

Unpaired electrons in molecules in solution interact isotropically with nuclei in these molecules if the nuclei have a magnetic moment and

if the orbitals of the unpaired electron and the nuclei overlap. The effect of this interaction on the EPR spectrum is called hyperfine structure. Equation 1.1 expanded to include hyperfine structure terms is

$$\mathcal{H} = g\beta H_o S_z + \sum_i a_i \underline{S}_i \underline{I}_i \qquad (1.5)$$

where $\underline{I}_i$ is the angular momentum vector in the ith nucleus and a_i, the hyperfine coupling constant, is a measure of the overlap of that nucleus and the unpaired electron. An energy level diagram which shows the effect of the hyperfine structure terms in the presence of a fixed magnetic field of strength H_o for a system containing one unpaired electron ($S_z = \frac{1}{2}$), one nitrogen nucleus ($I_z = 1$) and two protons (each with $I_z = \frac{1}{2}$) is shown in Fig 1.2. The dashed lines indicate the energy separations between the states, and the solid lines indicate some of the allowed EPR transitions ($\Delta m_s = \pm 1$, $\Delta m_I = 0$).

It can be seen that the hyperfine coupling with the nitrogen nucelus produces three lines of equal intensity, each of which is further split into three lines of relative intensity 1:2:1 by the two protons. The nitroxides studied in this work have similar spectra, except that there are either 16 or 18 protons instead of two as in the figure. Since a_N is about 15 Gauss and the a_H are less than 0.5 Gauss, the experimental spectra are triplets of equal intensity, which under certain experimental conditions show partially resolved proton hyperfine structure.

The nitrogen hyperfine coupling constants of nitroxides vary with the solvent, being larger in polar than in apolar media. This is due to the greater stabilisation by polar media of resonance form (I), which contains the unpaired electron on the nitrogen atom, over resonance form II,

FIG. 1·2. ENERGY LEVEL DIAGRAM FOR ONE ELECTRON, ONE NITROGEN NUCLEUS, AND TWO PROTONS

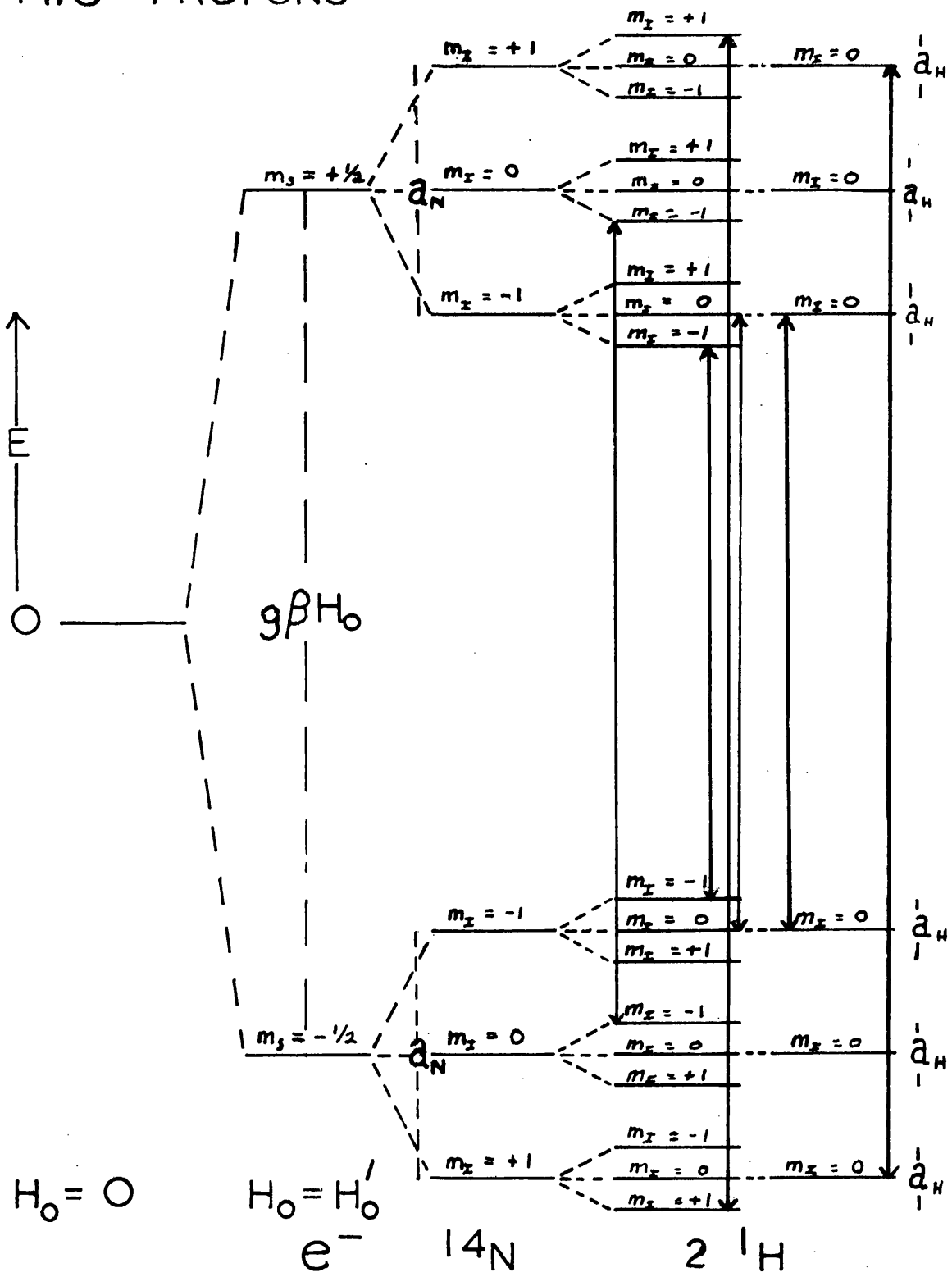

in which the unpaired electron is located on the oxygen atom. The Landé

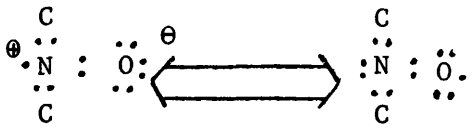

I II

g factor also changes with changes in the orbital occupied by the unpaired electron, and increases slightly as the solvent becomes more apolar. The resultant changes in a_N and g enable one to see separate spectra for a nitroxide in water and in a hydrocarbon solvent, as shown for di-tert-butylnitroxide in Fig 1.3[2]. The differences between the environments are greatest for the $m_I = -1$ peak. It is possible to determine the polarity of the nitroxide's environment from the measured a_N values, and this technique is generally used to determine the environment of spin-probes.

1.2.3. Rotational Mobility of Nitroxides

In addition to the isotropic interaction between unpaired electrons and nuclei mentioned in the previous section, an anisotropic interaction between the dipoles of the unpaired electron and any nucleus with a dipole moment also exists[3]. This interaction causes the energy levels of the system to vary as the orientation of the molecules comprising the systems is changed relative to the applied magnetic field. The Landé g factor is also anisotropic, leading to further changes in the energy levels of the system with changes in orientation[3]. For nitroxides, the resultant variation in line position with orientation is greater for the $m_I = -1$ line than for the $m_I = +1$ and $m_I = 0$ lines[4]. Molecular motion is much more rapid than the spread of possible line positions, measured in hz. Since this spread of line positions is greater for the

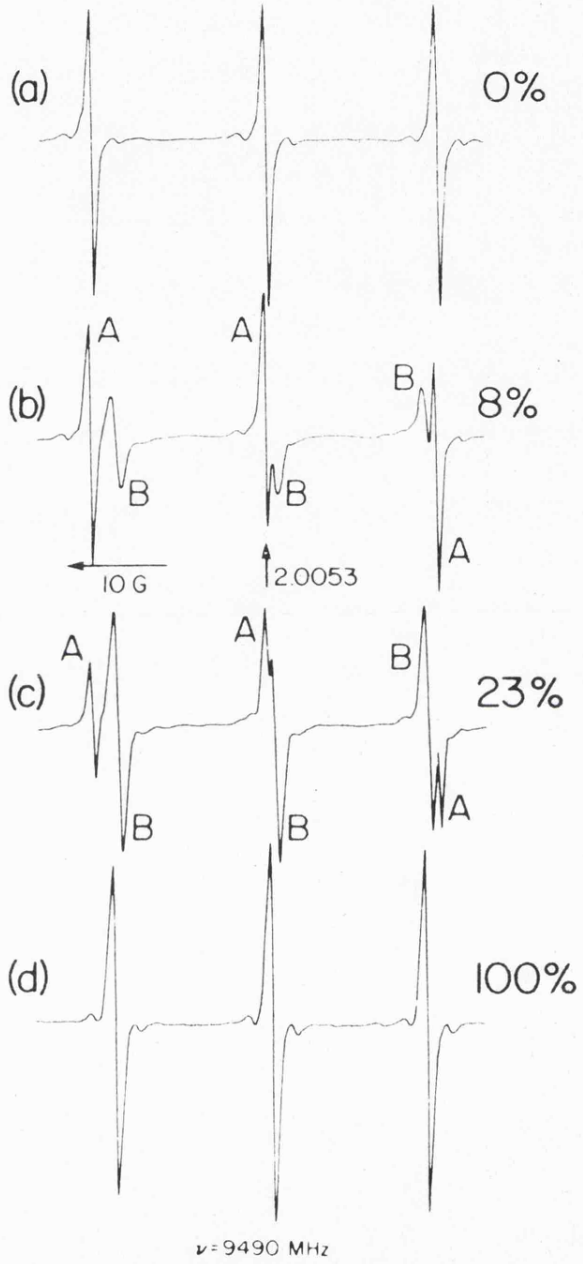

FIG.1.3. ESR spectra of DTBN in water (1a), lipostrate water emulsions (1b, c), and coconut oil (1d). The percentages indicated give the percent coconut oil by weight. The vertical arrow indicates $g = 2.0053$.

FROM REF. 2.

$m_I = -1$ line, for a given rotational correlation time τ_c the $m_I = -1$ line is often broader than the $m_I = 0$ and $m_I = +1$ lines, due to less complete averaging in the $m_I = -1$ case.

If one assumes isotropic molecular motion, no proton hyperfine structure, and almost axially symmetric g and dipole tensors, then the width of a nitroxide line with $m_I = M$, $\frac{2}{\sqrt{3}} \left[T_2(M)\right]^{-1}$, can be related to the rotational correlation time τ_c by[5]

$$\left[T_2(M)\right]^{-1} = \tau_c \left[\frac{1}{20} b^2 (3+7U) + \frac{1}{15}(\Delta\gamma H_o)^2 ({}^4/3 + U) + \frac{1}{8} b^2 M^2 (1-{}^U/5) + \frac{1}{5} b \Delta\gamma H_o M ({}^4/3+U) \right], \tag{1.6}$$

where $\Delta = {}^{\beta}/_{h} \left[g_z - {}^1/2\ (g_x + g_y) \right]$,

$b = {}^2/3 \left[A - {}^1/2\ (B + C) \right]$; $a_N = {}^1/3\ (A+B+C)$,

$U = \left[1 + \omega_o^2 \tau_c^2 \right]^{-1}$.

Here h is Planck's constant divided by 2π, ω_o is the Larmor frequency of the electron in the applied magnetic field H_o, and A, B, and C are the x,y, and z components of the dipole tensor. This type of analysis is used to estimate the rotational correlation times of nitroxide spin probes in various environments.

1.2.4. Exchange Phenomena

Some free radicals are capable of existing under different conditions in states or sites which give different EPR spectra. An example of this would be the nitroxide partitioned between water and oil environments shown in Fig 1.3.[2], in which the nitroxide gives a separate spectrum in each environment. If the individual nitroxide molecule spends a time much greater than the inverse of the separation (in hertz)

between the two sites in one or another of the sites, both of the sites will be observed. However, if the time spent by a nitroxide molecule in a site is much less than the inverse of the separation of the two sites, only one averaged spectrum will be observed. Thus the frequency with which a paramagnetic molecule exchanges between two environments can greatly affect the observed EPR spectrum.

The effect of increasing the electron spin exchange frequency P for the case of two equally populated sites is shown in Fig 1.4.[6] When P is small compared with the frequency separations the measured linewidth T_2^{-1} is related to the linewidth in the absence of exchange T_{2_o} by [6]

$$1/T_2 = 1/T_{2_o} + P, \qquad (1.7)$$

while if P is much greater than the separation of the initial frequencies $(\omega_A - \omega_B)$ the linewidth obeys the relationship[6]

$$\frac{1}{T_2} = \frac{f_A}{T_{2_oA}} + \frac{f_B}{T_{2_oB}} + \frac{f_A f_B (\omega_A - \omega_B)^2}{P_{AB} P_{BA}} \qquad (1.8)$$

where f_A and f_B are the fractions of spins in the A and B sites in the absence of exchange. In these two cases the exchange frequencies can be obtained from the measured linewidth if the linewidths in the absence of exchange and, in the fast exchange case, the fractional populations and frequency separations of the two sites are known. The application of this technique to the measurement of the monomer-micelle exchange frequency will be described in a later section.

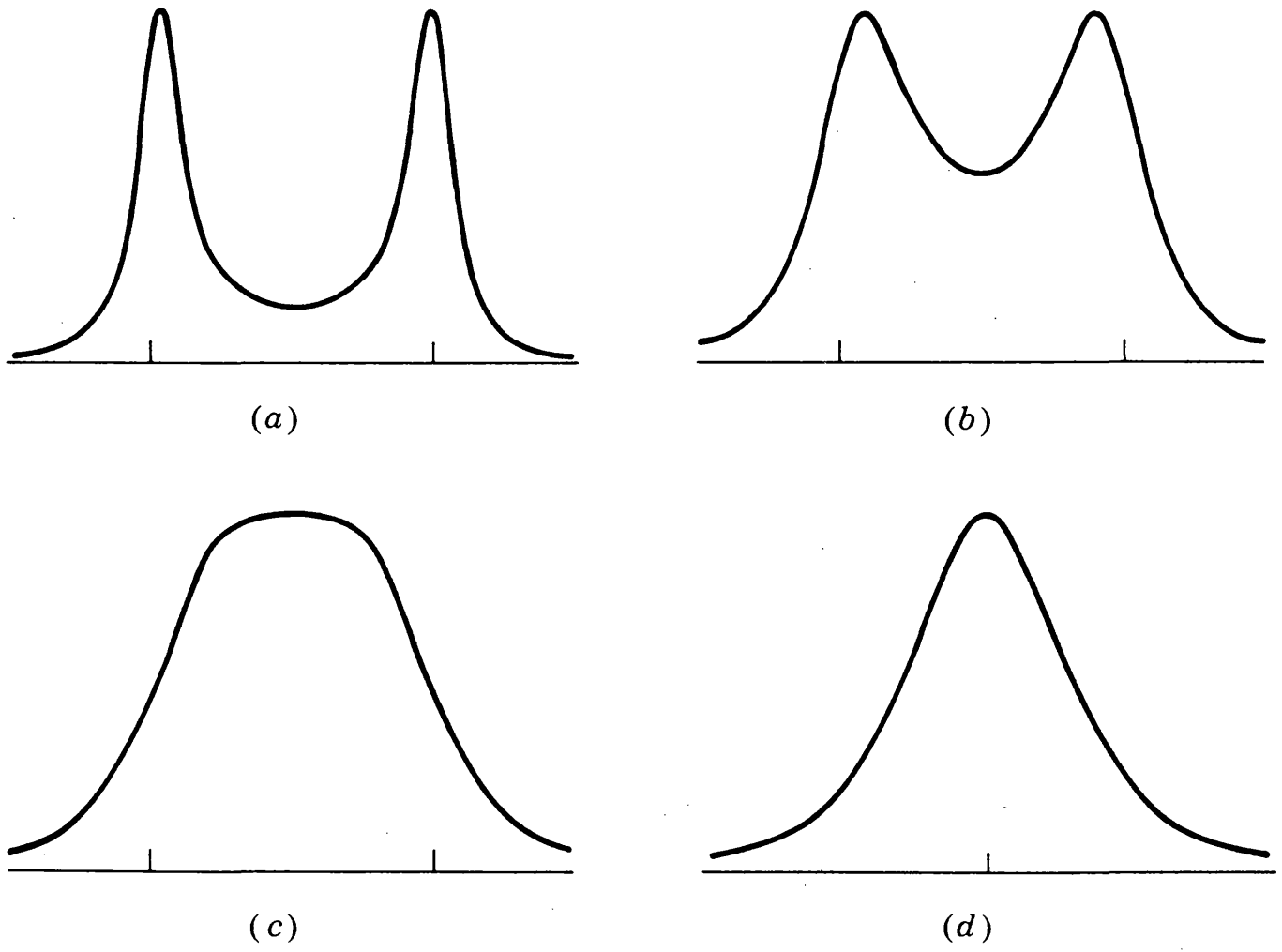

FIG. **1. 4.** Line shapes for a jumping spin. The ratio of the jumping rate P to the line splitting $(\omega_A - \omega_B)$ takes the values: (a) 1/10; (b) 1 5; (c) 1 2$\sqrt{2}$; (d) 1/2. The scale is adjusted so that each spectrum has the same maximum height. **From Ref. 6.**

1.3. The Micellization of Surfactants

Surface active agents which micellize contain both an apolar part, such as a hydrocarbon chain, and a polar part, such as an anionic or cationic headgroup or a headgroup consisting of several ethylene oxide units. Aqueous solutions of these compounds exhibit discontinuities in their conductance, surface tension, light scattering, and dye solubilization properties as the total surfactant concentration is increased through a region known as the critical micelle concentration, or c.m.c.[7]. These discontinuities can best be explained by the formation of surfactant aggregates, called micelles, at concentrations greater than or equal to the c.m.c. At surfactant concentrations up to several times the c.m.c., the micelle is generally spherical in shape, with the apolar parts of the surfactant molecules clustered together in the center of the micelle, and the polar parts of the surfactant molecules dissolved in the surrounding-water. This model of a micelle, developed by Hartley, is shown schematically for a cationic micelle in Fig 1.5.[7]

The major driving force for the micellization process is not thought to be the decreased enthalpy caused by the release of structured water about the hydrocarbon chains of monomers when these monomers enter a micelle. This increase in hydrogen-bonding is compensated for,at least in ionic micelles, by the increase in enthalpy caused by repulsion of the ionic micellar head groups, with the result that the measured changes of enthalpy upon micellization are small, and may be either positive or negative, depending on the surfactant and the temperature[8]. The major driving force for micellization is the increase in the entropy of both the hydrocarbon chains and the water molecules upon micellization[8]. The entropy of the hydrocarbon chains is greater

FIG. 1·5. A CATIONIC HARTLEY MICELLE

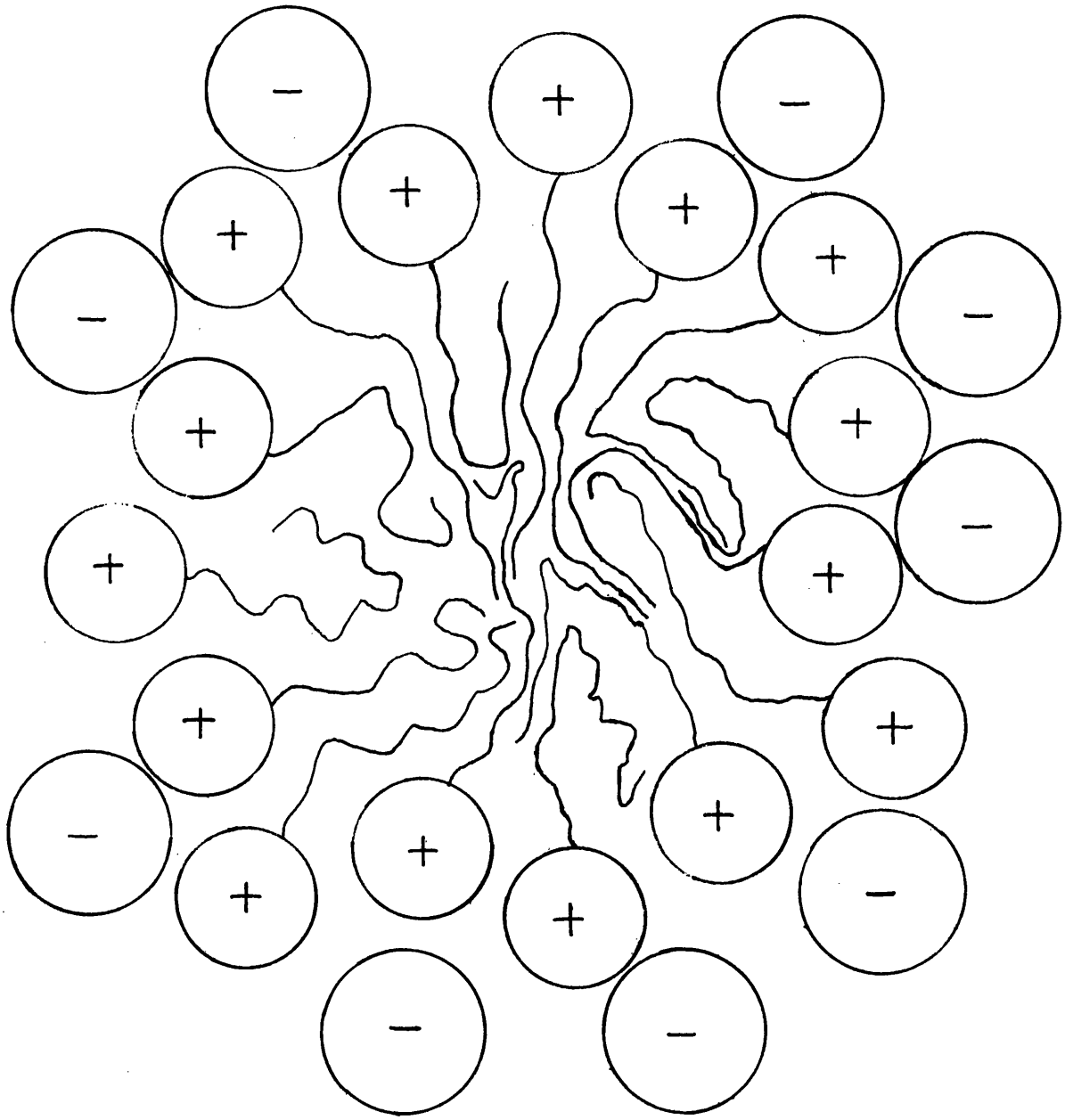

in a micellar environment because of their greater flexibility, while the release of the structured water about the former monomers increases the entropy of the aqueous phase as well. The decrease in the c.m.c. with increasing hydrocarbon chain length[7] qualitatively reflects these principles[8], being caused mainly by the increased entropy of the longer hydrocarbon chain in the micelle and the increase in both entropy and hydrogen bonding of the larger amount of structured water. Attempts at explaining micellar formations more quantitatively constitute much of the recent theoretical work in this field[8].

1.4. Previous Applications of EPR to Colloid Chemistry

The electron paramagnetic resonance (EPR) technique had been used in only a small number of investigations of micellar systems before 1971. The investigations were of two basic types, one using nitroxide molecules to probe the interior and/or double layer of micelles in which they were solubilized, the other studying the behaviour of paramagnetic counter-ions. A few applications of EPR to colloidal emulsions and to soap films had also been reported. A brief review of these investigations is given below.

1.4.1. Nitroxide Probes in Micellar Solutions

Nitroxide probes have been used to give information about the polarity of their environment (derived from the magnitude of the nitrogen hyperfine splitting constant a_n) and about the viscosity of this environment (determined from the totational correlation time τ_c of the nitroxide group, which is calculated from the relative widths of the three nitrogen hyperfine lines). A S Waggoner, O H Griffith, and C R Christensen[9] solubilised probes I and II (see Figure 1.6) in

FIG. 1.6. STRUCTURES OF NITROXIDE PROBES USED IN MICELLAR SYSTEMS

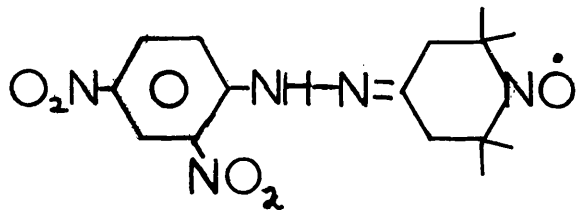

I

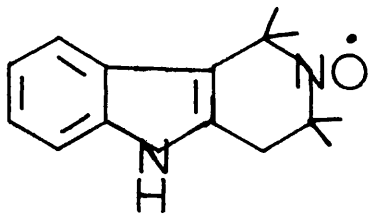

II

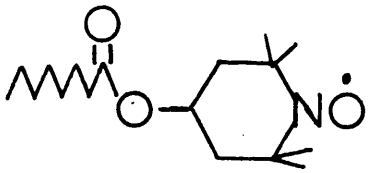

III

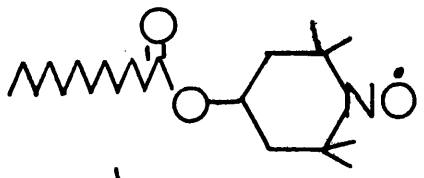

IV

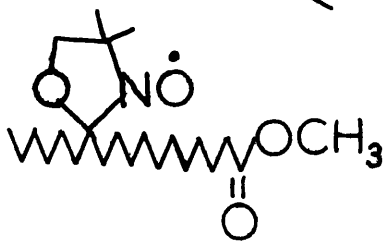

V

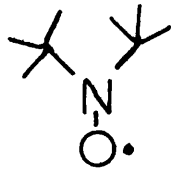

VI

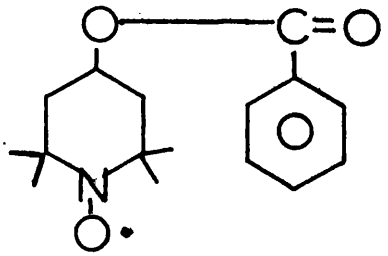

VII

FIG. 1.6. (CONT.)

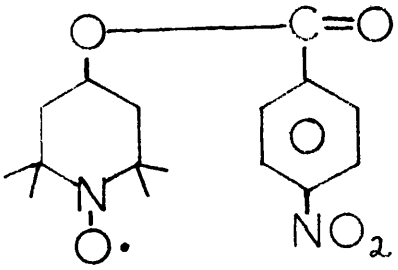

VIII

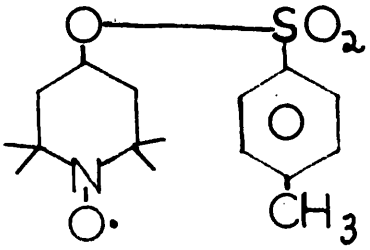

IX

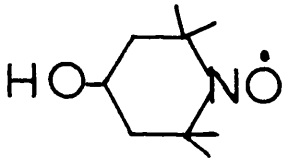

X

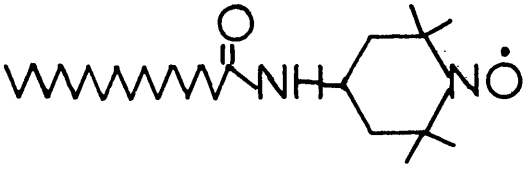

XI

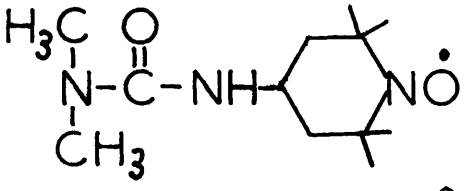

XII

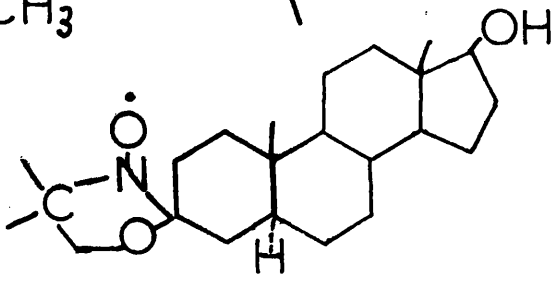

XIII

XIV

solutions of sodium dodecyl sulphate (henceforth SDS). The proton nuclear magnetic resonance spectrum of an SDS solution considerably above the critical micelle concentration (henceforth c.m.c.) was broadened when probes I and II were present, indicating that the probes were associating with the micelles. The magnitudes of the nitrogen hyperfine coupling constants a_n of the probes in SDS solution above the c.m.c. were intermediate in value between the a_n values of the same probes dissolved in aqueous and hydrocarbon media (see Table 1.1), thus indicating that the probes were in an environment of intermediate polarity.

TABLE 1.1

PROBE (see Fig I.6.)	a_n Value in Gauss in		
	Water	Dodecane	SDS (5%)
I	16.16	14.30	15.72
II	16.97	15.15	16.60
III	16.80	15.20	16.40
IV	-	15.20	16.20

The rotational correlation times τ_c of the probes were found to increase sharply at the c.m.c. (see Fig 1.7.), indicating that the micellar environment was slightly more viscous than the aqueous one. A Stokes law calculation eliminated the possibility that the probe was held rigidly in a solid micelle, since the correlation time expected for the probe in this case is almost two orders of magnitude lower than the observed corelation time[10].

The model of a relatively fluid micelle, with a viscosity about an order of magnitude greater than the viscosity of water, and an environment intermediate in polarity between aqueous and hydrocarbon media,

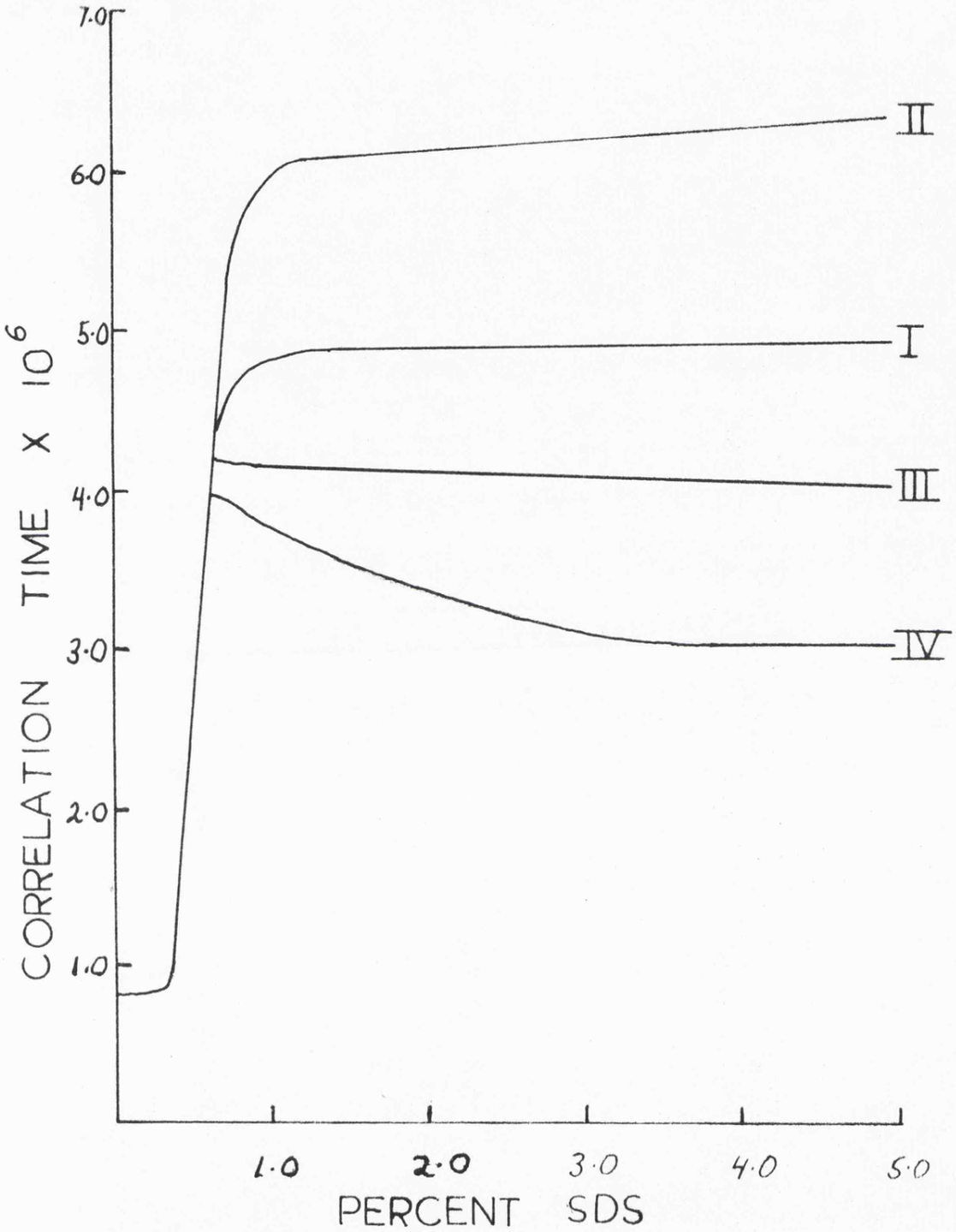

Fig.1.7. Plot of the rotational correlation time of nitroxides I-IV (see Fig 1.6.) in aqueous solution at 23°C vs. weight per cent sodium dodecyl sulphate. Data from Ref.10.

was further substantiated with probes III[10], IV[10], and V[11] (see Fig 1.6). A review of this work has been published by two of the authors[4]. The model was further substantiated by Rabold[12], using probes VI-IX, who showed in addition that the presence of either hexane or lauryl alcohol increased the viscosity of the probe's environment. Since the a_n value of the probe did not become smaller as hexane was added to the SDS system, it was postulated that the probe was localized near the surface of the micelle, which became more ordered as the micellar core was swollen with hexane. Rabold also suggested that the probe molecules were partitioned between the micellar environment and the "aqueous serum", and that the observed τ_c was a weighed average of the correlation times in the two environments. This would require that the exchange of the probe between the two environments be rapid on the EPR timescale, i.e. greater than about 10^9 sec^{-1}.

Goldfield et al[13] used probes III and X-XII to investigate micellar solutions of SDS and Tween 80 (a non-ionic detergent, sorbitanmono-oleate polyethyleneglycol -(10) ether). The dynamic nature of the micelle was again substantiated, especially in the region where only spherical micelles were present. At very high Tween concentrations, competition between the Tween and the nitroxide probes for water molecules was observed. Only Povich et al[14] and Lee et al[15] dissented from the concensus, showing that probe XIII was in a rigid hydrocarbon-like environment in SDS and hexadecyltrimethyl ammonium bromide micelles[14] and in micelles of cardiolipid[15]. In all of the studies mentioned above the nitroxide probe concentrations were kept very low (much less than one probe per micelle) to avoid complications caused by probe-probe interactions.

Ohnishi et al[16] studied the solubilization of the nitroxide biradical XIV (see Fig 1.6) in SDS micelles. The biradical was found to partition between the aqueous and micellar environments, with the exchange between the two environments being less than 10^7 sec^{-1}, the difference in J, the exchange interaction between the two inpaired electrons, and a_n for the biradical. The motion of the biradical within the micelle was relatively rapid, again indicating a fluid micellar interior. If biradicals in excess of one probe per micelle were present, the biradicals aggregated within the micelles, producing EPR spectra consisting of one broad line, caused by biradical-biradical interactions.

From the above a general picture of a micelle as having a fluid interior arises, except as experienced by the bulky, hydrocarbons probe XIII. The environment presented to most probes was intermediate between aqueous and apolar, probe XIII again being exceptional in that its environment was similar to a frozen hydrocarbon matrix. Only on the question of the rate of probe exchange between aqueous and micellar environments was there no concensus.

1.4.2. Paramagnetic Counter-Ions in Micellar Solutions

Rotational correlation times can be determined from the linewidths of paramagnetic ions. Hasegawa, et al[17,18] measured the linewidths of Mn^{++} ions in the presence of increasing amounts of SDS. The results are shown in Figure 1.8. The increase in τ_c in the presence of SDS micelles was interpreted as being caused by the formation of an outer sphere complex between the Mn^{++} counterion and the micelle. Sodium decyl sulphate micelles were also studied[18], and found to bind Mn^{++} less tightly than SDS micelles. Added paramagnetic and diamagnetic salts

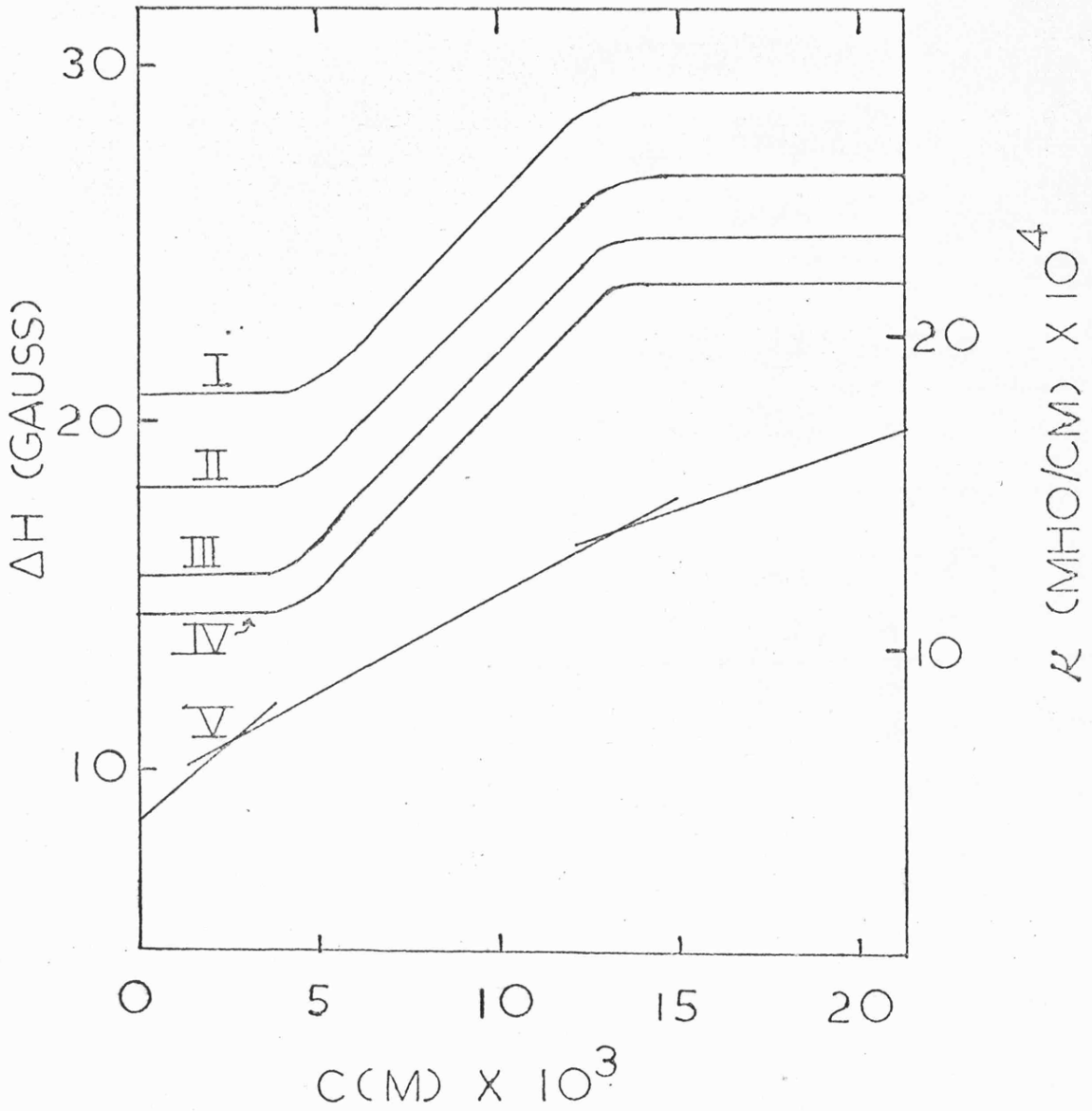

Fig.1.8. The dependences of the line width and specific conductivity (V) on the concentration of SDS at 50°C.

I = $M_I = -5/2$ III = $M_I = -1/2$

II = $M_I = -3/2$ IV = $M_I = +1/2$

Data from Ref.16.

slightly decreased the binding of Mn^{++} to the micelle, with the partial neutralization of the micellar surface charge by the added salt suggested as a reason for the effect.

Zaev[19] has compared the EPR of Cu (dodecyl-sulphate)$_2$ with the EPR of other Cu^{++} salts. The results are shown in Fig.1.9. At the c.m.c. the exchange narrowed resonance due to concentrated Cu^{++} ions in solution narrowed still further, because of increased Cu^{++} concentration at the micellar surface. Comparison with the spectra of other Cu^{++} salts showed that the counterion concentration at the micellar surface was equivalent to 0.5 to 1.0 M Cu^{++} in solution. The above results show that the EPR of paramagnetic ions can be used to give information about the strength and nature of counter-ion binding, and about the number of counter-ions bound to the micellar surface.

1.4.3. Electron Paramagnetic Resonance Studies of Colloidal Emulsions and Soap Films

Nitroxide free radicals have been used to probe colloidal emulsions and soap films. Bales and Baur[2] used probe VI (see Fig 1.6) to study coconut oil/water emulsions. The probe was found to partition between the two phases, separate high and low field EPR lines being obtained for each phase. The partion coefficient varied with temperature. Barratt et al[20] and Rottschaefer[21] investigated phospholipid vesicles, using probes I[20] and V[21]. The addition of cholesterol was found to decrease the motion of both probes. The motion of probe I[20] increased as the water content of the system increased up to about 25% water in the system. These studies indicated that spin probes could give information concerning correlation times in biological systems.

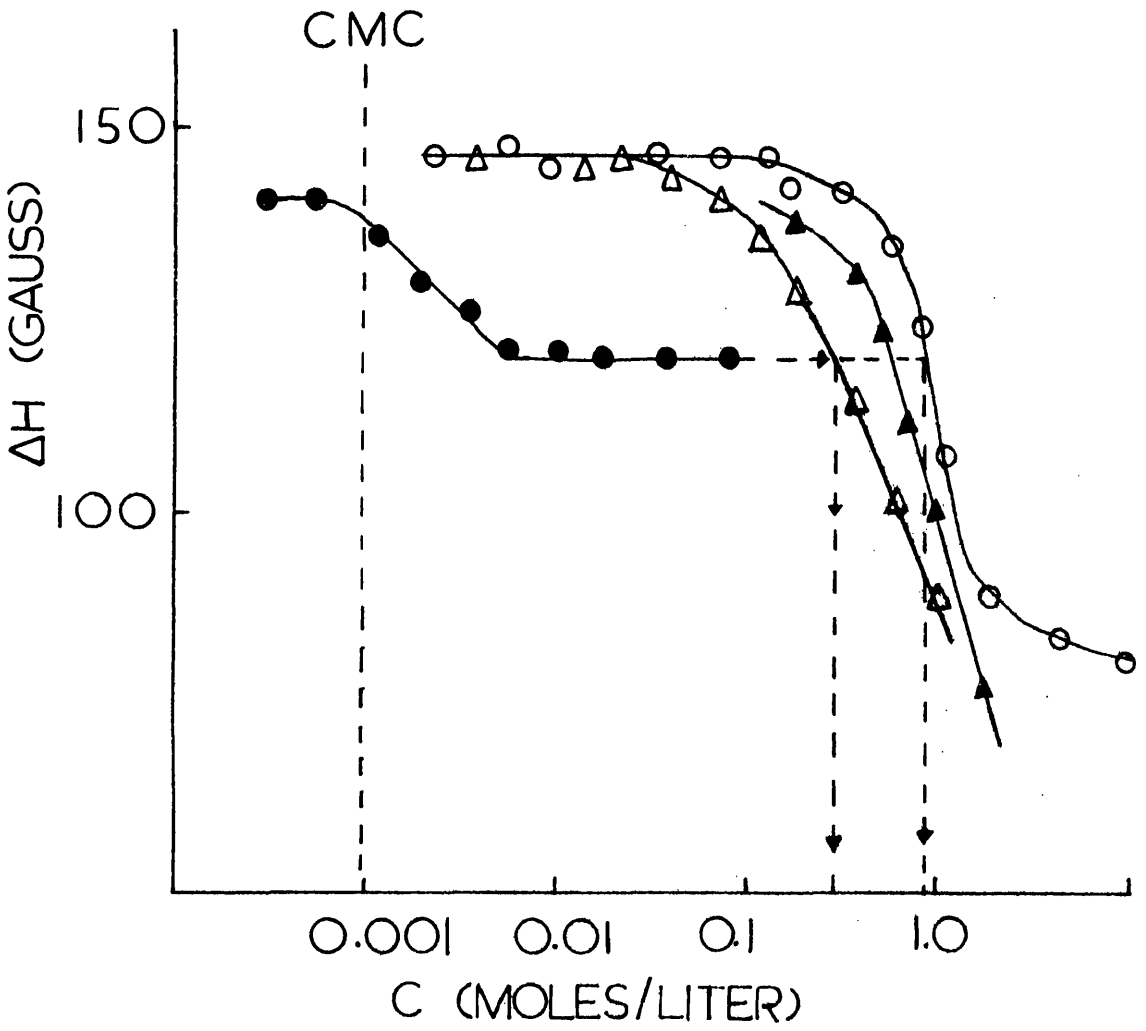

Fig.1.9. EPR line width as a function of concentration (c, moles/litre) in micellar $Cu(DS)_2$ and in homogeneous solutions of cupric salts.

○ $CuNO_3$ △ $CuSO_4$
● $Cu(DS)_2$ ▲ $Cu(ClO_4)_2$

Data from Ref. 18 .

Probe X has been used to study black (50-300Å thick) and silver (500-1200Å thick) soap films[23]. The probe showed a low correlation time in both films indicating that it was in a fluid environment. In the black film, the nitroxide lines were sharper than in the silver film or in bulk solution. Since the lines in the bulk solution and in the silver film were exchange broadened, this result indicated that the frequency with which one probe collided with another was reduced in the black film, although the tumbling rate of the probes was not reduced. Adsorbing the thin film on a quartz rod increased the correlation time of the probe, while the reduced collision frequency was maintained.

A few studies of paramagnetic colloidal systems have been reported[23-25]. King,et al[23] observed the EPR of metallic sodium electrons from the colloidal sodium in irradiated sodium azide. Smith, et al[24,25] studied the paramagnetic resonance of suspensions of $Cu[OP(C_6H_5)_3]_4(ClO_4)_2$ and $Cu[OAs(C_6H_5)_3]_4(ClO_4)_2$ in nitroethane. They were able to determine the mass of the small crystaline particles, and thus the molecular weight of the colloids, from the field dependence of the magnetization process. From the above, one can see that EPR can be used to determine molecular weights and collision frequencies as well as correlation times, environmental polarities, and the nature of the paramagnetic species.

1.5. The Frequency of Exchange Between Micelles and the Surrounding Solution

In the review of studies of nitroxide probes in micellar solutions (see 1.4.1. above) the lack of concensus concerning the frequency with which the probes exchanged between the micellar and aqueous environments was noted. Other experimental techniques designed to measure the frequency with which probes (such as dye molecules) exchanged between micellar and aqueous environments, or the related frequency with which

surfactant molecules exchanged between micellar and aqueous environments, also produced widely divergent results.

Nash[26], in a study of cetyltrimethylammonium salts, found that times on the order of tens of hours were needed for a micellar solution to reach a new equilibrium after having been diluted. Peper and Taylor[27] obtained comparable results with iso-nonyloctadecyl-dimethylammonium nitrate and bromide solutions, but found rapid equilibration with the chloride. Using a temperature-jump technique, Kresheck et al[28] found the dissociation rate of dodecylpyridinium iodide micelles to be 50 sec^{-1} at room temperature. Bennion et al[29,30] using a light-scattering temperature jump method, found dissociation rate constants ranging from 4 sec^{-1} at 35°C for dodecylammonium chloride and 17 sec^{-1} at 45°C for sodium dodecyl sulphonate up to 120 sec^{-1} at 35°C for dodecylpyridinium iodide.

Jaycock and Ottewill[31] measured the dissociation of several anionic and cationic surfactant micelles upon dilution, using a stopped flow conductance apparatus. Most of the dissociation was found to occur within the induction time of their apparatus. An upper limit of 10 milliseconds for the half-life of the dissociation was found. Mijnlieff and Ditmarsch[32], using a pressure jump technique, found a half-life for the dissociation of SDS micelles of 1×10^{-5} sec. Nuclear Magnetic Resonance spectra of ω-phenylalkyltrimethylammonium bromides[33] and of sodium 10, 10, 10-triflurocaprate[34] contained peaks which shifted from one position to approach a limiting value as surfactant concentration was increased above the c.m.c. The shift was interpreted to result from the spectrum being a weighed average of the spectra due to monomeric and micellar surfactant. This requires

that the exchange frequency between the two states be fast on the NMR timescale - i.e. greater than 10^4 exchanges per second. Muller and Birkhahn[34]'s work with the fluorocarbon surfactant indicated that the environment experienced by the ω-CF_3 group in the micelle was intermediate in polarity between aqueous and hydrocarbon media. Ultrasonic absorption measurements[35] of alkanoates of various short chain lengths and with different counterions indicated that the absorptions observed between 0.1 and 50 Mhz were probably due to surfactants exchanging between a micellar and an aqueous environment, rather than to counterions exchanging between free and bound environments. Development of a kinetic model from the ultrasonic absorption data was difficult,[36] with a preliminary treatment indicating that micelles might be poly-disperse.

The data presented above suggest that a method which would measure exchange frequencies which are higher than the frequencies measured by NMR and which would inherently indicate the species responsible for the exchange might help resolve the problem. Since EPR is capable of measuring exchange frequencies in this range[6] (from $\sim 10^5$ to $\sim 10^9$ exchanges per second), an EPR experiment was designed to investigate the monomer-micelle exchange frequency problem. This experiment is described below.

1.6. An EPR Investigation of the Monomer-Micelle Exchange Frequency

EPR will measure the frequency with which a paramagnetic molecule exchanges from one site to another if the sites are magnetically different. A paramagnetic surfactant dissolved in water in concentrations above its c.m.c. will exist in two magnetic environments - the micellar environment being dominated by rapid electron spin exchange between the paramagnetic surfactant molecules which constitute the micelle, the monomer environment being that of a single electron spin

in an aqueous environment. If the paramagnetic surfactant is a nitroxide, the expected micellar signal will consist of one exchange narrowed line, while the monomer signal will consist of the three sharp lines characteristic of a nitroxide tumbling rapidly in an aqueous medium. If the exchange of a nitroxide surfactant monomer between the aqueous and the micellar environments is slow on the EPR timescale, the observed spectrum will be a superposition of the broad micellar line and the three sharp monomer lines. If the exchange is fast, the observed spectrum will be a weighed average of the spectra expected from the monomeric and from the micellar sites. If the exchange is intermediate, the exchange frequency can be determined from the widths of the EPR lines.

The experiment proposed above differs from the experiments described in Section 1.4.1. in one important aspect. The use of a nitroxide surfactant analogue as the only surfactant present in the system ensures that the micellar environment, in which the signal from a given nitroxide is altered radically by the close proximity of the other nitroxide molecules which constitute the micelle, is distinctly different from the monomer environment. In contrast, the use of a low concentration of a nitroxide as a probe in a micellar system leads to very similar magnetic environments in the monomeric and micellar sites, as both sites contain isolated spins with slightly different a_n and g values. Resolution of the spectra from the two sites would be difficult, due to the proximity of the signals, if the frequency of probe exchange between monomeric and micellar environments were slow on the EPR timescale. The proposed experiment with the paramagnetic surfactant avoids this difficulty.

Two types of nitroxides which had been used as spin probes but which should micellize and therefore be possible paramagnetic surfactants were known. One of these was the sodium salt of the acid formed by hydrolysis of Probe V[11] (see Fig.1.6), a soap (anionic surfactant) analogue. The other, a cationic surfactant analogue[37], has the general formula

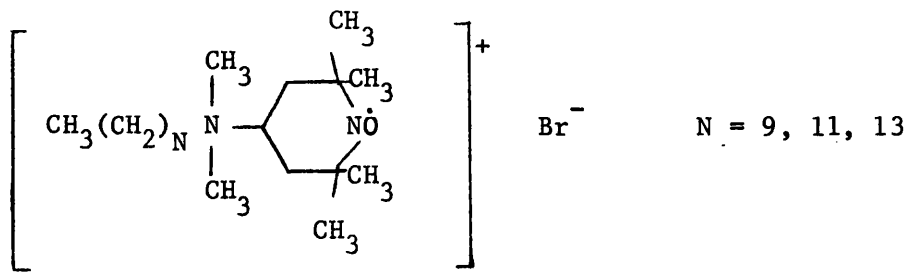

Br^- N = 9, 11, 13

The preparation and characterization of these paramagnetic surfactants is described below.

CHAPTER 2

PREPARATION AND CHARACTERISATION OF SOME NITROXIDE SURFACTANTS

2.1. Preparation of $CH_3(CH_2)_8$

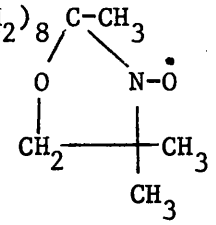

The nitroxide $CH_3(CH_2)_8$

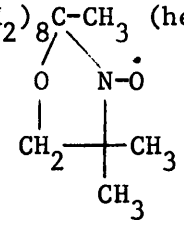

(henceforth I) was prepared in order to see

if the nitroxide moiety was polar enough to serve as a surfactant headgroup. The preparation, adapted from the preparation of

$CH_3(CH_2)_5$

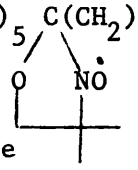

$C(CH_2)_{10}$ $COCH_3$ (=O) by Waggoner, et al[11], followed the reaction sequence

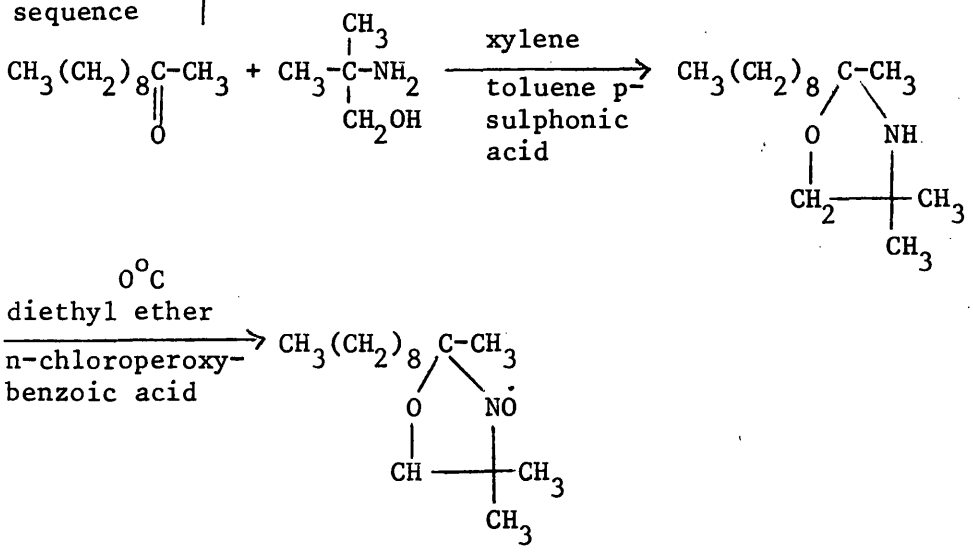

The reflux time of the first step was shortened from ten days to six hours, after which the oxazolidine product was isolated by distillation under vacuum. The nitroxide produced from the oxazolidine was not purified by chromatographic means as in reference 11, but was used directly. All other experimental conditions were as described in reference 11.

The nitroxide I was an orange oil, which did not dissolve in water to an extent great enough for micelles to be formed. Since the nitroxide moiety was not polar enough to serve as a surfactant headgroup, it seemed necessary to incorporate a nitroxide-containing group into a molecule which was itself a surfactant in order to obtain a paramagnetic surfactant molecule.

2.2. Attempted Preparation of Paramagnetic Anionic Surfactants

The sodium salt of the acid formed by hydrolysis of the methyl stearate nitroxide II, whose preparation is described in

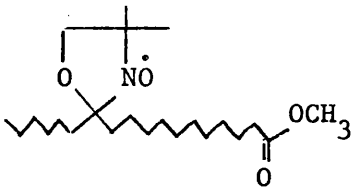

II

reference 11, should be a surfactant. It was decided to prepare this sodium salt, which will henceforth be referred to as sodium stearate nitroxide, and also the sodium salt of the acid formed by hydrolysis of the shorter chain length compound III, henceforth sodium laurate nitroxide.

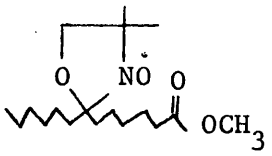

III

Preparation of II was as described by Waggoner, et al[11]. Nitroxide III was prepared from $CH_3(CH_2)_5\underset{\underset{O}{\|}}{C}(CH_2)_5\underset{\underset{O}{\|}}{C}OCH_3$, which was synthesized by Palmer Laboratories, Flintshire. The procedure followed for III was analogous to that for II. In each case about 2 g of product was obtained from about 15 g of ketone precursor.

Hydrolysis of both II and III was attempted, using an 0.05M solution of NaOH in methanol as described in Waggoner, et al[11] as the first step towards the preparation of the acid of II. After three days standing at 40°C, the methanol was removed by evaporation, leaving a dry, yellowish solid. Attempted re-crystallization of this material from a minimal amount of water did not succeed. The aqueous solution was then extracted with ether, and an orange water-insoluble oil representing about 25% of the starting material was recovered from the ether phase. Further recrystallization of the remaining material from water produced a white diamagnetic powder, which was probably Na_2CO_3 (produced from reaction of the NaOH with CO_2 obtained from the surrounding air). After repeated re-crystallizations had exhausted the system's supply of Na_2CO_3, recrystallization of the sodium salts from an 80/20 ethanol/water mixture was attempted. This recrystallization also failed. Evaporation of the solvent produced an orange oil in the case of sodium stearate nitroxide and a sticky orange solid in the case of sodium laurate nitroxide. It was postulated that the presence of the bulky nitroxide containing five-membered ring made it difficult for these sodium salts to fit into the sodium stearate or sodium laurate crystal structures.

Another recrystallization of sodium laurate nitroxide was attempted, this time from ethanol alone. This also failed, and evaporation of the solvent yielded a small amount of a sticky, orange, water soluble paramagnetic material. The EPR spectrum of an aqueous solution of this material indicated that a nitroxide surfactant had been formed, with the more concentrated solutions exhibiting a broad central line, characteristic of exchange-narrowing resonance produced by molecules associated in a micelle. However,

the signal intensity of the solutions decreased with time, with a half life of the order of a few weeks. Because of this intensity decrease and because not enough of the compound had been obtained to measure its surface chemical properties, further work with the anionic surfactants was abandoned.

2.3. Preparation of Cationic Surfactants

Cationic surfactants of the general structure IV were synthesized according to

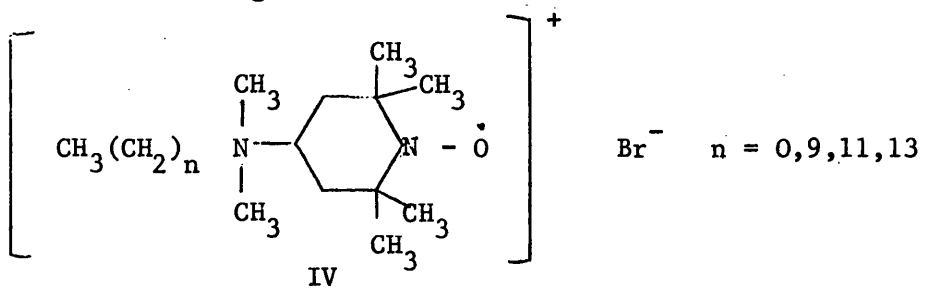

a procedure kindly supplied by Dr Wayne L Hubbell of Stanford University[37]. The reaction sequence is:

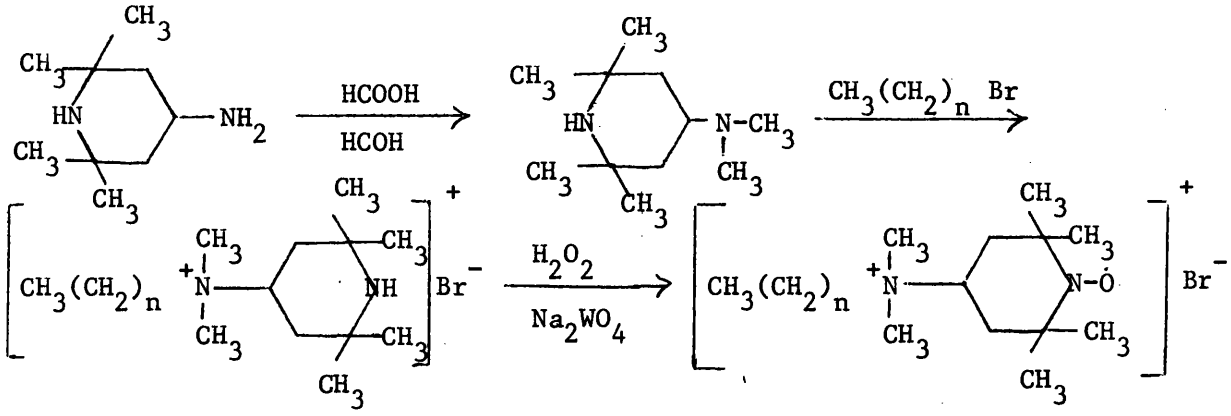

The details of the preparation for the n = 11 compound (henceforth C_{12}TABNȮ) are given below, followed by any changes in the procedure needed for the n = 0, n = 9, and n = 13 compounds (henceforth C_1TABNȮ, C_{10}TABNȮ, and C_{14}TABNȮ respectively).

2.3.1. Preparation of C_{12}TABNȮ

Ten grams of 4-amino-2, 2, 6, 6-tetramethylpiperidine (available from Aldrich Chemical Co) were added with cooling and rapid stirring

to 15.2 g of 98% formic acid solution. After addition was complete, 11.4 g of 37% aqueous solution of formaldehyde was added. The solution was heated on a steam bath under reflux for 10 hours, then cooled. Concentrated hydrochloric acid (7.3 g) was added, and the formic acid and any excess formaldehyde were evaporated under reduced pressure. The yellow residue (Hubbell's was reddish-brown) was dissolved in water and the solution was made strongly alkaline by the addition of solid sodium hydroxide. The solution separated into two layers; the yellow upper layer was collected, dried over barium oxide and distilled under reduced pressure. The clear distillate was used in the next step without further purification, as the NMR spectrum indicated that N, N-dimethyl-4-amino-2, 2, 6, 6-tetramethylpiperidine had been obtained. The yield was 3.84 g.

The 3.84 g of the dimethyl amine obtained above were mixed with 6.0 g of 1-bromododecane and heated in the dark to 60°C for 15 hours. The clear product was then stirred rapidly and cooled to 40°C, at which point white crystals began to precipitate from solution. The yield was increased by leaving the solution at 40°C for 4 hours. At the end of this time, diethyl ether was added, and the white crystals were collected by filtration and washed exhaustively with diethyl ether. Alternatively, the mixture of dimethyl amine and 1-bromododecane was heated in the dark at 40°C for 15 hours. The resulting white mass was titurated with diethyl ether, and the crystals formed were collected and washed as above. The yield was increased by removing the ether from the filtrate and repeating the reaction. The yield from the first procedure was about 2 g. The compound obtained above was dissolved in 75 ml of water containing 0.5 g of sodium tungstate and 0.5 g of disodium

EDTA. Then 10 ml of 30% hydrogen peroxide were added, and the reaction was allowed to stand for 12 hours. At this stage the solution was basic, with a pH of about 9. The water was then removed under reduced pressure, and the sticky, orange residue was dissolved in excess hot benzene and filtered. The benzene was removed from the filtrate under reduced pressure, leaving an orange solid.

If the product is still sticky at this stage, it should be re-dissolved in benzene, and the process repeated. This solid was then recrystallized from hot benzene. The crystalline material was dissolved in the minimum amount of water and chromatographed on 50 g of AG 2- x 8 anion exchange resin in the bromide form (Bio-Rad Laboratories), eluting with distilled water. The water was then removed by freeze-drying. At this stage, Hubbell suggests a final recrystallisation from hot water. However, the yield in this case was so small (~1 g) that this could not be performed. Instead, the compound was extracted for two weeks with 30°-40°C petroleum ether, and stored in a vacuum desiccator. In later preparations the final recrystallisation from hot water was employed, and was found to give a purer product.

2.3.2. Preparation of C_1, C_{10} and C_{14}TABNO$^{\bullet}$

The preparations of C_{10}TABNO$^{\bullet}$ and C_{14}TABNO$^{\bullet}$ were analogous to the preparation of C_{12}TABNO$^{\bullet}$ given above, with ease of purification increasing with the hydrocarbon chain length. In one instance it was difficult to dissolve the crude C_{10}TABNO$^{\bullet}$ in benzene, and it was necessary to dissolve it in chloroform instead. A dry solid was obtained upon evaporation of the chloroform.

The preparation of the N = O compound was complicated by the fact that, although both the CH_3Br and the 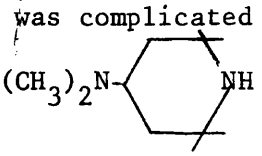

were chilled in an ice bath before being mixed together, the ensuing reaction was rather violent. After the reaction ceased, a white compound whose NMR spectrum corresponded with that of 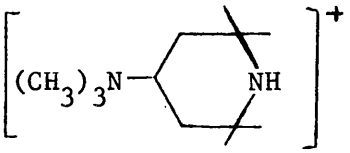 was scraped from the sides of the flask and oxidized according to Hubbell's procedure. Purification with benzene was very slow, but to date a better procedure has not been developed. The nitroxide, which is hydroscopic, has not yet been obtained in a crystalline state.

2.4. Characterization of the Cationic Surfactant Nitroxides

The cationic surfactants C_{10}, C_{12} and C_{14}TABNȮ whose preparation is described above were characterized according to several different procedures. The critical micelle concentration (cmc) of each compound at room temperature was measured by the depression of surface tension method, which also indicates the purity of the compound. A conductivity method was used to measure the cmc of each compound as a function of temperature. Finally the number of spins per molecule was measured by comparing the EPR spectra of each nitroxide surfactant with the spectra obtained from $CuSO_4.5H_2O$. The results of these experiments are described below.

2.4.1. Determination of the cmc from Surface Tension Measurements

The adsorption of surfactant molecules into the air-water interface causes a decrease in the surface tension of the interface. This decrease will continue with increasing surfactant concentration until the cmc, after which both the surface tension and the monomer concentration remain essentially constant[7,39]. The point at which

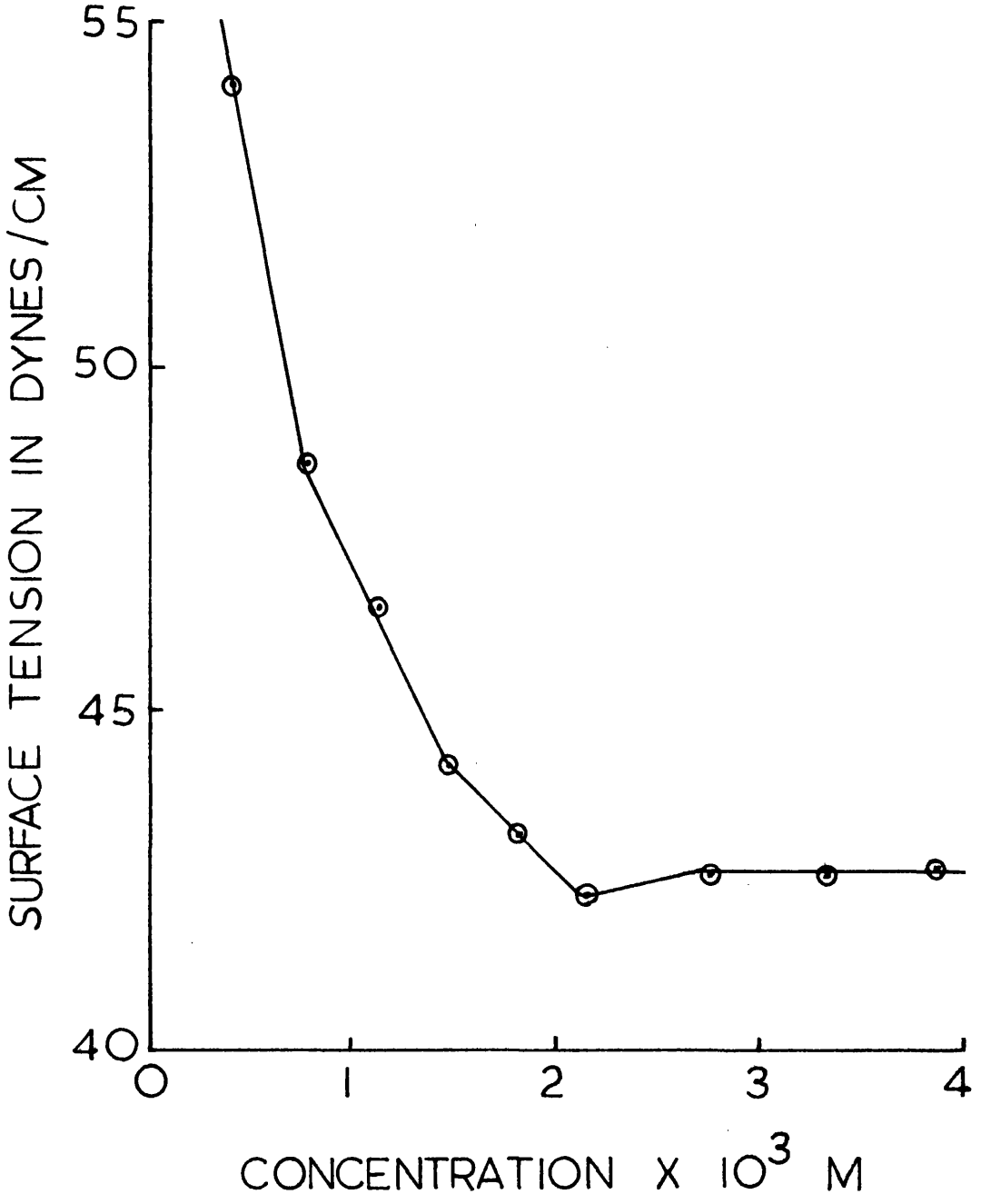

FIG. 2·1. DETERMINATION OF THE CMC OF C_{14}TABNO FROM SURFACE TENSION DATA

the surface tension becomes constant is taken to be the cmc. The presence of surface active impurities such as long chain alcohols will lower the surface tension still further, below the cmc, but above the cmc the surface tension will rise to the value determined by surfactant monomer adsorption in the air-water interface as the surface active impurities are adsorbed into the micelles[38]. Thus the presence of surface active impurities causes a minimum in the surface tension vs concentration curve.

The surface tensions of solutions of C_{10}, C_{12} and C_{14}TABNO were measured as a function of surfactant concentration with a du Noüy tensiometer[39]. The result for C_{14}TABNO is shown in Fig 2.1. All of the compounds prepared contained minima in the surface tension vs concentration curves even after repeated ether extractions and recrystallizations. The depths of the minima range from 0.4 dynes per centimeter for C_{14}TABNO to 3.4 dynes per centimeter for C_{10}TABNO to 5 dynes/cm for the initial preparation of C_{12}TABNO which was not recrystallized. The most probable contaminant is the alkyl bromide from which the compounds were prepared. If the contaminant is the alkyl bromide, previous experience with diamagnetic alkyltrimethylammonium bromide salts indicates that about 5% contaminant is present in the case of C_{12}TABNO, and less in the other cases. The measured values of the cmc were inaccurate because of the presence of the minima, but were close to the values obtained by the conductivity method described below.

2.4.2. Determination of the cmc by a Conductivity Method

The cmc of a surfactant solution can be determined from measurements of the electrical conductance of the solution as a function of surfactant concentration. Since the mobility of the surfactant ions when present in monomer form differs markedly

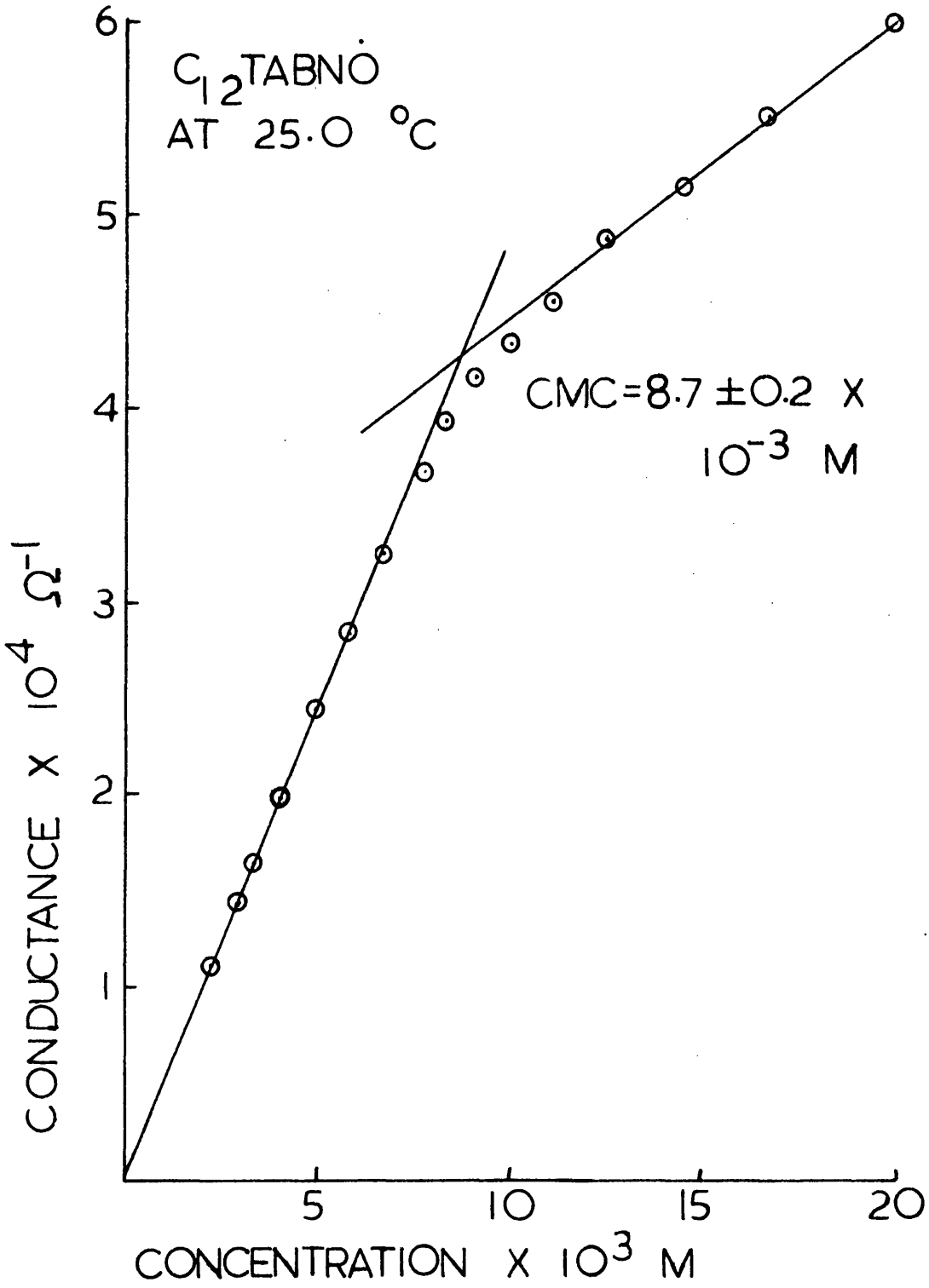

FIG.2.2. CONDUCTIVITY PLOT USED FOR DETERMINATION OF THE CMC

from the mobility of the same surfactant ions in aggregated or micellar form, there is an abrupt change in equivalent conductance at the cmc[17]. The cmc is then determined from the intercept of the line drawn through the points on the conductance vs concentration graph obtained at low concentrations with the line drawn through the points obtained at high concentrations. A conductance vs concentration plot for $C_{12}TABN\dot{O}$ is shown in Fig 2.2.

Experimentally, the resistances of surfactant solutions at known concentrations were measured with a Wheatstone bridge. The conductivity cell which was one arm of the bridge could operate with a minimum of 0.5 ml of solution, and was immersed in a water bath at the temperature desired for the measurement. The resulting profiles of the cmc as a function of temperature for C_{10}, C_{12} and $C_{14}TABN\dot{O}$ are shown in Fig 2.3. It was not possible to extend the temperature range above about 60°C, due to rapid evaporation of water from the solution in the conductivity cell.

2.4.3. Determination of the Number of Spins per Surfactant Molecule

The number of nitroxide groups present in a known weight of C_{10}, C_{12} and $C_{14}TABN\dot{O}$ was determined by comparing the EPR spectra of the solid state nitroxide surfactants with the spectra of freshly grown $CuSO_4.5H_2O$ single crystals. The double integral of an EPR first derivative absorption curve is equal to $2\pi^2\nu_o^2H_1^2 \frac{S(S+1)}{3kt} N_o g^2\beta^2$, where ν_o is the resonance frequency of the paramagnetic sample, H_1 the microwave field at the sample, N_o the total number of Spins, k Boltzman's constant, g the Landé g factor and β the Bohr magneton[40]. By keeping instrumental settings constant, ensuring that the samples to be compared are of the same general size and shape and occupy identical positions within the microwave cavity, and correcting for differences in the g factors, one may compare the number of spins in

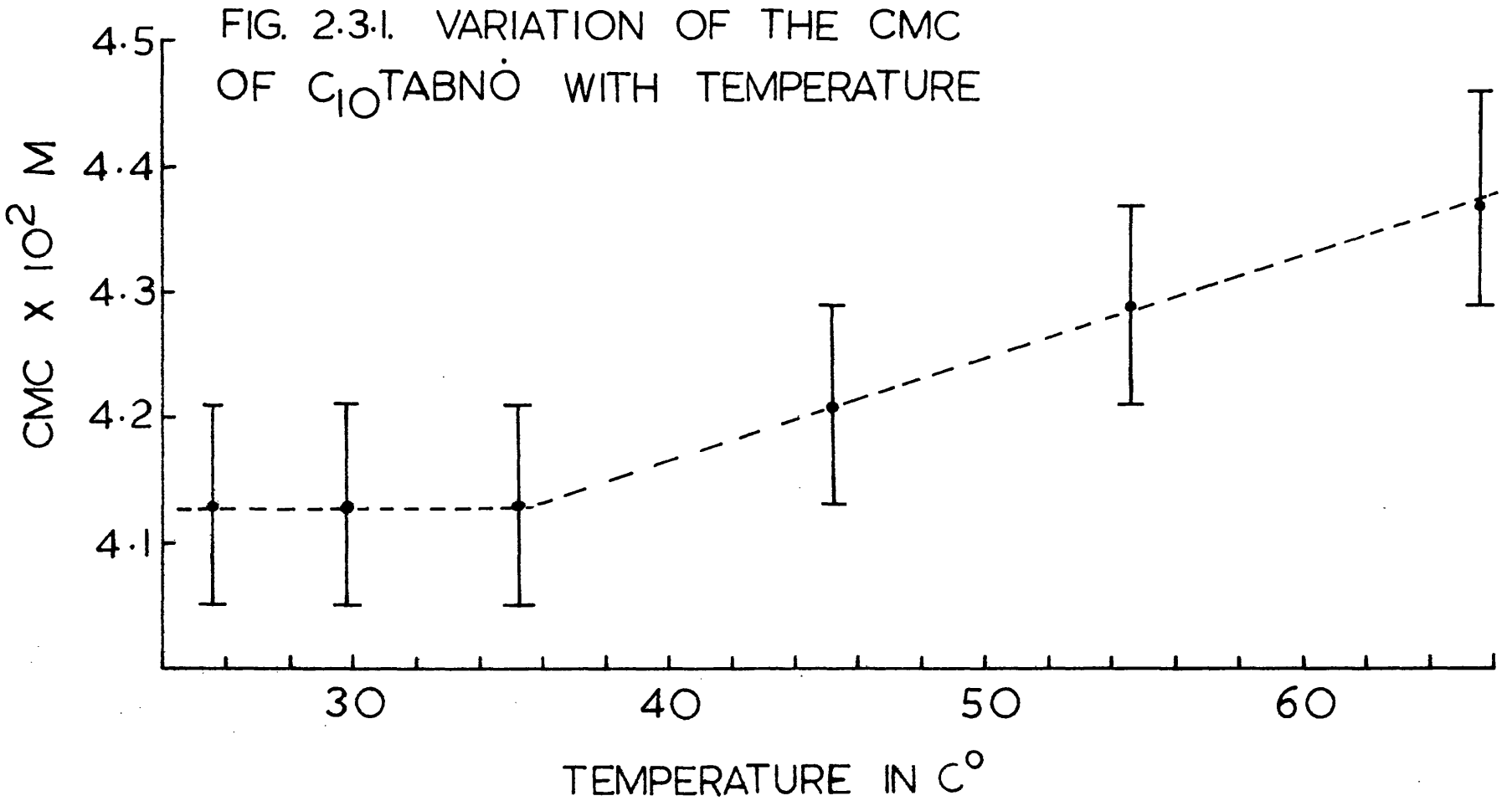

FIG. 2·3·1. VARIATION OF THE CMC OF $C_{10}TABNO$ WITH TEMPERATURE

FIG. 2·3·2. VARIATION IN THE CMC OF C_{12}TABNO WITH TEMPERATURE

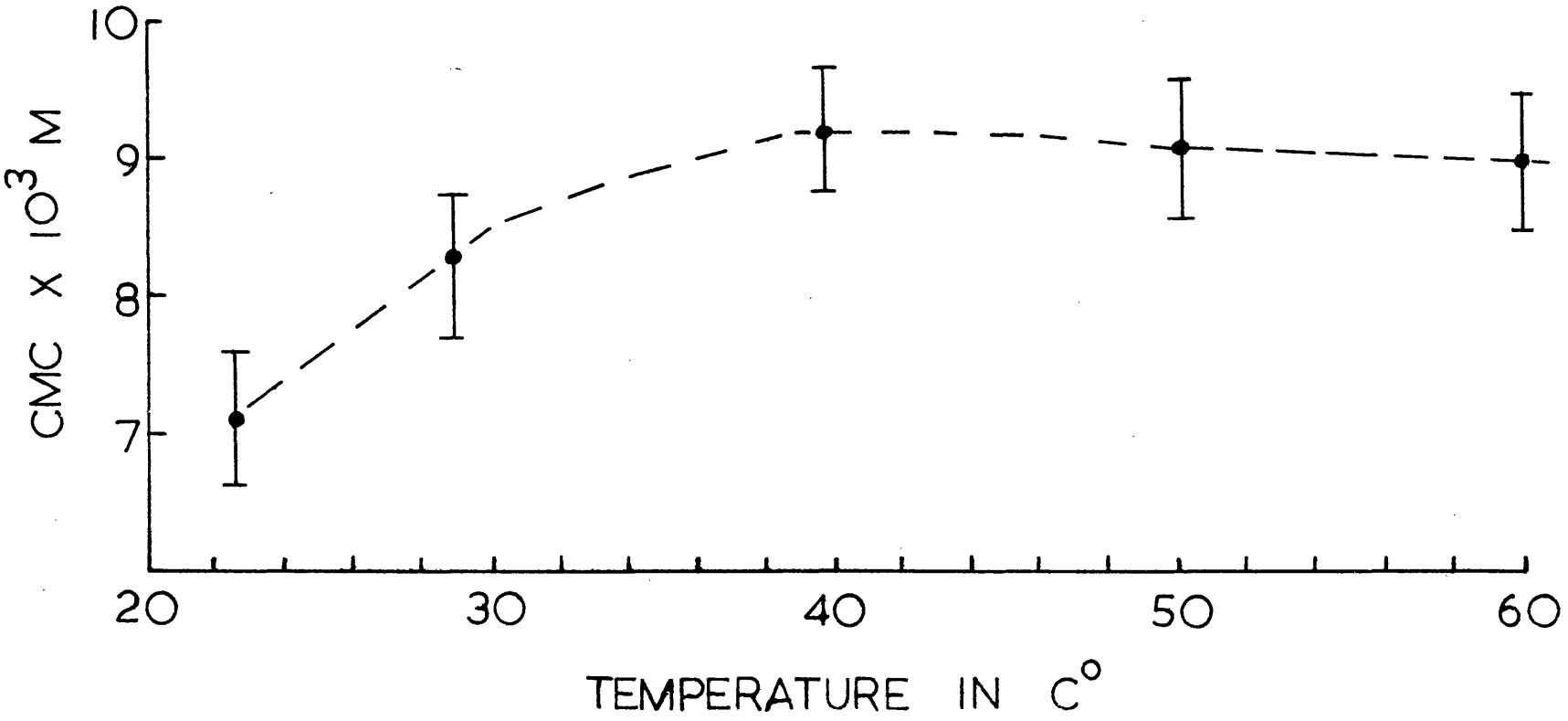

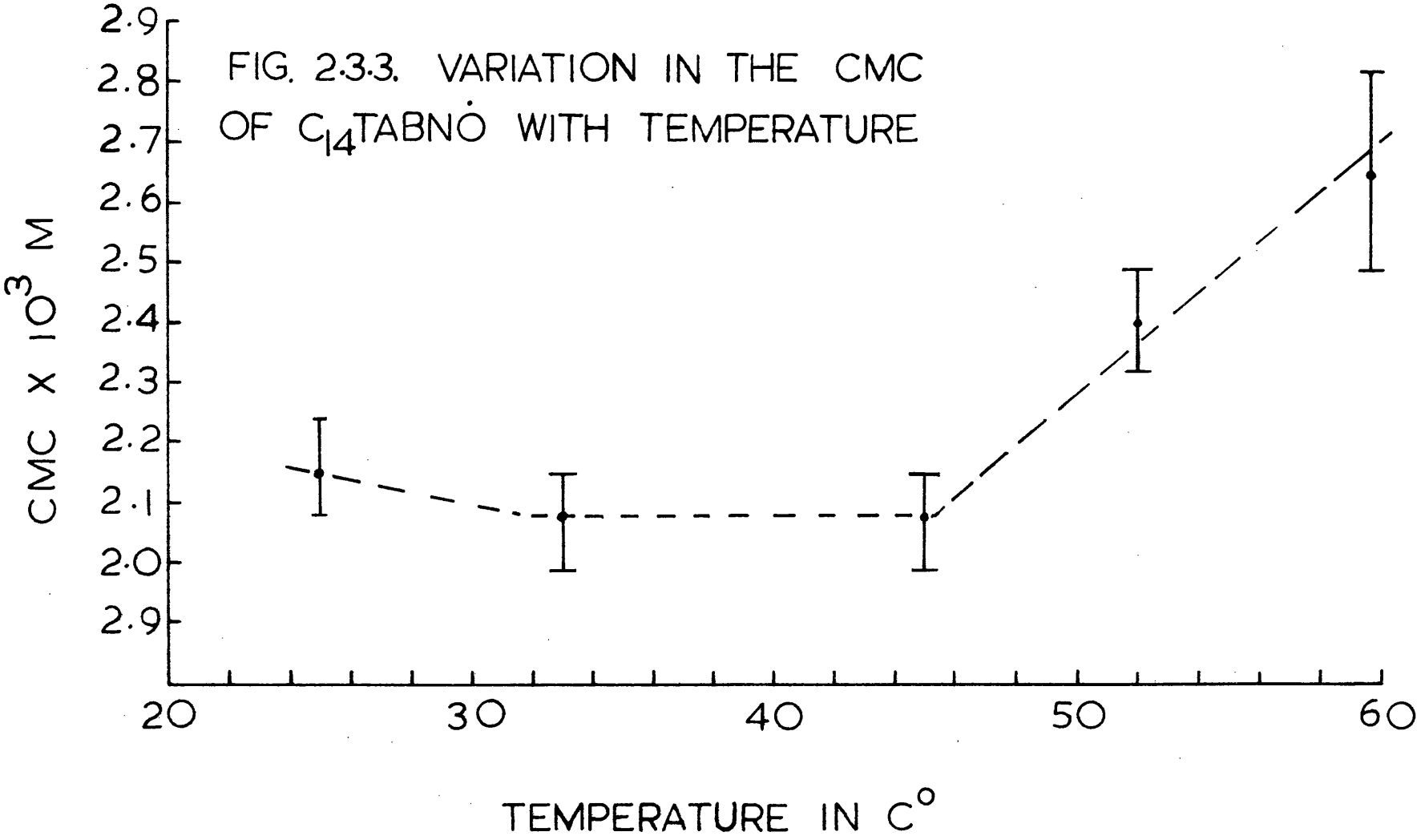

FIG. 2·3·3. VARIATION IN THE CMC OF C_{14}TABNO WITH TEMPERATURE

a standard sample with the number of spins in an unknown sample.

Two samples each of $C_{10}TABN\dot{O}$, $C_{12}TABN\dot{O}$, and $C_{14}TABN\dot{O}$ powder were packed into small capillaries and their weights determined. The spectra of these samples were compared with the spectra of four similarly sized $CuSO_4.5H_2O$ crystals recorded in a similar position in the EPR cavity. The double integrals of the spectra were measured by a nomogram method[41]. After corrections for the g factor difference had been made, it was found that relative to one spin per $CuSO_4.5H_2O$ molecule, $C_{10}TABN\dot{O}$ and $C_{14}TABN\dot{O}$ had 1.00 spins per molecule, while $C_{12}TABN\dot{O}$ had 0.95 spins per molecule. Since the accuracy of the method of comparison is $\pm$ 2% at best, these results indicate that C_{10} and $C_{14}TABN\dot{O}$ are >98% pure, while C_{12} is 95 $\pm$ 2% pure. Since the probable errors in the system tend to increase the intensity per gm of $CuSO_4.5H_2O$ (by evaporation of water) and to decrease the intensity per gm of the nitroxide surfactants (due to the presence of diamagnetic impurities), the $CuSO_4.5H_2O$, $C_{10}TABN\dot{O}$, and $C_{14}TABN\dot{O}$ used in this work were probably all pure enough to be used as secondary intensity standards.

CHAPTER 3

EARLY EXPERIMENTAL WORK WITH C_{12} TABNÒ

3.1. Experimental Results

The compound C_{12}TABNÒ was the first of the cationic surfactant analogues described in Chapter 2 to be prepared and characterized. This compound was used in the experiments described below.

The EPR results were obtained with a Varian E-3 spectrometer, which was very kindly made available by Liverpool University. Variable temperature results were obtained using the Varian V-4540 variable temperature control unit. Temperatures were measured using a copper-constantan thermocouple just above the cavity. It is estimated that these temperatures were known and controlled to $\pm$ 1°C. None of the solutions used were degassed.

3.1.1. Room Temperature Spectra

The EPR spectra were recorded for increasing concentrations of C_{12}TABNÒ in aqueous solution (see Figure 3.1). Below the cmc, the spectrum consists of three narrow lines, with a hyperfine coupling constant of 16.6 Gauss. This is consistent with a nitroxide in aqueous solution[9]. As the concentration of C_{12}TABNÒ is increased, the height of the EPR lines increases, while the widths remain almost the same, within experimental error. When the cmc is reached, the increase in height of the monomer spectrum ceases. At twice the cmc, the spectrum is that shown in Figure 3.1.B. The broad line has a width of 15.9 $\pm$ 0.1 Gauss, as determined from Figure 3.1.D, while the width of the central sharp component is 1.65 $\pm$ 0.05 Gauss. If it is assumed that the broad

FIG. 3·1. VARIATION IN $C_{12}TABNO^{\cdot}$ SPECTRA WITH CONCENTRATION

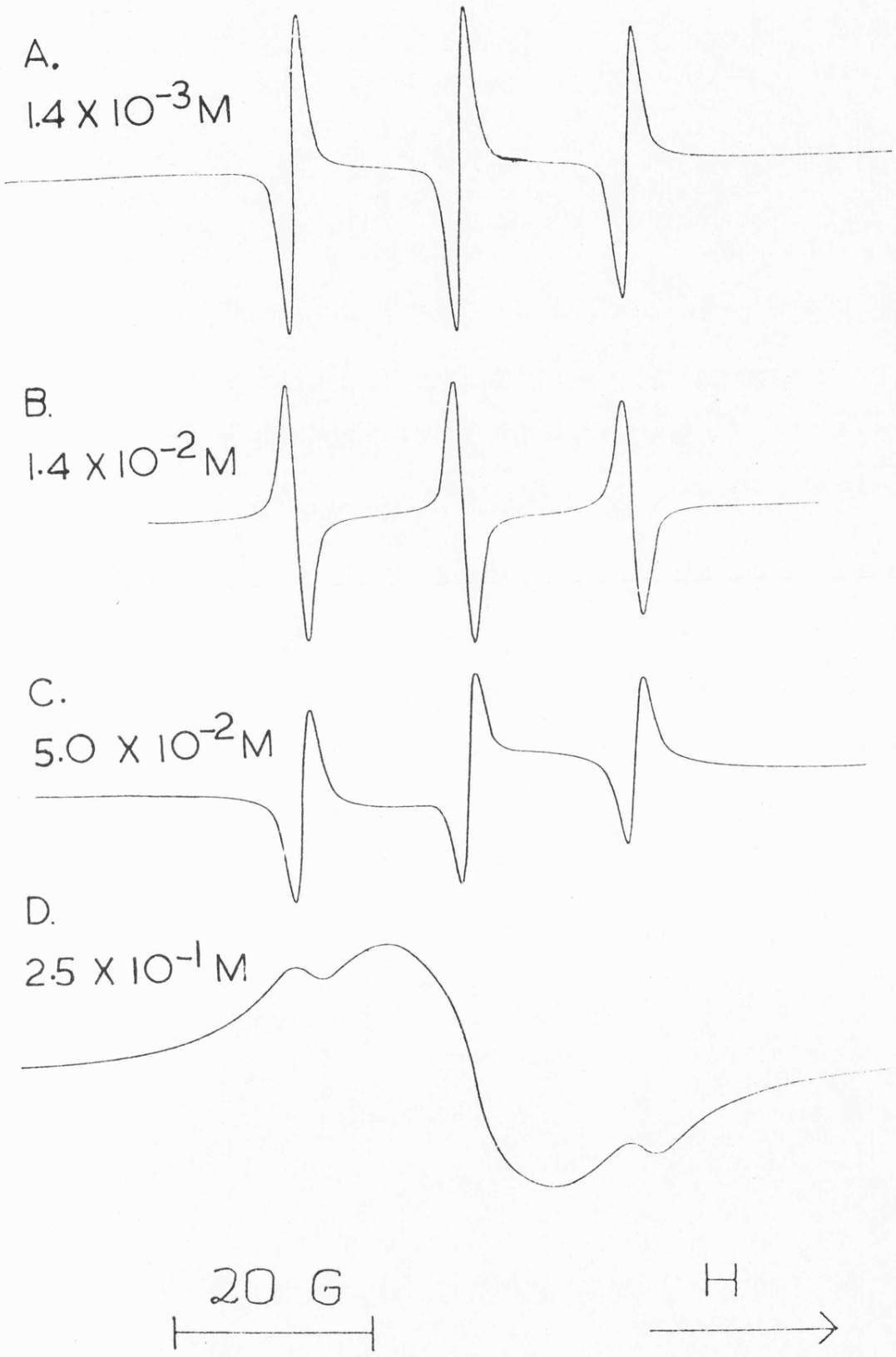

line is micellar in origin, while the sharp lines are due to monomers, then if the line shapes are Lorentzian, the intensity I will be proportional to the height, h, times the square of the width. At twice the cmc the total intensities of the two species should be equal, and the relative amplitudes of the two peaks can be calculated as follows:

$$3I_f = I_M$$

$$3(h_f)\ (1.65)^2 = h_M\ (15.9)^2$$

$$\frac{h_f}{h_m} = 31$$

Thus, it is reasonable that the micelle peak should still be too small to be seen. By 1.8×10^{-2}M, however, a broad peak underlying the sharp three lined spectrum is detectable $\left(\frac{h_f}{h_m} = 20\right)$, and at 5×10^{-2}M, the spectrum is that shown in Figure 3.1.C.

Increasing the concentration to 2.5×10^{-1}M gave the spectrum shown in Figure 3.1.D. The 5×10^{-2}M sample was centrifuged to remove any possible colloidal particles or oil droplets; the spectrum obtained from the centrifuged sample was identical with that from the uncentrifuged sample, suggesting that the exchange narrowed line is not due to undissolved radical aggregates. Thus it is seen that separate EPR signals are observed from the monomer and micellar species, and that therefore the monomer-micelle exchange frequency is in the slow region.

3.1.2. Dilution of the Paramagnetic Surfactant with a Diamagnetic Analogue

The centrifuged sample of 0.05M $C_{12}TABN\dot{O}$ was diluted with varying amounts of 0.05M cetyltrimethylammonium bromide ($C_{16}TAB$), a diamagnetic surfactant with a cmc of 8×10^{-4}M at 25°C[42]. The results are shown in Figure 3.2. At relatively low $C_{16}TAB$ levels, the height of the micelle signal begins to decrease relative to the height of the monomer. At higher $C_{16}TAB$ concentrations this becomes more apparent. This is the expected behaviour upon dilution of a paramagnetic micelle, for as the paramagnetic head groups are moved further apart by the intruding diamagnetic molecules, the electron exchange frequency ω_e will decrease. This will cause the micelle spectrum to become broader[6], and hence of smaller amplitude. As the relative amount of $C_{16}TAB$ is increased still further, three broad shoulders can be seen about the monomer lines. This is consistent with a diamagnetic micelle containing two or three paramagnetic molecules, where the paramagnetic molecules exhibit a hyperfine coupling constant somewhat smaller than that in water[9]. The resonances are broad because of spin-exchange effects due to the other paramagnetic molecules in the same micelle.

As dilution is increased still further, the broad lines sharpen, until in Figure 3.2.D. the height of the micellar nitroxide signal is greater than that of the aqueous nitroxide. Because of differences in the g and a values of the nitroxide radical in aqueous and micellar environments[4], this change is most clearly visible on the high field peak of the spectrum.

FIG. 3.2. DILUTION OF $C_{12}TABN\dot{O}$ WITH $C_{16}TAB$

$T = 40^{\circ}C.$ $[C_{12}TABN\dot{O}] + [C_{16}TAB] = 0.05\ M$

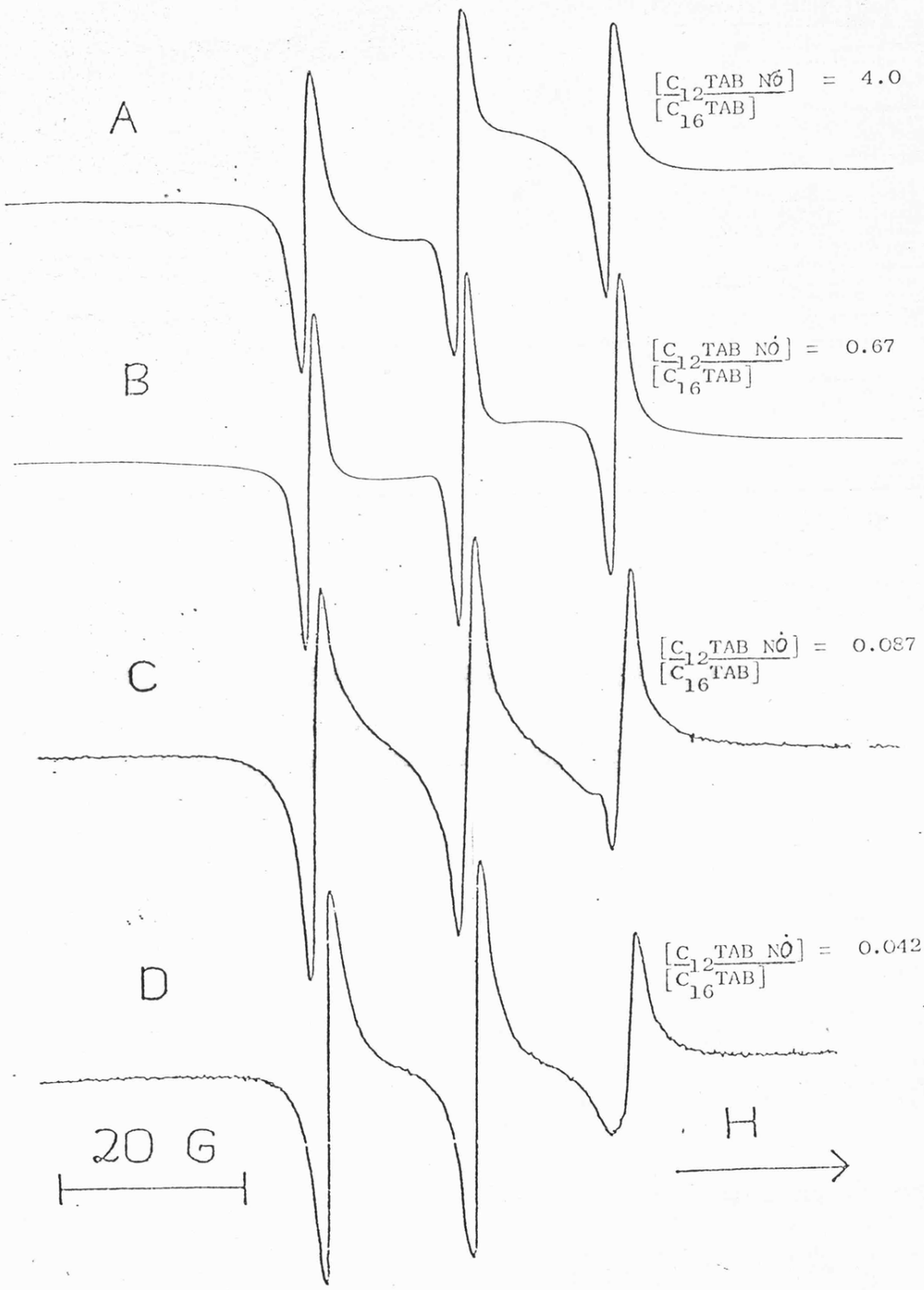

Since distinct signals are observed from the $C_{12}TABN\dot{O}$ in aqueous solution and the $C_{12}TABN\dot{O}$ solubilized in a $C_{16}TAB$ micelle, the spectra require that the frequency with which a $C_{12}TABN\dot{O}$ molecule solubilized in a $C_{16}TAB$ micelle exchanges between micellar and aqueous environment be slow. This work thus confirms the biradical results of Ohnishi, et al[16]. The spectra observed by workers[9,10,12] using nitroxide spin probes have subsequently been explained[43] as arising from two sets of overlapping spectra, one set due to probe molecules in the micelle, the other due to probe molecules in solution. The exchange frequency of a probe molecule between aqueous and micellar environments is thus slow on the EPR timescale, as is the monomer-micelle exchange frequency.

3.1.3. Temperature Dependence of $C_{12}TABN\dot{O}$ Spectra

Variable temperature studies have been carried out for several concentrations of $C_{12}TABN\dot{O}$. Below the cmc, the variation in line width with $^{T}/\eta$ is small; it is shown for two concentrations in Figure 3.3. Here η is the viscosity of the solution. The intensity dependence obeys the Curie Law[6], in that as the temperature increases, the intensity x" of the sample decreases according to

$$x'' = N \frac{g^2B^2S\ (S+1)}{3kT} \qquad (3.1)$$

where N is the total number of spins present, g is the Landé factor, B the Bohr magneton, S the electron spin quantum number ($\frac{1}{2}$ in this case), k is Boltzmann's constant and T is temperature (K).

FIG. 3.3. LINEWIDTH VS. T/η BELOW THE CMC

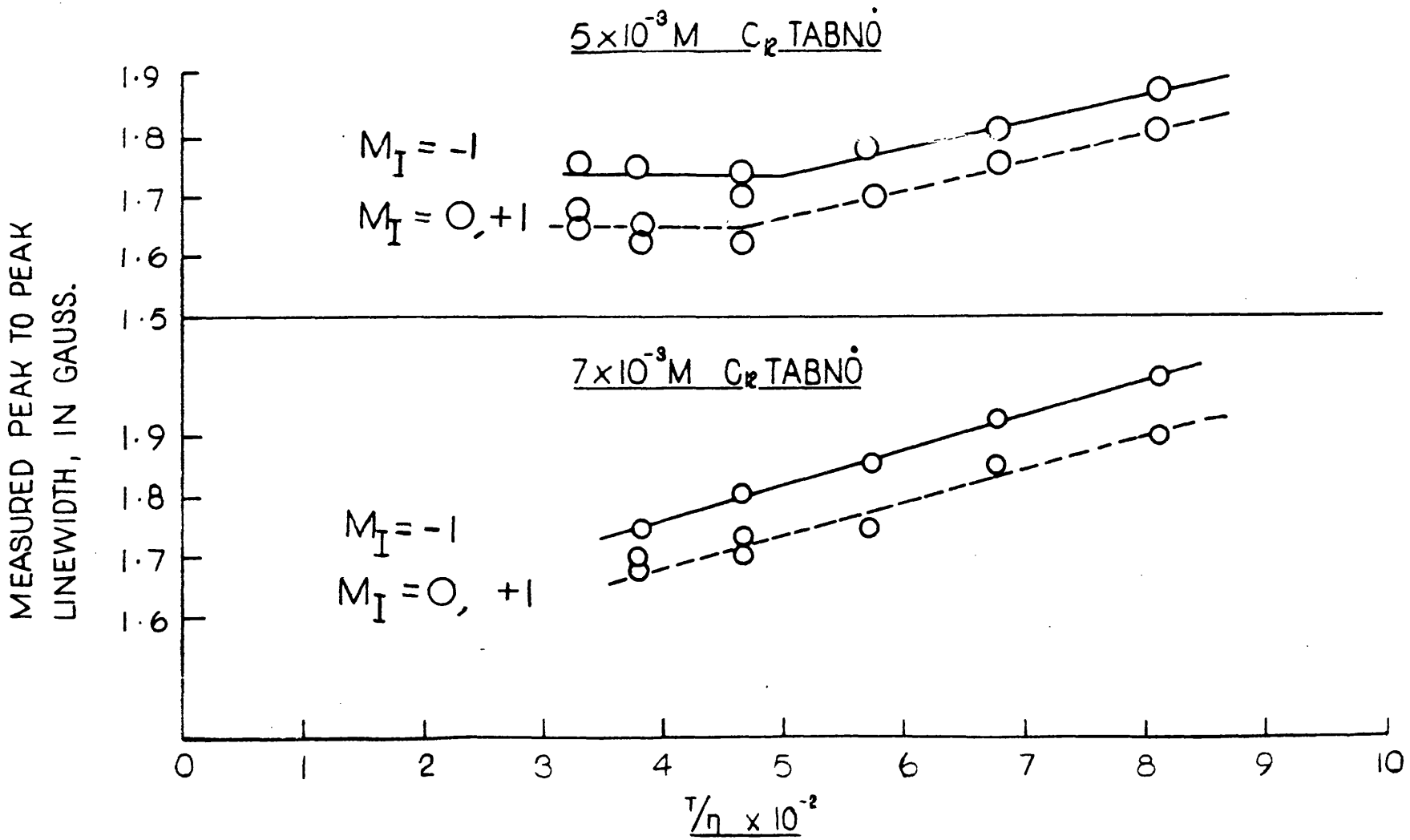

This is the temperature dependence expected for a free radical which is not in a thermally activated state. The behaviour of the compound above the cmc is shown qualitatively by the spectra in Figure 3.4. With increasing temperature the micellar spectrum sharpens, while the monomer spectrum broadens. The effect in Figure 3.4 is exaggerated somewhat by overlapping lines - in the spectra used for rate determination this overlap effect was not present, as the concentrations were between the cmc and the point of first observability of the micellar line.

3.2. Discussion

3.2.1. Establishment of the Species Responsible for the Observed Spectra

It is necessary to establish that the observed spectra are actually due to micelles and monomers. The sharp three-lined spectrum is assigned to a nitroxide tumbling fairly rapidly in aqueous solution and hence can be equated with the monomer, since uncharged nitroxides such as I should have been removed when the $C_{12}TABN\dot{O}$ was chromatographed

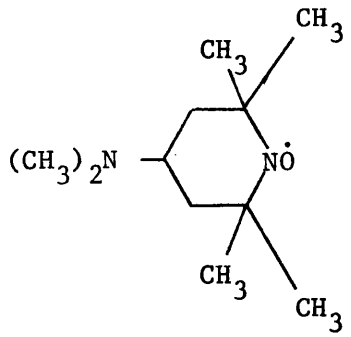

I

during preparation, while the presence of more than 1% of a charged nitroxide such as II would lead to a detectable increase in the apparent monomer concentration above the cmc, which was not observed.

FIG. 3.4. CHANGES IN 0.05M C_{12}TABNO SPECTRA WITH TEMPERATURE

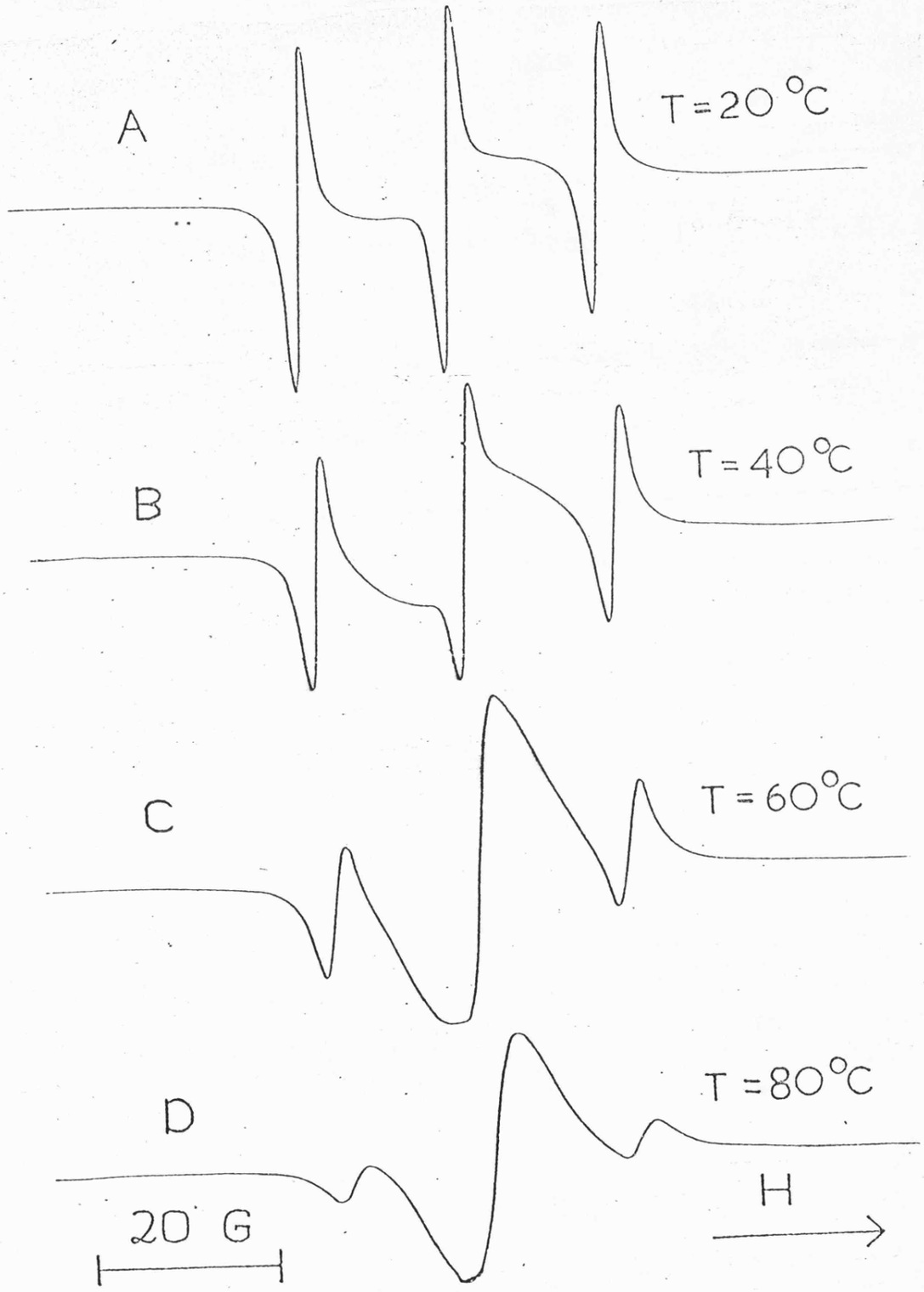

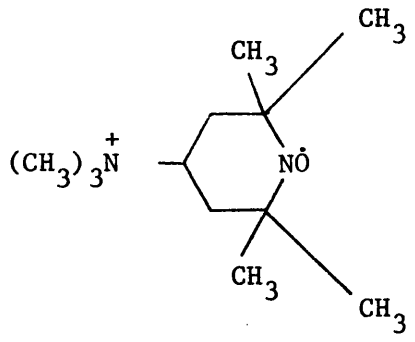

II

A broad line such as that attributed to the micelle could have other origins. The solution was centrifuged to eliminate the possibility of colloidal particles, microscopic solids, or oil droplets being present in solution. The variable temperature behaviour of the broad line is consistent with that of an exchange-narrowed aggregate, and inconsistent with that of a spin broadened by a dipolar mechanism, which should follow Curie Law behaviour. The behaviour upon dilution with a diamagnetic detergent is easily explicable if the system contains paramagnetic micelles with exchange narrowed signals. The appearance of the micellar EPR signal at a suitable interval after surface-tension and conductivity measurements have shown that micelles are present supports the assumption that the broad line is micellar in origin. Therefore, it is concluded that the broad component of the spectrum above the cmc is due to micelles, and the sharp component due to monomer detergent molecules.

3.2.2. Determination of Exchange Frequencies and Activation Energies

The discussion of exchange frequencies given here is a simplified analysis which was used in the early monomer-micelle exchange work. A more complete analysis of the monomer-micelle exchange problem which was developed later can be found in Chapter 5.

Since the frequency with which a paramagnetic surfactant molecule exchanges between aqueous and micellar environments is slow, i.e. much less than the hyperfine coupling constant[6], the observed EPR spectrum above the cmc consists of a broad line due to the micelles, upon which are superimposed three sharp lines due to the monomers. Since the hyperfine coupling constant of $C_{12}TABN\dot{O}$ in water is about 16 Gauss, the exchange frequency must be much less than 4.5×10^7 sec^{-1} to give two sharp, superimposed spectra. If the monomer-micelle exchange frequency had been fast, i.e. much greater than the hyperfine coupling constant, then the observed spectrum would have been a weighted average of the monomer and micellar signals. In the intermediate exchange region, as the exchange increases then the monomer lines will broaden according to[6,44]

$$\frac{1}{T_2} = \frac{1}{T_{2_o}} + P_{FM} \qquad (3.2)$$

where $\frac{1}{T_2}$ is $\frac{\sqrt{3}}{2}$ times the observed peak to peak first derivative line width,

$\frac{1}{T_{2_o}}$ is $\frac{\sqrt{3}}{2}$ times the first derivative peak to peak line width in the absence of exchange, and P_{FM} is the monomer-micelle exchange frequency.

The micellar signal would not be expected to broaden as the monomer-micelle exchange frequency increased, as it is already exchange narrowed due to electron spin exchange between the different head groups. Unless the monomer-micelle exchange frequency approached the electron spin exchange frequency in order of magnitude, the effect of monomer exchange upon the micellar signal should be negligible.

In the slow exchange region, the intensity of the monomer spectrum obeys the Curie Law. In addition to this, in the intermediate exchange region increasing the temperature should increase the rate of monomer exchange with the micelles, thus causing the increased broadening of the monomer spectrum (see equation 3.2). The micellar spectrum becomes narrower as the temperature is increased, due to the increase in the frequency of electron spin exchange within the micelle[6].

If the system is in the intermediate exchange region, equation 3.2. can be applied to the monomer spectrum to determine the frequency at which the monomer is exchanging with some other environment. It has been assumed that this other environment is the micelle, although the possibility of the existence of some sort of pre-micellar aggregate, with which the monomer might exchange with a similar effect upon its spectrum, cannot be ruled out. The small temperature dependence of the monomer linewidths below the cmc indicates that this other environment is present only above the cmc, however.

Before using the measured linewidth increases to calculate a monomer-micelle exchange frequency, it is necessary to account for any other contributions to the linewidth. In a system as concentrated as 10^{-2}M free radicals, EPR signals will be broadened by Heisenberg spin exchange[45]. This broadening is concentration dependent as well as showing dependence upon T/η. Broadening due to spin-rotational relaxation[46] may also be present,

but this does not appear to be concentration dependent[46]. The total broadening of the monomer spectrum with increasing temperature will thus be due to Heisenberg spin exchange between the monomers, spin-rotational relaxation of the monomers and exchange between the monomer and some other environment, presumably the micelle.

For the monomer spectrum in the presence of micelles:

$$\frac{1}{T_{2\ m\text{-}mic}} = \frac{1}{T_{2_o}} + \frac{1}{T_{2H}} + \frac{1}{T_{2S\text{-}R}} + \frac{1}{T_{2\ EXCH}} \qquad (3.3)$$

where $^1/T_2$m-mic is the observed $^1/T_2$ of the monomer in the presence of micelles, $\left(\frac{2}{\sqrt{3}}\right)$ $^1/T_{2_o}$ is the line width of the monomer due to unresolved proton hyperfine couplings, $^1/T_{2H}$ is the contribution to the observed $^1/T_2$ due to Heisenberg spin exchange, $^1/T_{2S\text{-}R}$ is the contribution to the observed $^1/T_2$ due to the spin-rotational interaction, and $^1/T_{2\ exch}$ is the contribution to the observed $^1/T_2$ due to exchange. For the monomer spectrum in the absence of micelles,

$$\frac{1}{T_{2M}} = \frac{1}{T_{2_o}} + \frac{1}{T_{2H}} + \frac{1}{T_{2S\text{-}R}} \qquad (3.4)$$

where T_{2M} is the observed transverse relaxation time of the monomer in the absence of micelles. It is necessary to show that $^1/T_{2H}$ and $^1/T_{2S\text{-}R}$ in equations 3.3 and 3.4 are equal, in order to write

$$\frac{1}{T_{2\ EXCH}} = \frac{1}{T_{2\ m\text{-}mic}} - \frac{1}{T_{2M}} \qquad (3.5)$$

In order to estimate the effects of monomer-monomer Heisenberg spin exchange and spin-rotational relaxation, the spectra of a 5 x 10^{-3}M (below the cmc) aqueous solution of C_{12}TABNÒ were taken at various temperatures. These spectra should show Heisenberg spin exchange and spin-rotational

relaxation but not monomer-micelle exchange. Since spin-rotational relaxation is not concentration dependent, its effect should be the same at 1.4×10^{-2}M, the concentration at which the monomer-micelle exchange frequency was measured. Heisenberg spin exchange is concentration dependent; but the following observations indicate that this concentration dependence is small in the region concerned.

1. At 24°C, the 5×10^{-3} and 1.4×10^{-2}M C_{12}TABNO$\dot{}$ spectral lines have the same width, within the experimental error of $\pm$ 0.03 Gauss. Thus the concentration dependence of Heisenberg spin exchange at 24°C does not exceed the experimental error.
2. Between 24°C and 68°C, 5×10^{-3}M and 6×10^{-3}M C_{12}TABNO$\dot{}$ have the same linewidth, within experimental error. Thus the concentration dependence in this region is too small to be measured.
3. The high field and low field lines of 1.4×10^{-2}M and 1.8×10^{-2}M C_{12}TABNO$\dot{}$ have the same widths, within experimental error. (The centre field line of 1.8×10^{-2}M shows the influence of the underlying micellar peak.) Thus in this region the monomer linewidth is independent of concentrations within experimental error.
4. A graph of linewidth vs. $^{T}/\eta$ for the 1.4×10^{-2}M C_{12}TABNO$\dot{}$ spectrum is shown in Figure 3.5. Below it is shown a typical graph of the same variables for Heisenberg spin exchange[45], with the observed deviation for increased concentrations shown as a dashed line[45]. It can be seen that the observed graph is not what would be expected for Heisenberg spin exchange.

FIG. 3.5. LINEWIDTH VS T/η

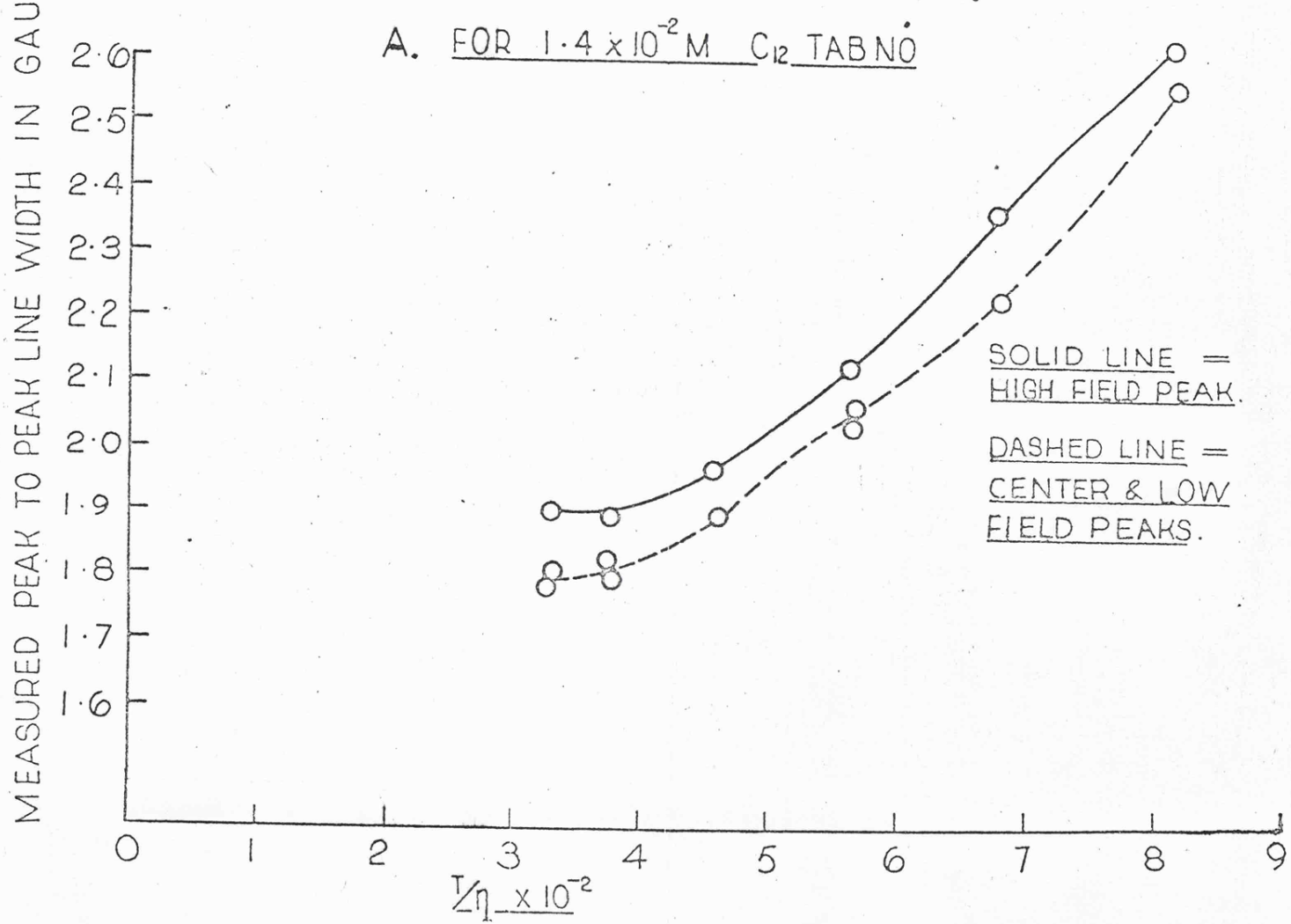

B. FOR DI-TERT-BUTYLNITROXIDE IN DME* – DATA FROM REF 45

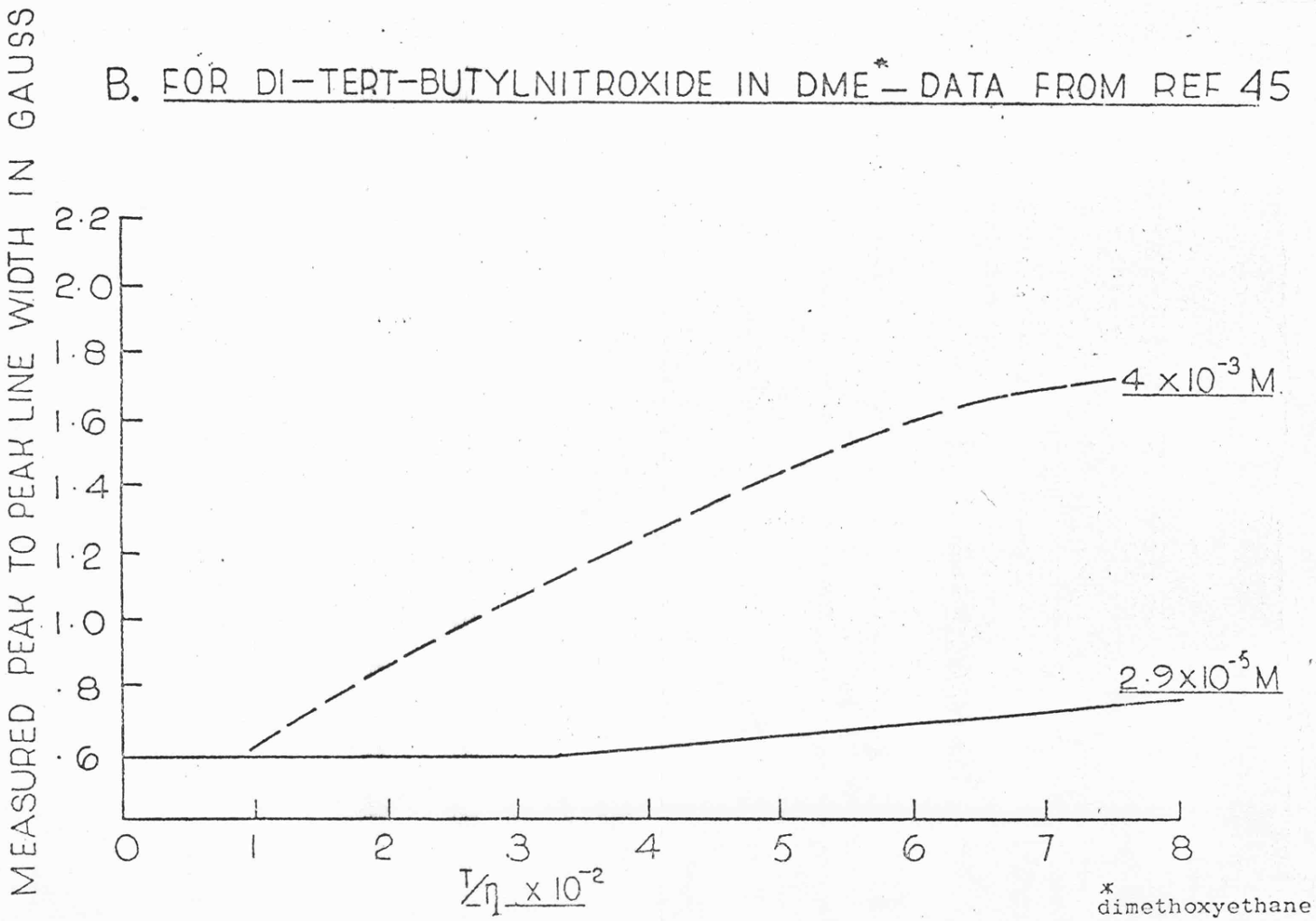

*dimethoxyethane

On the basis of the above, it was concluded that the concentration dependence of the Heisenberg spin-exchange contribution to the line width had a maximum value of the experimental error. Thus, in the calculations which follow, it has been assumed that only $T_{2\ EXCH}$ contributes effectively to the temperature dependence of the monomer line width.

Using the results at 5×10^{-3}M C_{12}TABNȮ and 1.4×10^{-2}M C_{12}TABNȮ the frequency of an exchange process, assumed to be monomer-micelle exchange, was calculated as a function of temperature, using equations 3.2 and 3.5. The results are shown in Table 1.

Table 1 - Monomer-micelle exchange rate as a function of temperature

Temp $^{o}C \pm 1^{o}C$	Average value of width at 1.4×10^{-2}M minus width of 5×10^{-3}M C_{12}TABNȮ in Gauss	Exchange Frequency $\times 10^{-5}$ sec^{-1}
24	0.06 ± 0.06	1.5 ± 1.5
30	0.09 ± 0.06	2.2 ± 1.5
39	0.16 ± 0.06	4.0 ± 1.5
49	0.30 ± 0.06	7.3 ± 1.5
59	0.44 ± 0.06	10.6 ± 1.5
68	0.69 ± 0.06	16.7 ± 1.5

The data given in Table 1 were used to obtain a rough estimate of the enthalpy barrier to the micelle-monomer exchange process. From an Arrhenius plot, as seen in Figure 3.6, an enthalpy of activation for the exchange process of between 8.1 and 11.6 k cal/mole was determined. The three most accurate (high temperature) points determined an activation enthalpy of 9.5 k cal/mole.

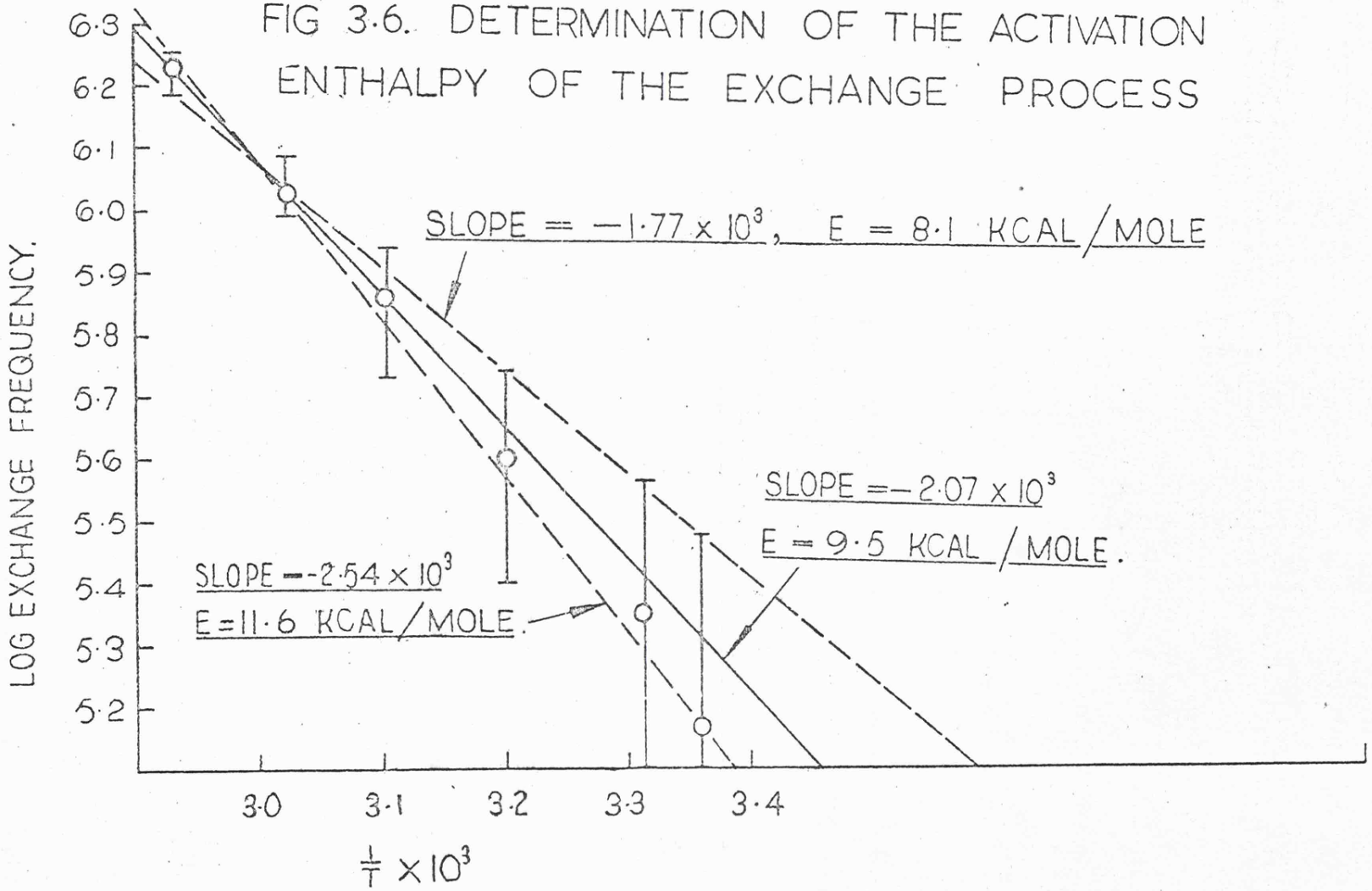

FIG 3·6. DETERMINATION OF THE ACTIVATION ENTHALPY OF THE EXCHANGE PROCESS

The exchange frequencies and activation enthalpy given above were assumed to be due to the exchange of paramagnetic surfactant molecules between an aqueous and a micellar environment[47]. Further work has, however, thrown considerable doubt upon the assumption that the measured frequencies are due to monomer-micelle exchange. This work will be described in the chapters which follow.

CHAPTER 4

FURTHER EXPERIMENTS WITH THE CATIONIC NITROXIDE SURFACTANTS

The initial purpose of the experiments described in this chapter was to measure the monomer-micelle exchange frequencies of $C_{10}TABN\dot{O}$ and $C_{14}TABN\dot{O}$ as functions of both temperature and surfactant concentration. It was hoped that the information obtained would, when taken in conjunction with the $C_{12}TABN\dot{O}$ data described in Chapter 3, allow one to determine the energetics of the micellisation process. However, the results of these experiments seemed to indicate that micellisation was not the only kinetic process occurring in these systems, and that any analysis of the energetics of micellisation would be premature. The experiments and the results obtained are described below.

4.1. Determination of the Energy of Activation of the Micellisation Process for $C_{14}TABN\dot{O}$

Solutions of $C_{14}TABN\dot{O}$ in water were prepared at 1.62×10^{-3}M (below the cmc) and at 4.05×10^{-3}M, 8.23×10^{-3}M, and 1.60×10^{-2}M (above the cmc). EPR spectra were recorded for each solution at temperatures ranging from 21°C to 98°C, using a Varian E-4 EPR spectrometer located at Unilever Research Laboratory, Port Sunlight. This spectrometer was used for the remainder of the EPR work described in this thesis. The temperatures were measured using a copper-constantan thermopile composed of four thermocouples in series, which was attached to a digital voltmeter which was sensitive enough to record twelve or thirteen digits per degree in the temperature range of interest. The thermopile was calibrated against a quartz thermometer. It is estimated that the temperatures recorded are known to $\pm$ 0.1 C° relative to each other and to $\pm$ 1.0 C° absolutely. The temperatures were measured by placing the thermopile in the center of the EPR cavity before and after the spectra had been recorded. As the temperatures measured before and after running the earlier samples agreed within $\pm$ 0.1°C, assuming at least two minutes were allowed for

the thermopile to reach equilibrium, one of the temperature measurements was often omitted for the later samples.

The spectra of the solution below the cmc showed a temperature independent linewidth for each peak, within the experimental error. The linewidths observed, 1.67 $\pm$ 0.02 G for the high field (m_I = -1), 1.63 $\pm$ 0.02 G for the centre (m_I = 0), and 1.64 $\pm$ 0.02 G for the low (m_I = 1) field peaks, were dominated by the proton hyperfine structure envelope, as will be discussed later. The spectra of the solutions above the cmc exhibited the three sharp monomer lines and the broad micellar line which characterised the micellar $C_{12}TABN\dot{O}$ solutions. This showed that the monomer-micelle-exchange frequency for $C_{14}TABN\dot{O}$ was slow on the EPR timescale. The linewidths remained constant as the temperature was increased up to about 70°C, after which the linewidths began to increase with increasing temperature. Since the 1.6 x 10^{-3}M $C_{14}TABN\dot{O}$ solution showed no such increase, it was assumed that the increased linewidth was due to the effect of monomer-micelle-exchange. Exchange frequencies were calculated as in Chapter 3, using equation 3.2 (4.1).

$$\frac{1}{T_2} = \frac{1}{T_{20}} + P_{F-M} \qquad (4.1)$$

Here $\frac{1}{T_2}$ is the transverse relaxation time determined from the measured linewidth in the presence of exchange, $\frac{1}{T_{20}}$ the transverse relaxation time in the absence of exchange, and P_{F-M} the frequency with which a monomer enters a micelle. The calculated exchange frequencies P_{F-M} were used to obtain the Arrhenius plots shown in figure 4.1. The activation enthalpies for the micellisation process which were obtained from these Arrhenius plots are shown in Table 4.1.

FIG. 4·1.

ARRHENIUS PLOTS FOR $C_{14}TABN\dot{O}$

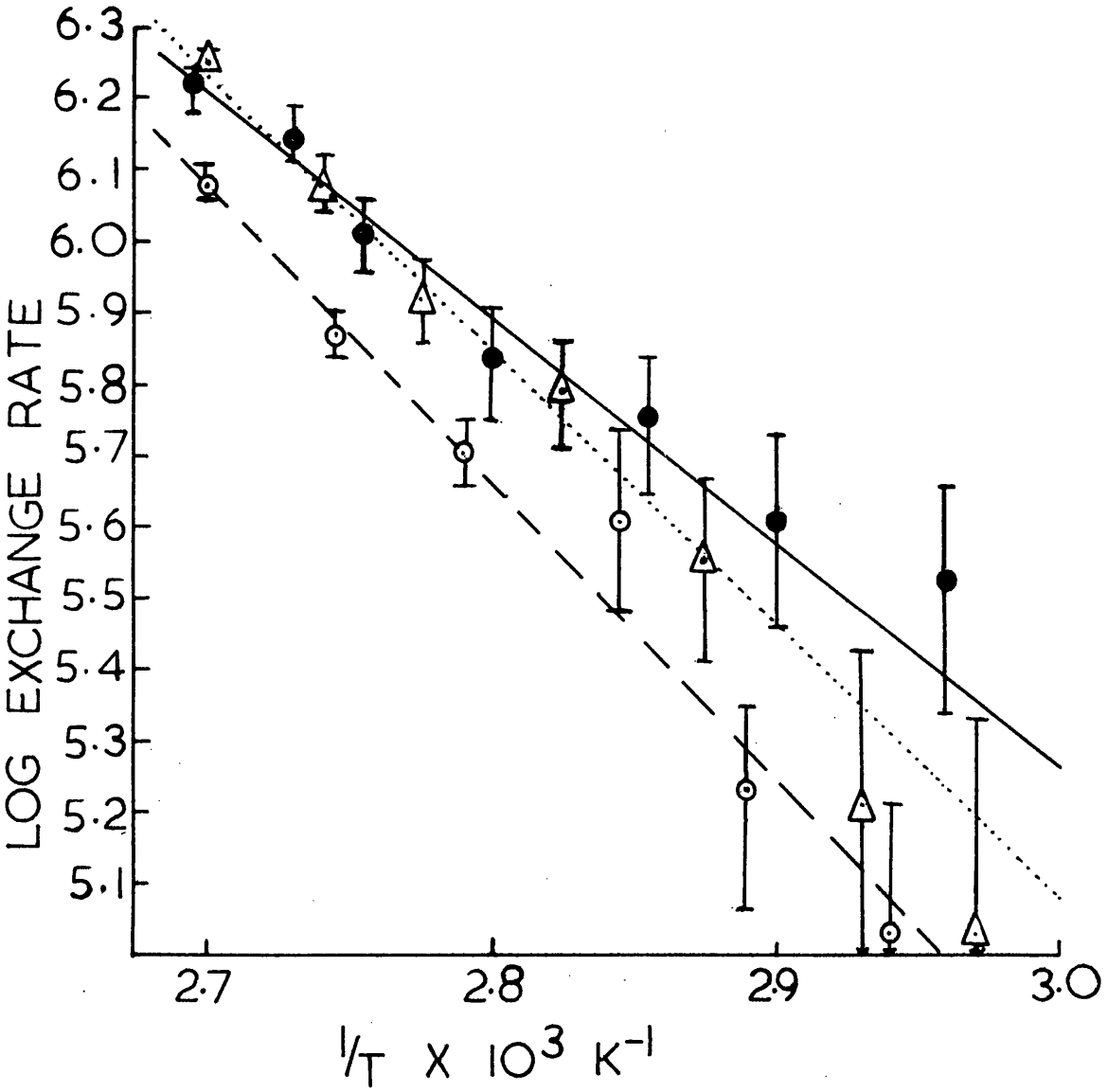

LEGEND:

—●— 1.60×10^{-2} M $C_{14}TABN\dot{O}$

·····△····· 8.23×10^{-3} M $C_{14}TABN\dot{O}$

– – ⊙ – – – 4.05×10^{-3} M $C_{14}TABN\dot{O}$

Table 4.1. Activation Enthalpies for the Micellisation Process for Several Concentrations of C_{14}TABNO

Concentration C_{14}TABNO,M	Activation Energy in kcal/mole
4.05×10^{-3}	20.2 ± 2.2
8.23×10^{-3}	18.0 ± 2.2
1.60×10^{-2}	15.3 ± 3.0

From Table 4.1 it is seen that the activation enthalpy needed for the micellisation process decreases as the concentration of surfactant increases. This result is in itself not unreasonable, as there could be models for the micellisation process with which it could be reconciled. The exchange frequency data from which the activation enthalpies were derived exhibit some strange behaviour, however. At the lower temperatures (higher $\frac{1}{T}$), the spectra of the more concentrated solutions have the broader lines, but as the temperature increases, the spectra of the 8.23×10^{-3}M solution broaden more than the spectra of the 1.6×10^{-2}M solution, until at the highest temperature recorded the linewidths are within the experimental error ($\pm$ 0.05 G) of each other. This either implies a limiting value of the monomer-micelle exchange frequency at high temperatures, or suggests that at high temperatures the dependence of the monomer-micelle exchange frequency on the micelle concentration is reversed from the dependence at lower temperatures. The spectra obtained by increasing the temperature to 98°C were reproduced when the temperature was decreased from 98°C so decomposition of the surfactant was not involved. None of the samples were de-gassed, however.

Since the temperature region 75°C-100°C was clearly of interest, attempts were made to measure the cmc of $C_{14}TABN\dot{O}$ at these temperatures. The conductivity cell described in Chapter 2 was immersed in an oil bath at 80°C and 93°C, and cmc values of $2.8 \pm 0.2 \times 10^{-3}$M and $3.6 \pm 0.3 \times 10^{-3}$M were obtained at 80°C and 93°C respectively. These values are uncertain, since at the high temperatures involved the rate of water evaporation from the sample was quite rapid. The cmc value obtained previously for $C_{14}TABN\dot{O}$ at 60°C was $2.6 \pm 0.1 \times 10^{-3}$M.

If this variation in the cmc is taken into account, the measured exchange frequencies seem even stranger. Since the results in the 70°C-80°C region indicate that the exchange frequency increases with increasing micelle concentration one would expect the higher cmc at higher temperatures to depress the exchange frequency. One would expect this depression of the exchange frequency and the resultant curvature of the Arrhenius plot to be greatest for the 4.05×10^{-3}M solution (36% micellar surfactant at 60°C, 11% micellar surfactant at 93°C) and smallest for the 1.6×10^{-2}M surfactant (84% and 78% micellar surfactant at 60°C and 93°C respectively). Yet none of this is observed. These results, taken in conjunction with the anomalous broadening of the most concentrated solution at high temperature, indicate that either the kinetics and energetics of the micellisation process are more complex than anticipated, or that the measured spectra are dominated by something other than the micellisation process.

4.2. Experiments with $C_{10}TABN\dot{O}$

Aqueous solutions of $C_{10}TABN\dot{O}$ were prepared at concentrations of 3.8×10^{-2}M (just below the cmc, which ranges from 4.1×10^{-2}M at 20°C to 4.7×10^{-2}M at 60°C), 4.6×10^{-2}M and 5.35×10^{-2}M. These solutions were not de-gassed. EPR spectra were obtained for these solutions at several temperatures between 25°C and 75°C. The spectra all exhibited the three lines due to monomeric $C_{10}TABN\dot{O}$ which were broadened to widths of between 3 and 6 G, the width increasing with surfactant concentration and with the temperature of the solution. The widths obtained for the 4.6×10^{-2}M sample are shown as a function of temperature in Table 4.2. It is noted that

Table 4.2 Widths of the $M_I = 1$, $M_I = 0$, and $M_I = -1$ lines of 4.6×10^{-2}M $C_{10}TABN\dot{O}$ as a Function of Temperature

T, °C	Width of $M_I = 1$ Line in Gauss	Width of $M_I = 0$ Line in Gauss	Width of $M_I = -1$ Line in Gauss
27.5	3.4 ± 0.1	3.2 ± 0.1	3.4 ± 0.1
35.8	3.7 "	3.6 "	3.6 "
44.4	4.3 "	4.1 "	4.2 "
55.0	5.0 "	4.8 "	5.0 "
65.6	5.6 "	5.5 "	5.6 "
74.4	5.8 "	6.1 "	5.9 "

at lower temperatures the $M_I = \pm 1$ lines are broader than the $M_I = 0$ line, while at the highest temperature this effect is reversed. These linewidth effects are at least partially due to the effect of overlapping lines, as is illustrated in Figure 4.2. Figure 4.2. contains lines of Lorentzian lineshape, which are more intense in the wings than the experimental lines, which have a lineshape intermediate between

FIG. 4.2.A. SUPERPOSITION OF THREE LORENTZIAN LINES OF EQUAL INTENSITY, EACH BEING 6G WIDE

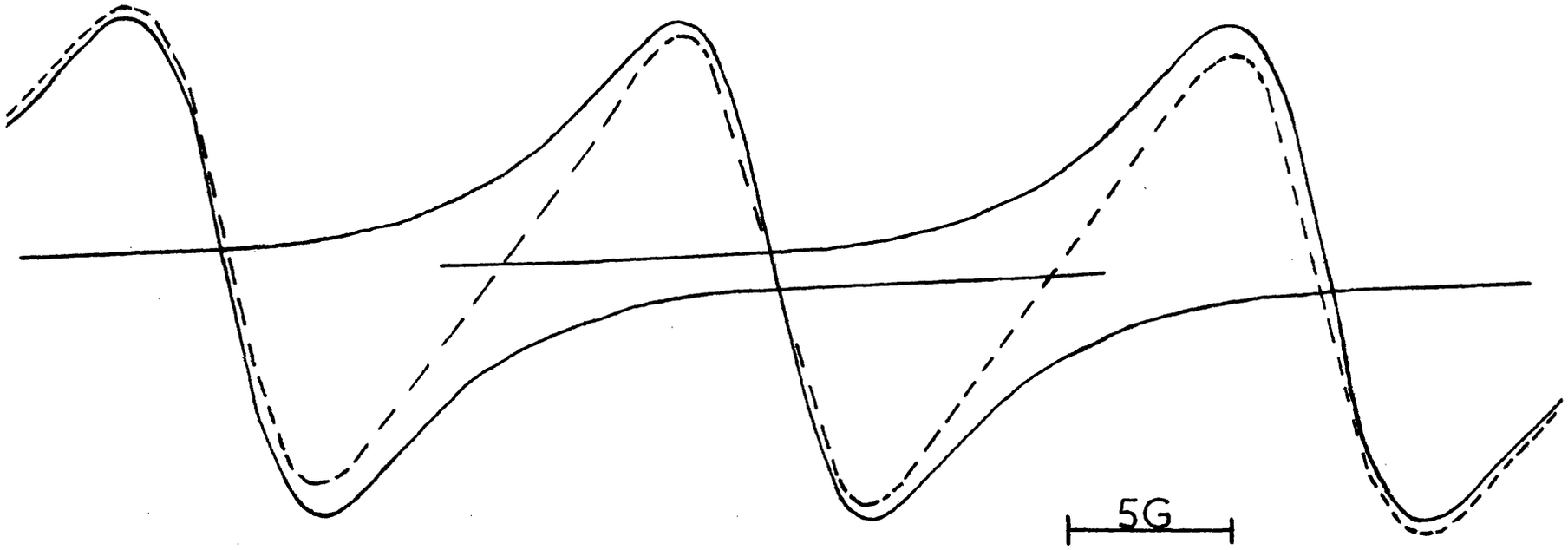

LORENTZIAN LINES 6G WIDE ————————————

SUPERPOSITION OF THREE SUCH LINES — — — — — — — — — —

FIG. 4.2.B. OVERLAP OF 3 LORENTZIAN LINES 6G WIDE WITH ONE LORENTZIAN LINE 10 G WIDE

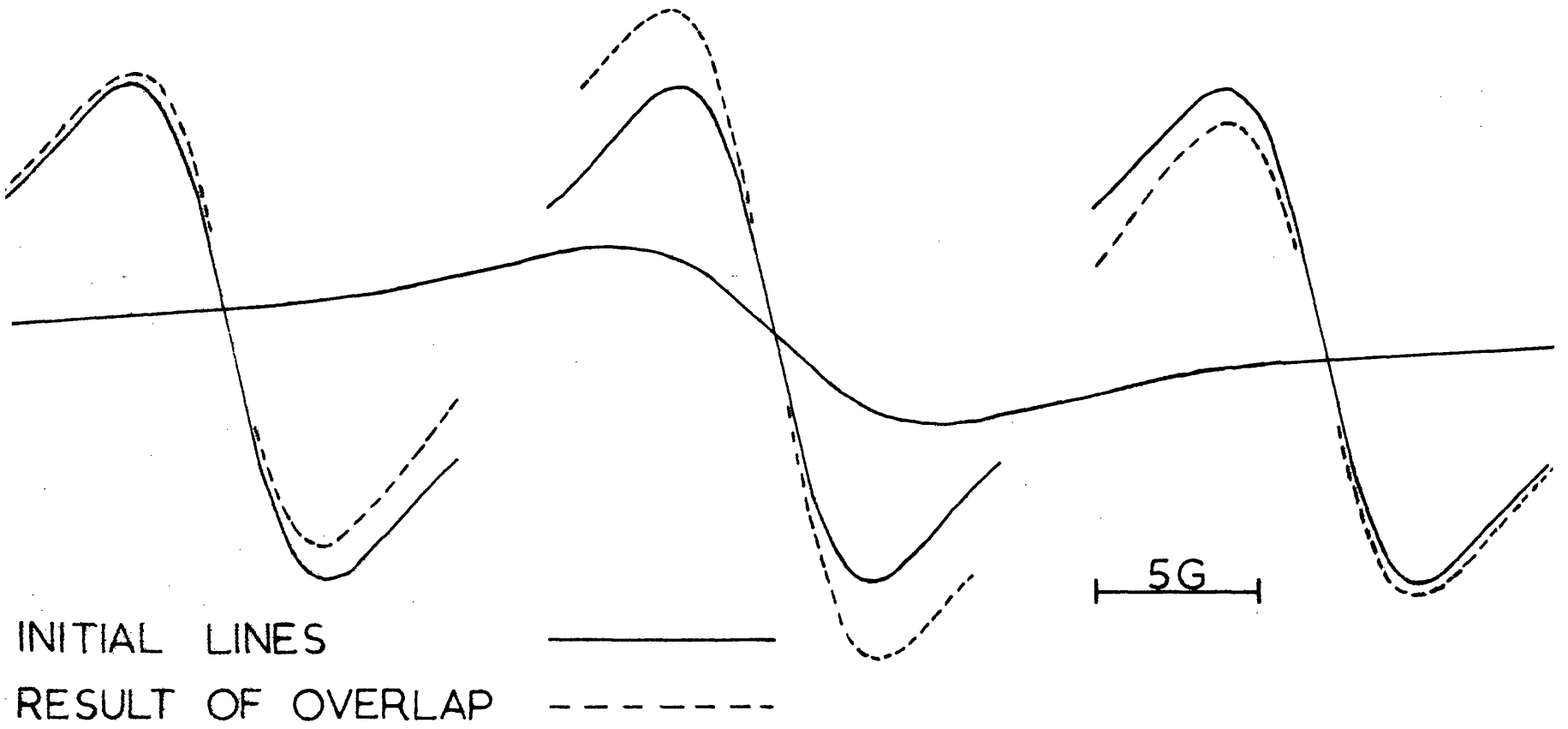

Gaussian and Lorentzian. Therefore the changes in the figure due to overlap will be larger than the changes observed experimentally. The results obtained from overlapping Lorentzian lines thus represent an upper limit for the experimental case.

Figure 4.2-A shows the effects of overlap on three Lorentzian lines 6.0 Gauss wide and 16.9 Gauss apart. Overlap with the other two lines causes the measured peak to peak width of the centre line to decrease by 0.33 G, while the outer lines decrease by 0.18 G in width due to overlap with the central peak. For three Lorentzian lines 16.9 Gauss apart and 3.0 G wide, however, the centre line decreases in width by only 0.01 G due to overlap, while the decrease in the width of the outer two lines is too small to be measured. Thus the overlap of the three monomer lines with each other becomes increasingly important as the monomer linewidth increases from 3.0 Gauss to 6.0 Gauss, and results in a decrease in the observed width of all of the lines, with the centre line being decreased preferentially.

The effect of superimposing upon the three 6.0 G wide lines a 10.0 G wide line concentric with the $M_I = 0$ monomer line and of intensity equal to it is shown in Figure 4.2-B. The overlap with the broad line causes the observed width of the centre line to increase by 0.63 G, while causing the outer lines to decrease in width by 0.18 G. If the overlap of the three monomer lines is considered as well, the net effect of overlap is to increase the central linewidth and to decrease the outer linewidth by about 0.3 Gauss. At lower temperatures the micellar spectrum is better approximated by a Lorentzian line 16.0 Gauss wide. The overlap of this line with three Lorentzian lines 3.0 Gauss wide and 16.9 Gauss apart broadens the central monomer line by 0.02 Gauss, the effect on the outer monomer lines being negligible. Thus at low temperatures and smaller monomer linewidths the effect of overlap is small.

The data in Table 4.2 show the effects of overlap in the high temperature region. In the low temperature region, however, the outer lines are consistently wider than the central line. This effect is the opposite of that expected for overlap with a micellar line, and is an order of magnitude larger than the effect expected from the overlap of the three monomer lines. Thus the observed preferential broadening of the outer lines cannot be due to overlapping spectra. Possible explanations for this effect will be given in Chapter 5.

The spectra of the 5.35×10^{-2}M solution showed the effect of the underlying micellar peak at all temperatures, with the $M_I = 0$ peak being broader and seemingly more intense than the other two peaks. Because of the width of the lines, direct observation of the micellar signal was not possible.

An attempt was made to calculate a monomer-micelle exchange frequency from the difference in the linewidths of the 3.8×10^{-2}M and 4.6×10^{-2}M $C_{10}TABN\dot{O}$ solutions. Since this difference did not change, within the experimental error, as the temperature of the solutions increased, it appeared that any monomer-micelle exchange present was being masked by the effects of Heisenberg spin exchange between the monomers. In an attempt to measure the activation energy of the Heisenberg spin exchange process, 2.01×10^{-2}M and 7.58×10^{-3}M solutions of $C_{10}TABN\dot{O}$ were prepared and their EPR spectra recorded. The linewidth determined by the proton hyperfine envelope (1.7 G) was subtracted from the measured linewidth for these two solutions, and also for the 3.8×10^{-2}M and 4.6×10^{-2}M $C_{10}TABN\dot{O}$ solutions. The results are shown in an Arrhenius plot in Figure 4.3. The slopes, and hence the activation energies, are seen to decrease as the

FIG. 4.3. ARRHENIUS PLOTS FOR $C_{10}TABNO$

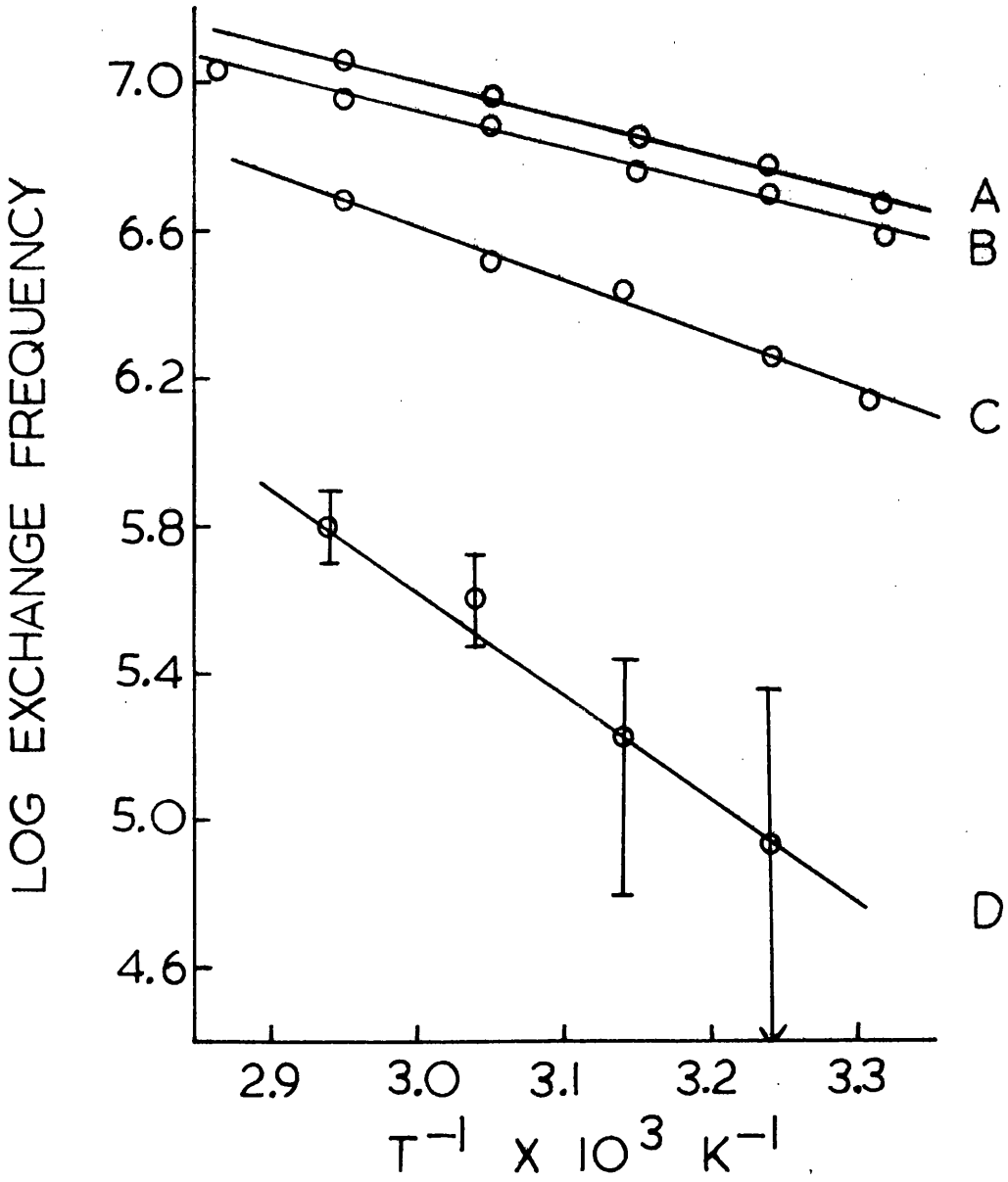

A = 4.6×10^{-2} M

B = 3.8×10^{-2} M

C = 2.0×10^{-2} M

D = 7.6×10^{-3} M

concentration of surfactant increases, the activation energies falling from about 13 kcal to about 4.5 kcal over the four concentrations shown. If Heisenberg spin exchange were the only process being monitored here, and if Heisenberg spin exchange is diffusion controlled, as has been assumed [45], then one would expect a constant activation energy at all concentrations of surfactant, of magnitude similar to the 5.3 kcal activation energy for the self-diffusion of water [48]. The 4.5 kcal activation energies observed just above and just below the cmc might be due to this process (note the negligible effect of the cmc upon the observed activation energy) but the activation energies at lower concentrations are too high to be accounted for by this process.

4.3. Addition of Inorganic Salts to the Cationic Nitroxide Surfactant Systems

The presence of inorganic salt lowers the cmc of ionic surfactants, the magnitude of the effect being dependent upon the charge of the ion whose charge is opposite in sign to the charge on the surfactant molecule [49]. For a given added salt, the cmc at first decreases rapidly with increasing salt concentration, and then at higher salt concentrations reaches a constant value [49]. The maximum amount that the cmc can be lowered with a given inorganic salt increases with the length of the hydrocarbon chain of the surfactant [49]. Thus 0.1 M NaCl lowers the cmc of both dodecyltrimethylammonium bromide ($C_{12}TAB$) and tetradecyltrimethylammonium bromide ($C_{14}TAB$) almost to the constant value, the lowering at 23°C being by a factor of three in the first case and by a factor of four in the second [50]. It was hoped that, by increasing the number of micelles present in a paramagnetic cationic surfactant solution by adding inorganic salt, the effects of Heisenberg spin exchange due to increasing paramagnetic surfactant concentration could be minimised.

Inorganic anions and cations have an effect on the structure of the water in which they dissolve, some enhancing this structure (structure making ions) and some disrupting it (structure breaking ions) [51,52]. Another purpose of these experiments was to investigate the effect of water structure on the activation energy required for the micellisation process by using inorganic salts of varying structure making or structure breaking abilities to lower the cmc of the cationic nitroxide surfactant.

A solution 1×10^{-3}M in $C_{14}TABN\dot{O}$, whose cmc ranges from 2.1×10^{-3}M at 25°C to 2.7×10^{-3}M at 60°C, and 2.3×10^{-1}M in NaCl was prepared. By analogy with $C_{14}TAB$[50], one would expect the salt addition to have lowered the cmc to the lowest value attainable, and that the magnitude of the cmc would be reduced by approximately a factor of four. Thus at room temperature about half of the surfactant present in this solution should be in micellar form. The EPR spectrum of this solution contained a broad line, as well as three sharp lines attributed to monomeric $C_{14}TABN\dot{O}$. Thus micelles were present in the solution. The three sharp lines showed proton hyperfine structure, which slowly disappeared as the sample was heated to 98°C. The proton hyperfine lines were not broadened enough to broaden their resultant envelope, however. These results mean that the monomer-micelle exchange frequency in this system is more than an order of magnitude slower than that observed in more concentrated $C_{14}TABN\dot{O}$ solutions in the absence of NaCl. Two possible explanations for this are either that NaCl, a slight net structure maker [51], has somehow greatly raised the activation energy needed for the micellisation process, or that the process which causes the line broadening at higher $C_{14}TABN\dot{O}$ concentrations is not monomer-micelle exchange.

The effect of added inorganic salt on the observed linewidths of $C_{12}TABN\dot{O}$ solutions between 25°C and 98°C is shown in Figure 4.4. By analogy with $C_{12}TAB$[50], the cmc should be decreased by a factor of about three from its normal value of around 9×10^{-3}M, and should not decrease greatly with increasing inorganic salt concentration, since the salt concentrations used are at or above 0.1 M. Micellar signals were observed in the 1.2×10^{-1}M NaCl/ 7.8×10^{-3}M $C_{12}TABN\dot{O}$, 1.2×10^{-1}M NaCl/9.75×10^{-3}M $C_{12}TABN\dot{O}$, and 1×10^{-1} LiF/1×10^{-3}M $C_{12}TABN\dot{O}$ solutions, and in the 1.47×10^{-2}M $C_{12}TABN\dot{O}$ solution used for comparison.

The line broadening was calculated by subtracting the line widths observed in either 2×10^{-3}M C_{12} $TABN\dot{O}$ solution containing 1.2×10^{-1}M NaCl or 1.0×10^{-1}M LiF, or a 5×10^{-3}M $C_{12}TABNO$ solution, as appropriate, from the line widths observed in the more concentrated solution. None of the solutions were de-gassed.

The monomer lines broadened as the temperature increased, but at temperatures above 70°C the rate of broadening decreased in most cases, resulting in a lower slope in the Arrhenius plots. This indicates that either the activation energy for the micellisation process changes abruptly at 70°C, or that at least two processes with different activation energies are occurring in the solution, with one process being dominant at lower temperatures and the other becoming dominant at higher temperatures. The slopes observed at low temperature range between 9.6 and 10.7 kcal $mole^{-1}$, while the lowest high temperature slope gives an activation energy of 5.9 kcal $mole^{-1}$. Heisenberg spin exchange may be the process responsible for at least one of the activation energies, and is probably responsible for the general increase in linewidth with increase in total surfactant concentration.

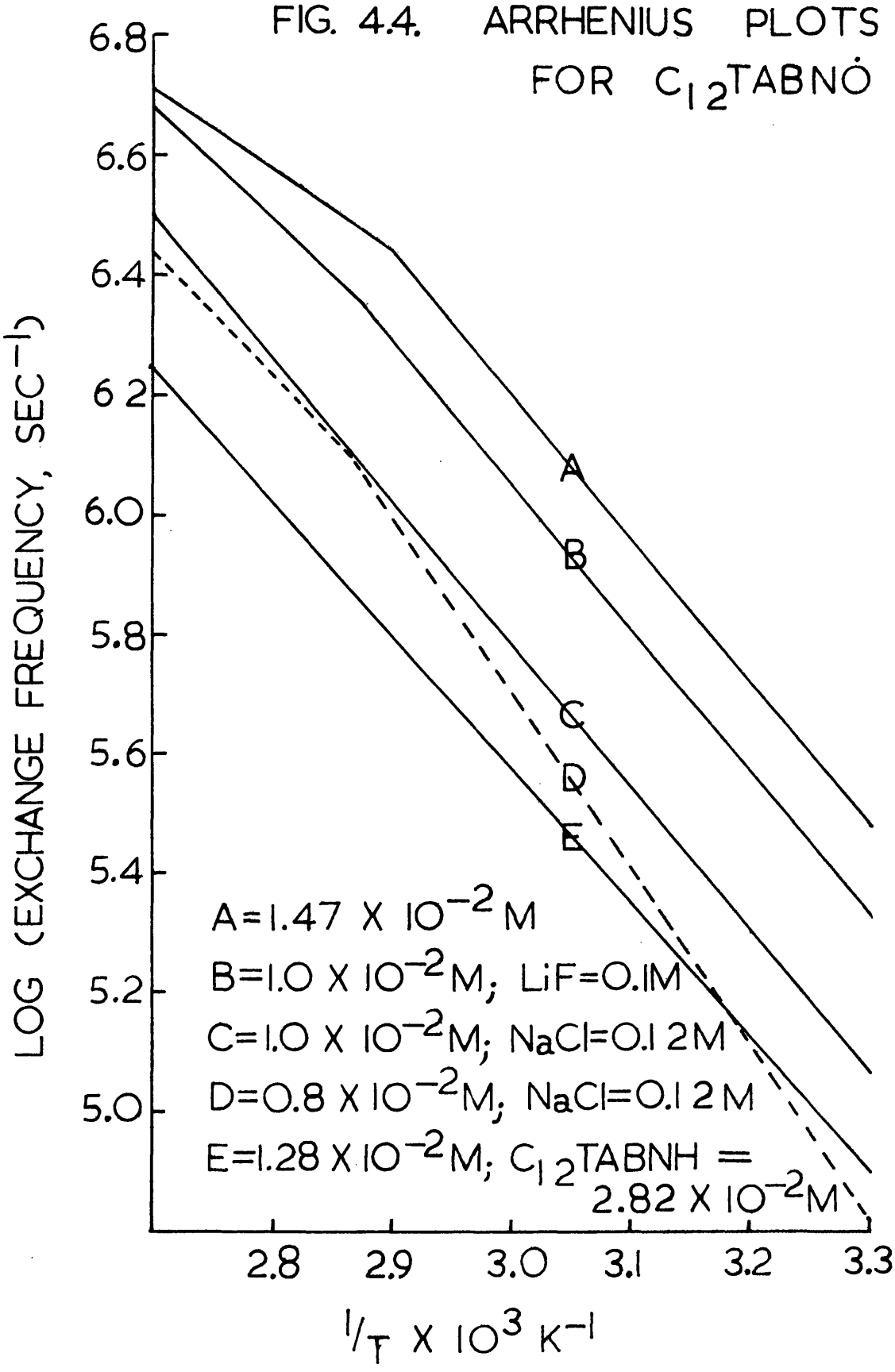
FIG. 4.4. ARRHENIUS PLOTS FOR $C_{12}TABNO^{\cdot}$
LOG (EXCHANGE FREQUENCY, SEC^{-1})
6.8
6.6
6.4
6.2
6.0
5.8
5.6
5.4
5.2
5.0
A
B
C
D
E
A=1.47 X 10^{-2} M
B=1.0 X 10^{-2}M; LiF=0.1M
C=1.0 X 10^{-2}M; NaCl=0.12M
D=0.8 X 10^{-2}M; NaCl=0.12M
E=1.28 X 10^{-2}M; $C_{12}TABNH$ = 2.82 X 10^{-2}M
2.8
2.9
3.0
3.1
3.2
3.3
$1/T$ X 10^3 K^{-1}

Figure 4.4 shows that LiF, which is a strong structure maker [50], has increased the linewidth of 1×10^{-2}M $C_{12}TABN\dot{O}$ solutions over the linewidth observed in the presence of a similar concentration of NaCl. From the $C_{14}TABN\dot{O}$ results in the presence of NaCl, one would have expected the stronger structure maker LiF to have depressed the monomer-micelle exchange frequency from that observed with NaCl, if the structure making properties of the salt were responsible for the apparent increase in the activation energy for monomer-micelle exchange. Thus these results make it more probable that the high concentration results observed with $C_{14}TABN\dot{O}$ are not due to monomer-micelle exchange.

Another way to change the monomer to micelle ratio of a paramagnetic surfactant solution is to add a diamagnetic surfactant to that solution. If the fraction of paramagnetic surfactant present is still relatively large, enough paramagnetic molecules will be present in each micelle to give a broad micellar signal, and to make the micellar environment distinctly magnetically different from the monomer environment. A solution of $C_{12}TABN\dot{O}$ containing the amine precursor to the nitroxide C_{12}TABNH should be suitable for this type of study, as the values of the cmc of each of these surfactants should be similar The main effect of the addition of C_{12}TABNH should be to increase the total number of mixed micelles, while decreasing the proportion of paramagnetic monomers in both micellar and aqueous environments.

A solution containing 1.28×10^{-2}M C_{12}TABNO$\dot{}$ and 2.82×10^{-2}M C_{12}TABNH was prepared. The EPR spectra of this solution contained a micellar peak. Spectra of the C_{12}TABNO$\dot{}$ in this solution were recorded at temperatures ranging from 25°C to 98°C. The samples were not de-gassed. The amount of broadening in excess of that found in a 5×10^{-3}M C_{12}TABNO$\dot{}$ solution was calculated, and used to compile an Arrhenius plot, which is included in Figure 4.4. Although the activation energy, 10.0 kcal mole^{-1}, is approximately the same as that found at lower temperatures for the other solutions involved in the figure, the total amount of broadening is significantly less. A less concentrated solution which contained 6.4×10^{-3}M C_{12}TABNO$\dot{}$ 1.4×10^{-2}M C_{12}TABNH was also prepared, but the EPR spectra of this solution were almost the same as the spectra of 5×10^{-3}M C_{12}TABNO$\dot{}$. The linewidth difference increased to 0.12 G at 98°C, which represents an exchange frequency of 2.5×10^{5} sec^{-1}. Although micelles would be expected to be present in this solution their spectrum was not intense enough to be detectable by EPR. Thus, if micelles are not present in this solution, the small increased broadening may represent the difference in the Heisenberg spin exchange frequencies in the two solutions. The result in the more concentrated solution is harder to explain, for it seems that C_{12}TABNH either reduces the monomer-micelle exchange frequency, the Heisenberg spin exchange present in the system, or the effectiveness of monomer-micelle exchange in producing line broadening. It was decided to examine the Heisenberg spin exchange in the systems under study to see if this could help resolve the problem.

4.4. Heisenberg Spin Exchange in the Cationic Nitroxide Systems

In order to observe Heisenberg spin exchange uncomplicated by the presence of monomer-micelle exchange, solutions of $C_1TABN\dot{O}$, which does not micellise, were prepared at various concentrations. Since the solid $C_1TABN\dot{O}$ was hygroscopic, the concentration of nitroxide was determined by comparison with a 1×10^{-2}M $C_{10}TABN\dot{O}$ solution, using EPR intensity data. $C_1TABN\dot{O}$ should have the same dependence of Heisenberg spin exchange on concentration as the longer chain nitroxides, since the magnitude and location of the positive charge and the molecular geometry near the nitroxide group are the same in both cases.

The Heisenberg spin exchange process is assumed to be diffusion controlled [41]. For such a process the rate constant k_1 for the reaction in which two monomers collide to form a dimer will be given by: [45]

$$k_1 = 4\pi dDf \qquad (4.2)$$

where d is the "interaction distance" for the exchange, f is a factor which contains the effects of like electric charges upon the collision frequency, and D is the diffusion coefficient. In a Stokes-Einstein model D is given by:

$$D = \frac{kT}{6\pi a\eta} \qquad (4.3)$$

where a is the molecular radius, T the temperature in K, the solvent viscosity, and k is Boltzmann's constant. By substituting equation 4.3 into equation 4.2 one finds that:

$$k_1 = \frac{2kd}{3a} \; (f) \; (\frac{T}{\eta}) \qquad (4.4)$$

Since the exchange frequency P_{FF} for a diffusion controlled process is given by:

$$P_{FF} = k_1 C \qquad (4.5)$$

FIG. 4.5. LINEWIDTH VS. T/η FOR 1.36×10^{-2}M C_1TABNO

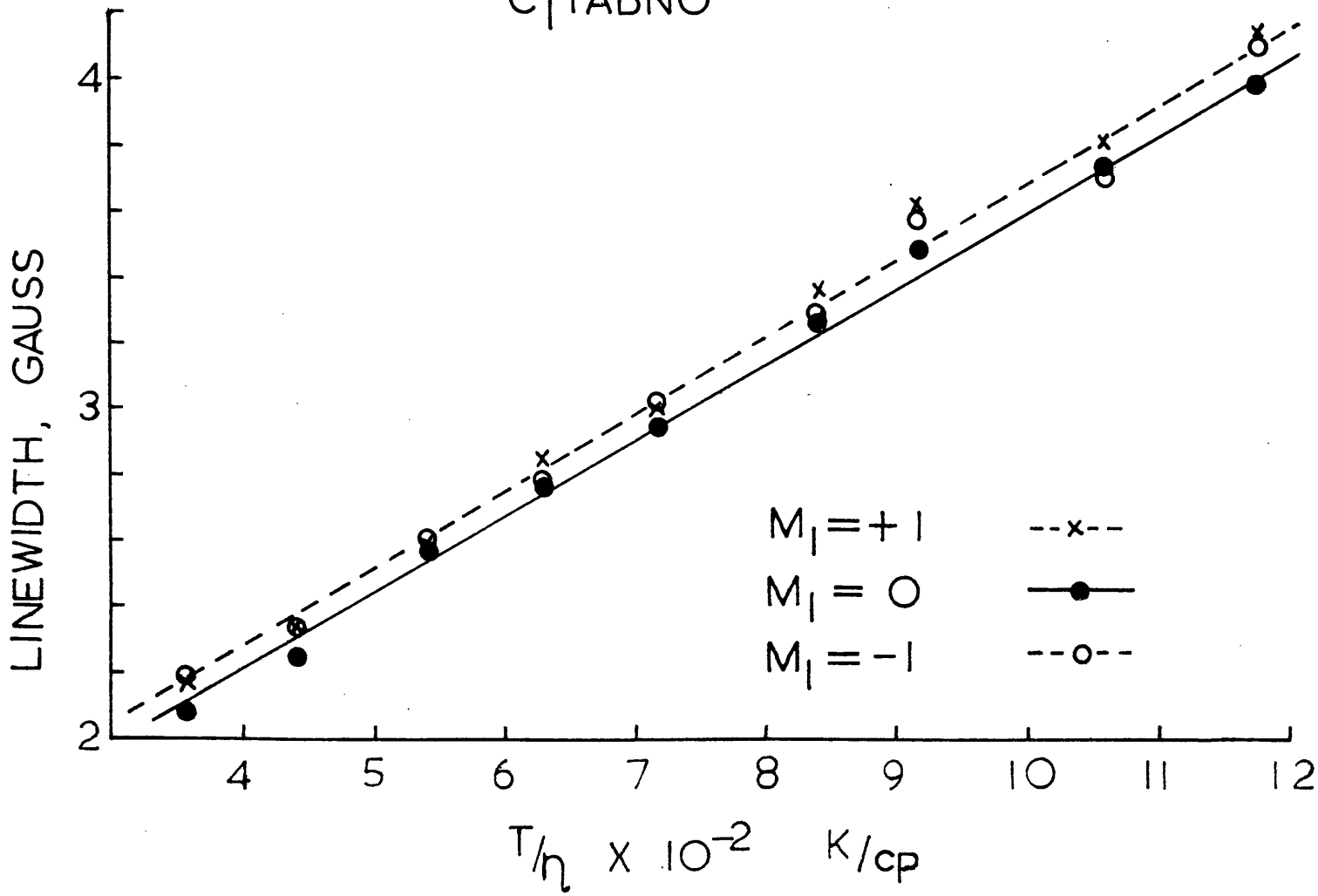

FIG. 4.6. LINEWIDTH VS. T/η FOR 8.34×10^{-3} M C_1TABNO

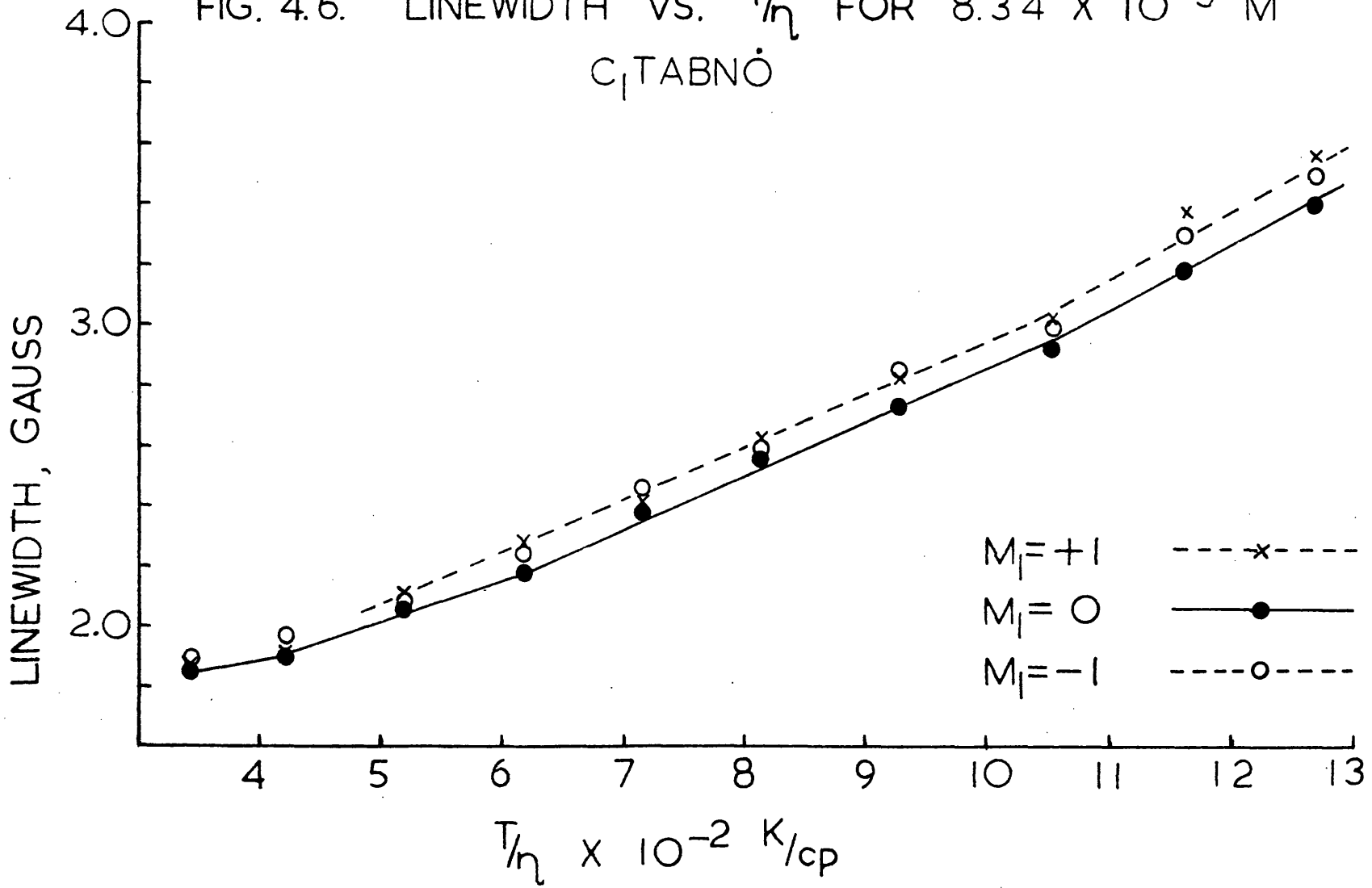

FIG. 4.7. LINEWIDTH VS. T/η FOR 4.18×10^{-3} M C_1TABNO

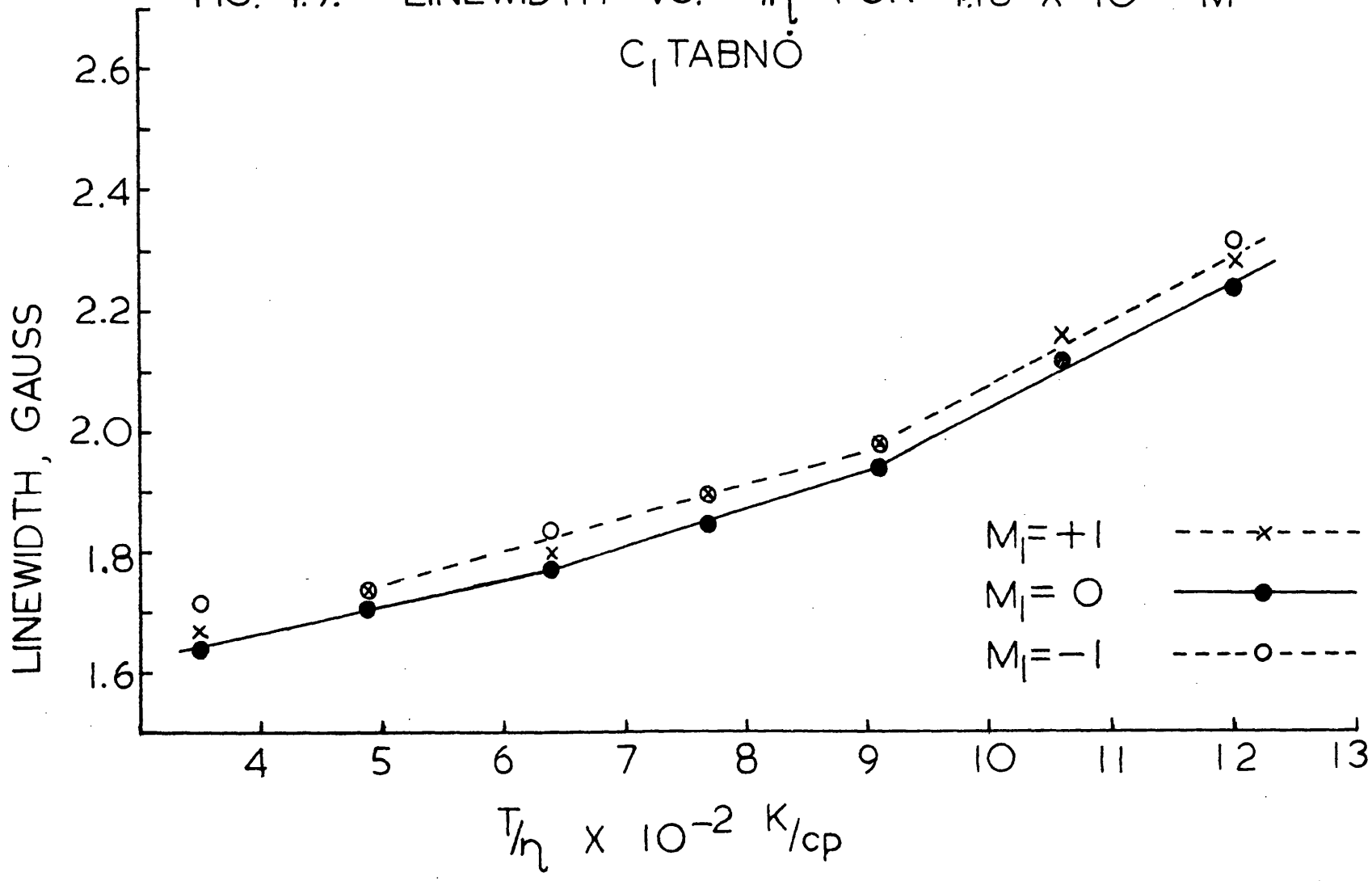

FIG. 4.8. LINEWIDTH VS. T/η FOR 2.48×10^{-3} M C_1TABNO

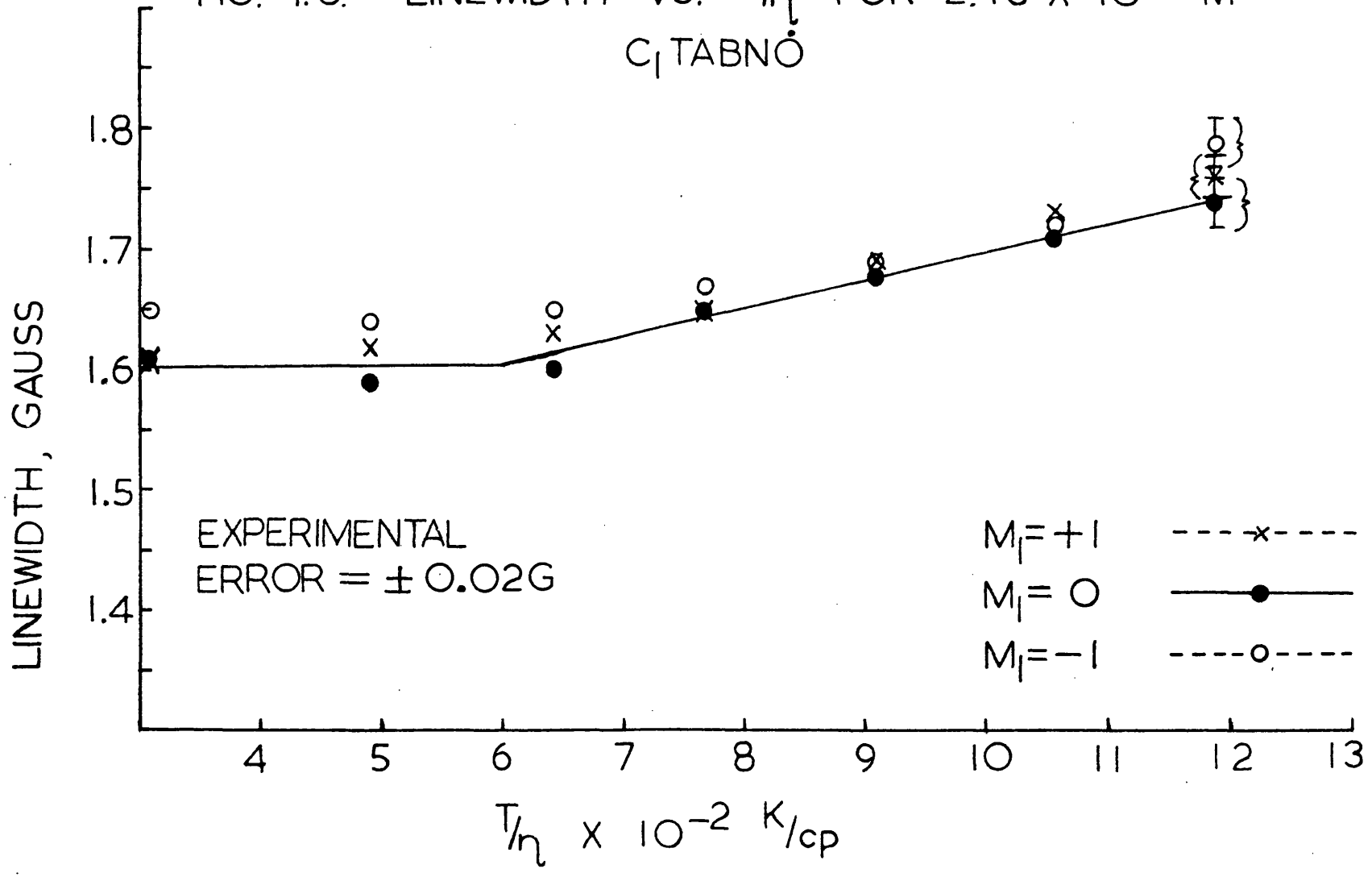

where C is the concentration of monomer radicals, by equation 4.1 the observed line broadening will be proportional to k_1, and hence to $\frac{T}{\eta}$. Thus for a given concentration of radicals undergoing Heisenberg spin exchange, a plot of the observed linewidth vs $\frac{T}{\eta}$ should yield a straight line.

Figures 4.5 to 4.20 contain experimental linewidth vs $\frac{T}{\eta}$ graphs for some $C_1TABN\dot{O}$, $C_{12}TABN\dot{O}$, and $C_{14}TABN\dot{O}$ solutions discussed earlier in this chapter. The $C_1TABN\dot{O}$ solutions shown in Figures 4.5 to 4.8 show the expected linear behaviour in the linewidth vs $\frac{T}{\eta}$ plots, with some deviation at low $\frac{T}{\eta}$ in the lower concentration samples due to the presence of proton hyperfine structure. The spectra for the more concentrated samples at higher temperatures show slight deviations from linearity, with the $M_I = \pm 1$ lines behaving differently from the $M_I = 0$ line. This will be discussed further in Chapter 5.

The $C_{10}TABN\dot{O}$ solutions in Figures 4.9 to 4.12 show the expected linear behaviour in the linewidth vs $\frac{T}{\eta}$ plot, except for the effect of proton hyperfine structure at low $\frac{T}{\eta}$. The high $\frac{T}{\eta}$ points in Figure 4.12 show deviations from linearity in the general directions expected from overlap with a broad micellar line, but otherwise the presence of micelles is not indicated, and no evidence of monomer-micelle exchange is seen.

Figures 4.13 to 4.18 give the linewidth vs $\frac{T}{\eta}$ data for $C_{12}TABN\dot{O}$ solutions, including solutions in the presence of either inorganic salts or the amine precursor of the nitroxide, $C_{12}TABNH$. The graph for 1.47×10^{-2}M $C_{12}TABN\dot{O}$, Figure 4.13, exhibits a marked departure from linearity in the central portion of the graph, unlike previous Figures. Similar non-linear behaviour is also seen in Figures 4.14 to

FIG. 4.9. LINEWIDTH VS. T/η FOR 2.58×10^{-3} M $C_{10}TABNO$

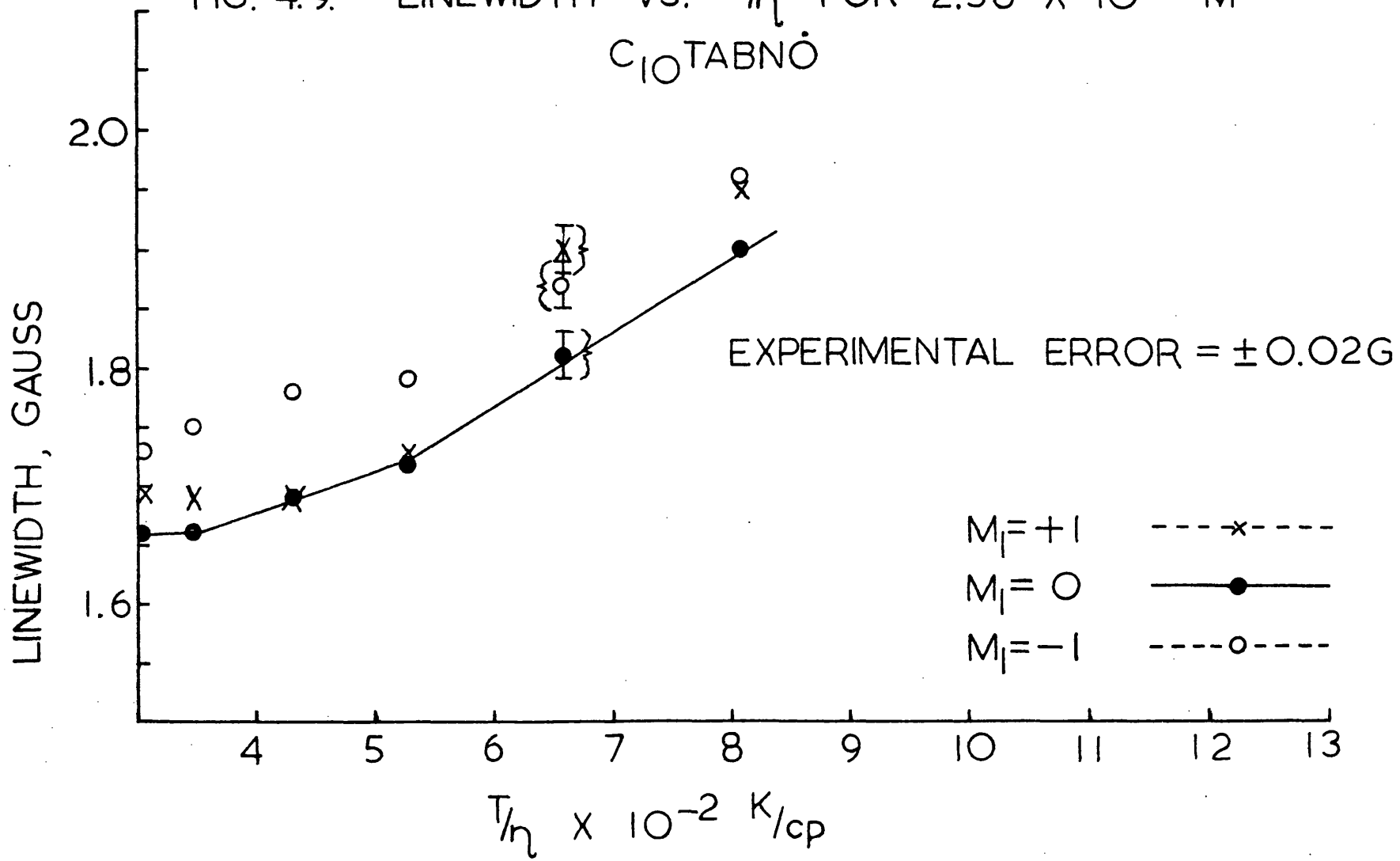

FIG. 4.10. LINEWIDTH VS. T/η FOR 2.0×10^{-2} M $C_{10}TABNO$

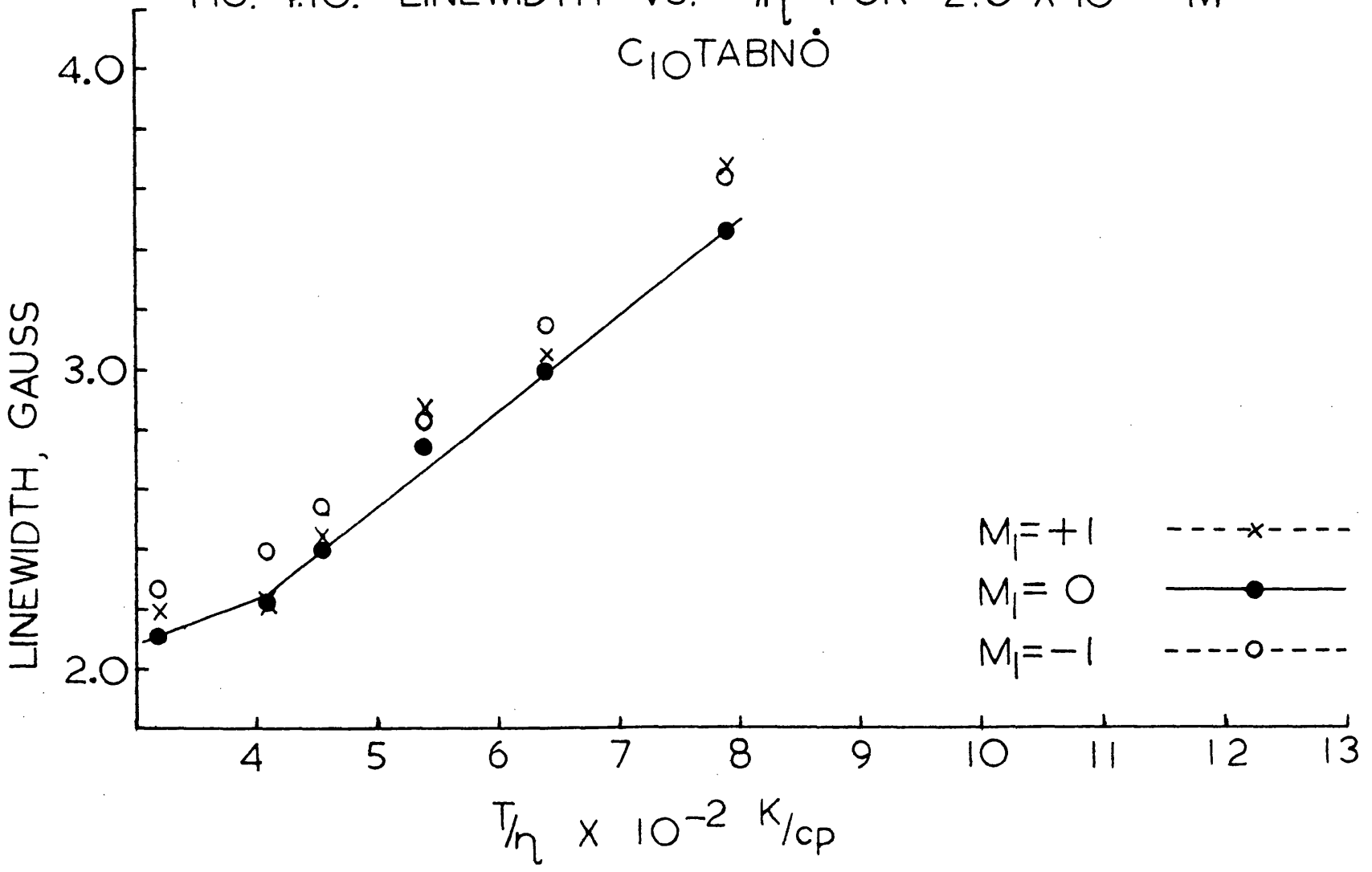

FIG. 4.11. LINEWIDTH VS. T/η FOR 3.8×10^{-2} M $C_{10}TABNO$

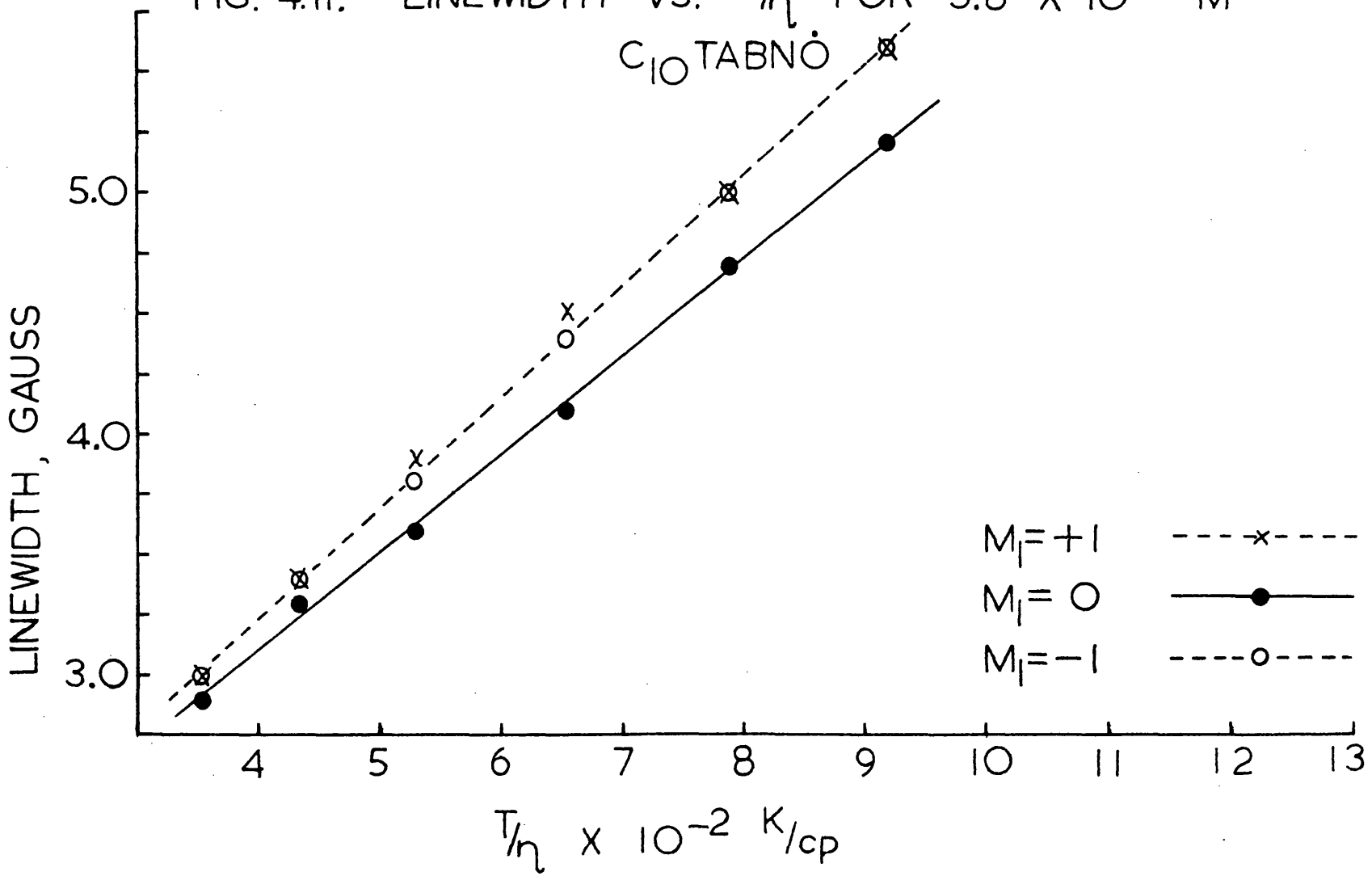

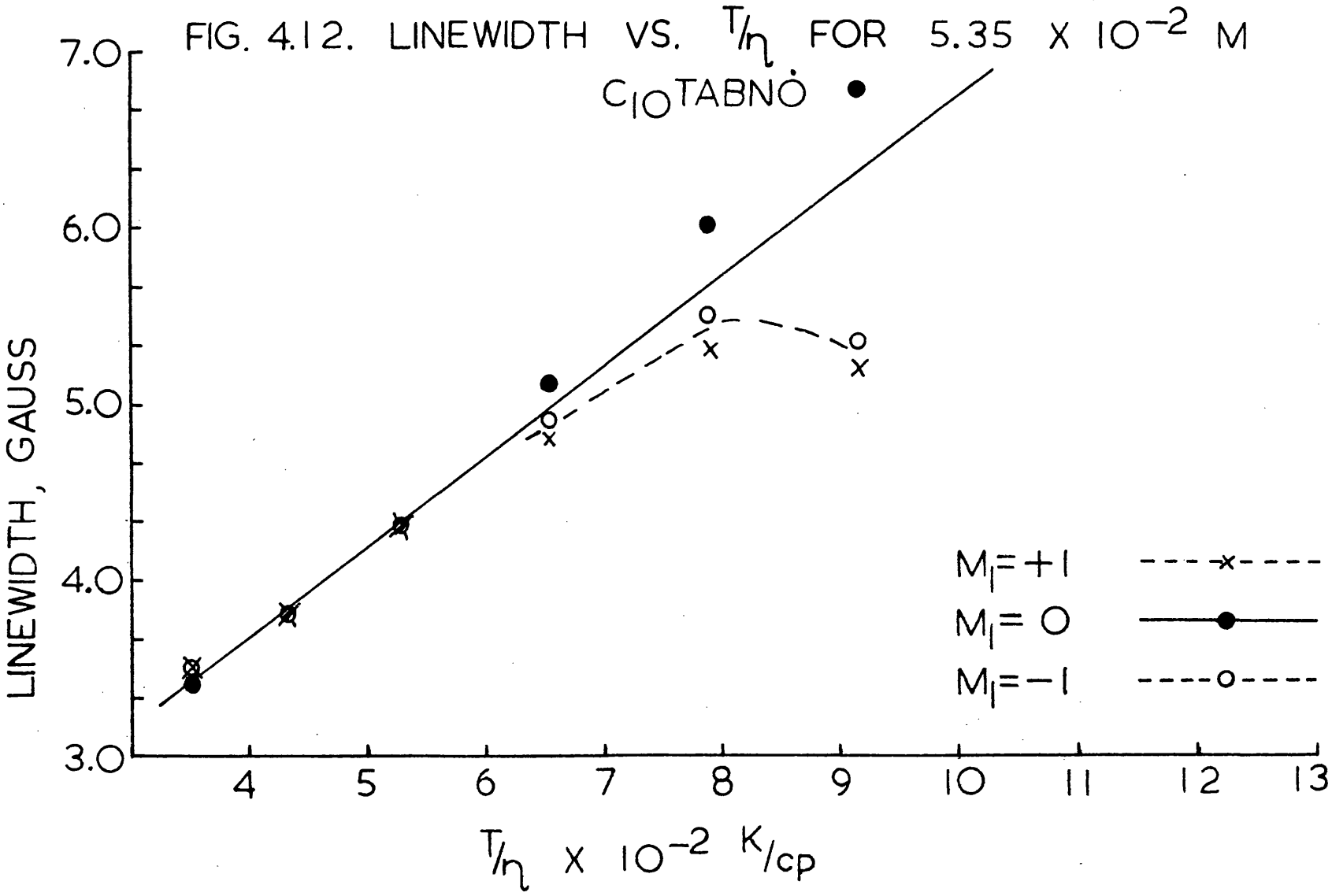
FIG. 4.12. LINEWIDTH VS. T/η FOR 5.35 X 10^-2 M
C10TABNO
LINEWIDTH, GAUSS
7.0
6.0
5.0
4.0
3.0
4
5
6
7
8
9
10
11
12
13
T/η X 10^-2 K/cp
M1=+1
M1= 0
M1=-1

FIG. 4.13. LINEWIDTH VS. T/η FOR 1.47×10^{-2} M $C_{12}TABNO$

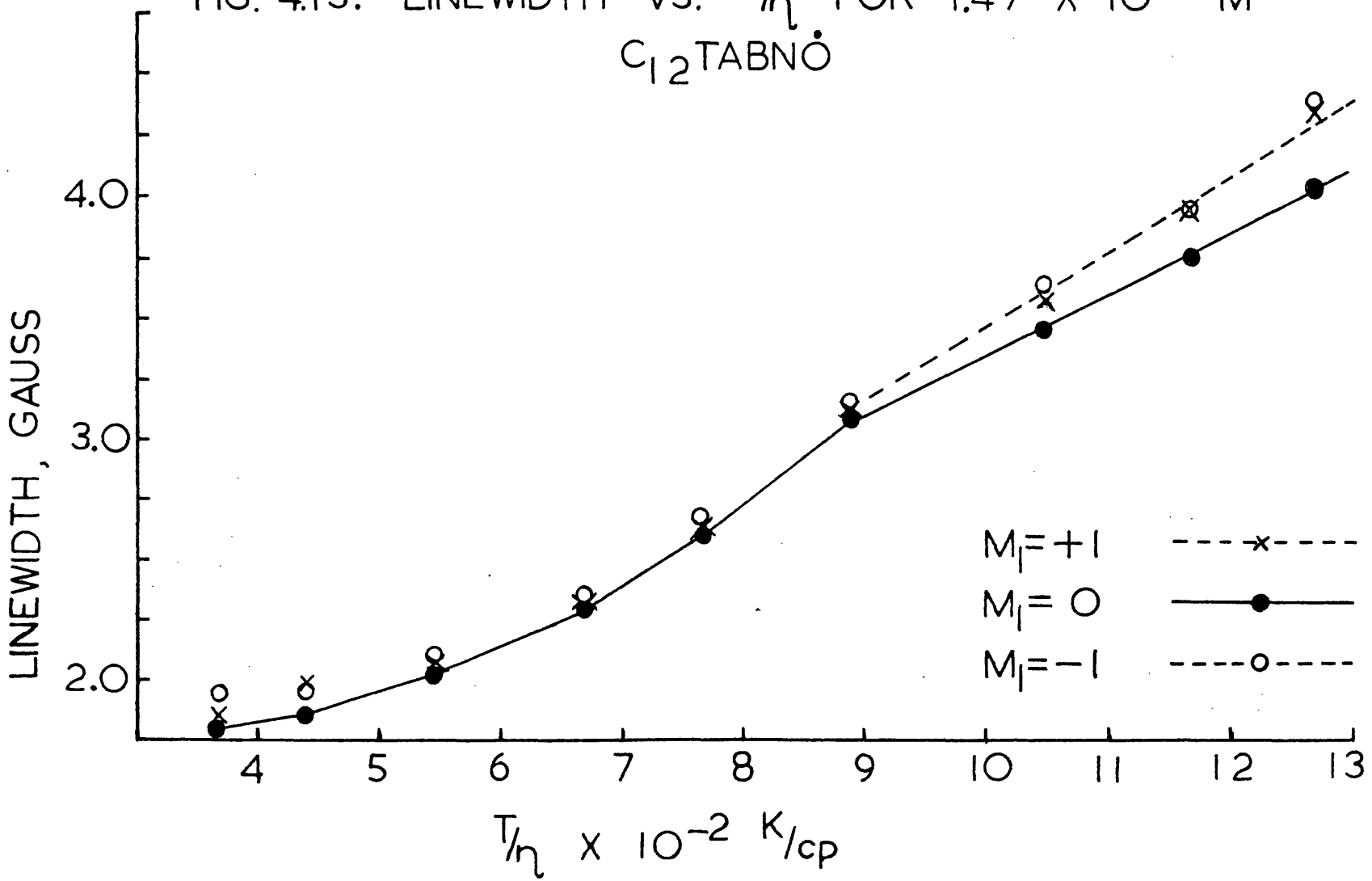

FIG. 4.14. LINEWIDTH VS. T/η FOR 1.36×10^{-2} M $C_{12}TABNH$, 0.64×10^{-2} M $C_{12}TABNO^{\cdot}$

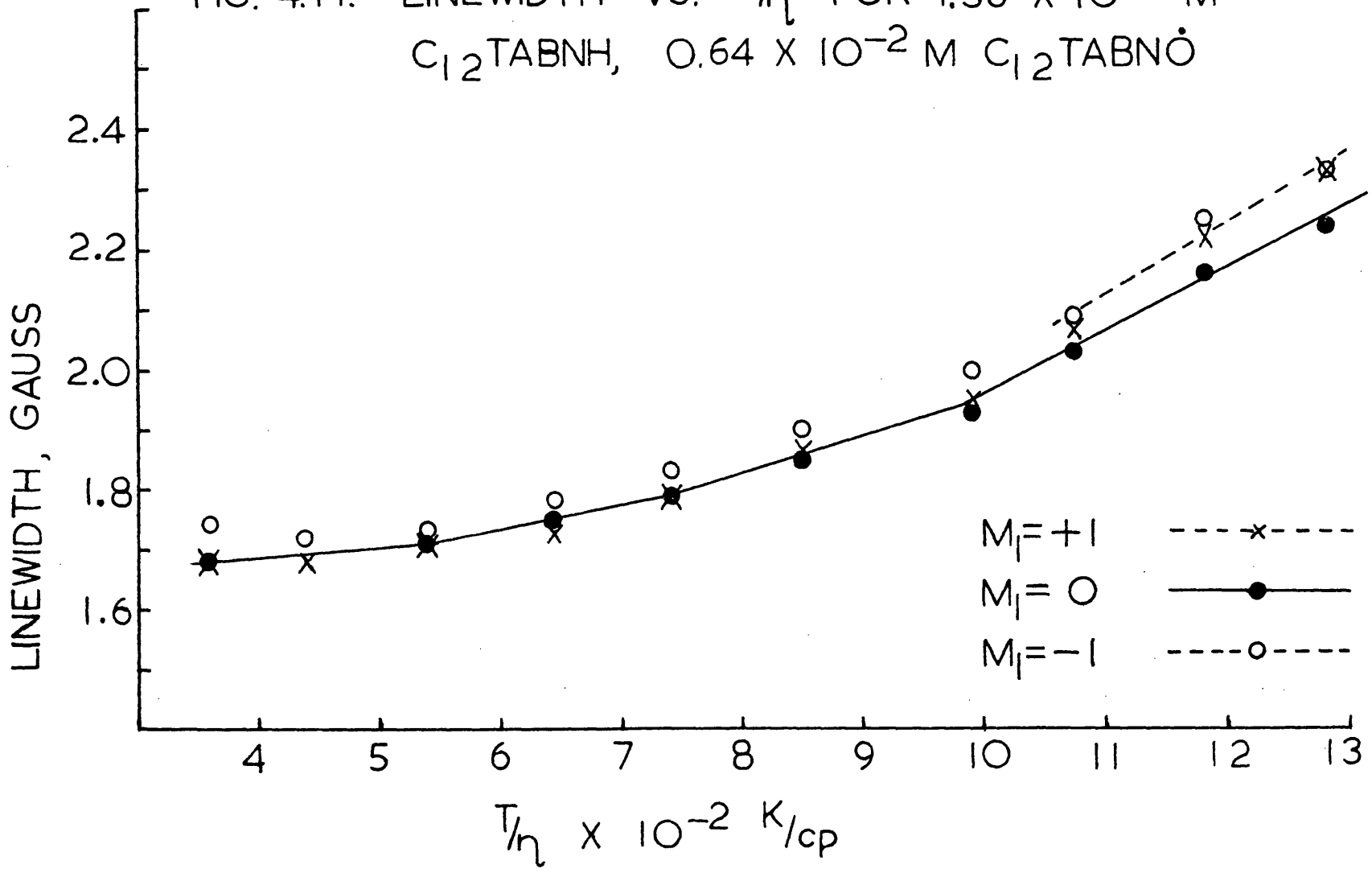

FIG. 4.15. LINEWIDTH VS. T/η FOR 2.72×10^{-2} M C_{12}TABNH, 1.28×10^{-2} M C_{12}TABNO

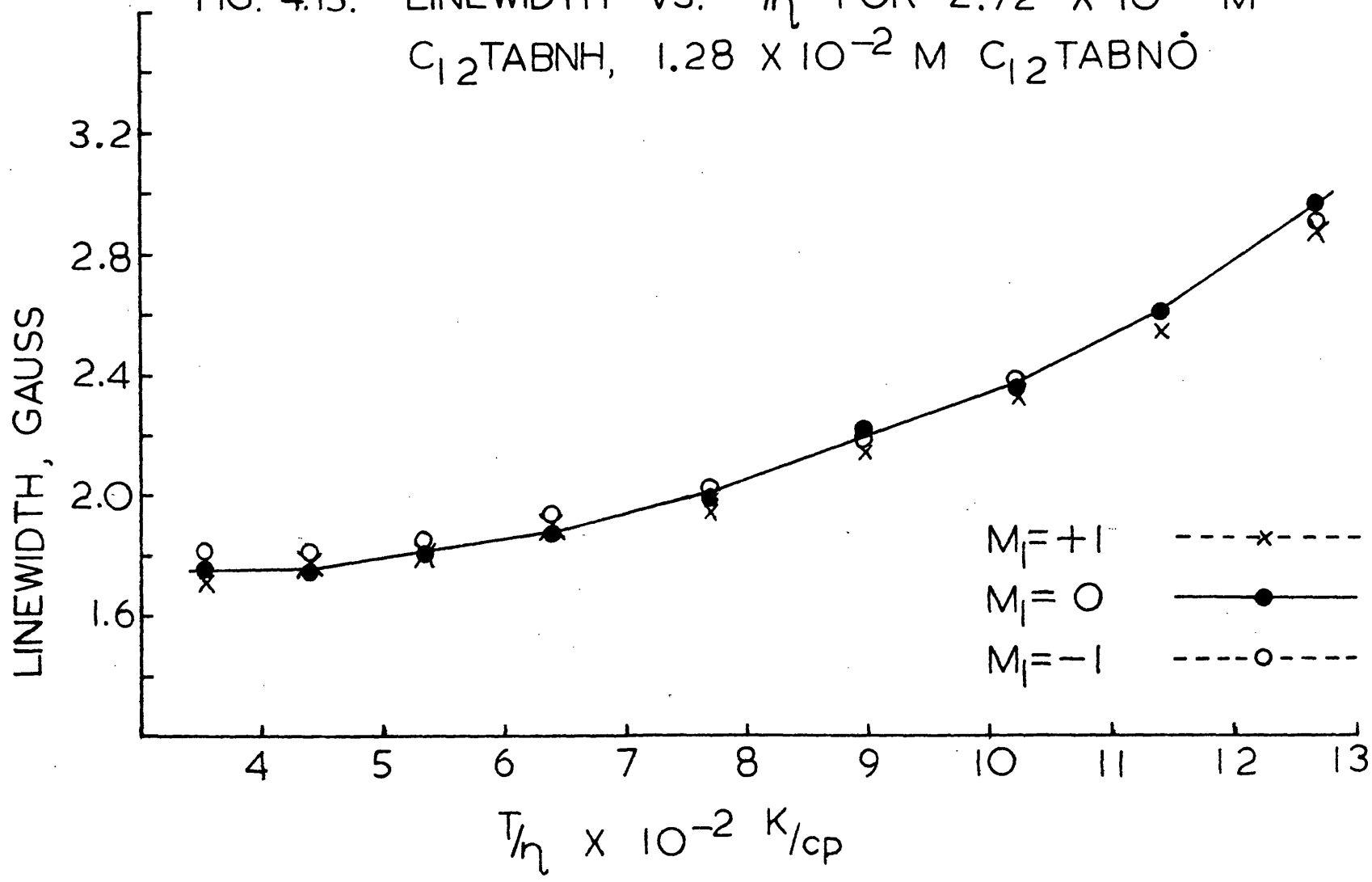

FIG. 4.16. LINEWIDTH VS. T/η FOR 1.0×10^{-2} M $C_{12}TABNO$, 0.1 M LiF

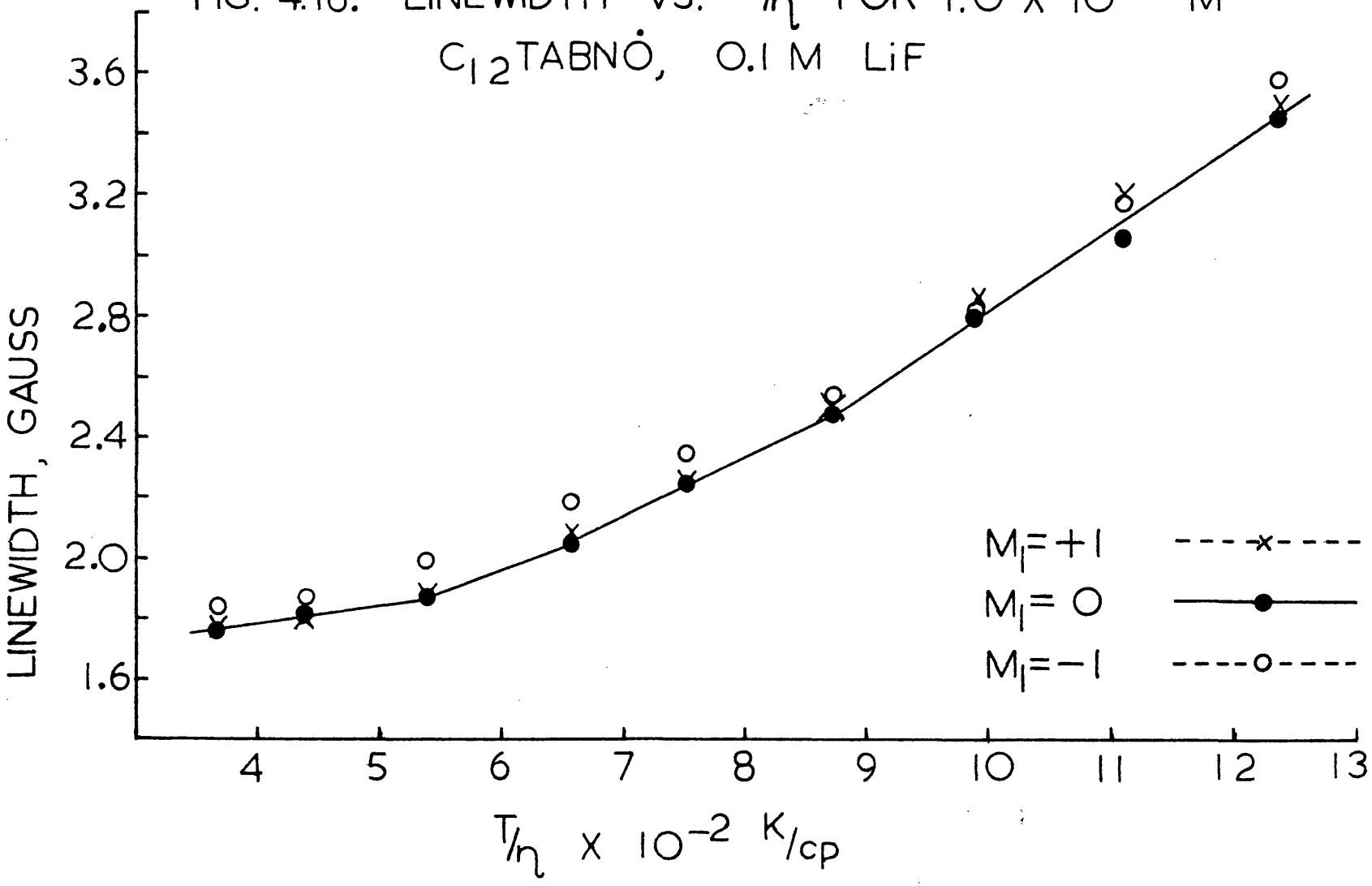

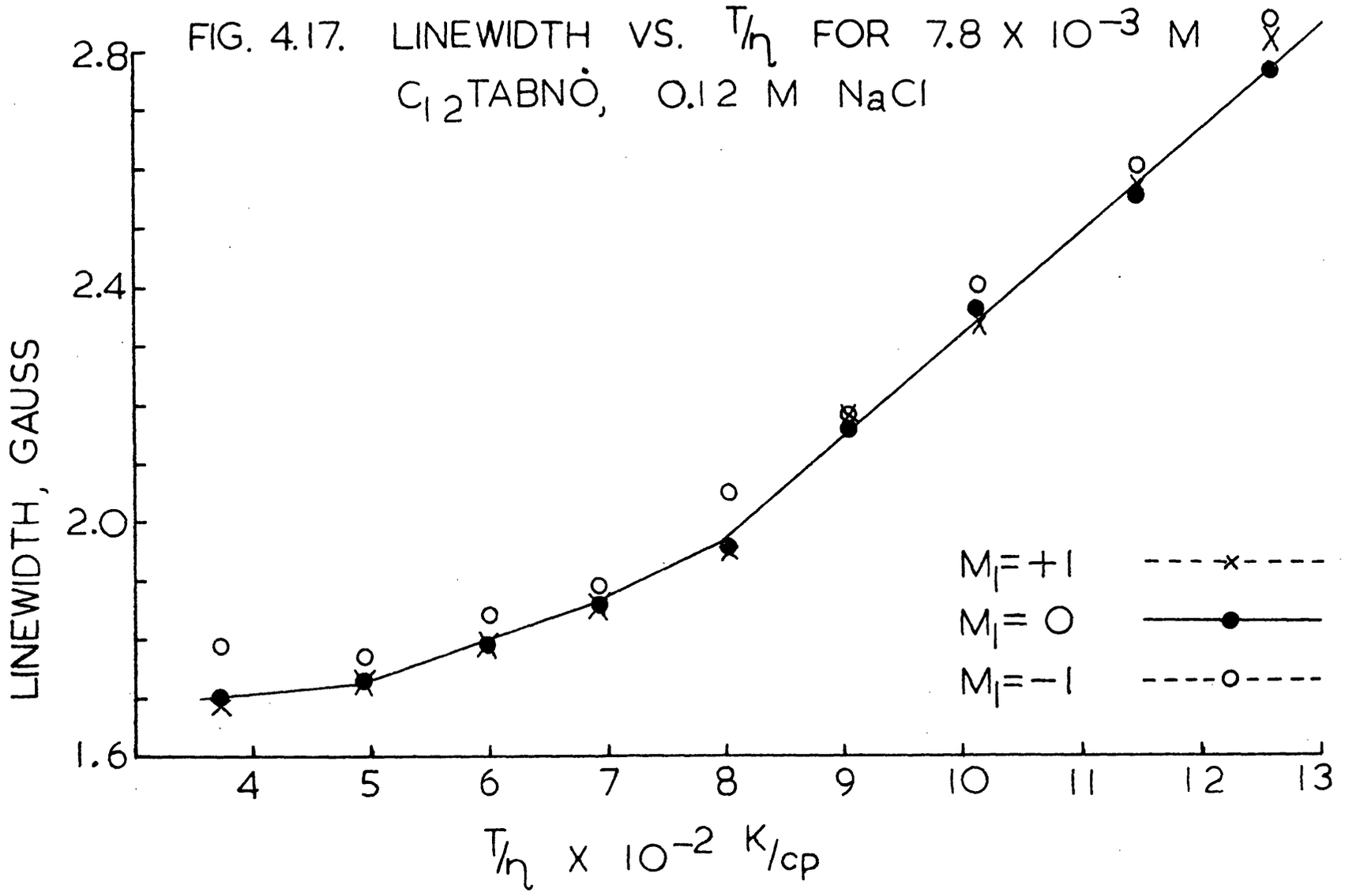
FIG. 4.17. LINEWIDTH VS. T/η FOR 7.8 X 10⁻³ M
C12TABNO, 0.12 M NaCl
LINEWIDTH, GAUSS
2.8
2.4
2.0
1.6
4
5
6
7
8
9
10
11
12
13
T/η X 10⁻² K/cp
M_I = +1
M_I = 0
M_I = −1

FIG. 4.18. LINEWIDTH VS. T/η FOR 9.75×10^{-3} M $C_{12}TABNO$, 0.12 M NaCl

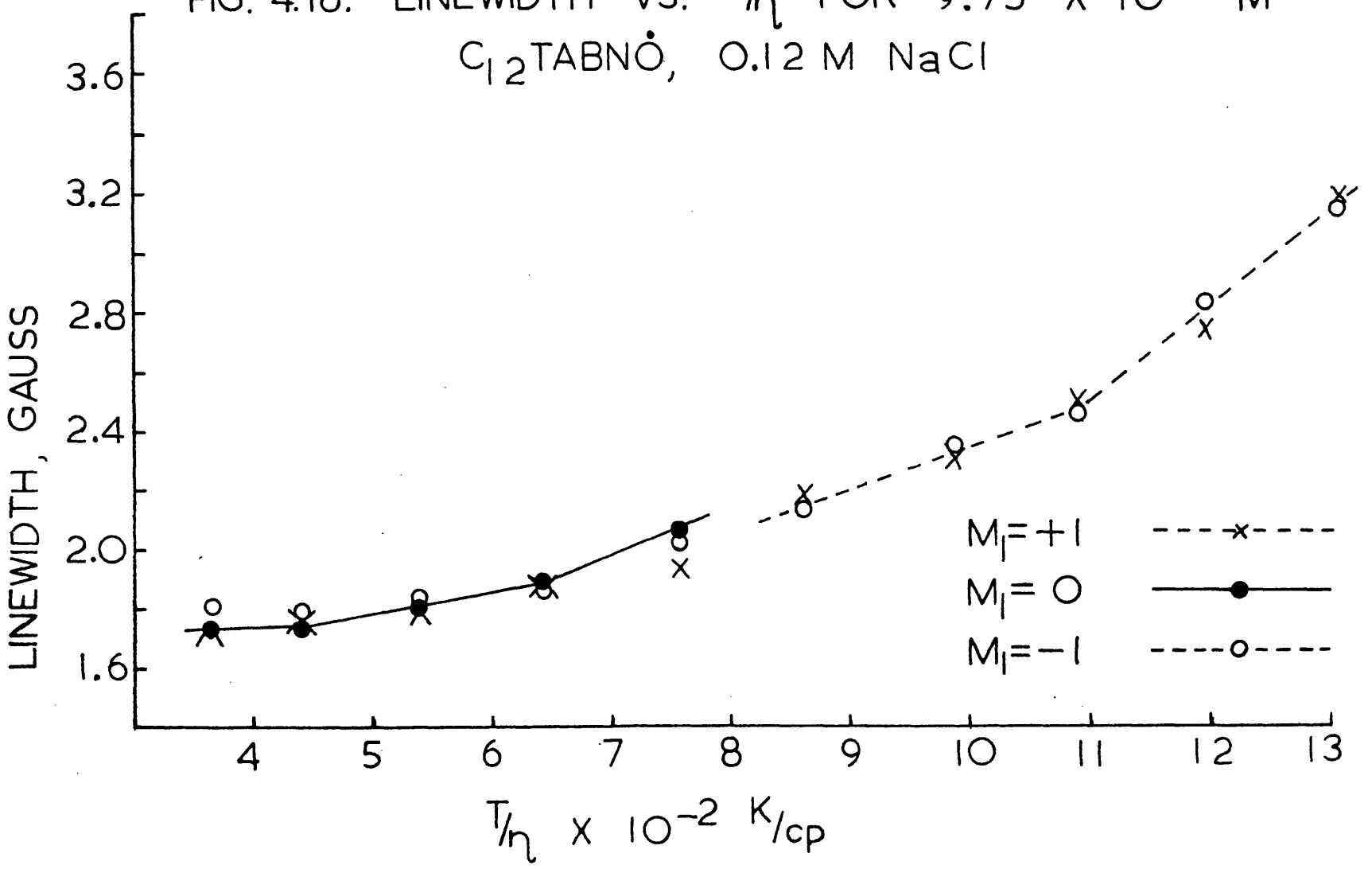

FIG. 4.19. LINEWIDTH VS. T/η FOR 4.05×10^{-3} M $C_{14}TABNO$

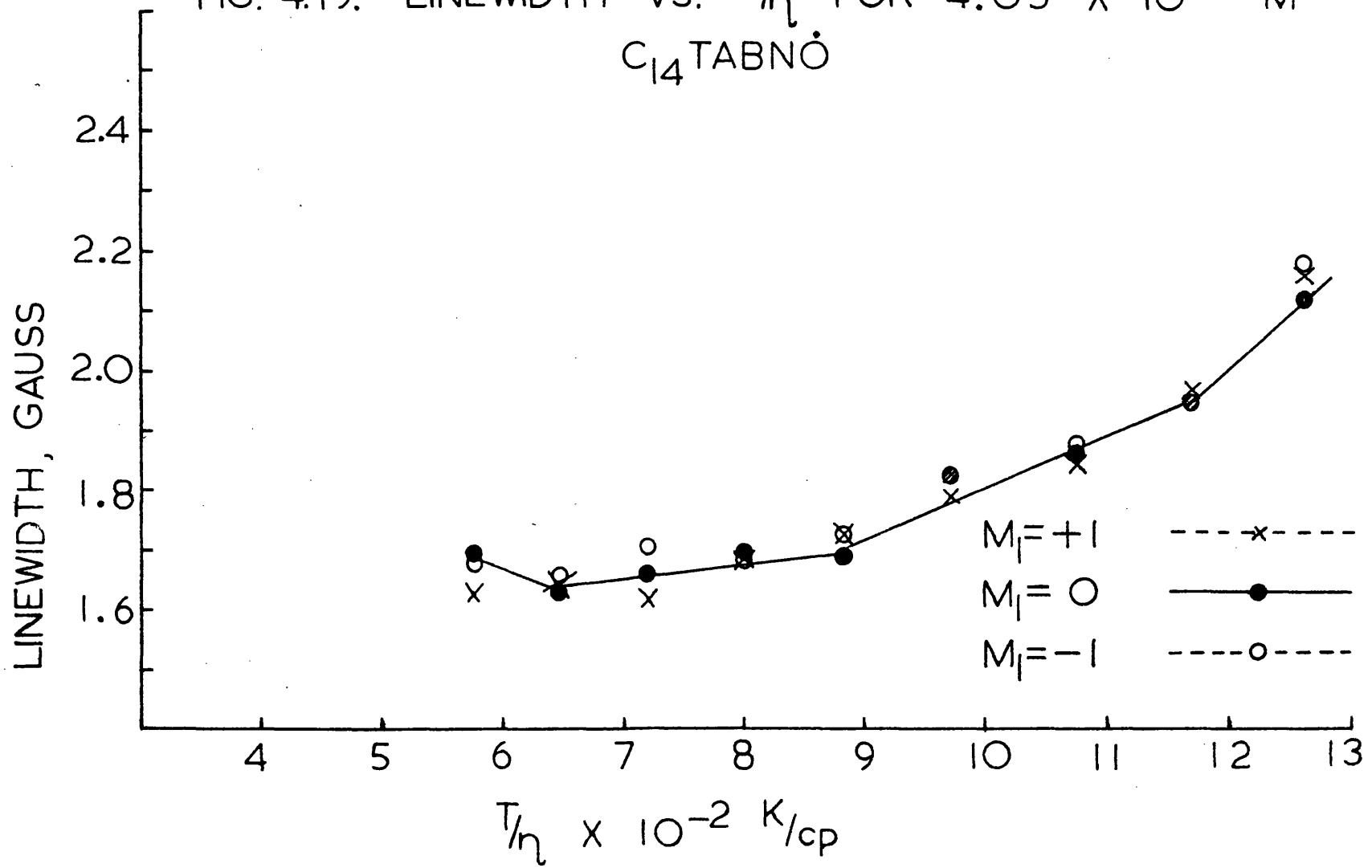

FIG. 4.20. LINEWIDTH VS. T/η FOR 8.23×10^{-3} M $C_{14}TABNO$

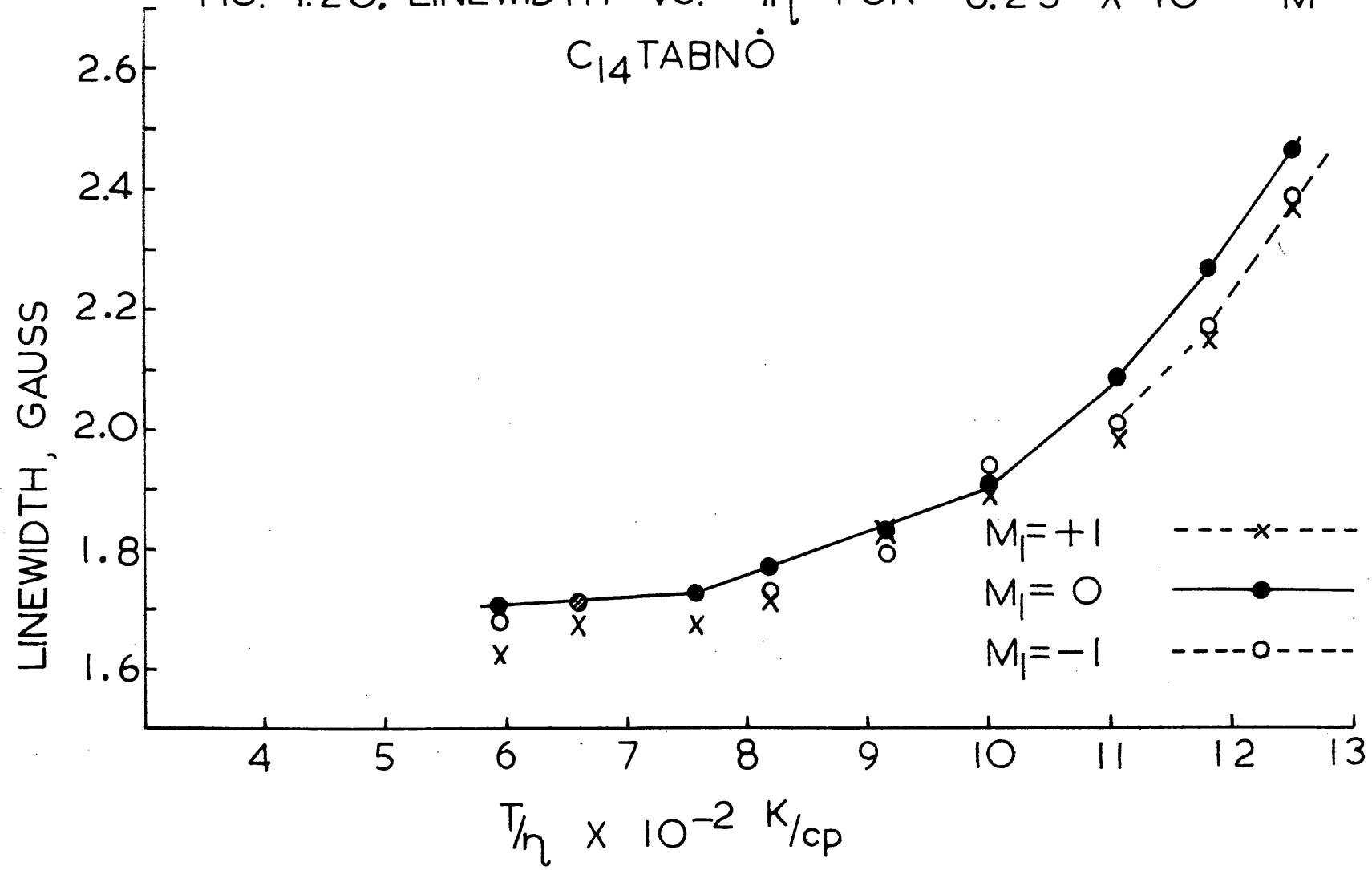

4.18, although in the solutions of lower surfactant concentration shown in Figures 4.14 and 4.17 some of the curvature may be due to proton hyperfine structure. The effect of proton hyperfine structure on the measured linewidth will be discussed in more detail in Chapter 6.

The $C_{14}TABN\dot{O}$ solutions, whose linewidths vs $\frac{T}{\eta}$ graphs also exhibit curvature, are shown in Figures 4.19 and 4.20. Here also part of the observed curvature may be due to the effect of proton hyperfine structure on the observed linewidth.

The results given above indicate that something more than simple Heisenberg spin exchange is taking place in $C_{12}TABN\dot{O}$ and $C_{14}TABN\dot{O}$ solutions above the cmc. Since some of the Arrhenius plots for these compounds showed changes in the activation energy at high temperatures, it was decided that two processes, one of which was Heisenberg spin exchange, might be occurring in these solutions. The results of this line of reasoning are presented below.

4.5. Expected Arrhenius Plots and Linewidth vs $\frac{T}{\eta}$ Graphs for a System Undergoing Two Rate Processes

Assume that two processes with different activation energies are taking place in solution. The lifetime of the monomer in the unperturbed state will be shortened by each of the two processes. For the ensemble of monomer spins, the average exchange frequency ck_o will be given by:

$$ck_o = P_1k_1 + P_2k_2 \qquad (4.6)$$

where c is the total monomer concentration, k_1 and k_2 are the rate constants for the high and low activation energy processes respectively, and P_1 and P_2 are concentration dependent parameters which can regulate the number of spins allowed to undergo each process. First assume that P_1 and P_2 are independent of temperature. In general,

$$k_o = \frac{kT}{h} e^{-\frac{\Delta E_{act}}{RT}}$$ [48]

where k is the Boltzmann constant, h is Planck's constant, T is the temperature in K, and ΔE act is the activation energy of the process under consideration.

Then: $$k_1 = \frac{kT}{h} e^{-E_1/RT} = \frac{kT}{Nh} e^{-E_1/kT} \qquad (4.8)$$

$$k_2 = \frac{kT}{h} e^{-E_2/RT} = \frac{kT}{Nh} e^{-E_2/kT}$$

Hence: $$k_o = \frac{kT}{Nh} \left(\frac{P_1 e^{-E_1/kT}}{C} + \frac{P_2 e^{-E_2/kT}}{C} \right) \qquad (4.9)$$

Let the second rate process be diffusion controlled, since from the experimental data the activation energies are approaching the experimental activation energy for the self-diffusion of water of 5.3 kcal/mole.[48] Then E_2 will be the same as the energy of activation for the diffusion process. The coefficient of viscosity η is given by:[48]

$$\eta = \frac{hN}{v} e^{E_2/kT} \qquad (4.10)$$

where v is the molar volume and N is Avogadro's number. Then, substituting 4.10 into 4.9:

$$k_o = \frac{T}{\eta} \frac{k}{v} \left[\frac{P_1}{C} e^{\frac{-(E_1-E_2)}{kT}} + \frac{P_2}{C} \right] \qquad (4.11)$$

Since observed values of E_1 are at least 22 kcal/mole, (E_1-E_2) will be about 17 kcal/mole. As the temperature increases from 300K to 370K, the first term in the bracket in equation 4.11 will increase from $4 \times 10^{-13} \frac{P_1}{C}$ to $9 \times 10^{-11} \frac{P_1}{C}$, an increase of 220 times the initial value. If only one exchange process is operative in the system, i.e. if $P_2 = 0$, the slope of a linewidth vs $\frac{T}{\eta}$ graph will increase by a factor of 220 as the temperature is increased from 300K to 370K, assuming that the difference in the activation energies between micellisation and diffusion is about 17 kcal/mole. If a diffusion controlled process is present as well, the change in slope will be less, and will depend upon the relative values of P_1 and P_2. If P_2 is present in any appreciable amount, say $P_2 \geqslant 1 \times 10^{-8} P_1$, the effect of the change in P_1 on the linewidth vs $\frac{T}{\eta}$ graph will become negligible. If P_2 is on the order of $1 \times 10^{-8} P_1$, the effect of P_1 upon the Arrhenius plot will be negligible since the logarithm of equation 4.9 becomes

$$\log k_o = \log \frac{NkT}{hc} + \log \left[P_1 e^{-E_1/kT} + P_2 e^{-E_2/kT} \right] \qquad (4.12)$$

with the value of the turn in brackets being $\left[P_1 \ (5 \times 10^{-17}) + 1 \times 10^{-8} \ P_1 \ (4.3 \times 10^{-4})\right]$ at room temperature. Only if $P_2 \simeq 10^{-12} \ P_1$ will the effects of both exchange processes be seen on the Arrhenius Plots and on the linewidth vs $\frac{T}{\eta}$ graphs. However, the effect upon the Arrhenius Plots will be in the opposite direction from that observed, as a higher slope will be present at high temperatures, rather than at low temperatures as observed. Thus the observed results are not due to the simple superposition of two rate processes.

Alternative explanations for the observed phenomena, involving one or more temperature-dependent activation energies and/or temperature-dependent concentration factors P_i, which are not subject to the constraint $\sum_i P_i = C$, could be attempted. Instead, it was decided to investigate more thoroughly the theoretical basis of both Heisenberg spin exchange and monomer-micelle exchange, to see if anything would emerge which would explain the observed behaviour of the cationic nitroxide surfactant systems. It was also decided to investigate the effect of proton hyperfine structure upon the observed broadening, to see what proportion of the observed effects were at least in part due to its presence. The results of these investigations are given in the two chapters which follow.

CHAPTER 5

THEORETICAL BASIS OF THE EXCHANGE EQUATIONS

Several types of exchange are possible in a solution consisting of paramagnetic micelles and paramagnetic surfactant monomers. Collisions between the monomers, whether at low concentrations in solution or at high concentrations in a micelle, are described by the equations for Heisenberg spin exchange as developed by Sack[53]. Equations describing the results of collisions between monomers and micelles require a different formulation. This chapter explores these two different types of exchange and their effects on the observed EPR spectra.

5.1. Equations for Monomer-Monomer Interactions

5.1.1. Heisenberg Spin Exchange

When two nitroxide molecules collide with each other, the electron spin magnetic moments of the two molecules may be exchanged. Each electron will have been coupled to a nitrogen nucleus (m_I = +1,0, or -1) before the exchange, and, if the small Boltzmann differences in the populations of the three nuclear spin states are ignored, will have an equal chance of being coupled to a nitrogen nucleus in each of the three nitrogen nuclear spin states after the exchange. The observed electron paramagnetic resonance spectrum will depend upon the exchange frequency, with the three nitrogen hyperfine lines broadening, coalescing, and the coalesced line narrowing as the exchange frequency increases from much less than to much greater than the hyperfine separation.

Using the method of Kubo[56] (also used by Zimmerman and Brittin - see 5.2.3. below) Sack[53] has found that, for the case of a symmetric triplet with equal probabilities P of exchange between the three sites, the spectral intensity I (ω) will be given by

$$I(\omega) \sim \frac{P(a_N^{\,2} + 27P^2 + 3\omega^2)}{\omega^2(a_N^{\,2} - \omega^2)^2 + 4P^2 a_N^{\,4} - 6P^2 a_N^{\,2}\omega^2 + 81\omega^2 P^4 + 18\omega^4 P^2} \qquad (5.1)$$

The three nitrogen hyperfine lines, in the absence of exchange, are located at frequences $+ a_N, 0$, and $- a_N$.

If one sets the second derivative of equation (5.1) equal to zero the resulting equation

$$\begin{aligned}
0 = {} & \omega^{18}\,(60P) \\
& + \omega^{16}\,(42E + 114PA) \\
& + \omega^{14}\,(72PA^2 + 24PB + 96\,AE) \\
& + \omega^{12}\,(12PAB - 90PC + 74A^2E + 58BE + 18PA^3) \\
& + \omega^{10}\,(-216PAC - 36PB^2 + 88ABE + 12CE + 12PA^2B + 20A^3E) \\
& + \omega^{8}\,(-12ACE + 22B^2E - 78PA^2C - 6PAB^2 + 38A^2BE - 204PBC) \\
& + \omega^{6}\,(-8A^2CE + 24AB^2E - 16BCE - 96PABC - 144PC^2) \\
& + \omega^{4}\,(4ABCE + 6EB^3 - 66PAC^2 - 18PB^2C - 30C^2E) \\
& + \omega^{2}\,(4B^2CE - 12PBC^2 - 12C^2AE) \\
& + \omega^{0}\,(-2BC^2E + 6PC^3)
\end{aligned} \qquad (5.2)$$

where $A = 18P^2 - 2a_N^{\,2}$

$B = a_N^{\,4} - 6P^2 a_N^{\,2} + 81P^4$

$C = 4P^2\, a_N^{\,4}$

$E = Pa_N^{\,2} - 27P^3$

relates the peak to peak width(s) of the first derivative EPR line(s) to the exchange frequency P for any given a_N. In the fast exchange region there will be two solutions, equidistant from $\omega = 0$; in the slow exchange region there will be two pairs of additional solutions, one pair equidistant from $+a_N$, the other pair equidistant from $-a_N$. Plachy and Kivelson[57] have calculated the widths of the three lines as a function of the exchange frequency in the slow exchange region, using a method similar to that used above. The results relative to the hyperfine coupling constant a_N are shown in Fig. 5.1. At values of $P/a_N > 0.2$ the widths of the three lines deviate from the width expected for a Lorentzian line, with the $m_I = 0$ line differing in width from the $m_I = \pm 1$ lines as indicated in the figure. For $a_N = 16.9$ Gauss, as it is for the cationic nitroxide surfactants in aqueous solution, the value of $P/a_N = 0.2$ is exceeded for lines of width greater than 3.4G. The $m_I = \pm 1$ lines will be broader than the $m_I = 0$ line until the three lines reach a width of 7.1G. For widths greater than 7.1G the $m_I = 0$ line will be broader than the $m_I = \pm 1$ lines, which will actually decrease in width with increasing exchange frequency.

5.1.2. The Micellar Line

The method described above can be used to calculate the frequency with which micellar surfactant molecules collide with each other. By substituting the value of the nitrogen hyperfine coupling constant a_N observed in aqueous non-micellar solutions of nitroxide surfactant molecules into equation 5.2, one obtains

FIG. 5.1.

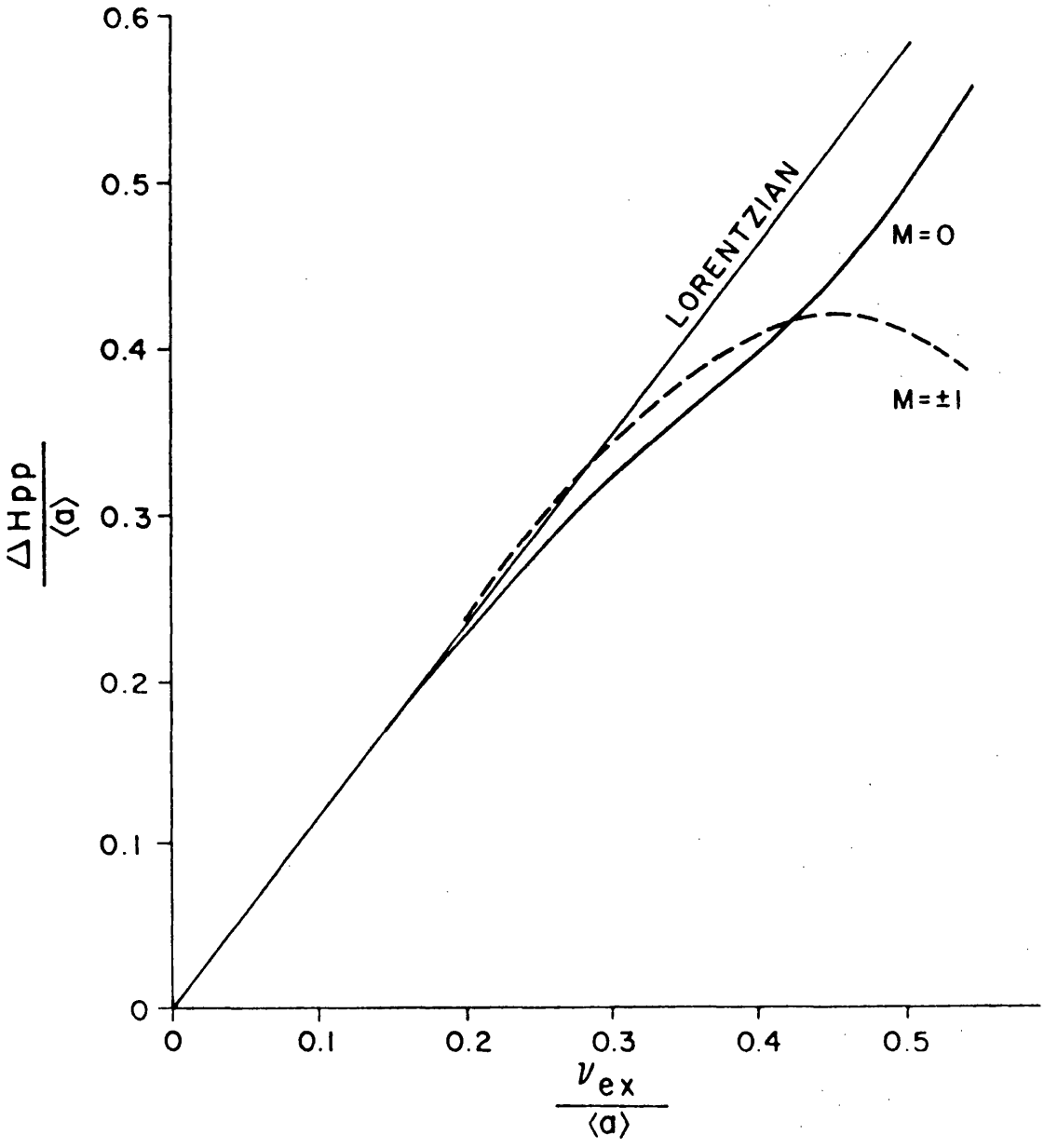

Plot of $\Delta H_{pp}/\langle a \rangle$ versus $\nu_{ex}/\langle a \rangle$ for three equivalent lines under exchange conditions.

FROM REF. 57.

$$
\begin{aligned}
0 = {} & \omega^{0}\,(-9.038\times10^{108}P^{5} - 3.634\times10^{94}P^{7} + 1.460\times10^{80}P^{9} - 1.768\times10^{66}P^{11}) \\
& + \omega^{2}\,(+4.516\times10^{108}P^{3} - 6.02\times10^{93}P^{5} + 5.919\times10^{80}P^{7} - 1.663\times10^{66}P^{9} \\
& \quad -2.228\times10^{51}P^{11} + 1.562\times10^{36}P^{13}) \\
& + \omega^{4}\,(1.693\times10^{108}P - 6.50\times10^{93}P^{3} + 5.36\times10^{80}P^{5} - 4.71\times10^{66}P^{7} \\
& \quad -1.28\times10^{51}P^{9} + 1.01\times10^{37}P^{11} - 1.51\times10^{22}P^{13} + 9.46\times10^{6}P^{15}) \\
& + \omega^{6}\,(-6.048\times10^{93}P + 1.67\times10^{79}P^{3} - 6.97\times10^{65}P^{3} - 6.33\times10^{50}P^{7} \\
& \quad +3.84\times10^{36}P^{9} - 1.41\times10^{22}P^{11} + 8.410\times10^{6}P^{13}) \qquad (5.3) \\
& + \omega^{8}\,(1.047\times10^{79}P - 3.608\times10^{64}P^{3} - 3.393\times10^{50}P^{5} + 3.146\times10^{36}P^{7} \\
& \quad -1.543\times10^{22}P^{9} + 2.740\times10^{7}P^{11}) \\
& + \omega^{10}\,(-8.145\times10^{63}P - 1.187\times10^{49}P^{3} + 5.907\times10^{35}P^{5} - 3.280\times10^{21}P^{7} \\
& \quad +6.921\times10^{6}P^{9}) \\
& + \omega^{12}\,(2.088\times10^{48}P^{1} + 3.896\times10^{34}P^{3} - 3.623\times10^{20}P^{5} + 8.973\times10^{5}P^{7}) \\
& + \omega^{14}\,(+6.014\times10^{32}P - 1.967\times10^{19}P^{3} + 7.193\times10^{4}P^{5}) \\
& + \omega^{16}\,(-4.165\times10^{17}P + 3.186\times10^{3}P^{3}) \\
& + \omega^{18}\,(60P)
\end{aligned}
$$

which relates the linewidth parameter to the exchange frequency P for these particular nitroxide surfactant systems.

The observed micellar line narrows as the temperature of the micelle-containing solution is increased, since with an increase in temperature the collision frequency P between the nitroxide molecules incorporated in a given micelle is increased. At a temperature of $90^{\circ}C$ the micellar linewidth is about 10G. Since the micellar linewidth is $(+\omega) - (-\omega)$ in the reference frame of equation (5.2), one can substitute $\omega = 5G$ into equation (5.3) and solve for the exchange frequency P. It is found that $P = 5.08\times10^{7}$ exchanges per second. At room temperature, the micellar linewidth is about 16G and the exchange frequency P is $3.70\times10^{7}\ sec^{-1}$.

As will be shown in the next chapter, the monomer lines which at high exchange frequencies coalesce to form the micellar line have an initial width of about half a gauss. If the lineshape is Lorentzian this corresponds to a transverse relaxation time T_2 of $8x10^{-5}$ sec, which means that the electron has a half-life of $8x10^{-5}$ sec in a given state. As exchange between states becomes greater than $8x10^{-5}$ seconds, an electron will become more likely to leave a state through exchange processes than through other forms of relaxation. In a nitroxide micelle at room temperature, the lifetime of a molecule in a given micellar state will be determined almost completely by the exchange frequency P. The half-life of an electron in a given micellar state will be P^{-1}, or $2.7x10^{-8}$ seconds. At a temperature of $90^{o}C$ the half-life of an electron in a given micellar state will be even shorter - about $2x10^{-8}$ seconds. It is this half-life of an electron in a given micellar state which is important in calculating the effect of exchange between the monomeric and the micellar states - in effect the micellar T_2 is equal to the inverse of the exchange frequency P.

5.2. Exchange between Monomeric and Micellar Sites

A nitroxide surfactant monomer in solution will have its unpaired electron coupled to a nitrogen nucleus in either the $m_I = +1$, $m_I = 0$, or $m_I = -1$ spin state. When an electron spin transition occurs, those molecules with nitrogen spin $m_I = +1$ will give rise to the EPR line located at $\omega_o - a_N$, while those molecules with nitrogen spin $m_I = 0$ and $m_I = -1$ will give rise to the EPR lines at ω_o and $\omega_o + a_N$ respectively. If this nitroxide surfactant monomer becomes incorporated in a micelle of similar nitroxide surfactants, rapid electron spin exchange will result in an EPR spectrum containing one broad line centred at ω_o[53].

Monomer-Micelle exchange will result in exchange between the broad micellar line centred at ω_o and the sharp monomer line centred at $\omega_o + a_N$ of the monomer nitrogen nucleus is in the $m_I = -1$ spin state. If the monomer nitrogen nucleus is in the $m_I = 0$ spin state, the exchange is between the sharp and broad lines centred at ω_o. If the monomer nitrogen nucleus has $m_I = +1$, exchange is between the broad line at ω_o and the sharp monomer line at $\omega_o - a_N$. Thus for $m_I = \pm 1$, exchange is between two lines with different T_2's separated by a frequency difference a_N, while for $m_I = 0$ exchange is between two lines with different T_2's but with the same resonance frequency ω_o.

5.2.1. Exchange Equations for the Central Line

The effect of exchange between the two sites for the cases $m_I = 0$ can be described by a modified set of Bloch equations[6,54]. If A and B represent the monomer and micellar sites respectively, and $\underline{M_A}$ and $\underline{M_B}$ represent the total magnetic moment of electrons in each of the sites, then in the presence of a strong magnetic field H_o perpendicular to a weak magnetic field H_1 the electrons will relax according to the Bloch equations:

$$\frac{d\hat{M}_A}{dt} + i\,(\hat{\omega}_A - \omega)\,\hat{M}_A = i\gamma H_1 M_{oA} \tag{5.4}$$

$$d\hat{M}_B + i\,(\hat{\omega}_B - \omega)\,\hat{M}_B = i\gamma H_1 M_{oB} \tag{5.5}$$

Here $\hat{M}$ is the complex magnetic moment $\hat{M} = u + i\,v$, M_o is the equilibrium magnetic moment, γ the gyromagnetic ratio of the electron, and $\hat{\omega}_o$ the complex frequency $\hat{\omega}_o = \omega_o - {}^{i}/T_{2O}$. If in addition the electron in site A has a time proportional transition probability $P_{AB}\,\delta t$ that it will transfer to site B during the time interval δt, and the electron in site B has a similar time-proportional

transition probability $P_{BA}\delta t$ of transferring to site A, then the change in magnetization due to electron transfer is described by the equations

$$\frac{d\hat{M}_A}{dt} = - P_{AB}\hat{M}_A + P_{BA}\hat{M}_B \quad , \tag{5.6}$$

$$\frac{d\hat{M}_B}{dt} = - P_{BA}\hat{M}_B + P_{AB}\hat{M}_A \quad . \tag{5.7}$$

Since in an equilibrium situation there will be $f_A = \frac{P_{BA}}{P_{AB} + P_{BA}}$ electrons in site A and $f_B = \frac{P_{AB}}{P_{AB} + P_{BA}}$ electrons in site B, the Bloch equations modified for chemical exchange can be written

$$\frac{d\hat{M}_A}{dt} = i\, f_A\, (\gamma H_1 M_o) - i\, (\hat{\omega}_A - \omega)\, \hat{M}_A - P_{AB}\hat{M}_A + P_{BA}\hat{M}_B \quad , \tag{5.8}$$

$$\frac{d\hat{M}_B}{dt} = i\, f_B\, (\gamma H_1 M_o) - i\, (\hat{\omega}_B - \omega)\, \hat{M}_B - P_{BA}\hat{M}_B + P_{AB}\hat{M}_A \quad . \tag{5.9}$$

The steady state solutions to these equations,

$$\hat{M}_A \left[(\omega - \hat{\omega}_A) + i\, P_{AB}\right] - i\, P_{BA}\hat{M}_B = -f_A\, (\gamma H_1 M_o) \quad , \tag{5.10}$$

$$\hat{M}_B \left[(\omega - \hat{\omega}_B) + i\, P_{BA}\right] - i\, P_{AB}\hat{M}_A = -f_B\, (\gamma H_1 M_o) \tag{5.11}$$

can be used to calculate the total magnetic moment $M = M_A + M_B$. The result is

$$\hat{M} = -\gamma H_1 M_o \; \frac{f_A(\omega - \hat{\omega}_B) + f_B\, (\omega - \hat{\omega}_A) + i\, (P_{AB} + P_{BA})}{\left[(\omega - \hat{\omega}_A) + i\, P_{AB}\right]\left[(\omega - \hat{\omega}_B) + i\, P_{BA}\right] + P_{AB}P_{BA}} \tag{5.12}$$

Since the $m_I = 0$ monomer state and the micellar state have the same resonance frequency, $\omega_A = \omega_B = \omega_R$, and equation (5.12) becomes

$$\hat{M} = \frac{-\gamma H_1 M_o \left[f_A (\omega-\omega_R + {}^{i}/T_{2B}) + f_B (\omega-\omega_R + {}^{i}/T_{2A}) + i (P_{AB} + P_{BA})\right]}{(\omega-\omega_R + {}^{i}/T_{2A} + i P_{AB}) (\omega-\omega_R + {}^{i}/T_{2B} + i P_{BA}) + P_{AB} P_{BA}} \quad (5.13)$$

The intensity of the resonance absorption will be proportional to the imaginary part of $\hat{M}$. One can solve for the width of the first derivative of an absorption peak by setting the second derivative of the absorption peak equal to zero and solving for ω - the width will be $2 (\omega-\omega_R)$.

For the special case of equal populations in the micellar state and in the monomer $m_I = 0$ state, $f_A = f_B = \frac{1}{2}$, $P_{AB}=P_{AB}=P$, and the absorption spectrum, or the imaginary part of $\hat{M}$, is

$$\text{Im } \hat{M} = \frac{+\gamma H_1 M_o \left[(\omega-\omega_R)^2 T_A T_B (T_A + T_B) + RQ\right]}{2\left[(\omega-\omega_R)^4 T_A^2 T_B^2 + (\omega-\omega_R)^2 S + R^2\right]} \quad (5.14)$$

where $S = T_A^2 + T_B^2 + 2P T_A T_B (2PT_A T_B + T_B + T_A)$

$R = 1 + P (T_A + T_B)$

$Q = T_A + T_B + 4P T_A T_B$

Setting the second derivative of the absorption spectrum equal to zero, one obtains

$$\begin{aligned}
&(\omega-\omega_R)^8 \left[+ 3T_A^5 T_B^5 (T_A + T_B)\right] \\
&+(\omega-\omega_R)^6 \left[+ 10T_A^4 T_B^4 RQ - ST_A^3 T_B^3 (T_A + T_B)\right] \\
&+(\omega-\omega_R)^4 \left[+ 9SRQT_A^2 T_B^2 - 12R^2 T_A^3 T_B^3 (T_A + T_B)\right. \\
&+(\omega-\omega_R)^2 \left[+ 3QRS^2 - 3R^2 ST_A T_B (T_A + T_B) - 6R^3 QT_A^2 T_B^2\right] \\
&+ R^4 T_A T_B (T_A + T_B) - SR^3 Q = 0
\end{aligned} \quad (5.15)$$

The linewidth will be $2(\omega-\omega_R)$. If the monomer line has a width of 1.6 Gauss in the absence of exchange, the micellar line a width of

10 Gauss, and the exchange frequency P is 1×10^6 sec^{-1}, then the width of the monomer line in the presence of exchange, calculated by means of equation (5.15), is 2.005 Gauss.

The above calculation is tedious, and becomes even more so for the general case $f_A \neq f_B$, $P_{AB} \neq P_{BA}$. Another approach, based on work by Zimmerman and Brittin[55], which involves less lengthy calculations is described in the next section.

5.2.2. Exchange Equations for the Central Line-Method of Zimmerman & Brittin

The system considered by Zimmerman and Brittin[55] consists of a finite number of phases, in all of which a spin has the same resonance frequency ω_o. Each phase is characterised by a single relaxation time T_{2i}, which will be different for different phases. Spins are able to transfer between phases, with the probability of a given transfer being independent of the previous history of the spin.

In the presence of a magnetic field, a spin in the ith phase will relax with a transverse relaxation time T_{2i} described by the equation

$$\frac{dM_\perp}{dt} = -\frac{M_\perp}{T_{2i}} \tag{5.16}$$

where $M_\perp$ is the magnetic moment of the sample in the plane perpendicular to the magnetic field. A spin-echo experiment will measure the average value of the transverse magnetization of an ensemble of spins, $\overline{M_\perp(t)}$. If T (t) is a random variable taking on the values T_{2i} as the spin jumps from phase to phase, then

$$M_{\perp}(t) = M_{\perp o} e^{-\int_o^t dt}/T(t) \tag{5.17}$$

where $M_{\perp}(t) = M_{\perp o}$ at $t = 0$. The relaxation process is described by the average value of the integral

$$I(t) = e^{-\int_o^t dt}/T(t) \tag{5.18}$$

where the average is taken over all possible initial states.

To obtain the average value $\overline{I(t)}$ of $I(t)$, let $I_{ij}(t)$ be the average value of $I(t)$ on the condition that the spin is initially in the ith phase and at time t is in the jth phase. Let P_i be the probability that the spin be found initially in the ith phase. Then

$$I(t) = \sum_{i,j} P_i I_{ij}(t) \tag{5.19}$$

The change $I_{ij}(t)$ with time will depend on the rate c_i at which spins leave the ith state for some other state, on the rate at which spins enter the jth state from all the other states, and on the probability of the spin relaxing while in the jth state. If p_{lj} is the conditional probability that if a spin leaves the lth state, it transfers to the jth state then

$$\frac{dI_{ij}(t)}{dt} = - I_{ij}(t)\,(c_j + {}^1/T_{2j}) + \sum_l I_{il}(t) c_l P_{lj} \tag{5.20}$$

If we let

$$F_{lj} = \delta_{lj}\,(c_l + {}^1/T_{2l}) - c_l P_{lj} \tag{5.21}$$

then using matrix notation $\underline{\underline{F}} = [F_{lj}]$, $\underline{\underline{I}} = [I_{ij}(t)]$, and equation (5.20) can be written

$$\frac{d\underline{\underline{I}}}{dt} = -\underline{\underline{I}}\,\underline{\underline{F}} \tag{5.22}$$

The solution to equation (5.22), subject to the boundary conditions $\underline{\underline{I}}\,(0) = \underline{\underline{1}}$ (i.e. at t = 0, the system is initially in the ith phase), is

$$\underline{\underline{I}} = e^{-\underline{\underline{F}}t} \tag{5.23}$$

The average $\overline{I\,(t)}$ will then be expressed as (compare equation (5.19))

$$\overline{I\,(t)} = \tilde{\phi}\, e^{-\underline{\underline{F}}t}\, \phi \tag{5.24}$$

$$\text{where } \tilde{\phi} = \begin{bmatrix} 1 \\ 1 \\ 1 \\ \cdot \\ \cdot \\ \cdot \\ 1 \end{bmatrix} \text{ and } \phi = \left[P_1 P_2 P_3 \ \ldots \ P_N\right] \tag{5.25}$$

Since $\underline{\underline{F}}$ is a finite, say N x N matrix, $e^{-\underline{\underline{F}}t}$ can be expressed as a polynomial in $\underline{\underline{F}}$. Hence

$$e^{-\underline{\underline{F}}t} = \sum_{m=o} g_m \underline{\underline{F}}^m \tag{5.26}$$

If $\underline{\underline{F}}$ has distinct eigenvalues $u_1 \ldots u_N$, then representations of $\underline{\underline{F}}$ and $e^{-\underline{\underline{F}}t}$ in the basis set of eigenvectors of $\underline{\underline{F}}$ are given by

$$\begin{bmatrix} u_1 & & & & \\ & u_2 & & & \\ & & \cdot & & \\ & & & \cdot & \\ & & & & \cdot u_N \end{bmatrix}$$

and

$$\begin{bmatrix} e^{-u_1 t} & & & \\ & e^{-u_2 t} & & \\ & & \cdot & \\ & & & \cdot \\ & & & \cdot\ e^{-u_N t} \end{bmatrix} = \begin{bmatrix} \sum_m g_m u_1^{\,m} & & \\ & \cdot & \\ & & \cdot \sum_m g_m u_N^{\,m} \end{bmatrix}$$

respectively. Hence

$$e^{-u_N t} = \sum_{m=0}^{N-1} g_m u_K^{\ m} \tag{5.27}$$

If one sets

$$e(t) = \begin{bmatrix} e^{-u_1 t} \\ \vdots \\ e^{-u_N t} \end{bmatrix} \quad ; g = \begin{bmatrix} g_0 \\ \vdots \\ g_{N-1} \end{bmatrix}$$

and $\underline{\underline{\Omega}} = [\Omega_{ik}] = |(u_i)^{-1}|^{k-1}$, i,k = 1, ...N, then equation (5.27) may be expressed as the matrix equation

$$\underline{e\ (t)} = \underline{\underline{\Omega}}\,\underline{g} \tag{5.28}$$

which has the solution

$$\underline{g} = \underline{\underline{\Omega}}^{-1}\ \underline{e(t)} \tag{5.29}$$

In a system consisting of only two phases, the above equations are simple to apply. Since P_{AB} is 1, the matrix $\underline{\underline{F}}$ will be given by

$$\underline{\underline{F}} = \begin{bmatrix} c_A + {}^1/T_{2A} & -c_A \\ -c_B & c_B + {}^1/T_{2B} \end{bmatrix} \tag{5.30}$$

whose eigenvalues u_A and u_B are

$$u_A = \tfrac{1}{2}\{ (c_A + c_B + {}^1/T_{2A} + {}^1/T_{2B}) - [(c_B - c_A + {}^1/T_{2B} - {}^1/T_{2A})^2 + 4c_A c_B]^{\frac{1}{2}}\} \tag{5.31}$$

$$u_B = \tfrac{1}{2}\{ (c_A + c_B + {}^1/T_{2A} + {}^1/T_{2B}) + [(c_B - c_A + {}^1/T_{2B} - {}^1/T_{2A})^2 + 4c_A c_B]^{\frac{1}{2}}\}$$

Equation (5.26) becomes

$$e^{-\underline{\underline{F}}t} = g_o(t)\underline{\underline{1}} + g_1(t)\underline{\underline{F}} \tag{5.32}$$

where, from equation (5.29),

$$\left.\begin{aligned} g_o(t) &= \frac{u_B e^{-u_A t} - u_A e^{-u_B t}}{u_B - u_A} \\ g_1(t) &= \frac{e^{-u_B t} - e^{-u_A t}}{u_B - u_A} \end{aligned}\right\} \qquad (5.33)$$

The relaxation integral, I (t), will be given by

$$I(t) = a_1 e^{-u_A t} - a_2 e^{-u_B t} ,$$

where

$$a_1 = \frac{u_B - {}^1/T_{AV}}{u_B - u_A} \qquad (5.34)$$

$$a_2 = \frac{u_A - {}^1/T_{AV}}{u_B - u_A} \qquad (5.35)$$

and

$${}^1/T_{AV} = {}^{P_A}/_{T_{2A}} + {}^{P_B}/_{T_{2B}}$$

Thus the spin-echo NMR experiment will be described by the equation

$$M_\perp (t) = M_{\perp o} \left[a_1 e^{-u_A t} - a_2 e^{-u_B t} \right] \qquad (5.36)$$

Equation (5.36) describes the relaxation of an exchangeless system containing fraction a_1 of its spins with relaxation time u_A and fraction $(-a_2)$ of its spins with relaxation time u_B. The apparent populations a_1 and $(-a_2)$ and the apparent relaxation times u_A and u_B can, assuming an appropriate (Gaussian or Lorentzian) lineshape function, be used to calculate first derivative EPR spectra. In the case of equal populations in the $m_I = 0$ monomer state and the micellar state, with a monomer linewidth 1.6G in the absence of exchange and a micellar linewidth of 10G, an exchange frequency of 1×10^6 sec^{-1} increases the monomer linewidth to 2.004G - essentially the same result as that obtained with the modified Bloch equations.

5.2.3. Exchange Equations for the Outer Lines

The exchange equations of Zimmerman and Brittin[55] have been extended by Woessner[44] to the case where the two exchanging species have unequal resonance frequencies. Woessner has solved the Bloch Equations (Equations 5.8 and 5.9) to obtain the time-dependent behaviour of the nuclear magnetization. He finds that, if the nuclear spin system was at thermal equilibrium at the beginning of the pulse, the in phase component of the total nuclear magnetization, $u = u_A + u_B$, and the out of phase component, $v = v_A + v_B$, evaluated at $\omega = \frac{1}{2}(\omega_A + \omega_B)$, are

$$U = - M_o \sin\theta \{F_-[dt] e^{-ct} + F_+[dt] e^{ct}\} e^{-\phi t} \qquad (5.37)$$

and

$$V = - M_o \sin\theta \{F_-[dt + \pi/2] e^{-ct} + F_+[dt - \pi/2]\} e^{-\phi t} \qquad (5.38)$$

Here the subscripts A and B refer to the two exchanging species, and $M_o \sin\theta$ is an amplitude factor composed of the total magnetization M_o and the fraction of that magnetization transferred into the transverse plane by the pulse, represented by $\sin\theta$. $F_+[T]$ and $F_-[T]$ are functions of the factor T given by

$$F_+[T] = - f \cos T - (1-g) \sin T$$

$$F_-[T] = - f \cos t T + g \sin T$$

where $T = dt$, $dt + \pi/2$, or $dt - \pi/2$ as required by equations 5.37 and 5.38.

$$\phi = \tfrac{1}{2}(C_A + C_B + {}^1/T_{2A} + {}^1/T_{2B}) , \qquad (5.39)$$

$$f = \tfrac{1}{2}\{c(P_B - P_A)(\omega_B - \omega_A) + d(P_B - P_A)({}^1/T_{2A} - {}^1/T_{2B}) + C_A + C_B\}/(c^2 + d^2) ,$$

$$g = \tfrac{1}{2} - \tfrac{1}{4}\{ c[(P_B - P_A)\,(^1/T_{2A} - {}^1/T_{2B}) + C_A + C_B] - d\,(P_B - P_A)\,(\omega_A - \omega_B)\} \,/\, (c^2 + d^2) \quad ,$$

$$c = [(X^2 + Y^2)^{\frac{1}{2}} + X]^{\frac{1}{2}} \,/\, \sqrt{8} \tag{5.40}$$

and

$$d = [(X^2 + Y^2)^{\frac{1}{2}} - X]^{\frac{1}{2}} \,/\, \sqrt{8} \quad ,$$

where $X = (^1/T_{2A} - {}^1/T_{2B} + C_A - C_B)^2 - (\omega_A - \omega_B)^2 + 4C_AC_B$ (5.41)

and $Y = -2(\omega_A - \omega_B)\,(^1/T_{2A} - {}^1/T_{2B} + C_A - C_B)$. (5.42)

In these equations P_A and P_B are the fractional populations of the A and B states respectively. The algebraic sign of d is always positive, and the sign of c is positive except for negative Y values.

One could fourier transform equations (5.37) and (5.38) to obtain the absorption spectrum as a function of frequency[58]. However, from equations (5.37) and (5.38) one can see that both U and V are the sum of two exponential curves, each with different initial amplitudes. One curve decays as $e^{-(\phi+c)t}$, the other as $e^{-(\phi-c)t}$. Thus the two relaxation times will be $T'_{2A} = \frac{1}{\phi - c}$ and $T'_{2B} = \frac{1}{\phi + c}$ which can be computed for differing values of ω_i, $^1/T_{2i}$, and C_i using equations (5.39) to (5.42).

5.3. The Effect of the Relative Numbers of Monomers and Micelles on the Observed Monomer Linewidth

In sections 5.2.2. and 5.2.3. it was shown that the monomer linewidth observed in the presence of exchange depended upon the transverse relaxation times of both the monomer and the micelle in the absence of exchange, the frequencies with which the

surfactant molecule left both the monomeric and the micellar states, and upon the difference in the resonance frequencies of the two states. The relationship between these factors has been shown in equations (5.31) and (5.39) to (5.42). If an equilibrium exists between monomeric and micellar surfactant, then

$$P_A C_A = P_B C_B \tag{5.43}$$

where P_A, the probability of a spin being initially in state A, is proportional to the population of state A. Similar relationships hold for state B. Since for a surfactant system at a given concentration P_A and P_B are known, the ratio of C_A to C_B can be determined from equation (5.43). One can then substitute $\frac{P_B}{P_A} C_B$ for C_A in equation (5.31) or (5.39) to (5.42), and, knowing the T_{2i}, solve for the U_i as a function of C_B (or C_A).

Suppose that one now adds more surfactant to the system considered previously. This will increase the population of the micellar state, while the population of the monomer state will remain the same. Equation (5.43) will still hold, assuming that the new system has reached equilibrium. From equation (5.43).

$$\frac{P_A}{P_B} = C_B/C_A \tag{5.44}$$

Thus the change in the ratio of P_A to P_B causes a change in the ratio of C_B to C_A. One cannot say a priori whether this is accomplished by a change in C_A or a change in C_B or by changes in both. A reasonable assumption might be that the frequency with which a surfactant molecule leaves a micelle remains almost constant as the total surfactant concentration is increased, at

least for concentrations at which the micelle size and shape remain constant. This would require that the frequency with which a surfactant molecule leaves the monomer state increases with increasing surfactant concentration, a result consistent with the increasing chance of a monomer finding a micelle. Alternatively one might assume that the frequency with which a monomer enters a micelle remains constant as the surfactant concentration is increased, and that the frequency with which a surfactant molecule leaves a micelle decreases with increasing surfactant concentration.

Figures 5.2 and 5.3 show the variations in the widths of the $M_I = 0$ and $M_i = \pm 1$ lines as a function of the ratio of the micellar population to the population of the monomer state ($m_I = +1, -1$, or 0) concerned. In Fig 5.2 the frequency with which a monomer leaves the micellar state has been fixed at 1×10^6 sec^{-1}, and the frequency with which a monomer enters a micelle varied as required by equation (5.44). In Figure 5.3. the frequency with which a monomer enters a micelle has been fixed at 1×10^6 sec^{-1}, and the frequency with which a monomer leaves a micelle varied correspondingly. The micellar relaxation time is 2.96×10^{-8} sec^{-1}, corresponding to a line 10G wide, while the monomer linewidth in the absence of exchange is 0.5G.

The major effect seen in Fig. 5.2. is the increase in monomer linewidth with increasing frequency of leaving the monomer state. The widths of the $m_I = \pm 1$ lines are slighly greater than the width of the $m_I = 0$ line, with the difference exceeding the experimental error for micelle to monomer ratios greater than two.

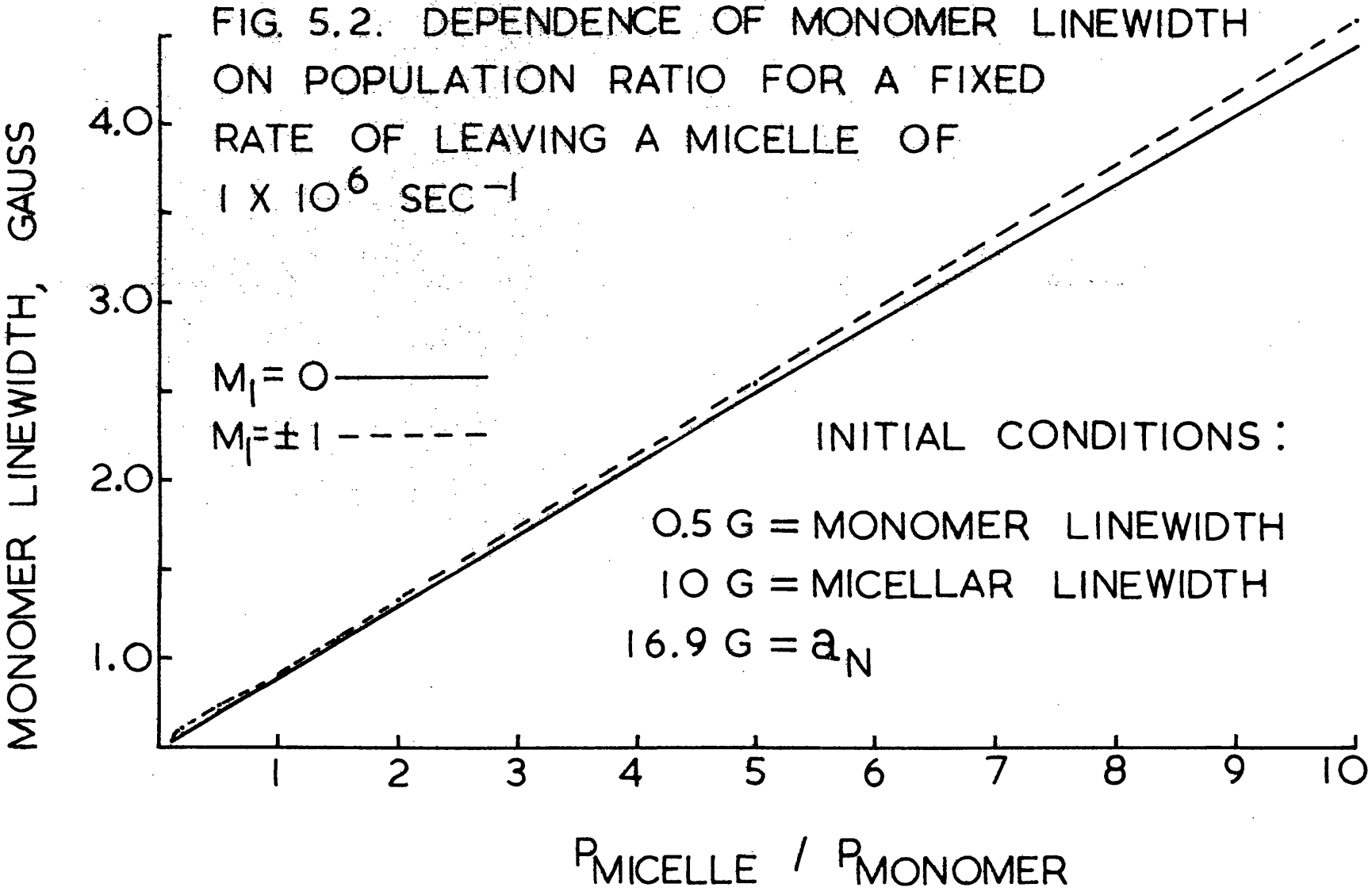

FIG. 5.2. DEPENDENCE OF MONOMER LINEWIDTH ON POPULATION RATIO FOR A FIXED RATE OF LEAVING A MICELLE OF 1×10^6 SEC^{-1}

FIG. 5.3. RATE OF ENTERING A MICELLE FIXED AT 1×10^6 SEC^{-1}

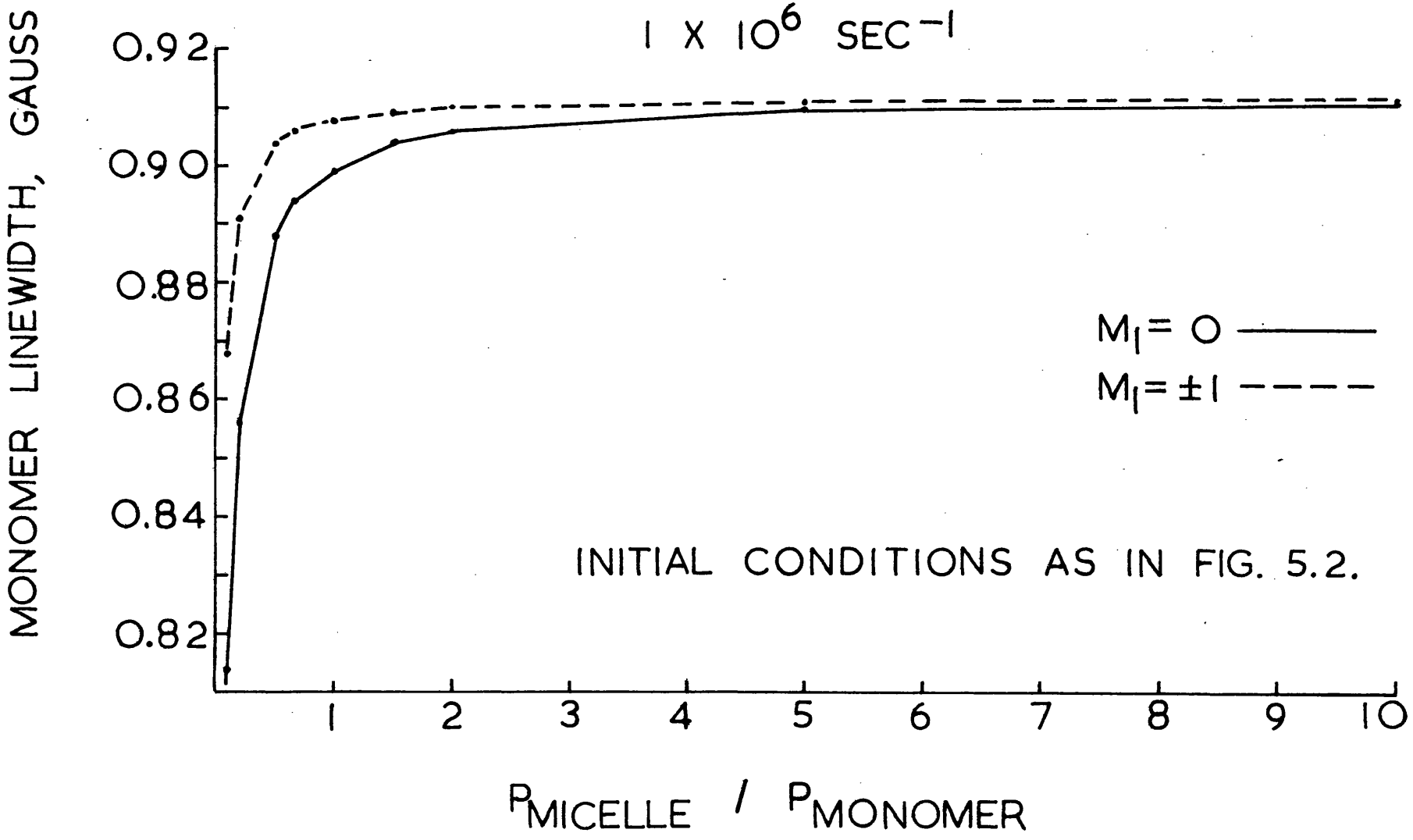

Figure 5.3. shows the effect of changing the frequency of leaving the micellar state on the monomer linewidth. At the low micelle to monomer ratios the linewidth is depressed from its value at higher micelle to monomer ratios, with the linewidth of the $m_I = 0$ line being smaller than that of the $m_I = \pm 1$ lines by more than twice the experimental error.

This effect is detectable for concentrations up to half the CMC, assuming initial linewidths and exchange frequencies as used in the figure.

Figures 5.2 and 5.3 represent limiting cases. The observed behaviour could be anywhere between these limits, in the absence of a specific model for the micellization process. However, observation of behaviour similar to that shown in either of the two figures would indicate that the micellization process was limited either by the frequency with which a monomer collides with a micelle (Fig 5.2), or by the energy required for a monomer to penetrate a micelle (Fig 5.3), and would thus help to define the micellization process.

In section 5.1.1. it was shown that Heisenberg spin exchange broadens the $m_I = \pm 1$ lines more than the $m_I = 0$ line for linewidths in excess of 3.4G. Figure 5.3 shows that, if a micellization mechanism which holds the frequency with which a monomer enters a micelle constant is operative, the $m_I = \pm 1$ lines may be broadened more than the $m_I = 0$ line at linewidths of less than 1G, assuming a suitable magnitude of the monomer-micelle exchange frequency and

a small micelle to monomer population ratio. Figure 5.2. shows that this linewidth effect may also be observable at linewidths less than 3.4G if the frequency with which a monomer leaves a micelle is held constant. Thus it may be possible to distinguish between Heisenberg spin exchange and monomer-micelle exchange by observing the differences in width of the $m_I = \pm 1$ and $m_I = 0$ lines as a function of surfactant concentration.

CHAPTER 6

DETERMINATION OF THE WIDTH OF THE PROTON HYPERFINE LINES

The various line-broadening mechanisms discussed in Chapter 5 broaden each of the proton hyperfine components of the nitroxide line. Experimentally, one records the superposition of these proton hyperfine lines. This chapter is concerned with extracting the width of the proton hyperfine lines from the spectrum obtained experimentally. In order to do this it is necessary to know the magnitude of the individual proton hyperfine splittings. Once the magnitude of these splittings is known, one can computer-simulate EPR spectra with these splittings, using linewidth as a variable parameter, and accept as the true linewidth that width which gives the best fit to the experimental spectrum under consideration. The methods used to determine the proton hyperfine splittings and the computer simulations performed with these splittings are described below.

6.1. NMR Measurements of Hyperfine Coupling Constants

6.1.1. The Theory of the Determination of Small Hyperfine Coupling Constants by NMR

If a nuclear magnetic moment $\underline{I}$ is coupled to an electron magnetic moment $\underline{S}$ in the presence of a strong magnetic field $\underline{H}$, the spin energy levels of the system tumbling freely in solution will be given by[59]

$$\mathcal{H} = g\beta HS_z - g_N\beta_N HI_z + aI_zS_z \qquad (6.1)$$

where g and g_N are the electronic and nuclear g factors respectively, β and β_N the Bohr and nuclear magnetons, and a the isotropic hyperfine constant for the coupling between the

nuclear and the electron spins. The part of the energy which is dependent on the nuclear spin orientation can be written as:

$$\mathcal{H} = -g_N\beta_N I_z \left(H - \frac{aS_z}{g_N\beta_N} \right) \qquad (6.2)$$

where $-\frac{aS_z}{g_N\beta_N}$ is the effective local field produced by the unpaired electron at the nucleus. The magnitude of the total field, $\left(H - \frac{aS_z}{g_N\beta_N} \right)$, will depend upon the sign of S_z if the electron spin relaxation time is long compared with the isotropic hyperfine coupling constant. However, if the electron spin relaxation time is short compared with the isotropic hyperfine coupling constant, the nucleus will see an average value of S_z which is weighted by the populations in each electron spin state. For a Boltzmann distribution of the electron spin populations and a temperature high enough that $\frac{g\beta H}{kT} << 1$, the weighted average value of S_z, $\langle S_z \rangle$, is given by

$$\langle S_z \rangle = - \frac{Hg\beta S(S+1)}{3kT} \qquad (6.3)$$

where k is the Boltzmann constant, T the temperature in Kelvins, and S the electron spin quantum number. Thus, for an electron spin relaxation time much shorter than the isotropic hyperfine coupling constant, (6.2) becomes[59]

$$\mathcal{H} = -g_N\beta_N I_Z H \left[1 + \frac{ag\beta S(S+1)}{3g_N\beta_N kT} \right] \qquad (6.4)$$

Compared with the nuclear resonance of a similar nucleus in a diamagnetic compound, the nuclear resonance peak of the paramagnetic compound is shifted downfield by an amount $\frac{g\beta}{g_N\beta_N} \cdot \frac{aS(S+1)}{3kT}$ if a is

positive, and upfield by the same amount if a is negative. From the observed shift the sign and magnitude of the isotropic hyperfine coupling constant can be determined if S and T are known[60-67].

6.1.2. The Pseudo-contact Interaction

Another type of interaction which can cause the resonance of a paramagnetic compound to shift from the position observed with a diamagnetic compound is called the pseudo-contact interaction. This shift is caused by the combined action of an anisotropic g tensor and a dipolar hyperfine coupling. For a paramagnetic ion with axial symmetry which is tumbling in solution, shift due to the pseudo-contact interaction is given by[68],

$$\Delta H = - \frac{H_o |\beta|^2 S(S+1)(3 \cos^2 x-1) g (g_{11}-g_{\perp})}{9 kT r^3} \qquad (6.5)$$

where x is the angle between the vector $\underline{r}$, connecting the nucleus and the unpaired electron, and the symmetry axis of the molecule, r is the magnitude of $\underline{r}$ and g_{11} and $g_{\perp}$ are the parallel and perpendicular components of the anisotropic g tensor respectively. If one assumes that $|r|$ for the nitroxide in question is 1Å, and that the molecular geometry allows cos x to be 1, the pseudo-contact shift observed on a 220 Mhz NMR spectrometer will be about 10 hz - which is less than the experimental error. Since formulations of equation (6.5) for other molecular geometries and other electron orbital occupation schemes give results of the same order of magnitude[69], the pseudo-contract contribution

to the shift observed in the NMR spectra of paramagnetic nitroxides is negligible. For this reason the pseudo-contact interaction has not been considered by others who have determined the isotropic hyperfine coupling constant from the shift observed in the NMR spectrum[60-67].

6.1.3. Determination of the Isotropic Proton Hyperfine Coupling Constants of the Paramagnetic Surfactants

In order to use equation (6.4) to determine the isotropic proton hyperfine coupling constants, one must ensure that the electron spin relaxation time τ_e is much less than the inverse of the coupling constant to be determined. Since the condition for observation of hyperfine splitting in the EPR spectrum is the converse of this, i.e. that $\tau_e a_i \gg 1$, one must increase the electron spin relaxation time of a paramagnetic compound whose EPR splitting is less than the EPR line-width considerably in order to observe the shifted NMR spectrum. This is usually done by increasing the radical concentration to the point where hyperfine structure is lost, since τ_e becomes increasingly determined by the radical-radical collision frequency and thus becomes less than $^1/a_i$ as the concentration, and thus the collision frequency, increase[60-62,64-67]. An alternative method is to dissolve the radical in a paramagnetic solvent such as di-tert-butylnitroxide[63].

The paramagnetic surfactant $C_{12}TABN\dot{O}$ was dissolved in a minimum amount of D_2O at 60°C. The sample was then heated to 97 ± 2°C, as measured from the temperature-dependent splitting

FIG. 6.1. NMR SPECTRUM OF $C_{12}TABNO$ IN D_2O

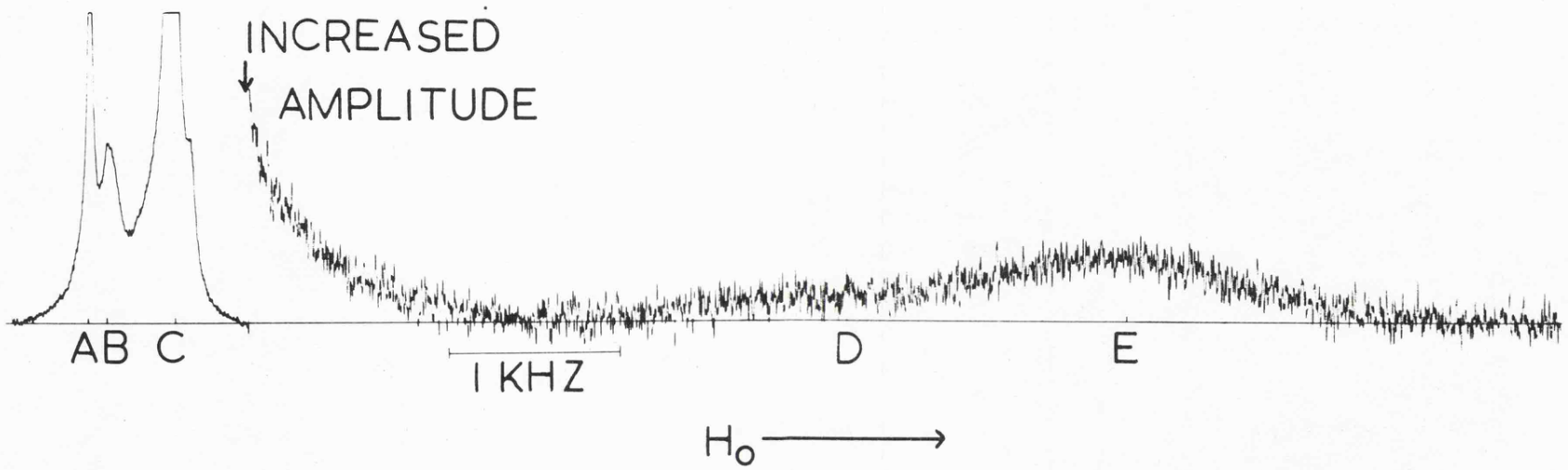

of a standard ethylene glycol sample, and the NMR spectrum recorded on the 220 Mhz spectrometer operated by TNO, Delft, the Netherlands. The spectrum obtained is shown in Figure 6.1. The resonances marked A, B and C are identified as broadened diamagnetic lines arising from $\underline{H}OD$, $(\underline{H}_3C)_3N$, and the hydrocarbon chain protons respectively. The resonances at D and E decreased as the sample was diluted with D_2O, and hence are due to protons coupled with an unpaired electron. From intensity considerations the high field line was assigned to the twelve methyl protons, and the shoulder to lower field to the four methylene protons. The spectrum was scanned 20,000 Mhz up-field and down-field of the diamagnetic resonances, but no other paramagnetically shifted peaks were observed. This is not surprising, in view of the low intensity of the observed paramagnetically shifted peaks.

The NMR spectrum of the diamagnetic precursor to C_{12}TABNO$^{\cdot}$, C_{12}TABNH, is shown in Fig. 6.2.A. Figure 6.2.B. shows the NMR spectrum of the head-group 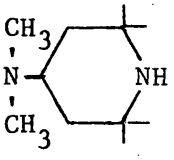

These spectra were obtained on a Perkin-Elmer T-60 NMR spectrometer located at Unilever Research Port Sunlight Laboratory. By comparing the spectra it can be seen that the positions of the methylene protons, the methyl protons, and the hydrocarbon chain protons are similar, at least within the accuracy required for the determination of the isotropic hyperfine coupling constant from NMR data. Therefore the diamagnetic hydrocarbon peak in Fig. 6.1 was taken as the diamagnetic position from which the methyl and methylene peaks had been shifted. Using the measured value of

FIG. 6.2.A. NMR SPECTRUM OF C_{12}TABNH IN ACETONE

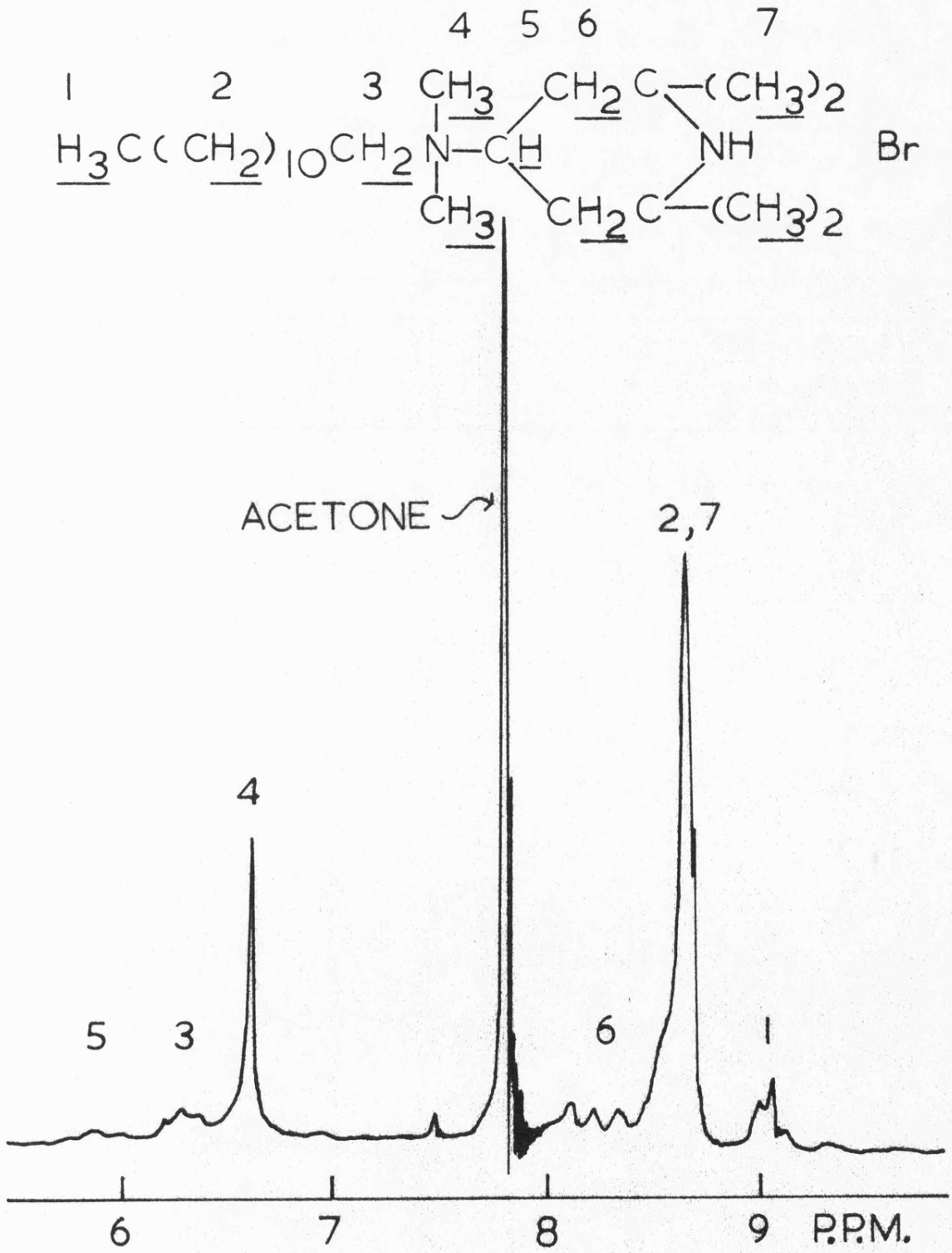

FIG. 6.2.B. NMR SPECTRUM OF

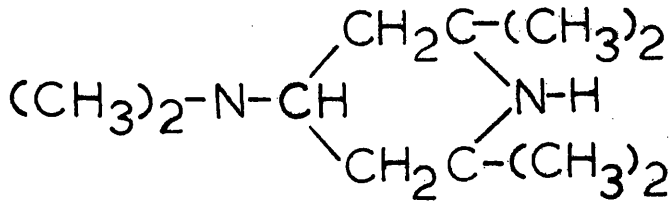

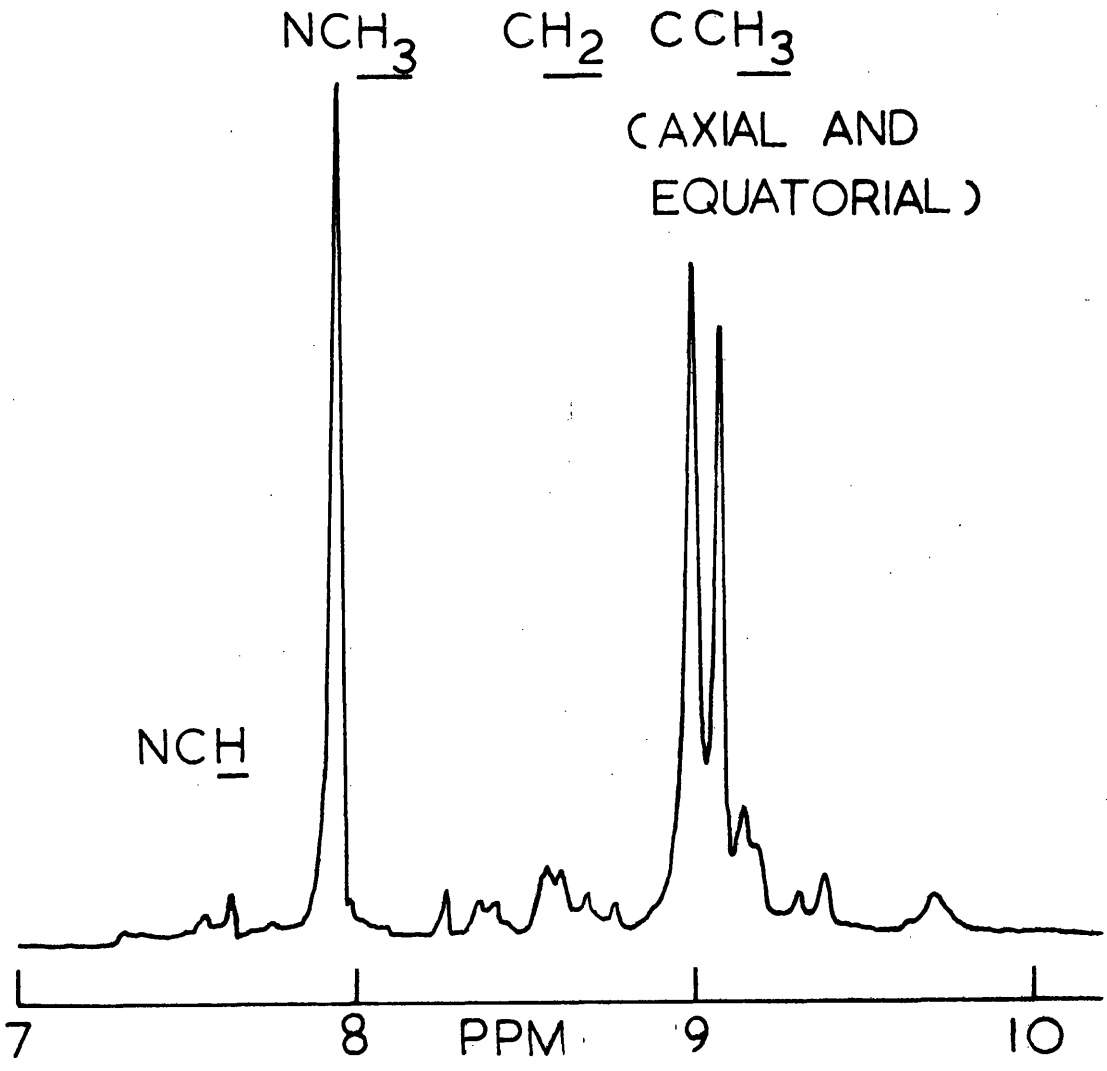

these shifts and the measured temperature of 97 $\pm$ 2°C, the isotropic hyperfine coupling constants were calculated, using equation (6.4), to be a_{CH_3} = - 0.425 $\pm$ 0.012 G, a_{CH_2} = - 0.030 $\pm$ 0.03 G.

Since the signals from which these coupling constants were obtained were quite weak, it was thought that more reliable results might be obtained from $C_1TABN\dot{O}$, which should be easier to solubilize in $D_2\dot{O}$. The NMR spectrum of a saturated solution of $C_1TABN\dot{O}$ in D_2O is shown in Fig. 6.3. This spectrum was obtained from the oscilloscope of the 220 Mhz NMR spectrometer at Delft. The large peaks at the left of the spectrum are the first sidebands of the diamagnetic peaks (the normally recorded spectrum). The central peaks are the paramagnetic peaks, and the right hand peaks the second sidebands of the diamagnetic peaks, shifted from the first sidebands by 10,000 hz. There is a possible paramagnetic peak to the left of the first sidebands of the diamagnetic peaks, which is much lower in intensity than the other paramagnetic peaks but might be caused by the proton at the γ position. The coupling constants obtained from the shift from the diamagnetic hydrocarbon peak are a_{CH_3} = - 0.44 $\pm$ 0.02 G, a_{CH_2} = - 0.31 $\pm$ 0.02 G, and perhaps a_{CH} = + 0.14 G $\pm$ 0.02 G.

The coupling constants obtained for $C_1TABN\dot{O}$ are in reasonable agreement with those obtained for $C_{12}TABN\dot{O}$. The coupling constants found in the literature for several compounds, shown in Fig. 6.4, which are similar to $C_1TABN\dot{O}$ and $C_{12}TABN\dot{O}$, are shown in Table 6.1.

FIG. 6.3. NMR SPECTRUM OF C_1TABNÒ IN D_2O

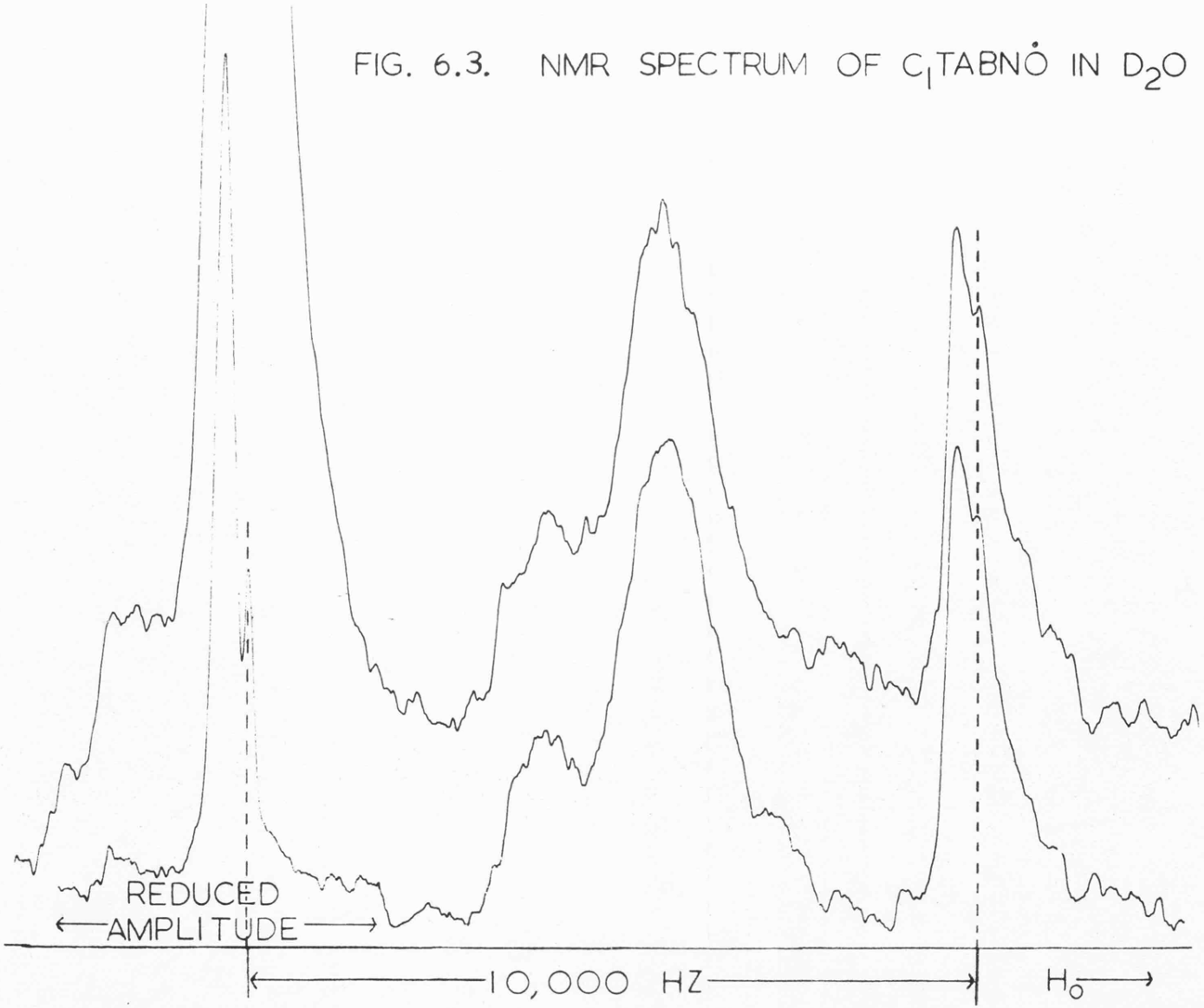

FIG. 6.4. NITROXIDES USED IN NMR STUDIES OF PROTON HYPERFINE STRUCTURE

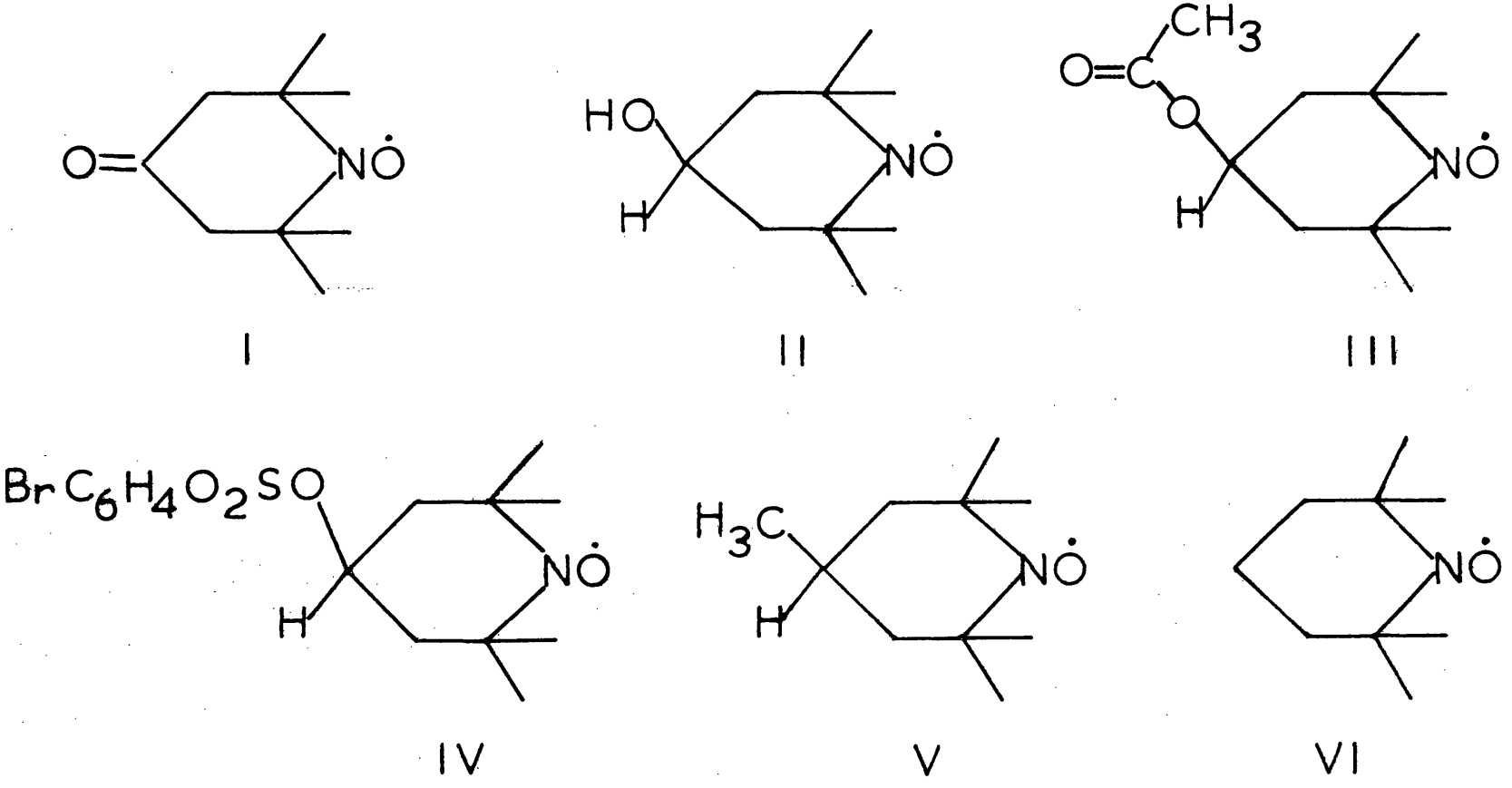

Table 6.1. - The Isotropic Hyperfine Coupling Constants of Several Nitroxides

Reference	Radical	a_{CH_3},G	a_{CH_2},G	a_{CH},G
65	I	- 0.11	- 0.01	
66	I	- 0.12	- 0.02	
65	II	- 0.43	- 0.29	+ 0.09
66	II	- 0.45	- 0.34	+ 0.07
65	III	- 0.41	- 0.29	+ 0.09
66	III	- 0.43	- 0.31	+ 0.08
66	IV	- 0.41	- 0.32	+ 0.06
66	V	- 0.40	- 0.27	0
65	VI	- 0.22	- 0.39	+ 0.18
66	VI	- 0.23	- 0.39	+ 0.18

From Table 6.1 one can see that the coupling constants assigned to C_1TABNO$^{\bullet}$ and C_{12}TABNO$^{\bullet}$ are in reasonable agreement with those which have been found for other similar nitroxides.

Studies of radicals I, II, III and VI have shown[65] that the temperature dependence of the coupling constants is small, especially at temperatures above 35°C. However, the variation in the magnitude of the coupling constants with concentration cannot be measured. It is thought that this may be the cause of small differences, of the order of 5-10%, between the values of the hyperfine coupling determined by NMR and the values of the hyperfine coupling constants necessary to reproduce the observed EPR spectrum[61,62,64,67]. For this reason the hyperfine coupling constants determined for C_{12}TABNO$^{\bullet}$ were varied by up to 10% of their magnitude in order to obtain a better fit between the observed EPR spectra and the computer simulated spectra. The computer-simulation of the EPR spectra is described in the next section.

6.2. Computer-Simulation of Nitroxide Spectra

6.2.1. Description of the Program used to Computer-Simulate EPR Spectra

The program used to computer-simulate EPR spectra was written by C S Johnson, Jnr.[70]. It has been modified by M K Ahn, Stirling Chemistry Laboratory, Yale University and by M A Turpin and Mrs J C Savage, Unilever Research Port Sunlight Laboratory. The program as modified is available from the Computer Sciences Section at Unilever Research Port Sunlight Laboratory, upon request.

The program calculates line positions and intensities from assumed hyperfine coupling constants, and then calculates and plots the resultant spectrum. The individual lines can have either Gaussian or Lorentzian lineshapes, and the spectrum can be calculated in either the adsorption mode or in the first or second derivatives thereof. The program assumes that each of the hyperfine lines has the same linewidth. The calculated spectra are first order approximations, and are strict superpositions of their components - i.e. any possible exchange between components is not taken into account.

6.2.2. Computer-Simulated Nitroxide-Surfactant Spectra

The program described above was used, in conjunction with the proton hyperfine coupling constants determined from NMR spectroscopy, to calculate simulated EPR spectra. It was assumed that only four methylene protons and twelve methyl protons contributed to the spectrum. When the experimentally determined coupling constants were used, it

was found that the experimental spectrum was not reproduced by the program. For an appropriately low linewidth (about 0.38 G),65 Lorentzian lines formed by splitting 13 lines of binomial intensity separated by 0.425 G each into 5 lines of binomial intensity separated by 0.300 G gave a first-derivative spectrum similar to that shown in Fig. 6.5. An experimental spectrum of the $M_I = 0$ line, obtained at low modulation amplitude (0.032 G) from a de-oxygenated sample in order to avoid extraneous line broadening, is shown in Fig. 6.6 for comparison. It can be seen that the feature numbered 1 on the simulated spectrum is too sharp, while the features numbered 3 and 4 are not sharp enough. If one keeps the linewidth narrow enough to allow the features of the line, determined by the proton hyperfine structure, to be observable, then the general shape of the line will be determined by the ratio of the proton hyperfine coupling constants, while the absolute distances such as the distance of any feature from the centre of the spectrum can be fixed by adjusting the magnitudes of the coupling constants after their ratio has been determined. It was decided to allow the magnitudes of the proton hyperfine coupling constants to vary through the experimental error in an attempt to improve the spectral simulation. The methyl coupling was fixed at 0.455 G and the methylene coupling constant in fact allowed to range from 0.200 G to 0.455 G, in steps of 0.001 G. No significant improvement was observed. Since experimental lineshapes are intermediate between Lortenzian and Gaussian, the computer-simulations were

FIG. 6.5. A TYPICAL COMPUTER-SIMULATED C_{12}TABNO SPECTRUM

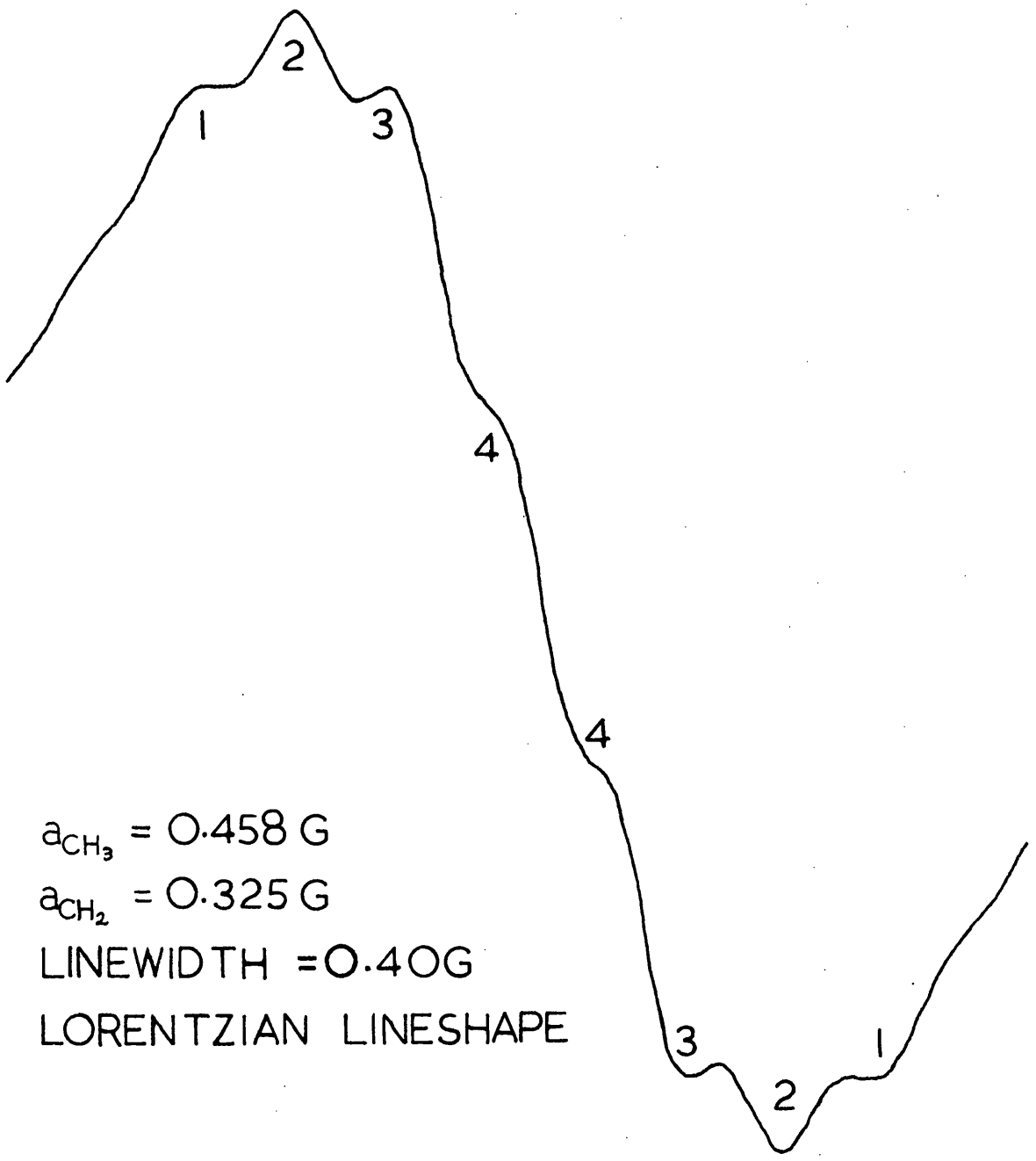

a_{CH_3} = 0.458 G

a_{CH_2} = 0.325 G

LINEWIDTH = 0.40G

LORENTZIAN LINESHAPE

repeated, using Gaussian instead of Lortenzian lines. The best result of this simulation is shown in Fig. 6.6. One can see that the feature numbered 1 is still too sharp, while the feature numbered 4 is not sharp enough.

Since the Gaussian character of EPR lines is often due to the presence of unresolved hyperfine structure, it was thought that a small coupling due to the proton in the γ position might be causing both the Gaussian lineshape and the lack of agreement between the computed and the experimental spectra. To check this assumption, each of the 65 lines in the simulated spectrum was split into two lines of equal intensity, separated by coupling constants ranging from 0.0001 G to 0.002 G in steps of 0.0001 G, from 0.002 G to 0.020 G in steps of 0.002 G and from 0.020 G to 0.150 G in steps of 0.005 G. The lineshapes in these simulations were Lorentzian. The best simulation increased the ratio of the height of peak 3 to the height of peak 2 from 0.939 in the absence of coupling to 0.940, while the worst simulations erased peak 3 completely. The agreement of features 1 and 4 with experiment was not significantly improved by the presence of the third coupling. Thus it was concluded that the possible Gaussian character of the lineshape was not due to the presence of a small hyperfine splitting due to the γ proton.

In a study of Heisenberg spin exchange[45], Freed and co-workers have shown that, when the strongest nuclear spin-dependent relaxation processes are due to exchange, in the slow exchange region the width of each hyperfine line depends upon the degeneracy of that line, according to equation 6.6.

FIG. 6·6. COMPARISON OF COMPUTED AND EXPERIMENTAL SPECTRA

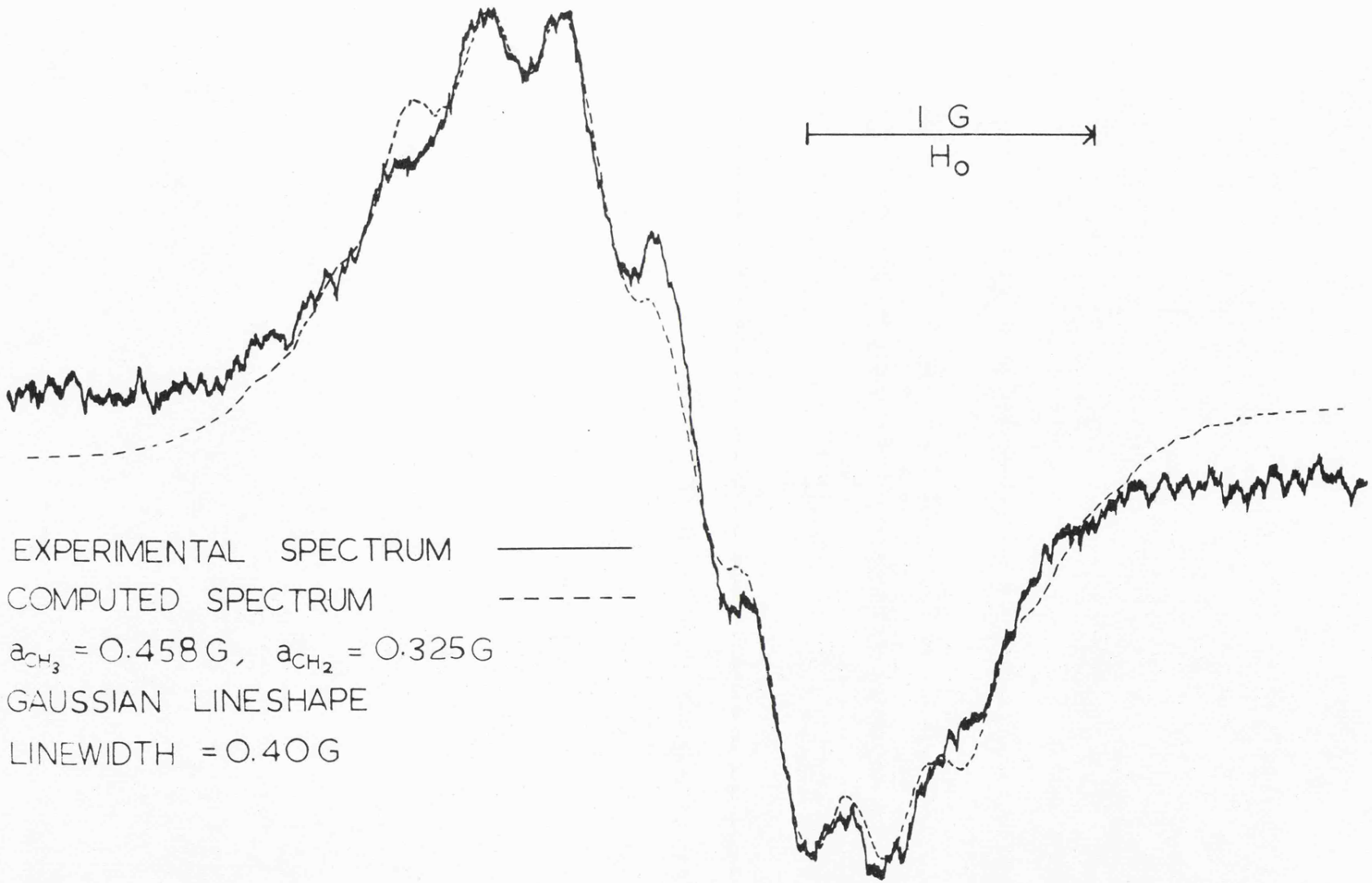

$$\left[\delta_M - \delta_M(0)\right] = \frac{2}{\sqrt{3}} W_{HE} \left(\frac{N-2D_M}{N}\right) \qquad (6.6)$$

In equation 6.6, $\left[\delta_M - \delta_M(0)\right]$ is the increase, in hz, in the width of the line of spectral index number M and degeneracy D_M caused by Heisenberg spin exchange at frequency W_{HE}. Here N is the total number of transitions. Since different nitroxide proton hyperfine lines will have different degeneracies, if exchange is present the widths of the lines will not be the same.

In Figure 6.7.A. a stick diagram is shown which contains the more intense (10% of the most intense line or greater) proton hyperfine lines. The encircled numbers above some of the lines are the nuclear magnetic moments of the methyl protons - for all of these lines the methylene proton magnetic moment is 0. Dashed lines connect these lines to other lines with the same methyl proton coupling but different methylene proton couplings. Of the lines shown here the one labelled by the encircled zero is the most degenerate, containing 6 out of 16 possible methylene states and 924 out of 4,096 possible methyl states for a total degeneracy of 5,544 out of 65,536. For this line the degeneracy factor $(N-2D_M)/N$ will be 0.83. Thus this line will have 0.83 of the width of a similar but non-degenerate line, if δ_M (0) is zero and the linewidth is determined entirely by Heisenberg spin exchange. If the inherent linewidth is greater than zero, the reduction in linewidth and accompanying increase in the height of the line will be less, with the maximum possible peak height being 1.45 times the height of a similar but non-degenerate peak.

FIG. 6.7. COMPUTER SIMULATION OF NITROXIDE SPECTRA

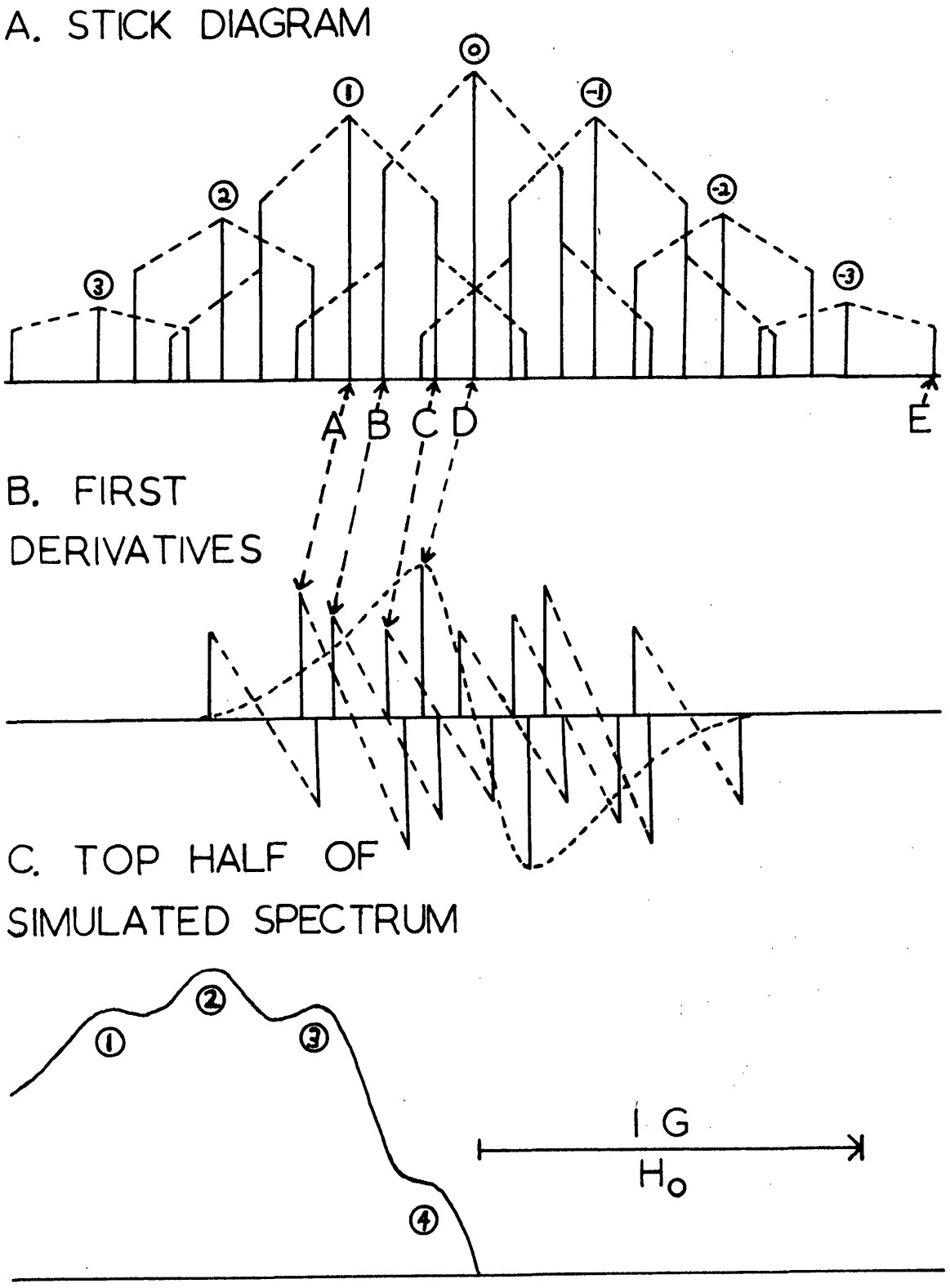

Figure 6.7.B. shows some first derivative maxima and minima obtained from some of the lines in the stick diagram. Only the most intense line is indicated by a Lorentzian curve; for the other lines a diagonal connecting the maximum and the minimum is used to indicate the Lorentzian lineshape. The degeneracies of the lines labelled A to E and the degeneracy factors $(N-2D_M)/N$ are given in Table 6.2 below:

Table 6.2 - Number of States and Degeneracy Factors for some Nitroxide Lines

Line	M_{CH_3}	M_{CH_2}	No of States	$(N-2D_M)/N$
A	+1	0	4,752	0.855
B	0	+1	3,696	0.887
C	+1	-1	3,168	0.903
D	0	0	5,544	0.831
E	-3	-1	880	0.973

It is seen that, if exchange were present, the effect would be to sharpen the central lines more than the outer lines of the spectrum, since the central lines are more degenerate.

Figure 6.7.C. shows the top half of a spectrum simulated from the stick diagram, assuming all lines are Lorentzian and are of equal width. If one looks at the first derivatives in Fig. 6.7.B. which combines to form feature 4, one can see that a narrowing of peaks in the order D > A > B > C > E would raise the peak of feature 4 (dominated by the positive half of line D), and increase the depression between that feature and feature 3 (dominated by the negative half of line A). Since

in general peaks (3) and (4) would be sharpened relative to peaks (1) and (2), the general effect of this mechanism would be to increase the correspondence between simulations such as that shown in Fig. 6.5 and the observed spectrum.

The experimental system used was designed to minimize Heisenberg spin exchange. The nitroxide concentration was kept low (2.0×10^{-5}M) and the system was de-oxygenated in order to eliminate exchange or any other sort of broadening from the system. That this attempt was not successful is consistent with data for 2.8×10^{-5}M di-t-butyl nitroxide[45], which indicate that at room temperature the linewidth in di-methoxyethane is constant at 0.6 G, and that therefore the Heisenberg spin exchange contribution to the linewidth was less than 0.6 G. By comparison with this system, a Heisenberg spin exchange mechanism accounting for 0.1 G to 0.4 G of the linewidth observed in the 2×10^{-5}M $C_{12}TABN\dot{O}$ system is not unreasonable - if one assumes the Heisenberg spin exchange frequency to be proportional to the radical concentration, the di-t-butyl nitroxide in dimethoxyethane data (reproduced in Fig. 3.5.B) indicate that 2×10^{-5}M $C_{12}TABN\dot{O}$ should have a Heisenberg spin exchange dominated linewidth of 0.36 G, which is in reasonable agreement with the observed linewidth. Thus it is reasonable to say that Heisenberg spin exchange is present in the 2×10^{-5}M $C_{12}TABN\dot{O}$ system, and that because of this the widths of the hyperfine lines are not the same, but will be given by equation 6.6, in which δ_M (0) may be zero and must be less than δ_M.

FIG. 6.8. ENVELOPE LINEWIDTH VS. WIDTH OF THE COMPONENT LINES

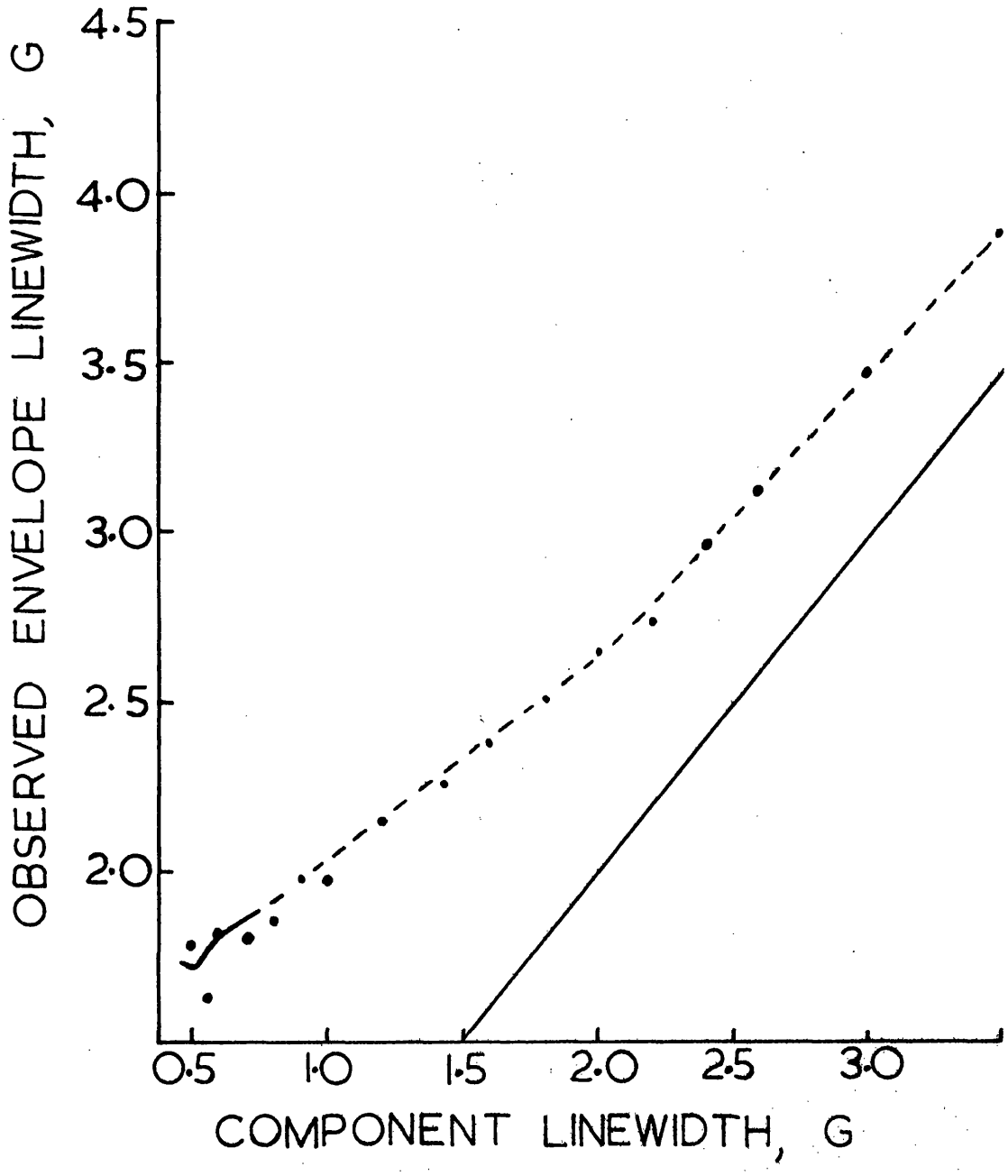

$a_{CH_3} = 0.458$ $a_{CH_2} = 0.325$

GAUSSIAN LINESHAPE

The computer-simulation procedure produced other evidence that exchange is probably present in the system. If one ignores the probable variation in the widths of the proton hyperfine lines and assumes that the computed spectrum shown in Fig. 6.6 adequately represents the experimental spectrum, then by increasing the width of the individual lines one can computer-simulate a series of spectra whose envelope linewidth can be correlated with the individual hyperfine linewidth by means of a graph similar to Fig. 6.8.[5] The points shown in Fig. 6.8 do not follow a smooth curve, especially in the region of low hyperfine component linewidth. The computer simulation program had a vertical sensitivity of one part in 10^8, however, and it was felt that one could only measure the maximum of an experimental spectrum to about one part in 10^2. An apparent maximum, defined as the mean on the horizontal scale of all points within 1% of the magnitude of the true maximum, was therefore calculated and its values used to define the solid line shown in Fig. 6.8. The real and apparent maxima for several linewidths are shown in more detail in Fig. 6.9. The horizontal sensitivity of the calculation is $\pm$ 0.010 G, which is about half the experimental error. These two figures show that the scatter of points allows one to correlate a measured envelope linewidth of 1.85 G or greater with a width of the component proton hyperfine lines to within $\pm$ 0.02 G, which is the experimental error, but that for envelope linewidths below 1.85 G the correlation can be qualitative only.

FIG. 6.9. EXPANDED LOWER LEFT CORNER OF PREVIOUS FIGURE

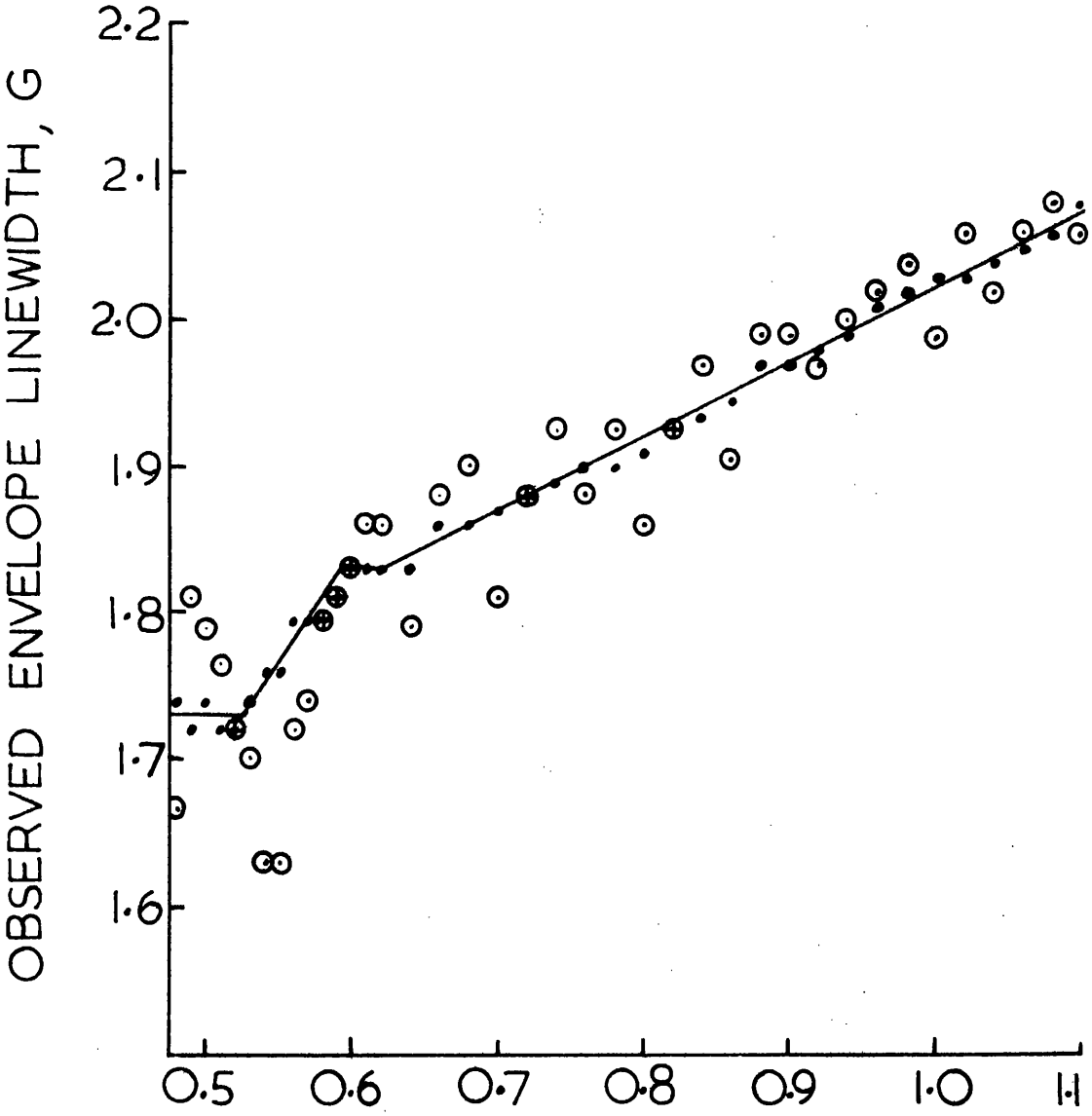

$a_{CH_3} = 0.458G$, $a_{CH_2} = 0.325G$

GAUSSIAN LINESHAPE

In Fig. 6.10, the points obtained for a similar graph using Lorentzian component linewidths are shown. It is seen that the points obtained define a much smoother curve than that obtained with Gaussian lineshapes, and that the resultant envelope linewidths are larger for Lorentzian than for Gaussian component lines. One would therefore expect a lineshape intermediate between Lorentzian and Gaussian to yield widths intermediate between the widths shown here.

Fig. 6.11 shows experimental linewidths obtained as a function of temperature from a de-oxygenated solution of 5.5×10^{-3}M C_{12}TABNO$\dot{}$ in the presence of 1.5×10^{-3}M C_{12}TABNH. As the temperature is increased, the number of collisions between paramagnetic molecules should increase, thus increasing the Heisenberg spin exchange broadening of the nitroxide lines. Thus Fig. 6.11 should be roughly equivalent to Figures 6.8-6.10. Since the nitroxide lines are not of equal height, the fast-tumbling limit has not been reached and it is conceivable that increasing the temperature could cause a linewidth decrease, especially to the high field line. The behaviour of the solutions at the higher temperatures show that Heisenberg spin exchange broadening dominates the linewidth behaviour in that region. The minimum linewidth obtained for the three lines is 1.65 G $\pm$ 0.02 G for $M_I = 0$, 1.67 G $\pm$ 0.02 G for $M_I = 1$ and 1.72 $\pm$ 0.02 G for $M_I = -1$. Experimental spectra of C_{12}TABNO$\dot{}$ with lower linewidths have been observed - a de-oxygenated sample whose concentration was lower than 1.4×10^{-3}M, which on heating loses the hyperfine structure on the central peak between 86°C and 96°C, has a width of 1.35 $\pm$ 0.05 G at 96°C. This indicates that broadening due to the slower tumbling rate probably dominates the lower temperature region of Fig. 6.11.

FIG. 6.10. ENVELOPE LINEWIDTH VS. COMPONENT LINEWIDTH

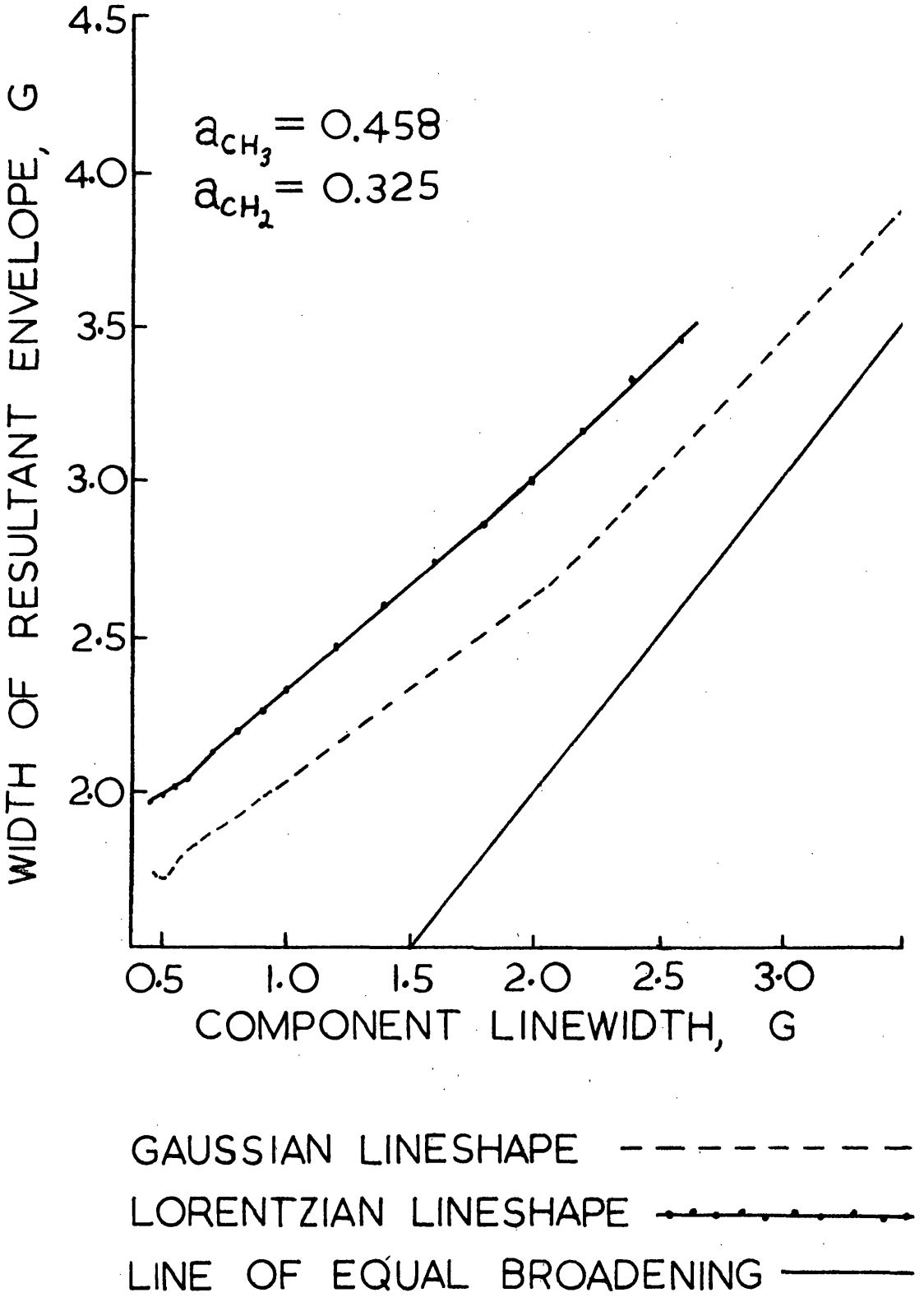

FIG. 6.11. MEASURED LINEWIDTH VS. TEMPERATURE FOR 1.5×10^{-3} M C_{12}TABNH, 5.5×10^{-3} M C_{12}TABNO

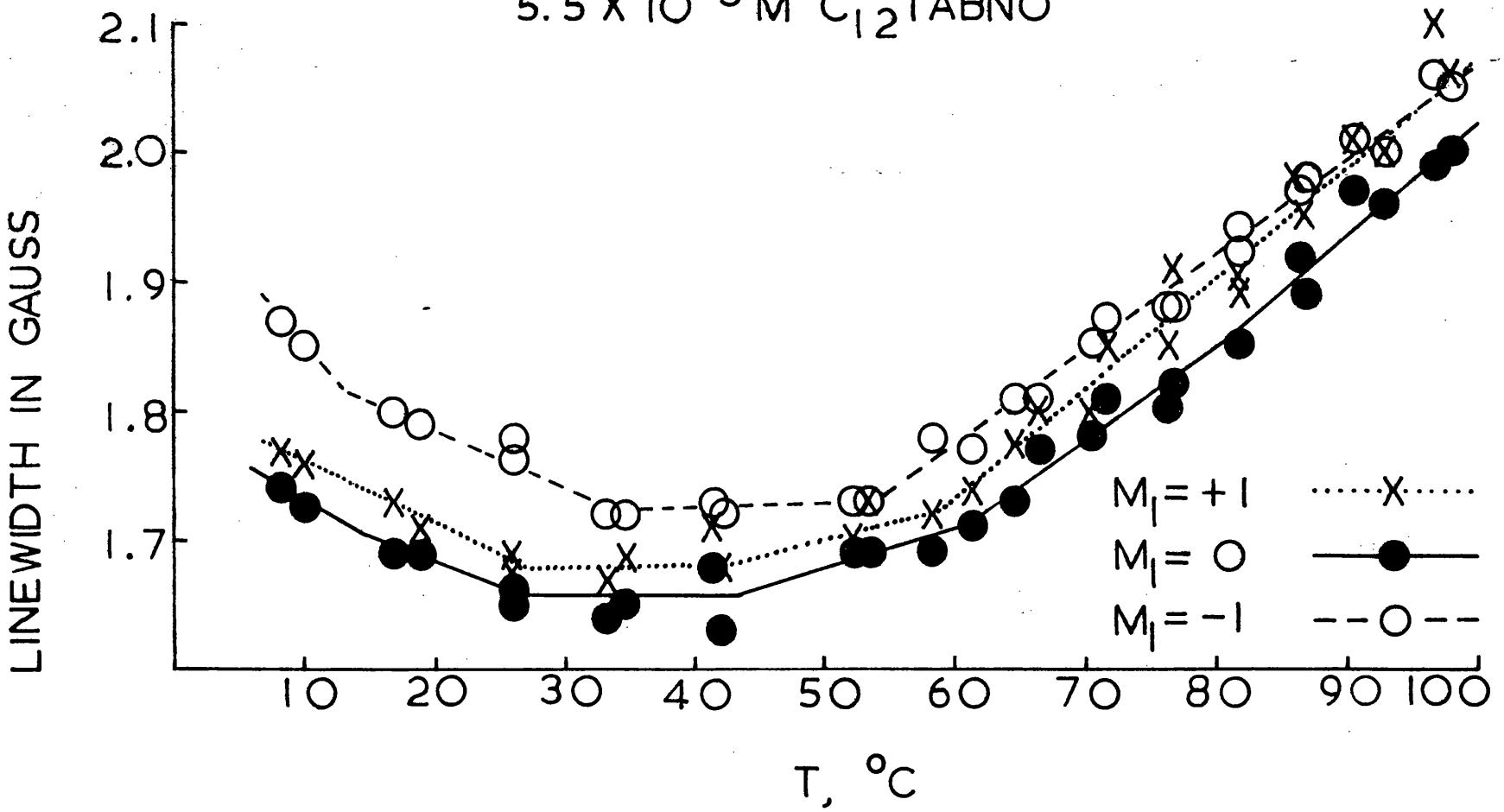

The computer-simulated spectra show hyperfine structure at envelope linewidths below 1.73 G for a Gaussian lineshape and 1.97 G for a Lorentzian lineshape. They clearly do not approach the experimentally observed width of around 1.35 G. However, spectra have been simulated with coupling constants of smaller magnitude but in the same ratio - the result of one of these simulations is shown in Fig. 6.12. The methyl and methylene coupling constants have been reduced from 0.458 to 0.430 and from 0.325 to 0.305 respectively, and the minimum envelope linewidth reduced from 1.73 G to 1.67 G. Clearly a much greater reduction in the coupling constants is needed to reduce the minimum to the experimentally observed value.

A reduction in the observed value of the proton hyperfine coupling constants is consistent with the presence of exchange between the proton hyperfine lines, since an exchange frequency of the order of magnitude of the separation of the hyperfine lines would cause the lines to move toward each other, thus reducing the apparent hyperfine coupling constants. Since the hyperfine coupling constants are of the same order of magnitude as the individual linewidths, which seem to be dominated by an exchange-broadening component, this hypothesis is not improbable.

Although it would be possible to correct the simulated spectra by modifying the program to give each hyperfine component a width determined by equation 6.6, it

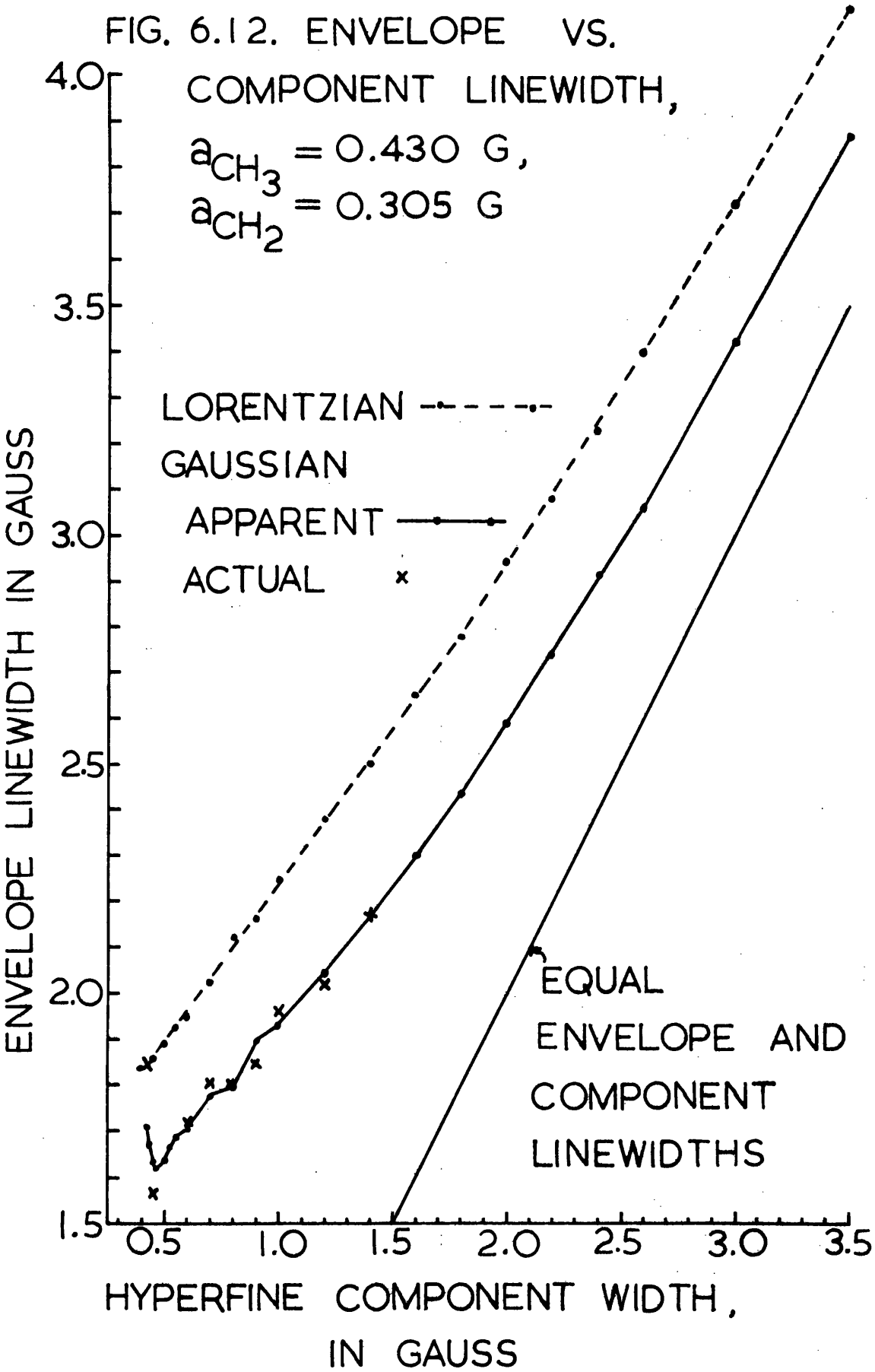
FIG. 6.12. ENVELOPE VS.
COMPONENT LINEWIDTH,
$a_{CH_3} = 0.430$ G,
$a_{CH_2} = 0.305$ G
LORENTZIAN
GAUSSIAN
APPARENT
ACTUAL
EQUAL
ENVELOPE AND
COMPONENT
LINEWIDTHS
ENVELOPE LINEWIDTH IN GAUSS
HYPERFINE COMPONENT WIDTH,
IN GAUSS
4.0
3.5
3.0
2.5
2.0
1.5
0.5
1.0
1.5
2.0
2.5
3.0
3.5

was decided that a complete solution to the problem of 65 exchanging lines, either by means of a Sack calculation[53] or by density-matrix methods[45], was too complicated to be attempted. One would need to have the full solution in order to obtain the exchange frequency from the observed envelope linewidth. However, the results obtained in this chapter are useful in a qualitative way in determining the exchange frequency which causes an observed envelope line broadening.

CHAPTER 7

PRE-MICELLAR ASSOCIATION

7.1. INTRODUCTION

In Chapter 5, exchange between a monomer and a micelle, or other aggregate giving one broad EPR line, was mentioned as a possible cause of the observed anomalous linewidth effects mentioned in Chapter 4. This chapter discusses the possible existence below the cmc of dimers or other pre-micellar aggregates, in order to establish whether the anomalous linewidth effects are indicative of micelle formation.

The possible existence of pre-micellar aggregates has been discussed in the chemical literature for several years[8,71-78]. Arguments favouring the existence of pre-micellar association have been collected in a review by Mukerjee[8]. In many instances the experimental errors of the techniques employed and the experimental results have been of the same order of magnitude. Sodium dodecyl sulphate has been studied by several authors and methods[71,75,76,78] and found, from conductivity measurements, to undergo pre-micellar dimerization,[71] with an equilibrium constant K_D for the dimerization reaction (7.1) of about 250. It has also been found,

$$DS^- + DS^- \rightleftharpoons (DS)_2^= \qquad (7.1)$$

from conductivity measurements[75], to behave as a completely disassociated electrolyte below the cmc. EMF measurements[76] yielded a maximum K_D of 10 (12% dimer at the cmc), with the suggestion that with theoretical modifications no dimers need be invoked, while measurements of solution density[78] resulted in a K_D of about 100.

Results from several series of surfactants are available which indicate that pre-micellar dimerization increases with increasing hydrocarbon chain length[72-74,79]. A conductivity method has been used to show that sodium n-alkyl sulphonates do not dimerize for hydrocarbon chain lengths ranging from two to twelve, but that for the sodium n-tetradecyl sulphonate the experimental data are best explained by a K_D of 340[74]. Alkyl trimethyl ammonium bromide salts have been found to undergo similar behaviour[73], a conductivity method indicating the presence of dimerization in C_{16} and C_{18}TAB but not in C_{12} and C_{14}TAB. Partition ratios for fatty acids between heptane and an aqueous buffer (pH 7.45)[79] have been interpreted[72] as showing that dimerization of the anion of the fatty acid takes place in the aqueous phase, with K_D ranging from 40 for the decanoate anion to 1.3×10^7 for the stearate anion. However, no dimerization was detected by light-scattering methods[77] in a series of zwitterionics whose hydrocarbon chain lengths ranged between ten and sixteen. In all cases where dimerization was found, the driving force of the reaction was considered to be the increase in stability obtained by the association of two hydrocarbon chains[8].

7.2. Measurements with C_{12}TABNO$^{\bullet}$

It is possible to use EPR methods to measure the amount of nitroxide which gives a sharp, three lined spectrum in solution. The intensity of this spectrum can be measured to $\pm$ 2% relative to a standard sample if care is taken in obtaining the EPR spectra. Thus, if a solution contains both a sharp, three lined signal and a broad signal such as has been observed from a micelle, one can measure the amount of the sharp component present and thus determine parameters such as the monomer to micelle ratio.

A series of measurements was carried out with $C_{12}TABN\dot{O}$ to determine the amount of monomeric surfactant present as the total surfactant concentration was increased through the cmc. A standard solution of 2×10^{-2}M $C_{12}TABN\dot{O}$ was prepared, and samples at other concentrations were prepared from this by dilution, using Agla syringes to measure both the volume of stock solution and the volume of water added. The concentrations thus obtained were known to be better than $\pm 1 \times 10^{-4}$M. The samples, which were not de-oxygenated, were placed in a Varian Room Temperature Aqueous cell, which was adjusted in the EPR cavity until the maximum possible signal ($\pm$ 0.5%) was obtained from the sample. The EPR spectra of the samples were obtained under identical conditions, excepting changes in the magnitude of the receiver gain control necessitated by the changing intensities. These changes were corrected for.

The intensities of the EPR spectra thus obtained were measured using a nomogram method described by Tolkachev and Mikhailov[41]. The method gave intensities for the three nitroxide peaks which were within $\pm$ 3% of the average value for the three peaks. The standard error (68% of the time, measurements of the mean will lie within one standard error of the true mean, while 95% of the time they will lie within two standard errors of the true mean)[80], averaged 1.25% and did not exceed 2.3%. The monomer concentrations were obtained from the measured intensities, using the 3×10^{-3}M peak as a standard. In Figure 7.1, the monomer concentrations thus obtained, enclosed by $\pm$ 2% error bars, are plotted as a function of the total surfactant concentration. Figure 7.2 shows a conductivity plot of the same compound, used to determine the cmc. In both figures there is a small deviation from

FIG. 7.1. VARIATION IN THE MONOMER CONCENTRATION OF $C_{12}TABN\dot{O}$ WITH TOTAL $C_{12}TABN\dot{O}$ CONCENTRATION

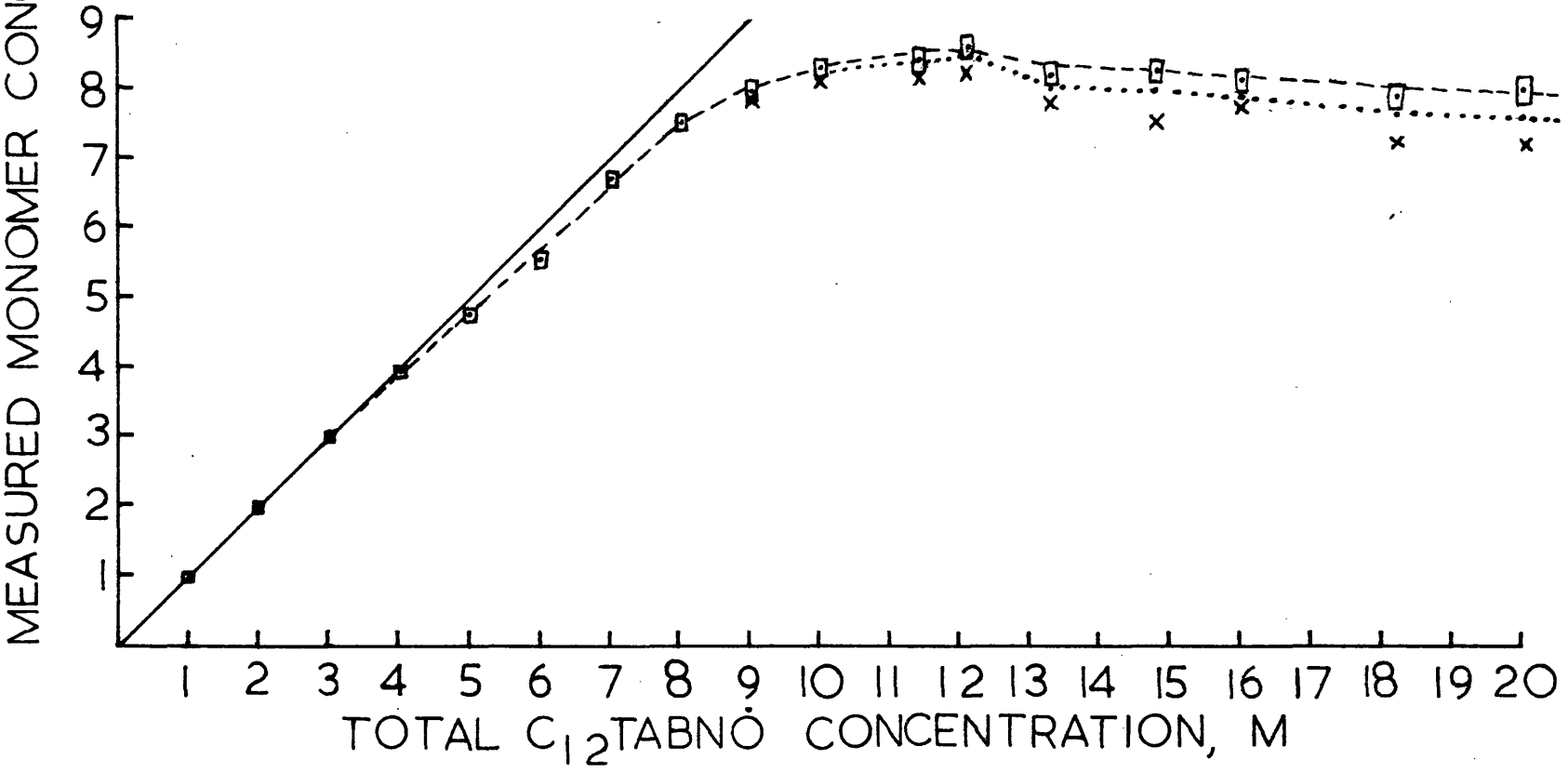

FIG. 7·2. CONDUCTIVITY OF C_{12}TABNO AT 25 °C

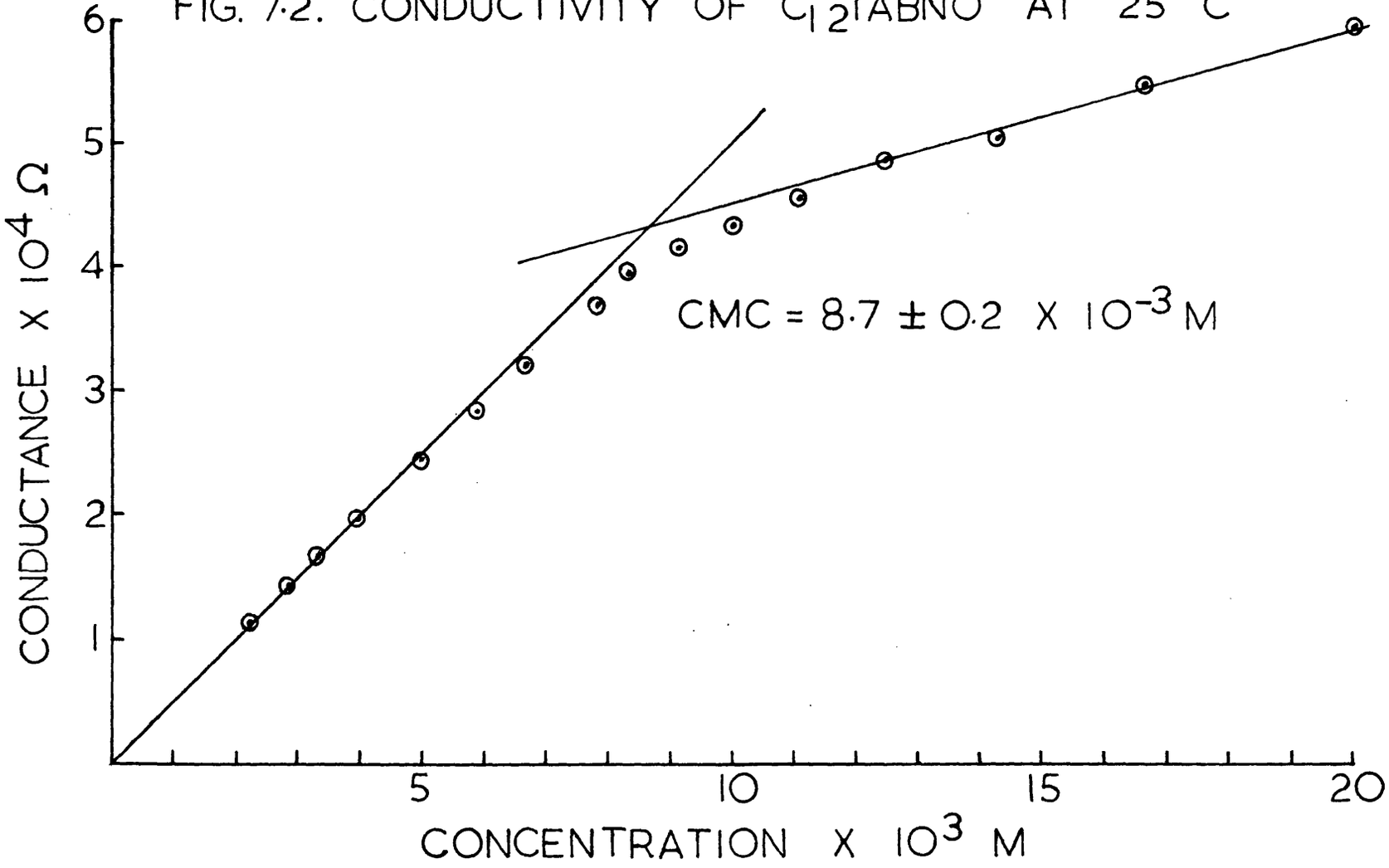

the expected behaviour in the region between about half the cmc and the cmc. Slightly less monomer than expected seems to be present, and the conductivity is decreased somewhat as well. This could be due to the formation of dimers below the cmc, or to the formation of a small number of micelles below the cmc. If one assumes that the deviations are caused by dimer formation, the data plotted in Figure 7.1 can be used to calculate an equilibrium constant K_D for the dimerization process. Several values of K_D and their error limits are shown in Table 7.1. The data at concentrations up to 8 x 10^{-3}M are consistent

Table 7.1 Dimerization constant K_D for $C_{12}TABNO$

Total $C_{12}TABNO$ concentration, T, x 10^3M	Measured Monomer Concentration, D, x 10^3M	$K_D = \frac{T - D}{D^2}$	$K_D^+ = \frac{(T+0.1)-(D-0.2D)}{(D-0.02D)^2}$	$K_D^- = \frac{(T-0.1)-(D+0.02D)}{(D+0.02D)^2}$
5	4.72	12.5	23.8	2.12
6	5.52	15.7	24.0	7.83
7	6.70	6.7	12.8	1.07
8	7.52	8.5	13.0	4.28
9	7.97	16.2	21.4	11.3
10	8.27	25.0	30.5	20.3

with a dimerization constant of about 10, but above that concentration an increasingly larger K_D is required, a result in fact due to the onset of micellization. The data are not accurate enough to establish beyond doubt that the decrease in monomer intensity below the cmc is due to dimerization rather than micelle formation, although they tend to support that view.

The intensities measured above the cmc are subject to an increasing error due to the presence of the underlying micellar line, which adds to the observed intensity of the $M_I = 0$ line and subtracts a smaller amount from the $M_I = \pm 1$ lines. Computer simulations assuming Lorentzian lineshapes for both monomer and micellar lines, a monomer linewidth of 1.8G, a micellar linewidth of 16.0G and a hyperfine splitting constant a_H of 16.9G showed that the true monomer intensity X was related to the observed intensity I (M) by

$$\left.\begin{aligned} X + Y &= I\ (0) \\ X - 0.25Y &= I\ (\pm 1) \end{aligned}\right\} \qquad (7.2)$$

where Y is the amount of micellar signal underlying the $M_I = 0$ monomer line and M is the spectral index number of the line concerned. However, micellar intensities obtained by this method were a magnitude lower than expected from cmc measurements. If the micellar line is 9G wide instead of 16, and is of Lorentzian lineshape, the micellar concentrations known to be present will have the observed effect on the spectra, and monomer intensities can be calculated using equations 7.3.

$$\left.\begin{aligned} X + Y &= I\ (0) \\ X - 0.1Y &= I\ (\pm 1) \end{aligned}\right\} \qquad (7.3)$$

Both sets of equations decrease the values of the monomer concentration, with the decrease becoming larger as the total surfactant concentration increases. Deviations of the lineshape towards the Gaussian lineshape would also tend to decrease the true monomer concentration. At present the most meaningful statement seems to be that the intensity measured above the cmc will be higher than the true intensity, which will lie somewhere between the intensity determined from the $M_I = \pm 1$ lines alone

and the average intensity. The dotted line in Figure 7.1 corrects the measured average intensity according to equation 7.2, while the crosses represent the average intensities from the $M_I = \pm 1$ peaks only. The resultant apparent decrease in monomer intensity above the cmc is consistent with the mass action approach to micellization[81], as explained briefly below.

If M is a micellar species at concentration C_M and D is a monomer species at concentration C_D, where N molecules of D constitute a micelle and $(1-\alpha)N$ counterions are associated with the micelle, then micellization can be described by

$$(1-\alpha)N\,C + ND \rightleftharpoons M \tag{7.4}$$

where C is the counterion. Equation 7.4 will have an associated equilibrium constant K_D, where

$$K_D = \frac{C_C^{N(1-\alpha)}\ C_D^N}{C_M} \tag{7.5}$$

Since mass balance requires that

$$C_C = C_D + N\,C_M \tag{7.6}$$

if no excess counterions are added to the system, Equation 7.6 can be substituted into Equation 7.5, yielding

$$K_D = \frac{C_C^{N(1-\alpha)} \cdot C_D^N \cdot N}{C_C - C_D} \tag{7.7}$$

Taking the logarithm of 7.7 and re-arranging, one finds that

$$\log C_D = \frac{\log K_D}{N} - (1-\alpha)\log C_C + \frac{1}{N}\left[\log (C_C - C_D) - \log N\right] \tag{7.8}$$

For a given system, the number of monomers per micelle and the degree of dissociation α will be fixed. Since C_C is also the total surfactant concentration, at high surfactant concentrations ($C_C >> C_D$)

$$\log C_D = K' - (1-\alpha^{-1}/N) \log C_C \qquad (7.9)$$

where $K' = \frac{\log K_D - \log N}{N}$. Thus in the limiting region of high total surfactant concentration the slope of a $\log C_D$ vs $\log C_C$ plot will be negative, with a value $(1-\alpha^{-1}/N)$. At lower total surfactant concentrations the slope will be larger in magnitude, but in the same direction. This is qualitatively the type of behaviour exhibited by C_{12} TABNO$^{\bullet}$, as shown in Figure 7.1.

7.3. Measurements with C_1TABNO$^{\bullet}$

In order to see whether or not the pre-micellar association observed with C_{12}TABNO$^{\bullet}$ was induced by the nitroxide head group, measurements of the intensity of C_1TABNO$^{\bullet}$ as a function of concentration were made. C_1TABNO$^{\bullet}$ solutions were prepared by dilution from a standard C_1TABNO$^{\bullet}$ solution whose concentration was not known exactly, both because of difficulties encountered in purifying the C_1TABNO$^{\bullet}$ sample and because the C_1TABNO$^{\bullet}$ was hydroscopic. Absolute intensities were determined by comparison of the intensities of the four least concentrated C_1TABNO$^{\bullet}$ samples with the intensity of a 4.78×10^{-3}M C_{10}TABNO$^{\bullet}$ sample, which was assumed not to dimerize. The intensity measurements were made using the nomogram method[41] used for the C_{12}TABNO$^{\bullet}$ samples, except that only the $M_I = 0$ peak was used in the measurement. Because of this, and because of probable errors involved in the standardization procedure, the error in the intensities determined is estimated at $\pm 5\%$.

FIG. 7·3. ASSOCIATION OF C_1TABNÒ IN SOLUTION

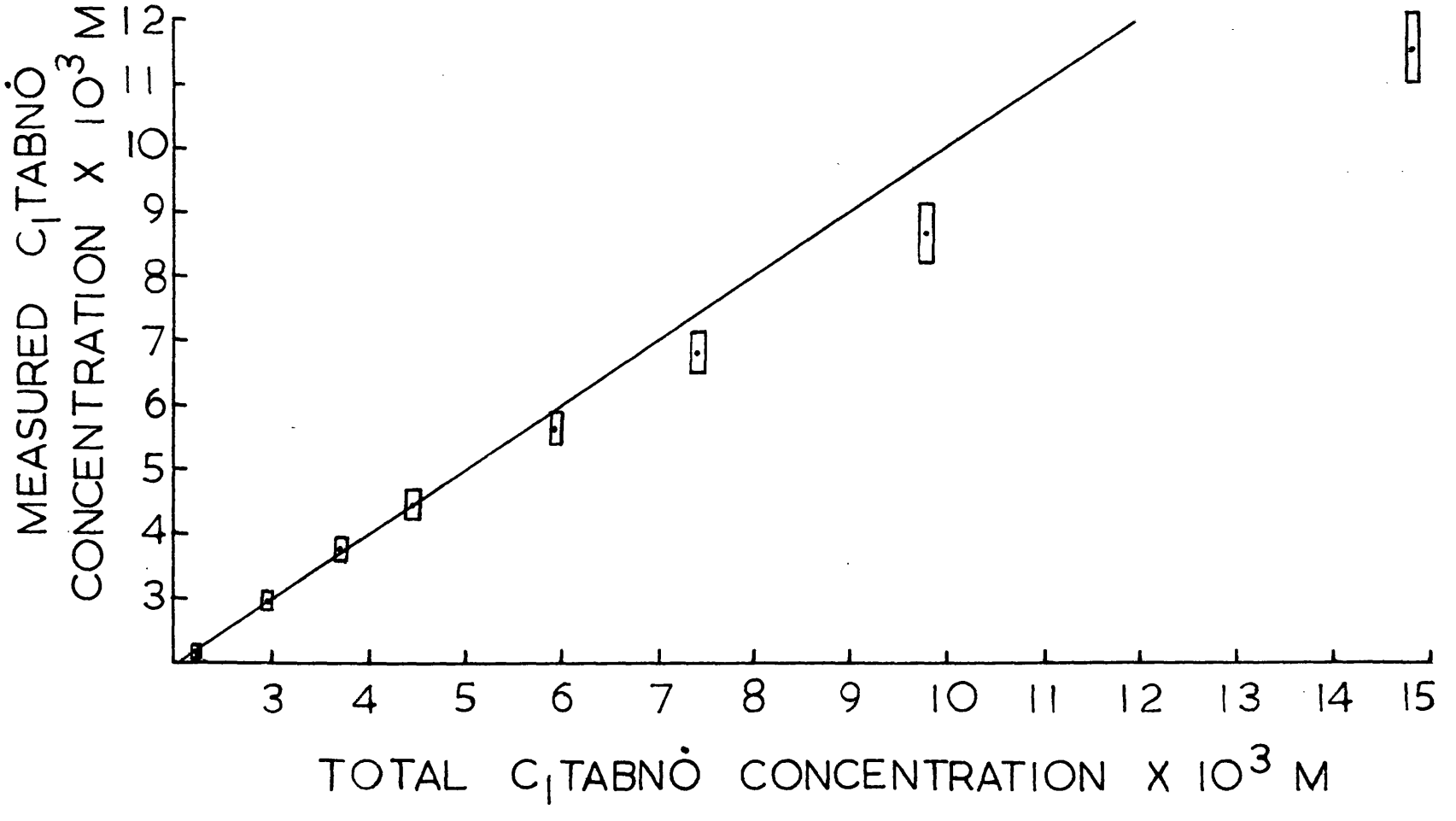

The resultant plot of measured monomer concentration versus total concentration is shown in Figure 7.3. At concentrations greater than 6×10^{-3}M a decrease in the measured monomer percentage is observed. If it is assumed that this decrease is due to dimer formation, one can calculate an equilibrium constant K_D for the dimerization reaction, as was done for $C_{12}TABN\dot{O}$ in the previous section. The results for C_1 $TABN\dot{O}$ are shown in Table 7.2.

TABLE 7.2

Total $C_1TABN\dot{O}$ concentration, T, x 10^3M	Measured Monomer. C_1 $TABN\dot{O}$ Concentration, M, x 10^3M	$K_D = \frac{T - M}{M^2}$	$K_D^+ = \frac{(T+0.1)-(M-0.05M)}{(M-0.05M)^2}$	$K_D^- = \frac{(T-0.1)-(M+0.05M)}{(M+0.05M)^2}$
5.92	5.63	9.15	19.9	0.29
7.40	6.80	13.0	22.8	4.89
9.78	8.70	14.3	22.3	7.67
14.80	11.60	23.8	31.2	17.7

As can be seen from Table 7.2, the results for $C_1TABN\dot{O}$ are not accurate enough to indicate whether or not dimerization is the only process occurring in the system. The calculated results could be explained by a dimerization constant of about 18, or by a dimerization constant of about 10 and the presence of larger aggregates at higher concentrations of total surfactant. It is certain, however, that some loss of expected monomer intensity is occurring in the system.

The results for $C_1TABN\dot{O}$ indicate that the monomer intensity loss observed for C_{12} $TABN\dot{O}$ does not have to be due to hydrocarbon-chain induced pre-micellar dimerization. It is likely that the interaction which causes $C_1TABN\dot{O}$ to associate is also operative in the $C_{12}TABN\dot{O}$

case, and that the association of $C_{12}TABN\dot{O}$ molecules below the cmc is caused by interactions between the paramagnetic head groups. The presence of an on-line computer would make it possible to reduce considerably the error margins in these experiments, allowing more accurate values of K_D to be obtained for $C_1TABN\dot{O}$ and for $C_{12}TABN\dot{O}$. Comparison of these more accurate K_D values should allow one to determine whether dimer formation or pre-cmc micelle formation is important for $C_{12}TABN\dot{O}$, and whether the $C_1TABN\dot{O}$ association and the $C_{12}TABN\dot{O}$ association are caused by the same mechanism.

7.4. Variable Temperature Measurements with $C_{10}TABN\dot{O}$

Data from $C_{10}TABN\dot{O}$ samples have been obtained which indicate that the number of monomers present in $C_{10}TABN\dot{O}$ below the cmc increases as the temperature increases from 25°C to about 60°C. The spectra were obtained from both a 6×10^{-3}M and a 1×10^{-2}M $C_{10}TABN\dot{O}$ solution, neither of which had been de-gassed. The solutions were placed in a Varian Variable Temperature Aqueous Cell, to which silicone rubber strips had been glued to ensure that the cell fitted tightly into the quartz dewar which was inserted in the EPR cavity. The dewar was fastened firmly in the cavity with similar strips. It was found that, using the standard Varian variable temperature apparatus modified in this way and measuring the intensities by the nomogram method[41] described earlier, it was possible to obtain intensities reproducible to ±3%. The temperatures were measured with the copper-constantan thermopile described in Chapter 4.

The measured intensities were corrected for the decrease in intensity with increasing temperature due to the progressive equalization of the number of spins in the $m_s = +\frac{1}{2}$ and $m_s = -\frac{1}{2}$ spin states (Boltzmann factor)[82], and for the decreasing intensity with increasing temperature due to the expansion of the solution[83] (the corrections used were those applicable to pure water). Errors due to the presence of air bubbles, which often form in solutions at higher temperatures (sometimes being visible in solutions at temperatures as low as 60°C) were not corrected for, and would cause a decrease in intensity at higher temperatures.

If one assumes that no air bubbles were present in any of the solutions, and that at the highest two temperatures recorded each of the solutions contained only monomeric C_{10}^{TABNO}, then by setting the average intensity at these two highest temperatures equal to 1 the relative monomer intensities at the other temperatures can be obtained. The results are shown in Figure 7.4 - the error bars represent a ±3% deviation in the measured intensity of the solution concerned. Figure 7.4 shows that there is some loss of intensity in the solutions at lower temperatures, and that there is probably a greater loss of intensity in the more concentrated solution. This is consistent with the formation of dimers which are more stable at the lower temperatures, and which would disassociate at higher temperatures to cause the observed increase in the number of monomers present. The decrease in intensity at the highest temperature is probably due to the formation of air bubbles, whose presence at other temperatures may have caused the percentage of monomers present at the lower temperatures to be less than that indicated on the figure. No calculations of dimerization constants were attempted, since the uncertainty in the data, coupled with the lack of accurate knowledge of the monomer intensity at high temperatures and the uncertainty that at high temperatures the solution

FIG. 7.4. FRACTION OF $C_{10}TABN\dot{O}$ PRESENT IN MONOMER FORM VS. TEMPERATURE

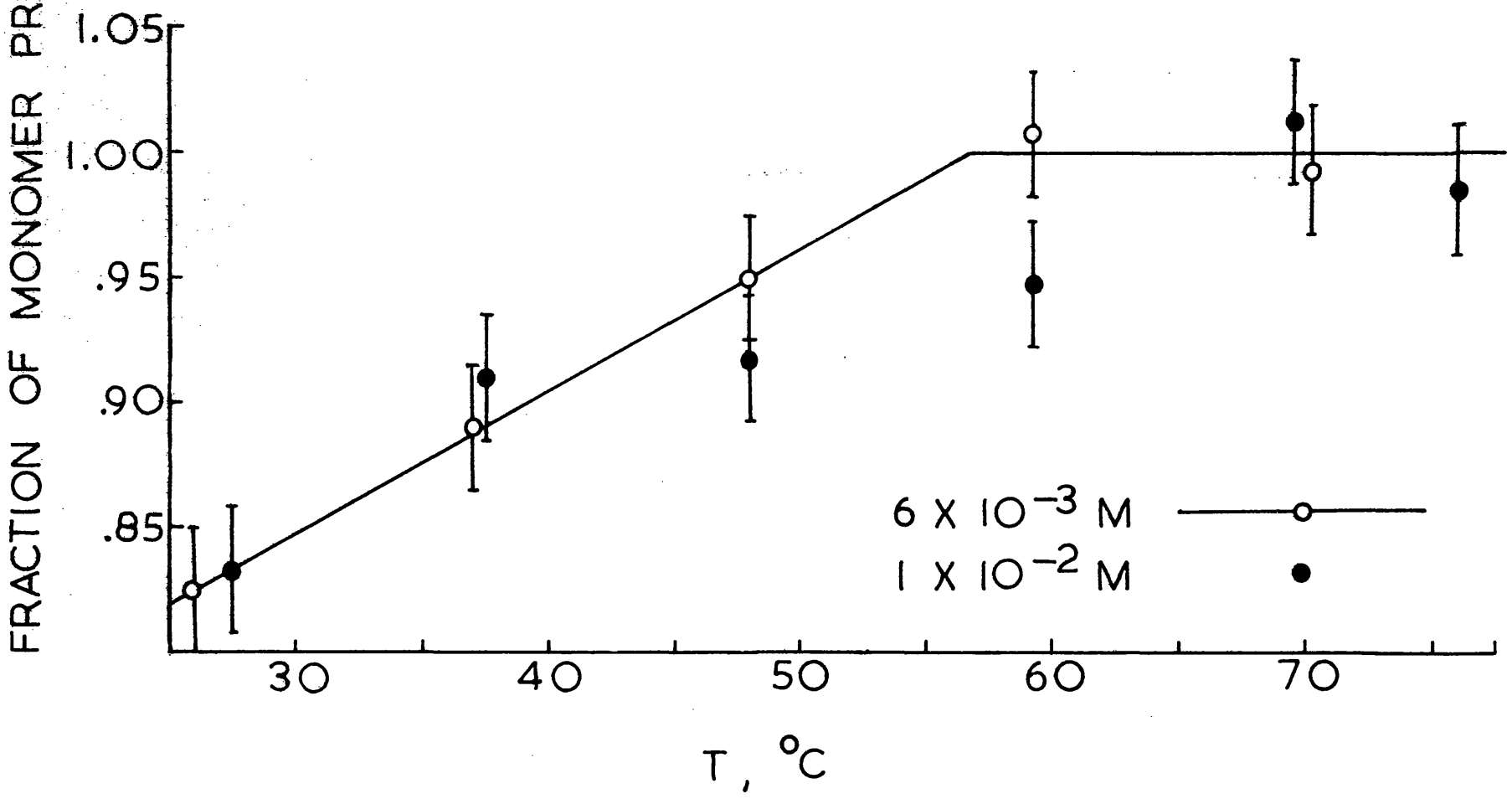

contained no associated cations, would make the results of the calculations meaningless. However, the data do show that the number of monomers in a $C_{10}TABNO$ solution decreases with temperature in the range $70^{o}C$-$25^{o}C$, and thus imply that some sort of pre-micellar association is taking place at the lower temperature.

7.5. An Attempted Detection of Pre-Micellar Association Using the Freezing Point Depression Method

Mr J H Boyd of the Department of Chemical Engineering at Birkenhead College of Technology has developed an apparatus which is accurate enough to detect dimerization with a K_D of 10 by the freezing point depression method[84]. Mr Boyd kindly agreed to test several $C_{10}TABNO$ solutions to see if any evidence of dimerization at about $0^{o}C$ could be found. Since the freezing point depression apparatus required about 500 ml of solution for each run, it was possible, due to the limited supply of $C_{10}TABNO$ available, to do only one run consisting of six different concentrations. Thus the accuracy of the technique was not as great as it would have been if data from the usual thirty or so points had been available.

The freezing point depression θ (in degrees centigrade) is related to the molality m of a solution of an ionic salt in which the cations may associate by

$$\theta/m = K_f \left[2 - K_D m\,(1-\alpha)^2\right] \qquad (7.10)$$

where K_D is the dimerization constant for the cation association, α is the degree of association, and K_f, the molal freezing point depression constant, has a value of 1.86.[88] If there is no cationic association, a plot of θ/m versus m will be a straight line with zero slope and

intercept $2K_f$. Association will cause the plot to have a negative slope, which will have the magnitude K_fK_D at small α and will decrease as α increases. Figure 7.5 shows a plot of $^{\theta}/2K_fm$ versus m which contains the theoretical lines for $K_D = 0$ and $K_D = 10$ as well as the experimental points. The experimental points are closer to $K_D = 0$ than to $K_D = 10$, and indicate that dimerization of the extent observed at room temperature does not occur at temperatures around 0^oC.

7.6. The Influence of Added Salt on the Pre-Micellar Association of $C_{10}TABN\dot{O}$

The addition of inorganic salt is known to decrease the cmc of ionic surfactants [49]. In order to see if the addition of inorganic salt had any effect on the pre-micellar association observed in $C_{10}TABN\dot{O}$ solutions at room temperature, 1×10^{-2}M NaBr was added to a 1×10^{-2}M $C_{10}TABN\dot{O}$ solution and the EPR spectrum was recorded. For comparison the spectrum of a 1×10^{-2}M $C_{10}TABN\dot{O}$ solution was recorded as well. Intensities of the nitroxide monomer were measured by the nomogram method in both cases, and after the volume effect of the added salt had been corrected for, it was found that the monomer intensity in the solution containing NaBr was more than 3% less than that in the solution without NaBr. This is slightly outside the experimental error of the nomogram method of intensity measurement. The quantity of salt added was not enough to have lowered the cmc of the surfactant appreciably.

The slightly increased aggregate formation in the presence of NaBr could be explained by the additional stability given to associated hydrocarbon chains by the increased ionic strength of the solution. Alternatively, it was felt that the Br- ion might stabilise the two cationic head groups which might associate to form a dimer. It was thought that, if the latter explanation were correct, there would be an effect on the

FIG. 7.5. DETERMINATION OF K_D BY A FREEZING-POINT DEPRESSION METHOD

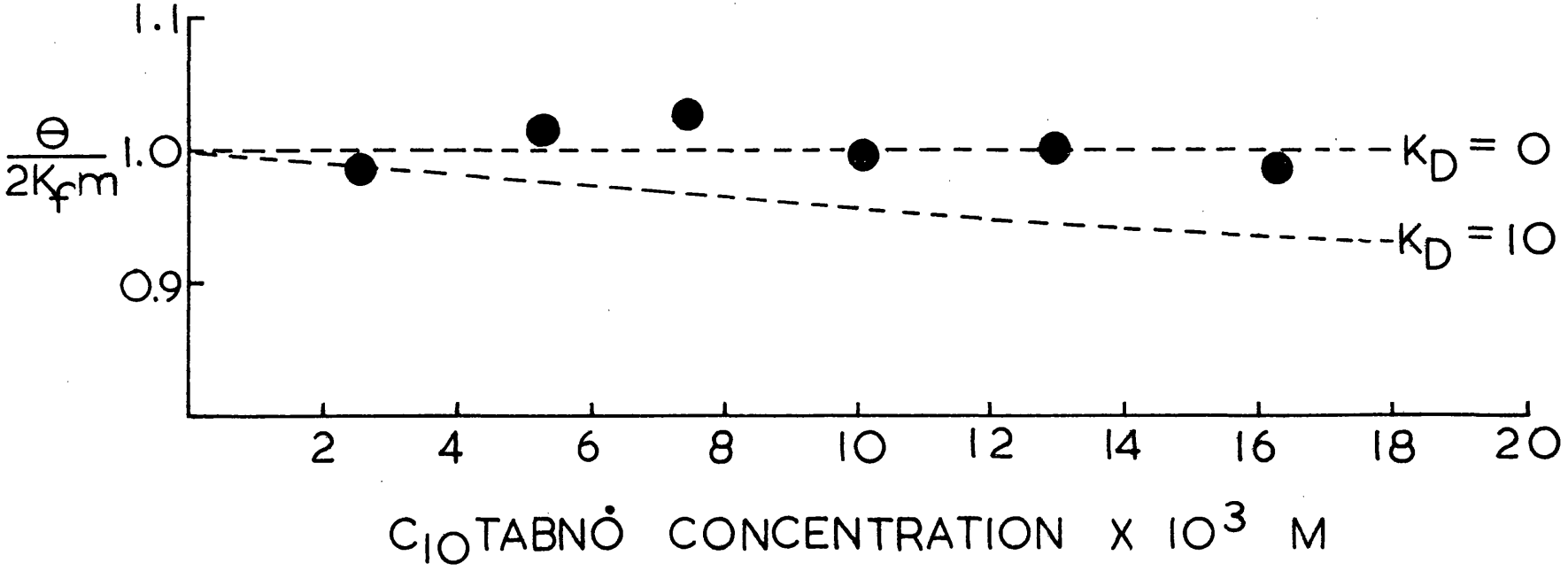

spin-spin and spin lattice relaxation times of the Br^- ion caused by its incorporation in a complex with paramagnetic head groups. The changes in the quadrupole interaction due to changes in the electric field at the $^{79}Br^-$ nucleus, the dipole-dipole interaction between the unpaired electron and the $^{79}Br^-$ nucleus, and the contact interaction between the unpaired electron and the nucleus would cause T_2 to decrease, while the first would decrease T_1 as well. Thus one would expect the addition of $C_{10}TABN\dot{O}$ to a $NaBr^-$ solution to broaden the Br^- resonances if a complex between Br^- and the surfactant headgroup were formed, and if fast exchange of the Br^- ion between complex and solution were taking place.

The experiment described above was attempted on the Brüker 90 Pulse NMR Spectrometer located at Unilever Research Port Sunlight Laboratory. Unfortunately, the low sensitivity of the $^{79}Br^-$ nucleus made it necessary to work with a 2.5 M NaBr solution, whose ionic strength caused the added $C_{10}TABN\dot{O}$ to precipitate out at concentrations above 1×10^{-3}M. Thus no information about the structure of the $C_{10}TABN\dot{O}$ dimer was obtained by this method.

7.7. Conclusions

The data obtained by EPR methods indicate that, at room temperature, some sort of aggregate is present in pre-micellar solutions of $C_1TABN\dot{O}$, $C_{10}TABN\dot{O}$ and $C_{12}TABN\dot{O}$ The fact that $C_1TABN\dot{O}$ solutions exhibit this behaviour makes it unlikely that the association is caused by the surfactant hydrocarbon chains. If one assumes that the aggregate is a dimer, the data can be explained by a dimerization constant K_D of about 10. EPR data indicate that the number of aggregated molecules decreases

as the temperature is increased, while freezing point depression data indicate that aggregates are not present at $0^{o}C$ to the same extent that they are present at $25^{o}C$. Thus the aggregates probably exhibit a minimum in the free energy of formation versus temperature curve similar to that found for many micellar species above the cmc. The influence of the pre-micellar species upon the EPR spectra observed above the cmc will be discussed in the next chapter.

CHAPTER 8

CONCLUDING EXPERIMENTS WITH THE CATIONIC NITROXIDE SURFACTANTS

8.1. Introduction

The three previous chapters have indicated several things that should be considered when interpreting the EPR spectra of the cationic nitroxide surfactants. In chapter five it was shown that, under certain conditions, one can distinguish between Heisenberg spin exchange and exchange between a monomer and an aggregate by a differential line-broadening effect, in which the $m_I = \pm 1$ lines broaden more than the $m_I = 0$ line for monomer-aggregate exchange, at exchange frequencies for which Heisenberg spin exchange causes all three lines to broaden equally. However, chapter seven showed that at room temperature there were two types of aggregate present in solution, micelles above the cmc and a pre-micellar aggregate, which may be a dimer, below the cmc and presumably, if a dimer, above it. The small magnitude of the linewidth effects and the complications caused by three possible interactions in solution made it desirable to remove a fourth type of interaction, that of the various components of the system with dissolved oxygen, from the system. For this reason oxygen was removed from the systems studied in this chapter. Even with the removal of dissolved oxygen, however, the measured linewidths of the monomeric nitroxide surfactant can not be quantitatively related to the exchange frequency of the monomeric nitroxide surfactant with some other environment since, as indicated in chapter six, the calculations necessary to do this are too complicated. Thus only qualitative information about the exchange frequency has been obtained from the measured linewidths. The qualitative information obtained from further experiments with the cationic nitroxide surfactant systems is described below.

8.2. De-oxygenation of the Surfactant Solutions

Dissolved oxygen was removed from most of the samples studied in this chapter using a glove-box filled with nitrogen, from which any oxygen present had been removed by bubbling through three consecutive traps containing a solution of alkaline pyrogallol[85]. The nitrogen stream then passed through two traps containing water, and thence into the glove box. A valve was available which allowed part of the nitrogen to be diverted through a tapered tube into the sample, and open solutions of alkaline pyrogallol were present in the glove box to adsorb any oxygen given off by the sample. A schematic drawing of the de-oxygenation apparatus is shown in Figure 8.1.

It was found that it was not possible to de-oxygenate the samples successfully by passing the nitrogen stream through the sample, as the loss of bubbles containing excess surfactant made the resultant concentrations highly unreliable. Therefore the samples were prepared inside the glove box by adding water which was de-oxygenated by the nitrogen stream to flasks containing weighed amounts of powdered surfactant. The powdered surfactant was allowed to stand in the nitrogen atmosphere for several hours before measured amounts of the de-oxygenated water were added with an Agla syringe. The samples were then left for several hours, to ensure complete dissolution. The EPR tube, generally the Varian variable temperature aqueous cell, was filled with sample inside the glove box, and sealed at the bottom with a rubber stopper and at the top with an ordinary pipette teat. The EPR spectra from samples prepared in this way were reproducible, and the sealed EPR cell did not admit a detectable amount of oxygen for at least forty-eight hours. The glove box was used for storage of de-oxygenated stock solutions as well as for sample preparation and transfer.

FIG. 8.1. GLOVE BOX AND DE-OXYGENATION APPARATUS

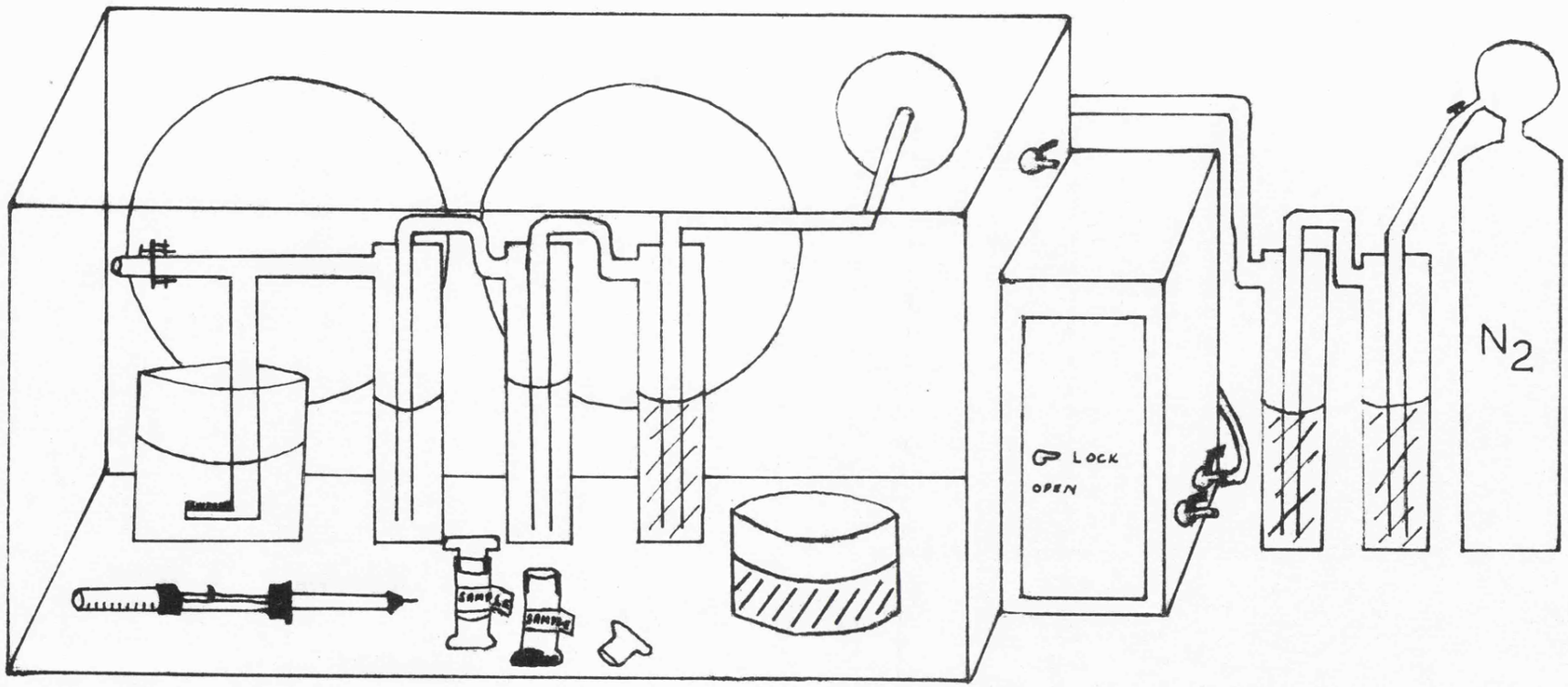

SOLUTIONS:

☐ = WATER

▨ = ALKALINE PYROGALLOL

8.3. Experiments with $C_{14}TABN\dot{O}$

Although earlier work (see chapter four) had shown that the monomer-micelle exchange frequency in $C_{14}TABN\dot{O}$ solutions was very small, it was thought that, using de-oxygenated solutions, some change in the EPR spectra which might be attributable to monomer-micelle exchange might be detected. A solution 2×10^{-3}M in $C_{14}TABN\dot{O}$ and 8×10^{-3}M in $C_{14}TABNH$ was prepared, the total surfactant concentration being more than twice the cmc of the mixed surfactant. Oxygen was then removed from the solution by passing de-oxygenated nitrogen gas through it - a procedure which would have removed some surfactant from the solutions. The resulting de-oxygenated solution was above the cmc of the mixed surfactant, as inciated by the presence of micellar peaks in the EPR spectrum described below. The $C_{14}TABN\dot{O}$ concentration was kept low, to minimise the formation of $C_{14}TABNO/C_{14}TABN\dot{O}$ dimers, and $C_{14}TABNH$ was added in order to micellize the mixed surfactant. The low $C_{14}TABN\dot{O}$ concentration was also intended to minimize Heisenberg spin exchange effects.

The EPR spectra obtained from this sample at room temperature is shown in Figure 8.2. The micellar signal consists of three broad lines, since the micellar nitroxide spin exchange frequency is reduced by the intervening $C_{14}TABNH$ molecules. The nitroxide monomer signals show proton hyperfine structure. Even if monomer-micelle exchange were present in this system it would be more difficult to detect than in the case where the micelle gives one broad EPR line, as the exchange in the present case would be between two lines at the same frequency with T_2's differing by a factor of less than 10.[55] By increasing the temperature to 70°C, one has increased the frequency of inter-micellar

FIG. 8.2. EPR SPECTRUM OF 2×10^{-3} M $C_{14}TABN\dot{O}$, 8×10^{-3} M $C_{14}TABNH$, AT ROOM TEMPERATURE

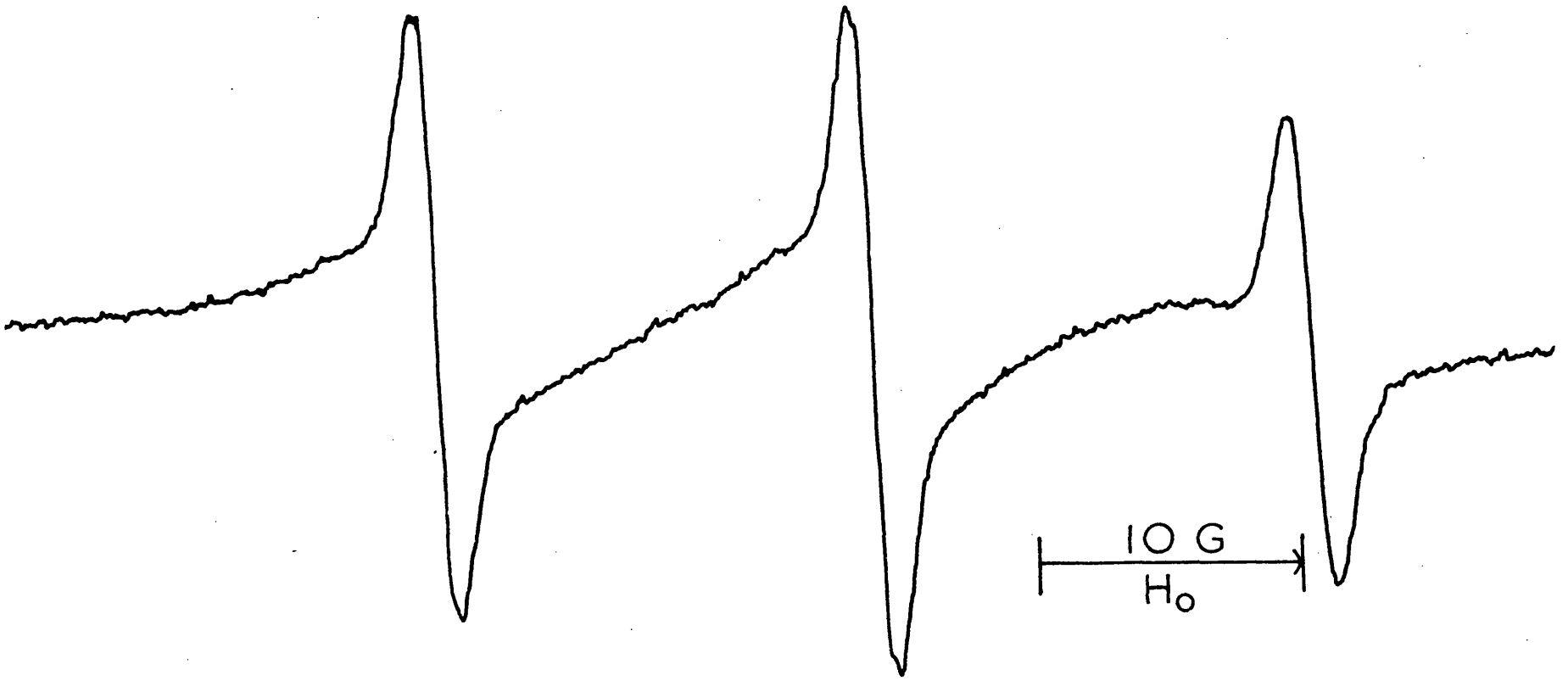

exchange, so that many of the micelles give the micellar spectrum consisting of one broad, exchange-narrowing line. The monomer spectrum consists of three sharp lines with increased proton hyperfine structure resolution. The most probable cause of the increased resolution is the narrowing of the linewidth due to the increased tumbling rate of the molecule at the higher temperature - the monomer-micelle exchange frequency is therefore not large enough to overcome this effect. Thus the monomer-micelle exchange frequency in the $C_{14}TABN\dot{O}/C_{14}TABNH$ system studied here, and by inference in $C_{14}TABN\dot{O}$ systems in general, is too low to be detected by this EPR technique.

8.4. Experiments with $C_{12}TABN\dot{O}$

A series of experiments was performed with $C_{12}TABN\dot{O}$ solutions in an attempt to measure the monomer-micelle exchange frequency. The first of these involved 7×10^{-3}M $C_{12}TABN\dot{O}$ solutions in the presence and absence of 0.1M NaCl. The solutions were de-oxygenated as described in section 8.2. The NaCl decreased the cmc of the NaCl containing solution so that micelles were present in it throughout the temperature range studied. The 7×10^{-3}M $C_{12}TABN\dot{O}$ solution should not have contained micelles, and certainly would not have done so at temperatures above 35°C.

The widths of the $M_I = 0$ lines of $C_{12}TABN\dot{O}$ in the presence and absence of 0.1M NaCl are shown as a function of temperature in Figure 8.3. It is seen that at the higher temperatures the lines in the NaCl containing solution are broader than those in the system containing $C_{12}TABN\dot{O}$ alone, while at intermediate temperatures the position is perhaps reversed (the difference in linewidths being just outside the combined experimental errors). Figure 8.4 shows the widths of all three nitroxide lines for the solution containing NaCl, while Figure 8.5 contains similar information for the solutions without NaCl. It is seen that in both solutions at higher temperatures there is a tendency for the $m_I = \pm 1$

FIG. 8.3. LINEWIDTH VS. TEMPERATURE FOR THE $M_I = 0$ LINES OF:

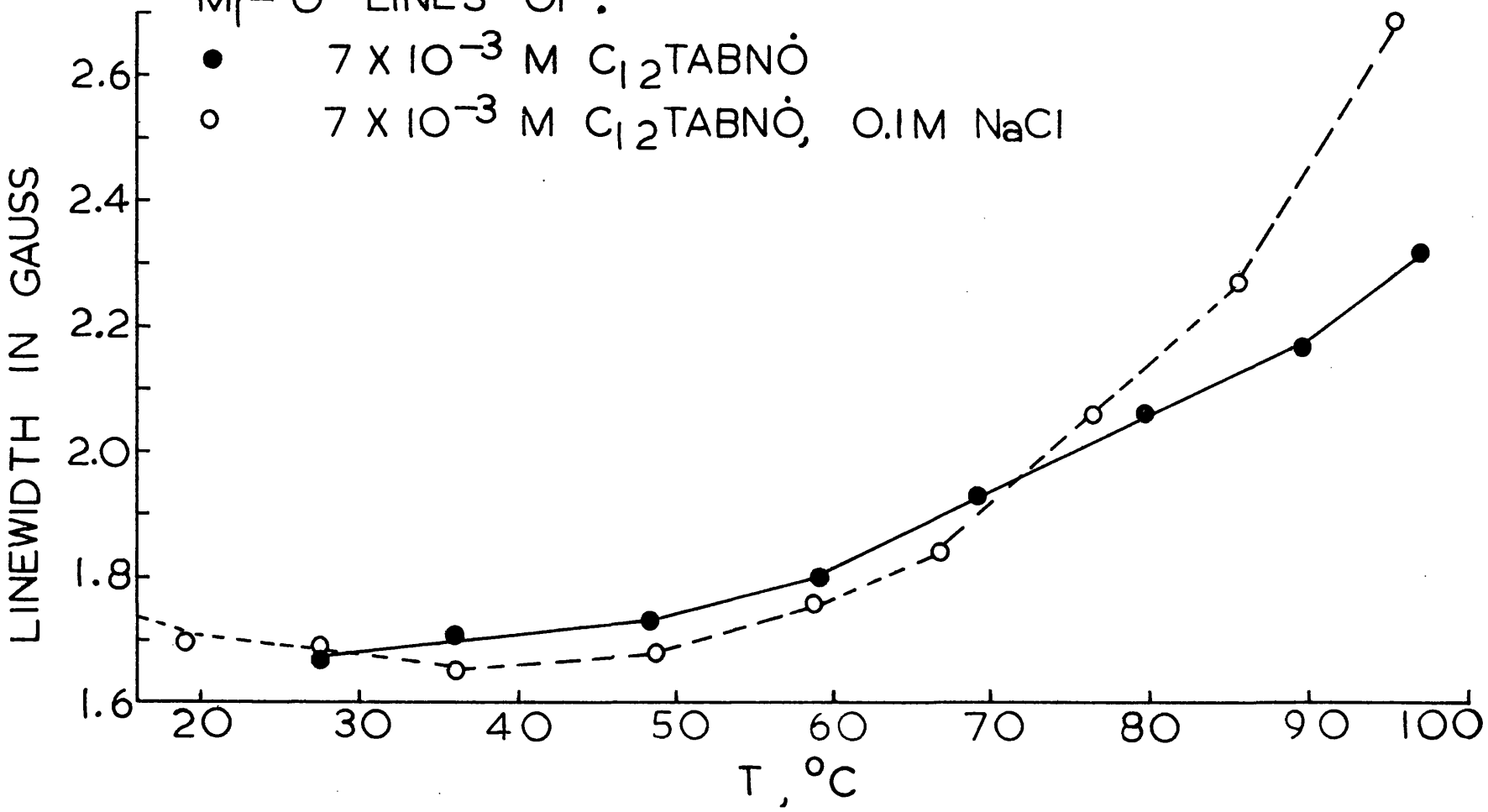

FIG. 8.4. LINEWIDTH VS. TEMPERATURE FOR 7×10^{-3} M C_{12}TABNO, 0.1 M NaCl

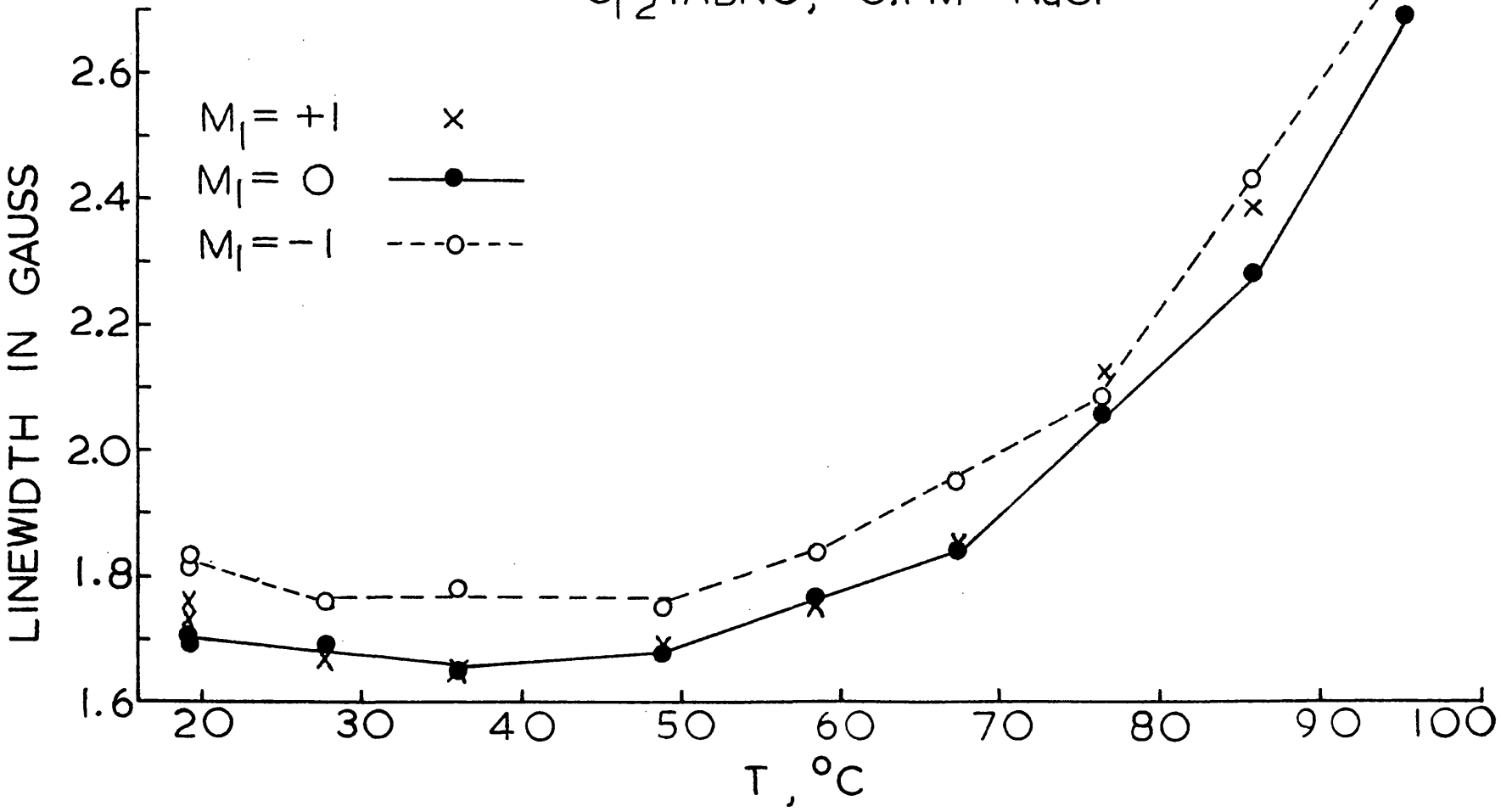

FIG. 8.5. LINEWIDTH VS. TEMPERATURE FOR 7×10^{-3} M C_{12}TABNO

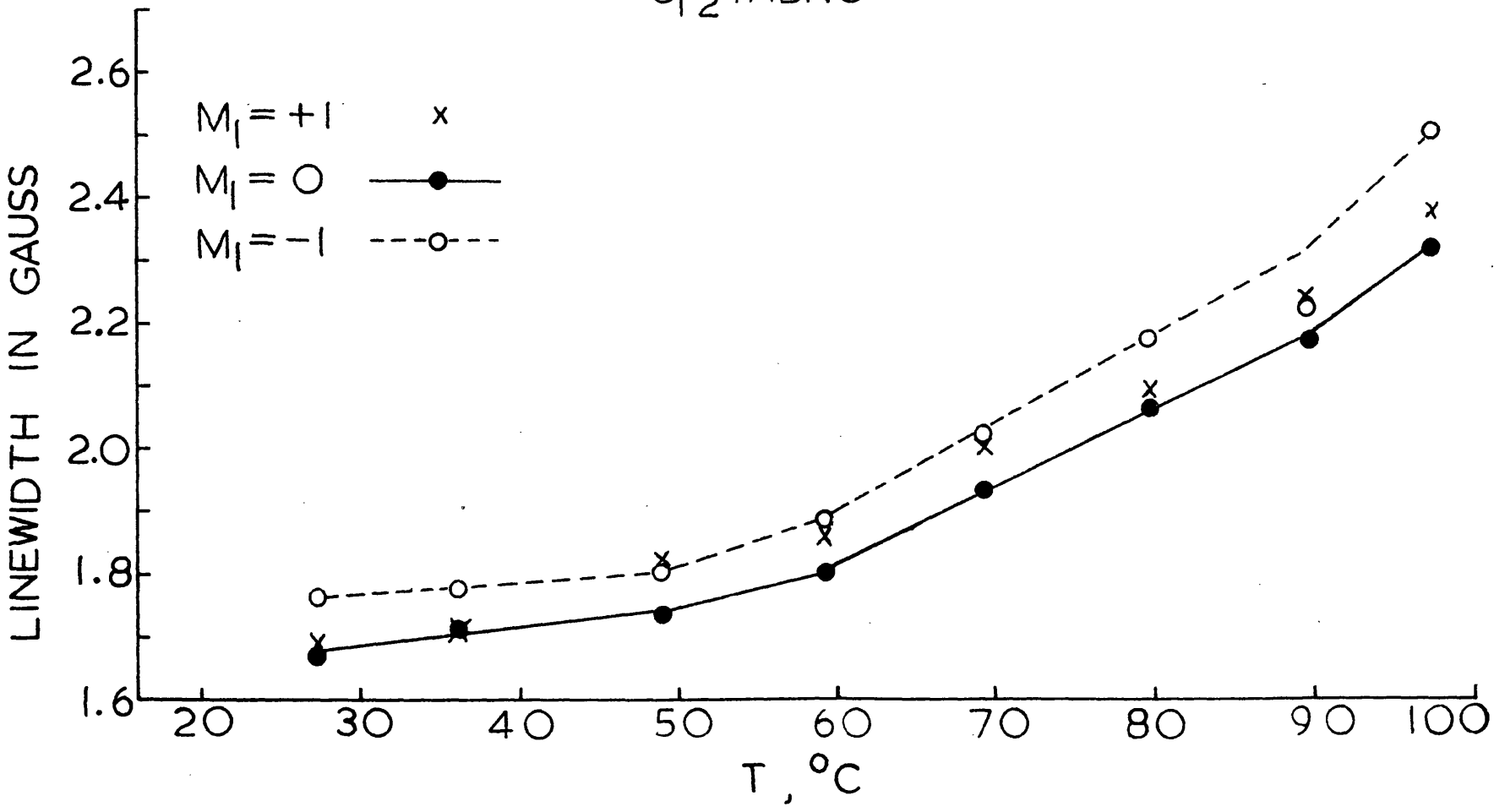

lines to be broader than the $m_I = 0$ line, and that this effect is apparent at lower temperatures in the solution without NaCl.

A possible explanation for Figure 8.3 is that the increased broadening at high temperatures in the presence of NaCl is due to monomer-micelle exchange, while the slightly reduced broadening at lower temperatures is caused by a reduction in either Heisenberg spin exchange or monomer-dimer exchange, due to the presence of a smaller number of monomers (and therefore dimers) in solution. The slightly greater width of the $m_I = \pm 1$ lines of the solution without NaCl in this temperature region would indicate monomer-dimer exchange, while the absence of the effect in the micellar solution would be due to the smaller number of monomers and dimers present there. Further experiments have shown this explanation to be only partially correct, however.

Further experiments were performed with samples containing less C_{12} TABNO. A series of variable temperature experiments was performed with de-oxygenated 5.5×10^{-3}M C_{12}TABNO with and without 0.1M NaCl, and with both of these systems also containing 1.5×10^{-3}M C_{12}TABNH. An analogous series of experiments was performed using 4.0×10^{-3}M C_{12}TABNO, 2×10^{-3}M C_{12}TABNH, and 0.1M NaCl. Only the results of this latter series will be reported in detail - the results of the former series were similar, except that the linewidths were somewhat broader throughout.

The results with the 4×10^{-3}M C_{12}TABNO solutions are shown in Figure 8.6 A-D. All four of the solutions exhibit slightly greater broadening of the $M_I = \pm 1$ lines over that exhibited by the $m_I = 0$ line. The two solutions containing NaCl had identical linewidths, within the experimental error of $\pm$ 0.02 G, as did the two solutions not containing NaCl.

FIG. 8.6.A. LINEWIDTH VS. TEMPERATURE FOR 4×10^{-3} M $C_{12}TABNO$

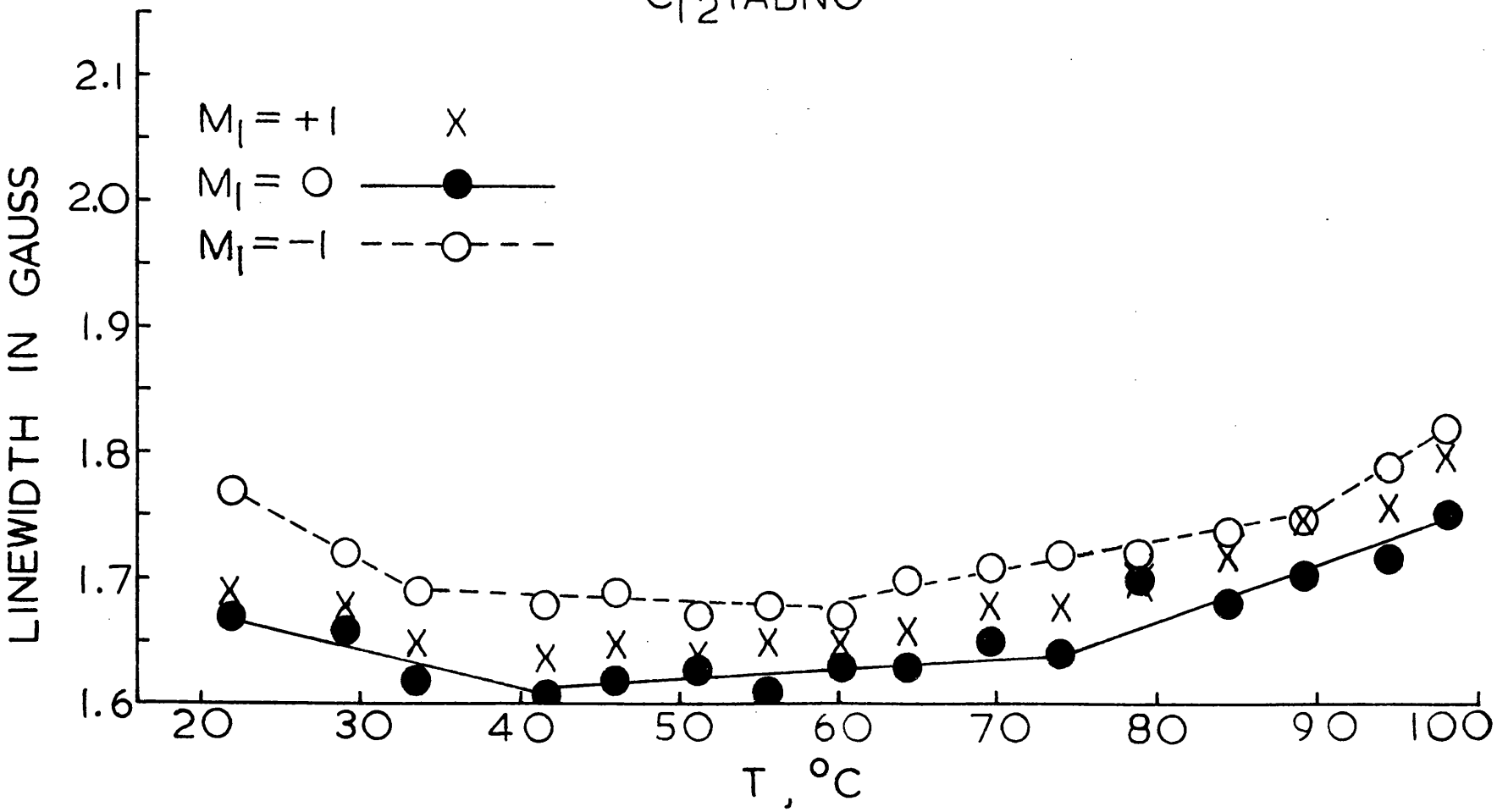

FIG. 8.6.B. LINEWIDTH VS. TEMPERATURE FOR 4 X 10^{-3}M $C_{12}TABN\dot{O}$, 0.1 M NaCl

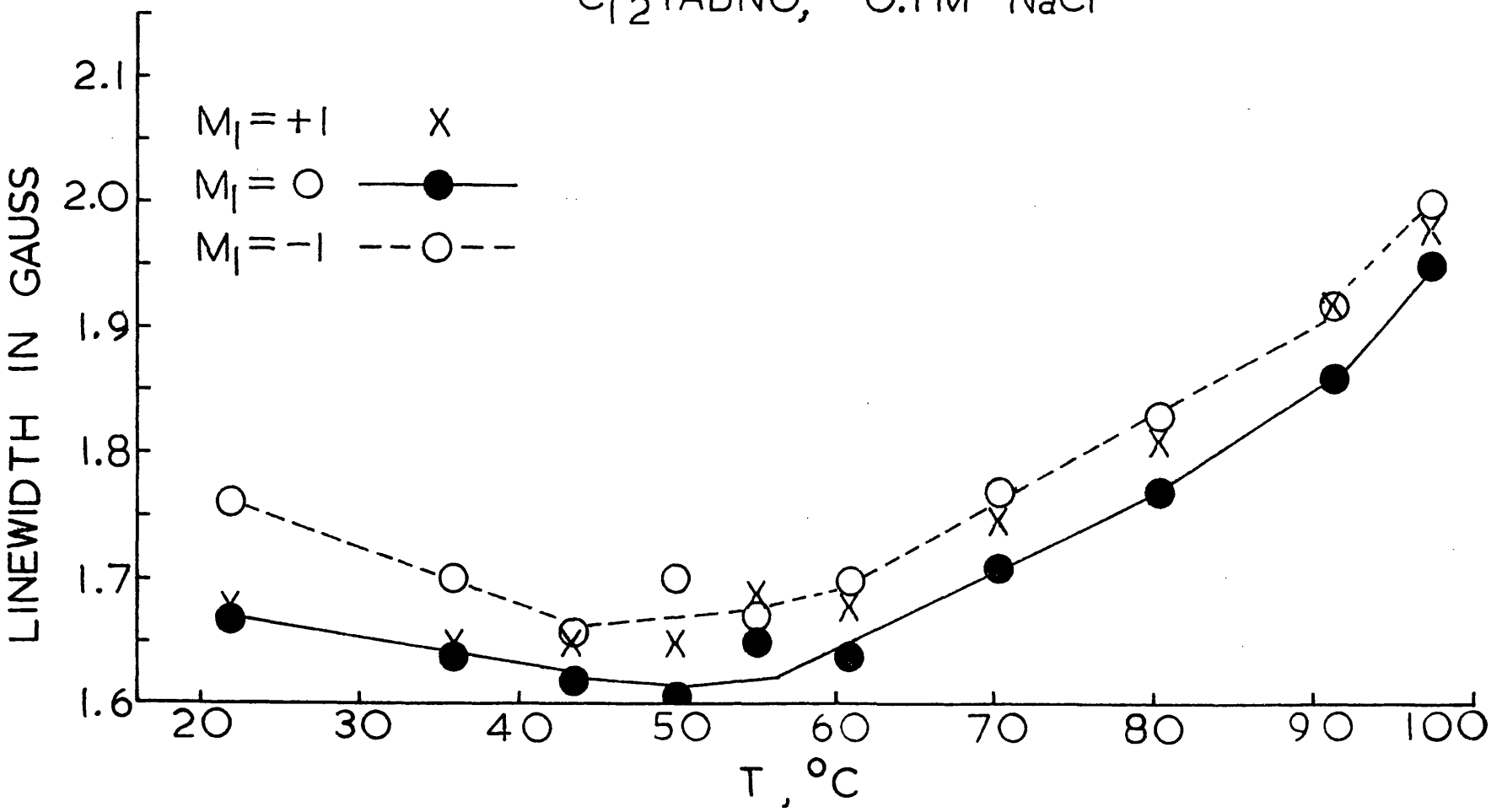

FIG. 8.6.C. LINEWIDTH VS. TEMPERATURE FOR 4 X 10^{-3}M C_{12}TABNO, 2 X 10^{-3}M C_{12}TABNH

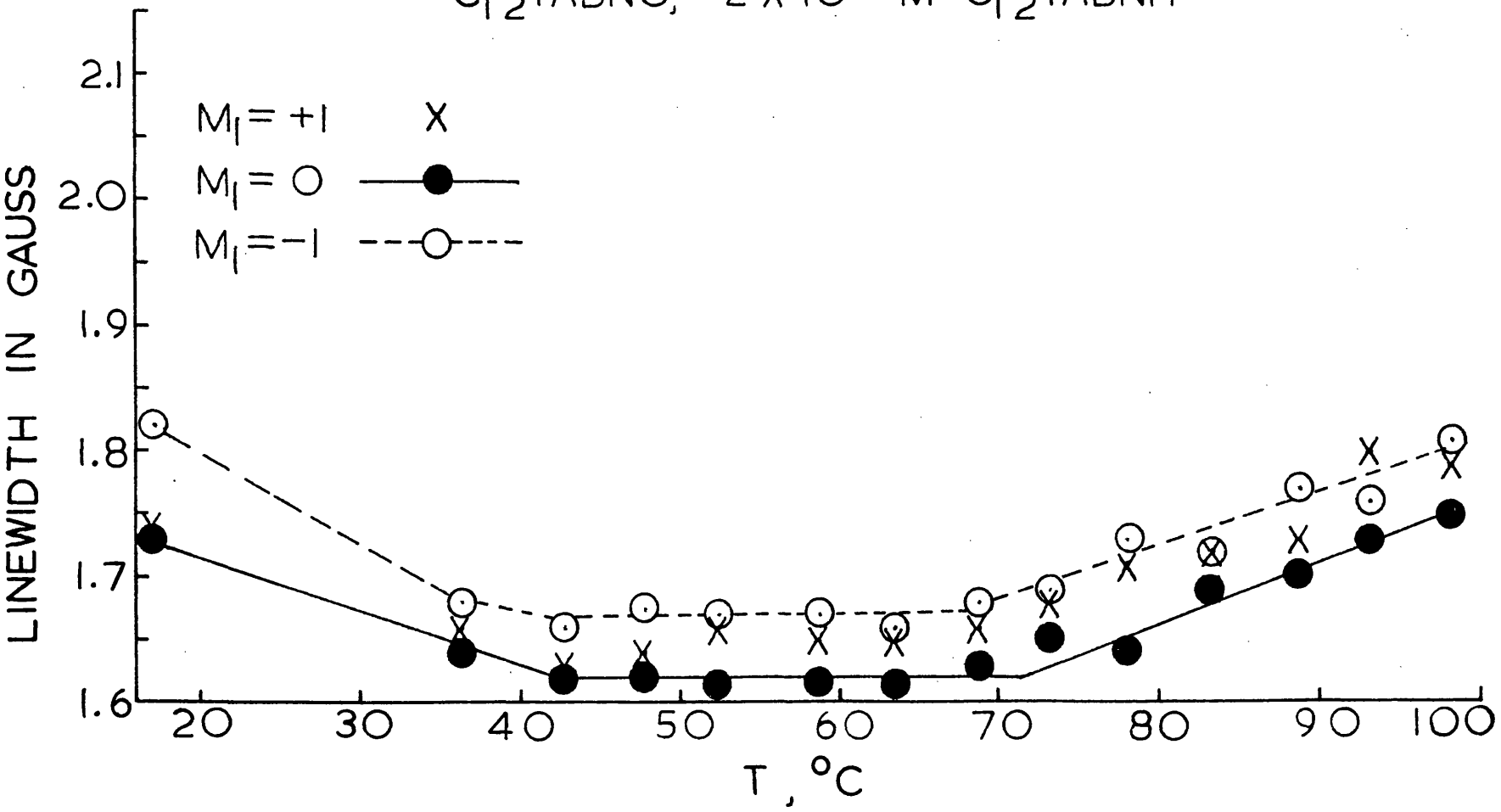

FIG. 8.6.D. LINEWIDTH VS. TEMPERATURE FOR 4×10^{-3} M $C_{12}TABNO^{\cdot}$, 2×10^{-3} M $C_{12}TABNH$, 0.1M NaCl

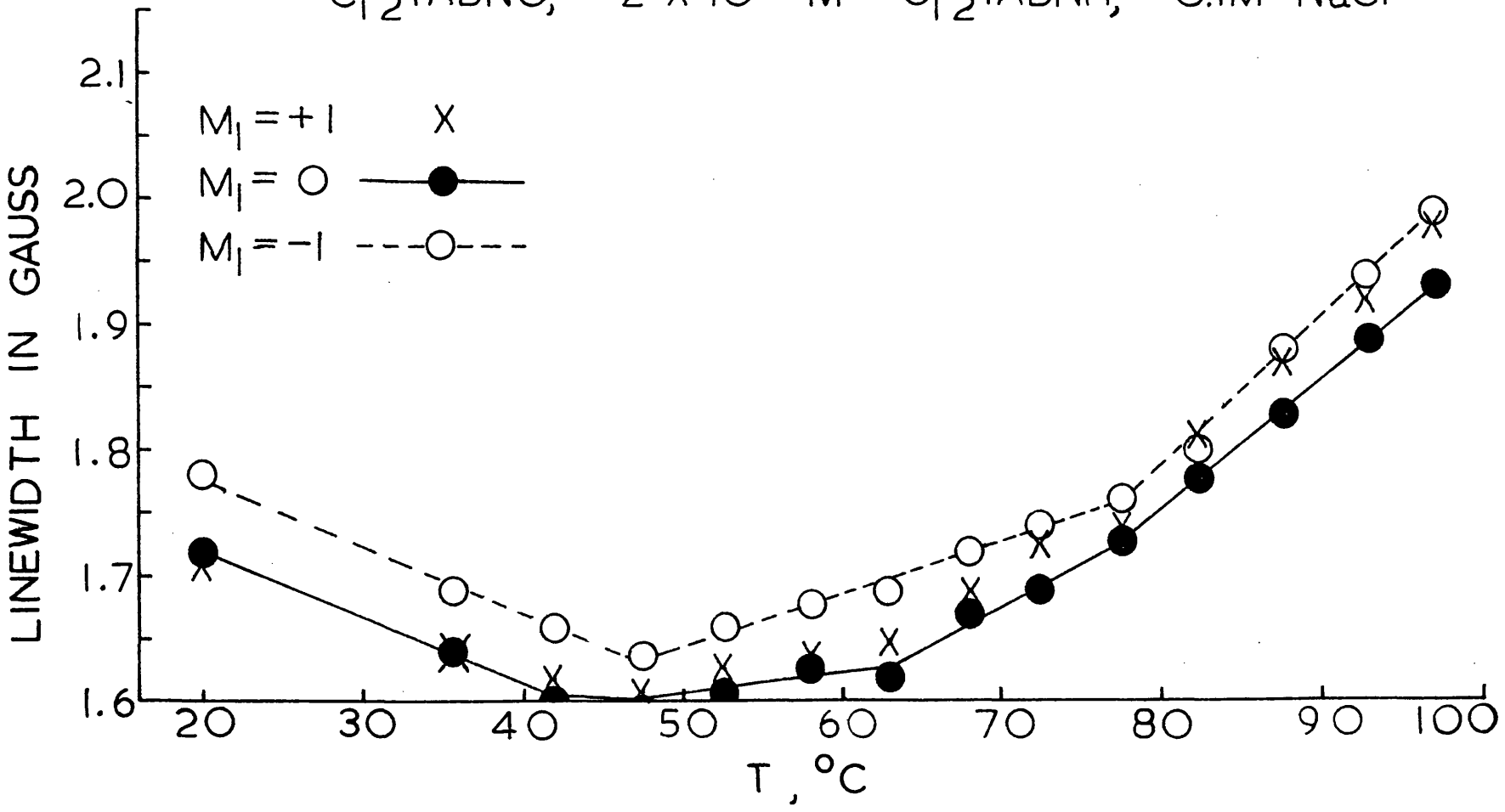

Rough intensity measurements were taken, by the method of assuming the lineshapes to be Lorentzian and equating the intensity with the product of the height and the square of the width of each peak, which estimated the number of monomers in each solution. Since at lower temperatures the linewidths in all four solutions were within the experimental error of each other, this method was more accurate than in the usual case of different linewidths. The measurements showed that at room temperature the solution containing $C_{12}TABN\dot{O}$ only and the solution containing $C_{12}TABNH$ as well had the same intensity, while the solution containing $C_{12}TABN\dot{O}$ and 0.1M NaCl showed about 77% of the monomer intensity of the other two solutions. The monomer intensity of the solution containing all three compounds was only 63% of the intensity in the absence of NaCl. As the temperature increased up to 60°C the intensities in each solution stayed almost constant. Accurate intensity measurement in the region above 60°C was not possible due to the formation of vapour bubbles in the solutions.

The above results were consistent with the presence of micelles in the solutions containing NaCl, and the presence of monomer-micelle exchange causing the increased broadening observed there. However, it was thought prudent to check that the observed broadening was not a property of the NaCl alone, to ensure that it was due to the presence of the micelles caused by the NaCl.

Accordingly de-oxygenated solutions 4×10^{-3}M in $C_{10}TABN\dot{O}$ in the presence and absence of 0.1M NaCl were prepared. Neither of these solutions contained micelles. The broadening caused by the presence of NaCl was the same as that observed with the 4×10^{-3}M $C_{12}TABN\dot{O}$ solutions both with and without $C_{12}TABNH$. The intensity

loss in the $C_{10}TABN\dot{O}$ solution containing NaCl was 15%, as compared with the 23% intensity drop observed with the $C_{12}TABN\dot{O}$ solutions. In the $C_{10}TABN\dot{O}$ case the intensity drop is probably due to increased dimer formation with added salt, while in the $C_{12}TABN\dot{O}$ case both micelle and dimer formation may be involved. The increased linewidth in the presence of NaCl could reflect monomer-dimer exchange, or it could reflect increased Heisenberg spin exchange for the monomers that are left in solution, the increased ionic strength of the solution making it easier for two cationic nitroxides to approach each other in solution. The observed, but small, increase in broadening of the $m_I = \pm 1$ lines over the $m_I = 0$ line in all the solutions observed argues for the former explanation.

If the presence of NaCl causes increased monomer-dimer exchange, perhaps due to the presence of more dimers, then the high temperature line broadening shown in Figure 8.3 for the solution containing NaCl could reflect the creation of more dimers due to micellar breakdown at high temperature. If this caused the solution containing NaCl to contain more dimers than the solution without NaCl, the excess broadening in that solution would be explained.

Figure 8.7 shows the changes in the width of the $m_I = 0$ line of two solutions, one containing 5.5×10^{-3}M $C_{12}TABN\dot{O}$, the other containing in addition 1.5×10^{-3}M $C_{12}TABNH$. If one assumes that dimers will be formed in both of these solutions, with a K_D of 10 for the dimerization process, and that $C_{12}TABN\dot{O}$ and $C_{12}TABNH$ behave alike as far as the dimerization reaction is concerned, then one can

FIG. 8.7. LINEWIDTH VS. TEMPERATURE FOR THE $M_I = 0$ LINES OF:

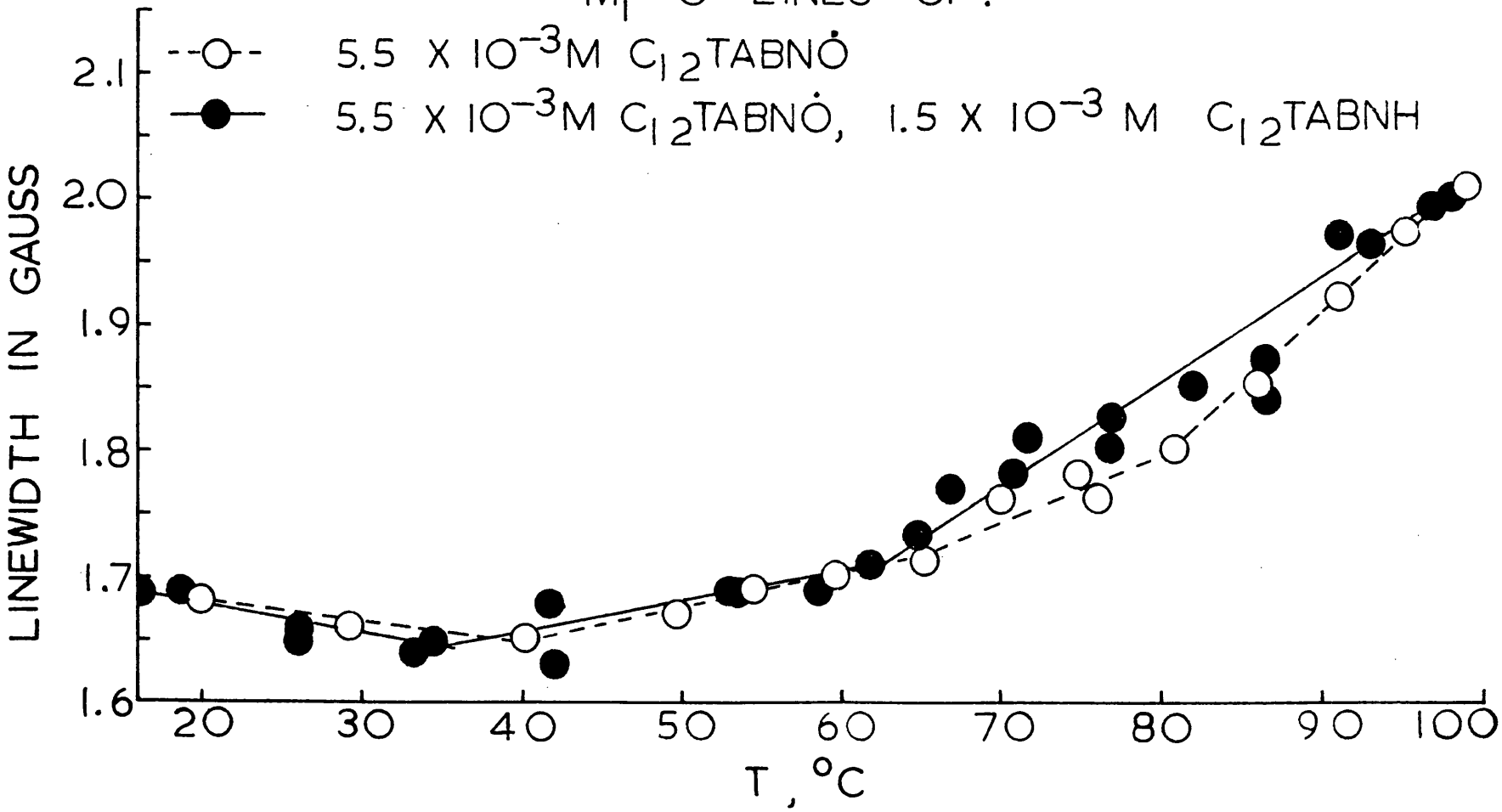

calculate that the sample without C_{12}TABNH should contain 1.25 x 10^{-3}M nitroxide dimers, while the sample with C_{12}TABNH should contain 1.50 x 10^{-3}M nitroxide dimers. The broadening pattern is similar for the two samples except in the region around 75°C, where the broadening of the sample containing C_{12}TABNH is greater. If the cause of broadening were a general salt effect due to the presence of the C_{12} TABNH, one would expect to see small differences at all temperatures. The broadening pattern shown in Figure 8.7 can be explained if one invokes both an increasing monomer-dimer exchange frequency with increasing temperature and a decreasing K_D with increasing temperature, the latter being consistent with data presented in chapter seven.

Accurate measurements of the monomer intensity, and also of the micelle and dimer intensities, in these solutions would provide the information necessary to decide what is happening in these systems. Unfortunately the interesting temperature region is that in which the EPR intensity measurements, which might yield accurate monomer intensities, are of doubtful value, due to the presence of vapour bubbles in the solutions. Other techniques such as conductivity are also doubtful due to rapid evaporation of solution. Thus it seems that for the present only indirect evidence of the type presented above is available to aid in discerning the process which are taking place in these systems.

In order to avoid the complications caused by the use of NaCl to induce micellisation it was decided to use the diamagnetic nitroxide-analogue C_{12}TABNH to increase the total surfactant concentration to above the cmc. A solution 7 x 10^{-3}M in C_{12}TABNO$^{\bullet}$ and 8 x 10^{-3}M C_{12}TABNH

was prepared, de-oxygenation being performed as described in section 8.2. The EPR spectra of this sample showed one broad micellar peak at temperatures ranging between 44°C and 93°C, as well as the usual three-lined monomer spectrum. The width of the $m_I = 0$ line as a function of temperature is shown in Figure 8.8, where the width of the $m_I = 0$ line of 7×10^{-3}M $C_{12}TABN\dot{O}$ in the absence of added surfactant is shown for comparison. It is seen that the linewidths of the two systems are similar, with the width in the non-micellar system exceeding the width in the micellar system by about three times the experimental error in the region around 64°C. The major effect of the addition of micelles to this system seems to be the removal of paramagnetic monomers from solution, and the concomittant reduction in either monomer-dimer or Heisenberg spin exchange. At 64°C and below the linewidth behaviour in both systems indicates the presence of Heisenberg spin exchange only, while above that temperature the $m_I = +1$ line begins to approach the $m_I = -1$ line in width. Thus at the higher temperatures monomer-dimer exchange could be important in both systems.

The experiments described above show that monomer-micelle exchange does not effect the linewidths observed in $C_{12}TABN\dot{O}$ solutions. The major linewidth effects can be explained if Heisenberg spin exchange is taken into account, although in certain solutions and at certain temperatures linewidth effects suggest that monomer-dimer exchange may contribute to the observed linewidth as well.

8.5. Experiments with $C_{10}TABN\dot{O}$

In order to see if monomer-micelle exchange could be detected in $C_{10}TABN\dot{O}$ solutions, two solutions each 1.8×10^{-2}M in $C_{10}TABN\dot{O}$ were prepared. One solution was also 5.8×10^{-2}M in $C_{10}TABNH$, which increased the total surfactant concentration to above the combined cmc for the surfactant mixture. The other solution contained $C_{10}TABN\dot{O}$ only, and was thus below the cmc.

FIG. 8.8. LINEWIDTH VS. TEMPERATURE FOR THE $M_I = 0$ LINE OF:

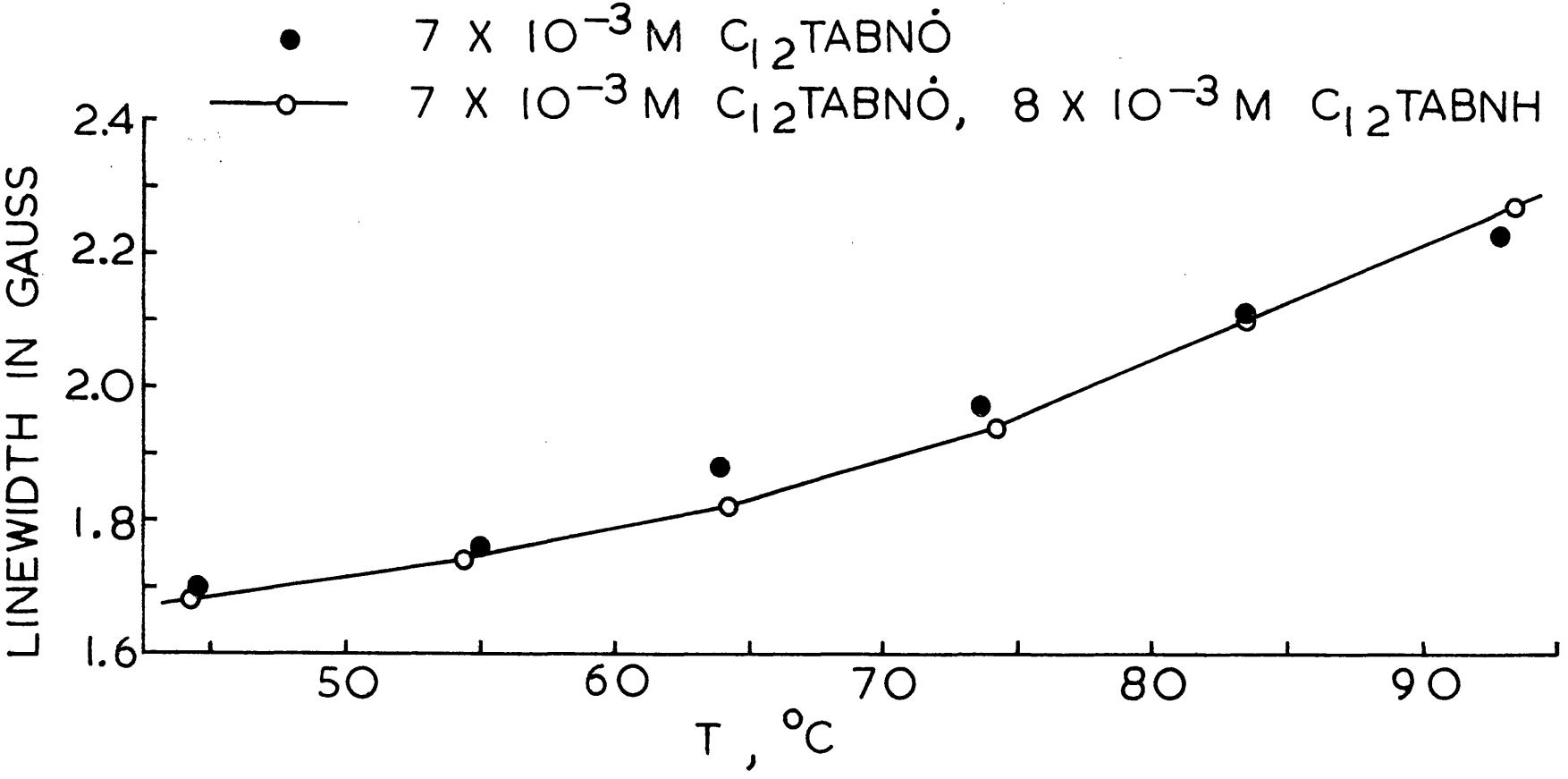

Spectra of both solutions obtained at 76.7°C consisted of three broad lines. In the sample containing C_{10}TABNH the m_I=0 line was more intense relative to the $m_I = \pm 1$ lines than the $m_I = 0$ line in the other sample, a result which is consistent with the presence of an underlying micellar peak in the first sample. This effect, although diminished in magnitude, was still present at 54.8°C. Thus the sample containing C_{10}TABNH contained micelles at both temperatures studied, although the micellar signal was sharper at the higher temperature, due to increased inter-micellar exchange.

The linewidths obtained from the samples at both temperatures are shown in Table 8.1.

Table 8.1 Linewidths of C_{10}TABNO• Samples

Sample	T°C	Width of $m_I = +1$ line,	Width of $m_I = 0$ line,	Width of $m_I = -1$ line,
1.8×10^{-3}M C_{10}TABNO•	54.8	3.82 ± 0.05	3.65 ± 0.05	3.85 ± 0.05
1.8×10^{-3}M C_{10}TABNO•	76.7	5.00 ± 0.05	4.65 ± 0.05	5.05 ± 0.05
1.8×10^{-2}M C_{10}TABNO• 5.8×10^{-2}M C_{10}TABNH	54.8	2.98 ± 0.05	2.98 ± 0.05	3.05 ± 0.05
1.8×10^{-2}M C_{10}TABNO• 5.8×10^{-2}M C_{10}TABNH	76.7	4.10 ± 0.05	3.98 ± 0.05	4.15 ± 0.05

At both temperatures the widths of the lines in the solutions containing micelles are less than the widths of the lines in the non-micellar solutions. Thus the major effect of creating micelles is not the introduction of monomer-micelle exchange, but the removal from

the solution of monomers and/or dimers which had undergone either monomer-dimer or Heisenberg spin exchange in the non-micellar solution. Monomer-micelle exchange may be present in this system, but if so its magnitude is not great enough to compensate for the loss of monomer-dimer and/or Heisenberg spin exchange.

In both solutions at 76.7°C and in the non-micellar solution at 54.8°C the widths of the $m_I = \pm 1$ lines are longer than the widths of the $m_I = 0$ lines. At total linewidths of these magnitudes, however, Heisenberg spin exchange will have this effect on the linewidths[57], so monomer-dimer exchange is not necessarily occurring here. Analogy with the other nitroxide surfactant systems makes its presence likely, however.

Unfortunately it was not possible, because of the high cmc and the independent effects of inorganic salts on the observed linewidths, to study the micellization of $C_{10}TABNO^{\bullet}$ at a lower total nitroxide concentration, for which the effects of Heisenberg spin exchange would have been reduced. However, the present experiments allow one to put an upper limit of about 0.2G on the linewidth increment that would be possible for monomer-micelle exchange, and thus to estimate that monomer-micelle exchange in the $C_{10}TABNO^{\bullet}$ systems should be less than 5×10^5 sec^{-1}.

8.6. Conclusion

The results presented above show that monomer-micelle exchange is not detectable by EPR methods in the $C_{10}TABNO^{\bullet}$, $C_{12}TABNO^{\bullet}$, and $C_{14}TABNO^{\bullet}$ surfactant systems. The major effects observable in these systems are caused by Heisenberg spin exchange, while monomer-dimer exchange may

affect the observed spectra at certain temperatures and concentrations of surfactant. The effects which have been described in chapters three and four which were originally attributed to monomer-micelle exchange can be adequately explained by monomer-dimer exchange and Heisenberg spin exchange if the variations in both the cmc and the dimerization constant K_D with temperature are taken into account. However, it has been possible to show that in the three surfactant systems studied monomer-micelle exchange is slow on the EPR timescale, and that for $C_{14}TABN\dot{O}$ in particular the monomer-micelle exchange frequency is less than 5×10^4 sec^{-1}. Thus EPR is one of the many techniques which yield an upper limit to the monomer-micelle exchange frequency, but are unable to measure that frequency accurately.

APPENDIX I

SOIL REMOVAL STUDIES INVOLVING A PARAMAGNETIC SOIL

In addition to the EPR investigation of monomer-micelle exchange described above, certain EPR experiments of a more applied nature were also performed. These experiments investigated the applicability of the EPR technique to practical problems such as the determination of detergency mechanisms and the measurement of soil removal and soil re-deposition. The results of these experiments are described below.

A-1.1. Introduction

The electron paramagnetic resonance spectrum of a nitroxide probe contains information concerning the probe's environment. From the EPR spectrum one can determine whether the probe is in the solid state or in solution, and if in solution whether the solvent is hydrophobic or hydrophilic.

The distance between paramagnetic molecules can be determined qualitatively from the EPR spectra as well. If the nitroxide probe is also a model oily soil, then the EPR spectra can yield information concerning the state of that soil both on fabric and in detergent solution. In the present study, the paramagnetic nitroxide (I)[11] has been used as a model oily soil. The

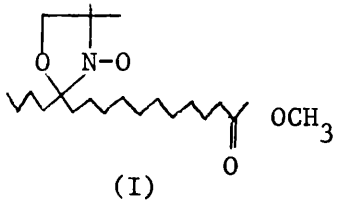

(I)

physical state of this model oily soil in other soils and on fabrics, its removal from fabrics and its redeposition onto nylon are described below.

A-1.2. The Paramagnetic Probe as a Component of Other Soils

Dilute solutions (less than 10^{-3}M) of I in both methyl oleate and sebum-H, a synthetic sebum prepared by Dr M Hull at the Unilever Research, Port Sunlight Laboratory and kindly donated by him, were prepared. Dr Hull also provided test cloths of unfinished cotton, rayon, and nylon, from which threads were unravelled and coated with the labelled soils.

EPR spectra were recorded on the apparatus located at Unilever Research, Port Sunlight Laboratory which is described in Chapter 4. In all cases the EPR spectra of (I) with fabric present were identical to spectra of (I) in the given soil, and indicated that (I) was in the liquid state, tumbling rapidly in a hydrocarbon environment (a_N = 14.5G). The spectra were obtained at room temperature for methyl-oleate, and at 65 $\pm$ 1°C for Sebum-H. Thus these experiments indicated that the average soil molecule in a thick layer of soil on fabrics sees only other soil molecules, and does not itself interact with the fabric.

A-1.3. Dilute Paramagnetic Probe as the Only Soil Present

In order to detect the physical state of the model soil on the fabric itself, unsoiled threads were pulled through a dilute solution of (I) in acetone, and allowed to dry. The acetone solution was diluted until spin-exchange effects did not dominate the EPR spectra of the dried samples, indicating that the probe molecules were associating with the fabric, and not with each other. It was found that, in order to obtain reproducible spectra, the samples must not be touched by the preparer - otherwise spectra of (I) in varying amounts of human sebum were obtained. The spectra obtained from untouched samples are shown in Fig A-1-1. The motion of the probe is slower on cotton than on nylon, as shown by the sharper spectral

FIG. A.I.I-A. STEARATE NITROXIDE ON COTTON

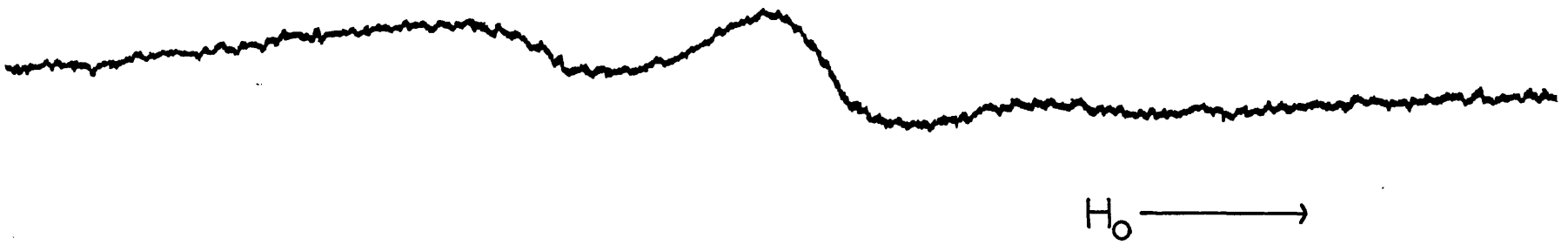

B. STEARATE NITROXIDE ON NYLON

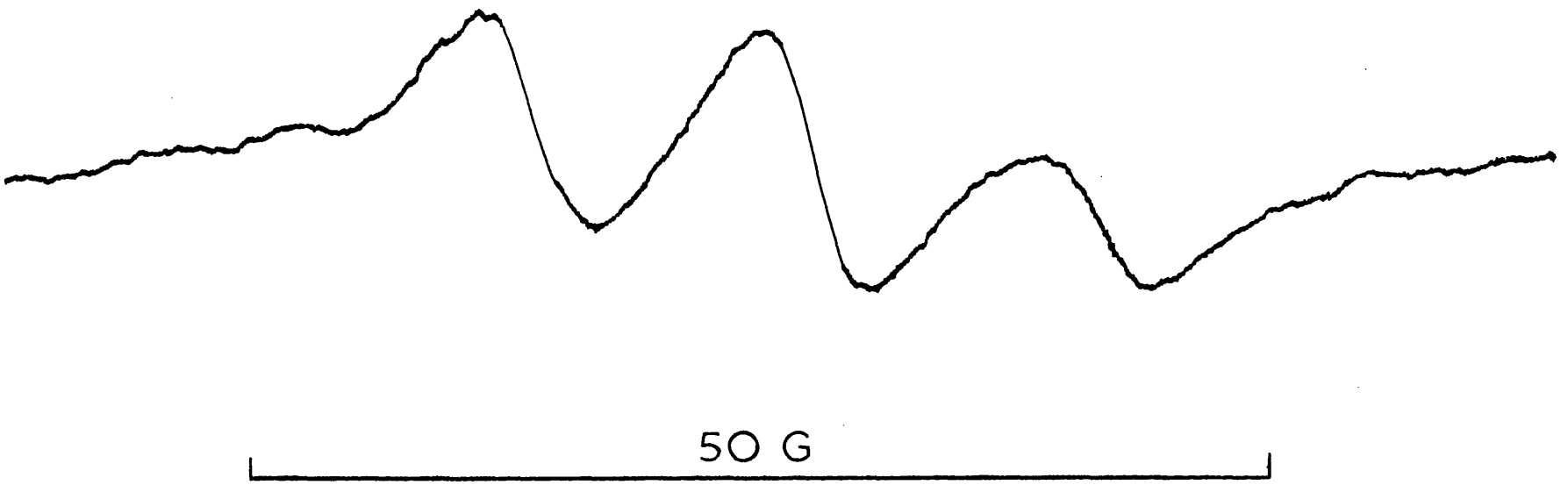

lines in the nylon case. The motion in both cases is slower than that of the probe in an oily environment such as methyl-oleate.

A-1.4. Removal of Soils From Fabrics

The soiled threads were washed both with water and with 9×10^{-3}M sodium dodecylsulphate in a capillary washing chamber which fits inside the Varian E-4 EPR spectrometer. A description of the capillary washing chamber may be found in Appendix II. Several threads were packed into the capillary at one time, to enhance the observed signal, and also to increase the Reynolds number[86] of the system to the point of turbulent flow. Turbulent flow is indicated by a Reynolds number of 2100 or greater[87] - with an average spacing between threads of 0.1 mm and a pumping frequency of 2 cycles per second, the Reynolds number of the system was 12,000. This, combined with the machine's rapid reciprocal pumping action, ensures that the capillary washing machine is an effective washing machine simulator[88]. The removal of soil will be described in two sections, one pertaining to soil films, and the other to individually deposited soil molecules.

A-1.4.1. Removal of Soil Films

Threads previously coated with either probe-containing Sebum-H or probe-containing methyl-oleate were washed with water at room temperature and at 65°C. In each case the spectrum was identical to the spectrum of the probe in the soil concerned. The spectrum of individual probe molecules in an aqueous environment was <u>not</u> detected, even though this spectrum is easily detected in a sample containing only pure (I) and water. Thus, it seems that (I) has a lower chemical potential in Sebum-H and in methyl-oleate than it has as a pure liquid. It was noted visually that agitation removed much of the soil from the fabric, although no change was discernible in the EPR spectrum.

Threads previously coated with probe-containing Sebum-H were washed in 9 x 10^{-3}M sodium dodecylsulphate (SDS) at 65°C. Again, no change was observed in the spectrum, the hyperfine coupling constant remaining at 14.5G. The threads were removed from the washing chamber and the clear wash liquor was examined, giving a spectrum identical to those obtained before. Thus the nitroxide group is present in a hydrophobic environment, and not in a more polar environment such as that found near the surface of a micelle. Again, no aqueous probe was observed, indicating that essentially all of the soil in the wash liquor is contained in large hydrophobic domains.

A-1.4.2. Removal of Individual Soil Molecules

Nylon and cotton threads soiled with dilute paramagnetic probe deposited from an acetone film were washed in water at 65°C. With nylon, the spectrum was similar to that obtained in the absence of water, but with cotton, the spectrum of aqueous nitroxide molecules was also detected (see Fig A-1-2.). The relative intensity of the aqueous component of this spectrum is similar to that of a sample containing only (I) and water. Thus, the model oily soil shows an affinity for nylon, but no affinity for cotton.

The model oily soil also shows different behaviour on cotton and on nylon threads in the presence of 9 x 10^{-3}M SDS at 65°C. Although the cmc of pure SDS is about 1.1 x 10^{-2}M at this temperature[89], oily soils lower the cmc to below 9 x 10^{-3}M, as evidenced by Fig A-1-3B (see below). After a 5 minute washing, the spectrum of (I) on nylon had become somewhat sharper (see Fig A-1-3A.). The a_N value was unchanged, indicating that (I) was still in a hydrophobic environment. Examination of the wash liquor without the nylon revealed the presence of a weak spectrum with a slightly greater a_N value (a_N = 14.8G). At

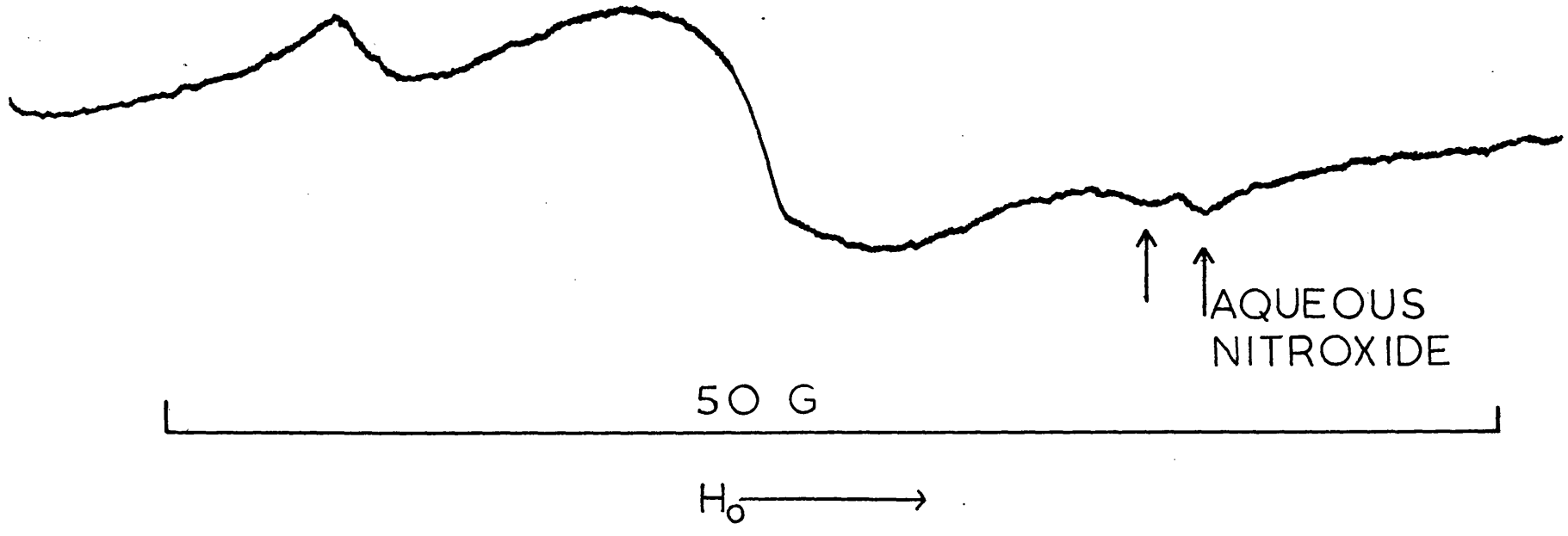

FIG.A.1.2. STEARATE NITROXIDE ON COTTON IN WATER

present the origin of this spectrum is unknown - (I) dissolved in micellar SDS has a_N = 15.2G, so in this case (I) is in an environment more hydrophobic than the micellar one. Possible explanations are (I) in miniscule nylon bits which have been broken off by agitation, or (I) in some sort of oil which, unknown to us, has contaminated the nylon. The more intense spectrum with a_N = 14.5G is associated with the nylon and not with the solution, indicating that it is due to (I) still located on or in the nylon fibre. Since the increase in spectral sharpness was accompanied by an increase in the centre peak to high field peak height ratio, the major effect of 9×10^{-3}M SDS is to reduce the intramolecular electron spin exchange, accompanied by a probable slight reduction in the molecular motion of the nitroxide associated with the nylon.

The spectrum of (I) on cotton after a 1 minute washing with 9×10^{-3}M SDS at 65°C is shown in Fig. A-1-3B. The sharp three lined component of the spectrum has a_N = 15.2G, as does the three lined spectrum obtained from (I) solubilised in SDS, presumably in the micelle. ((I) in water has a_N = 16.0G.) Thus, this component of the spectrum is due to (I) which has become solubilised in micellar SDS. The assymetry of the spectrum indicates the presence of an underlying solid state signal, due to (I) still remaining on the cotton. There may also be a broad underlying line, indicative of several molecules of (I) solubilized in a given SDS micelle - if so, its magnitude is similar to the experimental error. Removal of (I) from the cotton can be measured by comparing the intensities of the micellar and solid state spectra - loss of assymetry would indicate high removal.

FIG. A.1.3-A. STEARATE NITROXIDE ON NYLON IN 9×10^{-3}M SDS

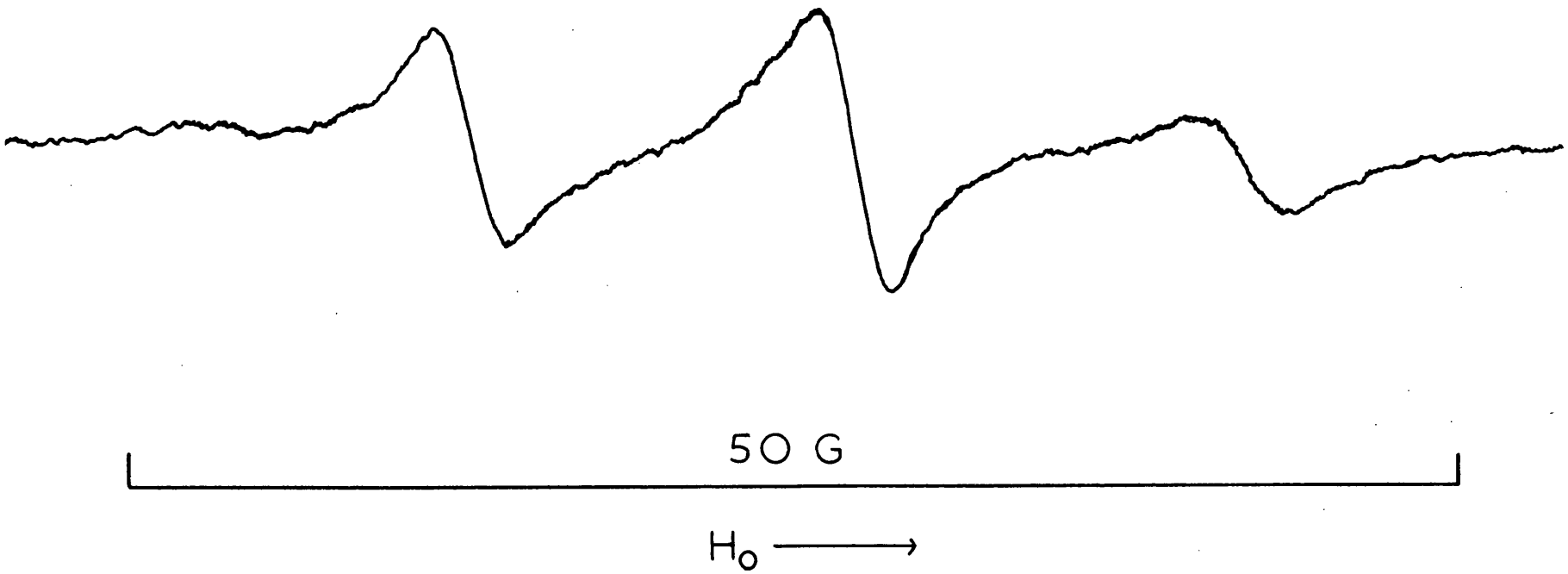

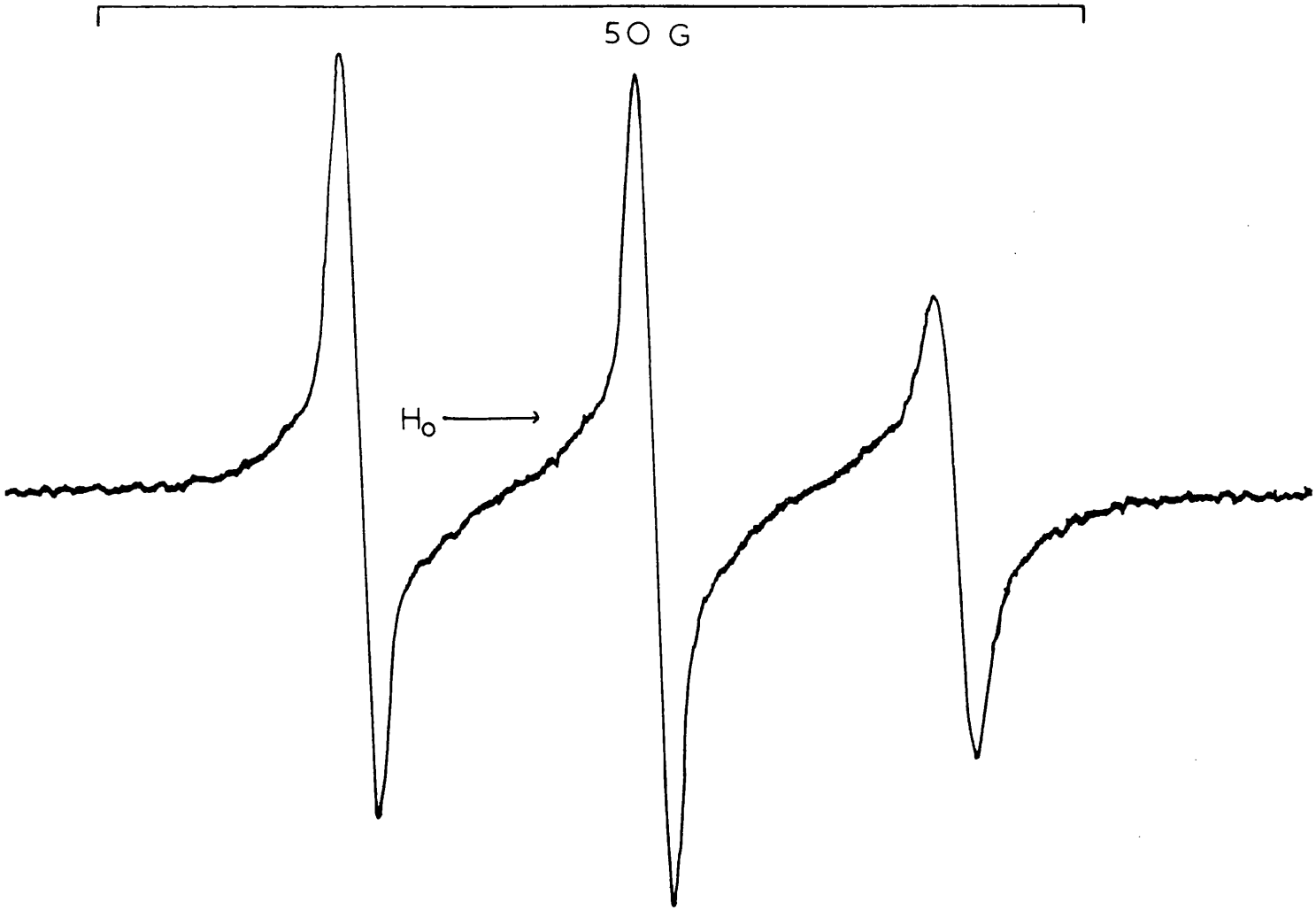

FIG. A.I.3-B. STEARATE NITROXIDE ON COTTON IN 9×10^{-3} M SDS

A-1.5. Redeposition of (I) onto Nylon from SDS Solution

The model oily soil (I) was added to a 5 x 10^{-2}M SDS solution until the EPR spectra indicated that several molecules of (I) were present in each micelle. Clean nylon threads were placed in the capillary washing chamber, and were washed with the soiled detergent solution at room temperature. The EPR spectra of the nylon-containing sample contained a broad peak due to partially immobilized (I), as well as the three broad peaks due to micellar (I). When the nylon was removed from the sample, the signal due to partially immobilized (I) disappeared. The nylon threads were washed several times with distilled water and then placed in a clean capillary. The EPR spectrum of the rinsed threads showed only the partially immobilized signal; no signal due to micellar (I) was detectable. Thus, EPR is an effective method for monitoring simultaneously the immobilized soil associated with the fabric and the soil incorporated in micelles in solution.

A-1.6. Conclusions

The experiments described above illustrate some of the types of information that can be obtained from an EPR study of a paramagnetic oily soil. Using this technique, it has been shown that under normal washing conditions removed oily soil is not solubilized in micelles, but instead exists in oily drops with surfactant probably adsorbed at the oil-water interface. The EPR spectra also reflect the greater affinity of oily soil for nylon rather than for cotton, and give information about the molecular motion of the oily soil adsorbed on each substrate. It is possible, using EPR, to measure redeposition uncomplicated by uncertainties introduced in the rinsing process, since one can observe the spectrum of the adsorbed soil in the presence of soil in the solution. These results show that EPR can be used to obtain useful information about detergency processes and mechanisms.

APPENDIX II

A SIMULATED WASHING MACHINE EPR SAMPLE CELL

A-II.1. Introduction

In order to investigate the removal of a paramagnetic model oily soil from fabrics under normal washing conditions, an EPR sample cell in which these washing conditions can be approximated is required. This cell must be small enough to fit into the cavity of the EPR spectrometer with the variable temperature accessory in position, and must be shaped and positioned so that dielectric absorption of the water molecules does not repress the EPR signal. Also it must be possible to insert and remove fabric from the cell with comparative ease. An EPR sample cell which meets these requirements is described below.

A-II.2. Cell Description

The basis of the Simulated Washing Machine EPR Sample Cell is the capillary washing chamber, a glass capillary less than 1 mm inner diameter which is open at both ends. One or more threads of the fabric to be washed are inserted at the lower end of this chamber, to which is then attached a flexible silicone rubber tube whose other end is stoppered by a glass bead. This tube expands or contracts to compensate for the movement of a syringe, which is attached to the upper end of the capillary washing chamber, thus allowing the washing solution contained in the syringe to be pumped back and forth over the threads of fabric in the washing chamber.

The cell is assembled as shown in Figure A-II.1.A. Short lengths of silicone rubber tubing (1 mm inner diameter) are slipped over each end of the capillary washing chamber, making a water-tight junction with the 3 mm outer diameter silicone rubber tubing which is next slipped over each end of the capillary. The lower piece of silicone tubing, about 22 mm in length, is stoppered at the end opposite the capillary by a glass bead, about which is a ring of 1 mm silicone tubing to water-proof the junction. The upper, short piece of silicone tubing serves to water-proof the junction between the capillary and the teflon tubing (3 mm inner diameter, 15 mm long) into which the upper part of a disposable syringe has been inserted.

The position of the cell in the Varian E-4 EPR spectrometer is shown in Figure A-II.1.B. The variable temperature insert dewar is positioned with the glass dimples about 30 mm below the resonant part of the cavity, so that signals are obtained from the contents of the capillary washing chamber. A teflon adaptor which positions the capillary in the centre of the dewar to ensure maximum sensitivity is shown in Figure A-II.2. This adaptor was made by cutting wedges in a short length of the 6 mm outer diameter teflon tubing. One cut breaks the tubing, to enable the adaptor to fit easily around the capillary; the other wedges allow the nitrogen gas to pass through the variable temperature assembly.

A-II.3. Discussion

The cell is filled by removing the bladder assembly and inserting one or more soiled threads into the capillary. The washing solution is placed in the syringe, which is then pressed

CAPTION TO FIGURES

Figure A-II.1.A. Assembly of washing machine cell.

1 - Glass bead

2 - A, B and C. Silicone rubber tubing approximately 3 mm long, 1 mm outside diameter.

3 - Silicone rubber tubing approximately 22 mm long, 3 mm outside diameter.

4 - Capillary less than 1 mm inside diameter, suitable for EPR use with aqueous solutions.

5 - Silicon rubber tubing approximately 4 mm long, 3 mm outside diameter.

6 - Teflon tubing 3 mm inner diameter, ~ 15 mm in length.

7 - Disposable syringe from which needle has been removed.

Figure A-II.1.B. Assembled cell in variable temperature dewar.

1 - Temperature control coils.

2 - Variable temperature dewar.

3 - Glass dimples.

4 - Silicone rubber expansion tube.

5 - Region which is inside EPR cavity during operation.

6 - Fabric.

7 - Adaptor.

8 - Syringe.

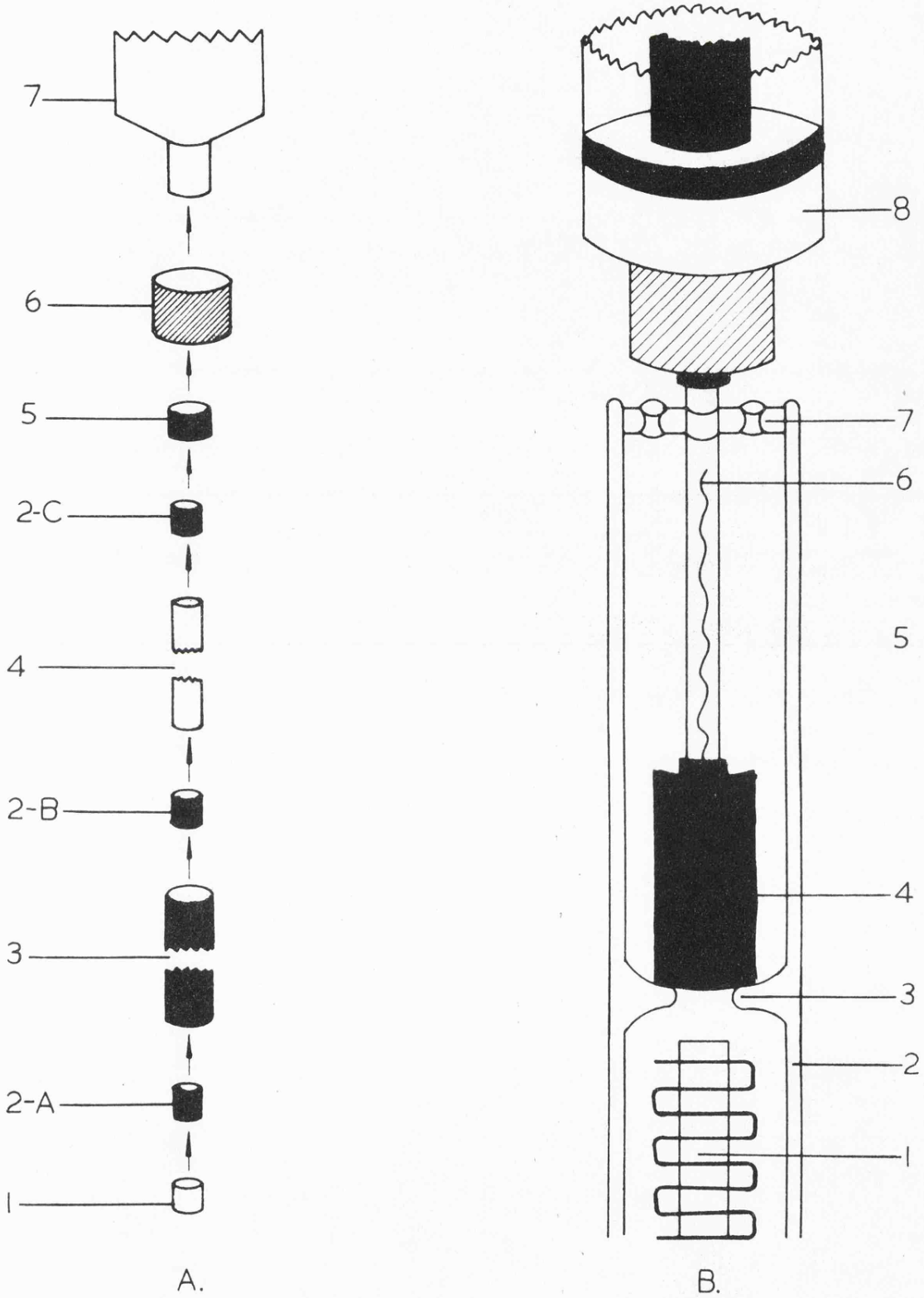

FIG. A.II. I. SIMULATED WASHING MACHINE EPR CELL

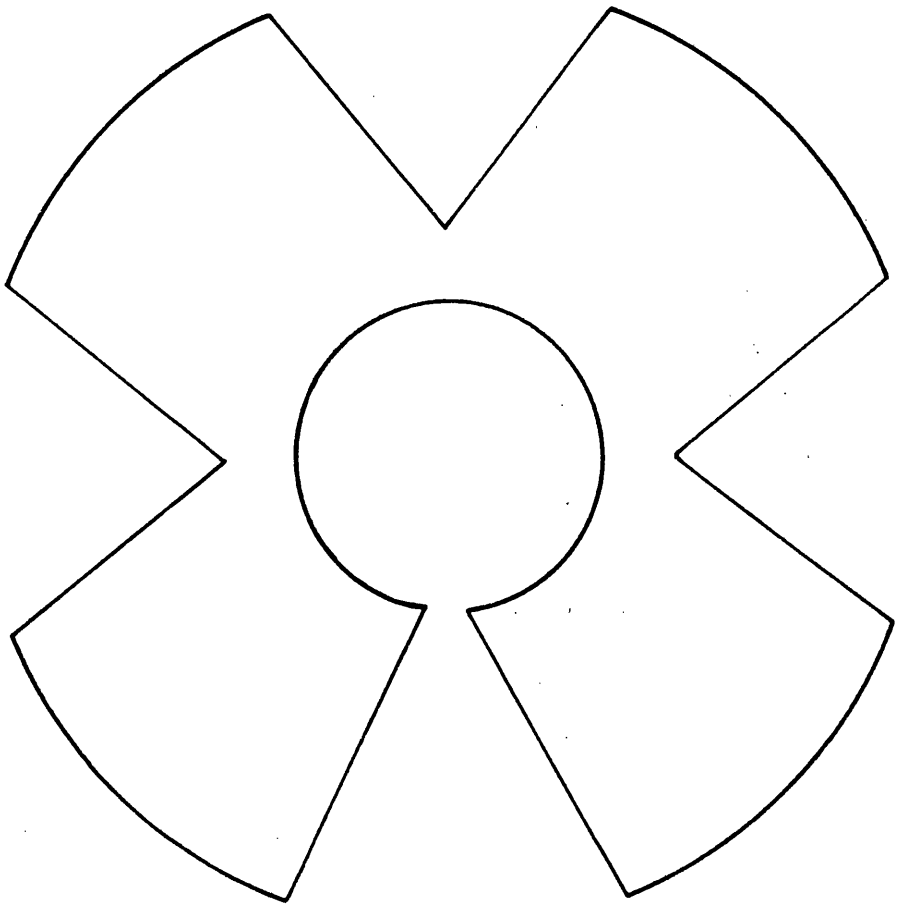

FIG. A.II. 2. TEFLON ADAPTOR

until the washing solution fills most of the capillary. The bladder assembly is evacuated by pressing it with one's fingers, and is then re-joined to the capillary. When the bladder is released the washing solution is drawn into the remaining part of the capillary. The cell is then placed in the variable temperature apparatus in the EPR cavity, which has been set at the desired wash temperature. Agitation is effected by gently moving the plunger of the syringe.

In practice, it is possible to agitate while recording a spectrum, but the more usual procedure is to agitate the sample between recordings. The cell has been found to be completely water-tight, and there is no loss in sensitivity over that of an ordinary capillary. Sample changing is facilitated by using several washing chambers, one for each sample, and by using a new disposable syringe for each solution.

A-II.4. Conclusions

The "Simulated Washing Machine" EPR sample cell enables one to study both paramagnetic soils and paramagnetic surfactants under simulated washing conditions. The construction and use of the cell are described above.

REFERENCES

1. A Carrington and A D McLachlan, Introduction to Magnetic Resonance, Harper and Row, New York, 1967. Chapter 1.

2. B L Bales and M E Baur, Chem.Phys.Letters, 7(3), 341 (1970).

3. A Carrington and A D McLachlan, Introduction to Magnetic Resonance, Harper and Row, New York, 1967. Chapter 7.

4. O H Griffith and A S Waggoner, Accounts Chem.Res., 2, 17 (1969).

5. G Poggi and C S Johnson, Jr. J.Mag.Res., 3, 436 (1970).

6. A Carrington and A D McLachlan, Introduction to Magnetic Resonance, Harper and Row, New York, 1967. Chapter 12.

7. K Shinoda, T Nakagawa, B Tamamushi and T Isemura, Colloidal Surfactants: Some Physico-Chemical Properties, Academic Press, New York, 1963. Chapter 1.

8. P Mukerjee, Advances in Colloid and Interface Science, 1, 241 (1967).

9. A S Waggoner, O H Griffith and C R Christensen, Proc.Nat.Acad.Sci., US, 57 (5), 1198 (1967).

10. A S Waggoner, A D Keith and O H Griffith, J.Phys.Chem., 72 (12), 4129 (1968).

11. A S Waggoner, T J Kingzett, S Rottschaefer and O H Griffith, Chem.Phys.Lipids, 3, 245 (1969).

12. G P Rabold, J.Polymer Sci., Part A-1, 1, 1187 (1969).

13. M G Goldfeld, V K Kolkover, E G Rosantzev and V I Suskina, Kolloid-Z, und Z Polymere, 243, 62 (1971).

14. M J Povich, J A Mann and A Kawamoto, J.Colloid and Interface Sci., 41 (1), 145 (1972).

15. C P Lee, H Drott, B Johansson, T Yonetaric and B Chance, Probes of Structure and Function of Macromolecules and Membranes, Proc.Collog. 249 (1971).

16. S Ohnishi, T J R Cyr and H Fukushima, Bull.Chem.Soc. Japan, 43, 673 (197C

17. M Miura, A Hasegawa and Y Michihara, Bull.Chem.Soc. Japan, 41 (2), 534 (1968).

18. A Hasegawa, Y Michihara and M Miura, Bull.Chem.Soc. Japan, 43 (10), 3116 (1970).

REFERENCES (cont'd)

19. E E Zaev, Kolloidnyi Zhurnal, 34 (2), 304 (1972).

20. M D Barratt, D K Green and D Chapman, Chem.Phys.Lipids, 3 (2), 140 (1969).

21. S Rottschaefer, PhD Thesis, University of Oregon, 1970. Dissertation Abs. B, 1971, July, 214.

22. M J Povich, J A Mann and D E Holmes, J.Coll.Interface Sci., 35 (1), 176 (1971).

23. G J King, B S Miller, F F Carlson and R C McMillan, J.Chem.Phys., 32, 940 (1960).

24. J R Wasson, C Trapp, C I Shyr and D Smith, J.Chem.Phys., 49 (11), 5197 (1968).

25. D Smith and C Trapp, J.Chem.Phys., 52 (9), 4923 (1970).

26. T Nash, J.Coll.Sci., 14, 59 (1959).

27. H Peper and E G Taylor, J.Coll.Sci., 18, 318 (1963).

28. G C Kresheck, E Hamori, G Davenport and H A Scheraga, J.Am.Chem.Soc., 88 (2), 246 (1966).

29. B C Bennion, L K J Tong, L P Holmes and E M Eyring, J.Phys.Chem., 73 (10), 3288 (1969).

30. B C Bennion and E M Eyring, J.Coll.Interface Sci., 32 (2), 286 (1970).

31. M J Jaycock and R H Ottewill, 4th Intern.Congr.Surface Active Substances (Brussels), Sept 1964, Section B, Paper 8, 545.

32. P F Mijnlieff and R Ditmarsch, Nature 208, 889 (1965).

33. T Nakagawa and H Choue, 4th Intern.Congr.Surface Active Substances (Brussels), Sept 1964, Section B, Paper 11, 569.

34. N Muller and R H Birkhahn, J.Phys.Chem., 71 (4), 957 (1967).

35. E Graber, J Lang and R Zana, Kolloid Zeitschrift und Zeitschrift für Polymere, 238 (1-2), 470 (1970).

36. E Graber and R Zana, Kolloid Zeitschrift und Zeit Schrift für Polymere 238 (1-2), 479 (1970).

37. Wayne L Hubbell, Private Communication.

REFERENCES (cont'd)

38. J T Davies and E K Rideal, Interfacial Phenomena, Second Edition, Academic Press, London, 1963. Chapter 4.

39. Ibid, Chapter 1.

40. P B Ayscough, Electron Spin Resonance in Chemistry, Methuen & Co.Ltd., London, 1967. Chapter 1.

41. V A Tolkacher and A I Mikhailov, Pribor.Tekhn.Eksper., 9, 95 (1964).

42. B W Barry, J C Morrison and G F J Russell, J.Colloid and Interface Sci., 33 (4), 554 (1970).

43. J Oakes, Nature 231, 38 (1971).

44. D E Woessner, J.Chem.Phys., 35, 41 (1961).

45. M P Eastman, R G Kooser, M R Das and J H Freed, J.Chem.Phys., 51, 2690 (1969).

46. P W Atkins and D Kivelson, J.Chem.Phys., 44, 169 (1966).

47. K Fox, Trans.Faraday Society, 67 (9), 2802 (1971).

48. S Glasstone, K J Laidler and H Eyring, The Theory of Rate Processes, McGraw Hill Book Company, Inc., New York, 1941.

49. M L Corrin and W D Harkins, J.Am.Chem.Soc., 69, 683 (1947).

50. L M Kushner, W D Hubbard and R A Parker, J.Res.Nat.Bureau of Standards, 59 (2), 113 (1957).

51. H G Hertz, Microdynamic Behaviour of Liquids as studied by NMR Relaxation Times, in J W Emsley, J Feeney and L H Sutcliffe, Eds. Progress in Nuclear Magnetic Resonance Spectroscopy, Vol. 3, Pergammon Press, Oxford, 1967. Chapter 5.

52. R E Verrall, Infrared Spectroscopy of Aqueous Solutions, in Felix Franks, Ed. Water, A Comprehensive Treatise, Vol. 3, Plenum Press, New York, 1973. Chapter 5.

53. R A Sack, Mol.Phys., 1, 163 (1958).

54. H M McConnell, J.Chem.Phys., 28, 430 (1958).

55. J R Zimmerman and W E Brittin, J.Phys.Chem., 61, 1328 (1957).

56. R Kubo, J.Phys.Society, Japan, 9, 935 (1954).

REFERENCES (cont'd)

57. W Plachy and D Kivelson, J.Chem.Phys., 47 (9), 3312 (1967).

58. I J Lowe and R E Norberg, Phys.Rev., 107 (1), 46 (1957).

59. A Carrington and A D McLachlan, Introduction to Magnetic Resonance, Harper and Row, New York, 1967. Chapter 13.

60. R W Kreilick, J.Chem.Phys., 45 (6), 1922 (1966).

61. K H Hausser, H Brunner and J C Jochims, Mol.Phys., 10, 253 (1966).

62. A Calder, A R Forrester, J W Emsley, G R Luckhurst and R A Storey, Mol.Phys., 18 (4), 481 (1970).

63. R W Kreilick, Mol.Phys., 14 (5), 495 (1968).

64. J A Pedersen and K Torssell, Acta.Chemica.Scandinavica, 25, 3151 (1971)

65. R W Kreilick, J.Chem.Phys., 46 (11), 4260 (1967).

66. R Briere, H Lemaire, A Rassat, P Rey and A Rousseau, Bull.Chim.Soc., France, 1967, 4479 (1967).

67. G F Hatch and R W Kreilick, J.Chem.Phys., 57, 3696 (1972).

68. H M McConnell and R E Robertson, J.Chem.Phys., 29, 1361 (1958).

69. R J Kurland and B R McGarvey, J.Mag.Res., 2 (3), 286 (1970).

70. R Chang and C S Johnson, Jr. J.Chem.Phys., 41, 3272 (1964).

71. P Mukerjee, J.Phys.Chem., 62, 1397 (1958).

72. P Mukerjee, J.Phys.Chem., 69, 2821 (1965).

73. E J Bair and C A Kraus, J.Am.Chem.Soc., 73, 1129 (1951).

74. J S Clunic, J F Goodman and P C Symons, Trans.Faraday Soc., 63, 754 (1967).

75. G D Parfitt and A L Smith, J.Phys.Chem., 66, 942 (1962).

76. F van Voorst Vader, Trans.Faraday Soc., 57, 110 (1961).

77. K W Herrmann, J.Colloid and Interface Sci., 22, 352 (1966).

78. F Franks and H T Smith, J.Phys.Chem., 68, 3581 (1964).

79. D S Goodman, J.Am.Chem.Soc., 80, 3887 (1958).

REFERENCES (cont'd)

80. C Mack, Essentials of Statistics for Scientists and Technologists, Heinemann Educational Books Ltd., London, 1966.

81. D G Hall, Private Communication.

82. C P Poole, Jr. Electron Spin Resonance, Interscience Publishers, New York, 1967.

83. R C Weast, Ed. Handbook of Chemistry and Physics, 45th Edition, The Chemical Rubber Company, Cleveland, Ohio, 1964.

84. J H Boyd, Thesis submitted in partial fulfilment of the requirements for the degree of Master of Philosophy of the Council for National Academic Awards, 1972. Copies may be obtained from Mr Boyd at the Birkenhead College of Technology.

85. L F Fieser, J.Am.Chem.Soc., 46, 2639 (1924).

86. R C L Bosworth, Physics in Chemical Industry, MacMillan and Co.Ltd., London, 1950.

87. C O Bennett and J E Myers, Momentum, Heat and Mass Transfer, McGraw-Hill Book Company Inc., New York, 1962. Chapter 1.

88. H A Barnes, Private Communication.

89. P Mukerjee and K J Mysels, CMC's of Aqueous Surfactant Systems, National Bureau of Standards Publication NSR DS/NBS 36, 1971.

MAGNETIC RESONANCE OF MICELLAR SYSTEMS

Abstract

The frequency with which a surfactant monomer enters and leaves a surfactant micelle has been the subject of much discussion. It is possible, using EPR, to measure the frequency with which a paramagnetic molecule changes to a magnetically different environment if that frequency is between 10^5 and 10^9 sec^{-1}, or alternatively to state whether the exchange frequency is faster or slower than these limits. If the paramagnetic molecule were also a surfactant, this technique would give information about the exchange frequency between monomer and micelle, since these have magnetically different environments.

A series of paramagnetic surfactants (I) was prepared. The EPR spectra of micellar solutions of these surfactants consisted of one broad line due to

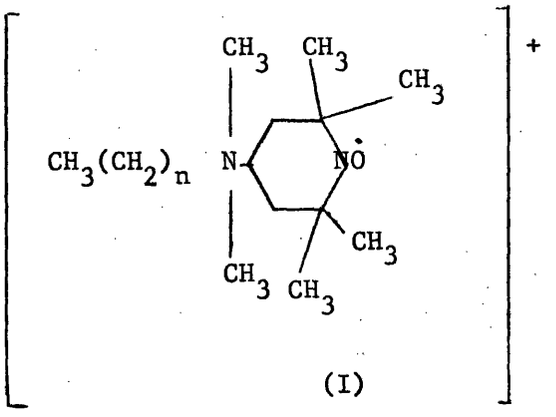

(I)

the micelles, superimposed upon three sharp lines due to the monomeric nitroxide surfactant. This showed that the monomer- micelle exchange frequency was in the slow region. Increasing the temperature increased the width of the monomer lines, and it was initially thought that this was indicative of measurable monomer-micelle exchange. Further experiments produced inconsistent results. In an attempt to understand

these results, a theoretical investigation of the linewidth behaviour expected for monomer-aggregate exchange was made, which indicated that under certain conditions the $m_I = \pm 1$ nitroxide lines might broaden more than the $m_I = 0$ line. This would enable one to distinguish monomer-aggregate exchange from Heisenberg spin exchange. Since these linewidth effects were small, an attempt was made, by computer-simulation, to take into account the effect of proton hyperfine structure on the observed linewidth. This attempt was not successful as the proton hyperfine coupling constants were found to decrease with increasing exchange frequency in the region of interest. The problem was further complicated by the presence of pre-micellar aggregates, which seem to be caused by the nitroxide head group and not by the hydrocarbon chains of the surfactant. A final series of experiments showed that the observed linewidth increases were not due to monomer-micelle exchange, but to a combination of monomer-dimer exchange and Heisenberg spin exchange. Thus this EPR technique yields only the information that the monomer-micelle exchange frequency is slower than 10^5 sec^{-1}.

Other EPR experiments involving the nitroxide analogue of an oily soil are described. The physical state of the paramagnetic soil on fabric, the removal of the soil under different conditions, and the re-deposition of the soil are described, as is the construction of a capillary washing chamber, an effective washing-machine simulator which operates in the cavity of an EPR spectrometer and in which these experiments were performed.